Inaugural dissertation

for

obtaining the doctoral degree

of the

Combined Faculty of Mathematics, Engineering and Natural Sciences

of the

Ruprecht - Karls - University

Heidelberg

Presented by

Dipl. Ing. (FH) Jessica Kehrer

Born in: Heidelberg, Germany

Oral examination: 28.05.2024

Identification and functional characterization of micronemal proteins in *Plasmodium berghei* parasites

Referees: Prof. Dr. Michael Lanzer

Prof. Dr. Friedrich Frischknecht

SUMMARY

Malaria, a life-threatening disease caused by *Plasmodium* parasites, poses a significant global health challenge. Despite efforts to combat malaria through prevention, diagnosis, and treatment, it continues to claim a high number of lives, particularly among vulnerable populations such as young children and pregnant women.

The motility of *Plasmodium* ookinetes and sporozoites in the mosquito vector as well as in the mammalian host is a crucial aspect of the parasite life cycle. Ookinetes play a critical role in the establishment of an infection in the mosquito. Motility enables these parasite forms to traverse the midgut epithelium, a key step during parasite development. Sporozoites need to be motile to egress from oocysts, to enter salivary glands and during their transmission to the mammalian host. During an infectious mosquito bite, sporozoites exhibit remarkable motility, allowing them to navigate through the skin, invade blood vessels and reach the liver, where they establish an infection.

Understanding the mechanisms underlying parasite motility is essential for developing effective strategies to target and disrupt their life cycle, ultimately aiding in the control and eradication of the disease.

Parasite motility relies on the secretion of specialized secretory vesicles at the apical side of the cell, to present proteins on the cell surface needed to interact with host cell surface receptors. In my thesis, I first focused on identifying novel proteins residing in the secretory vesicles of ookinetes and sporozoites using two different proteomics approaches. For ookinetes, I employed Apex2-based proximity labeling to determine the protein content of micronemes. However, a similar approach in sporozoites proved unsuccessful due to a high background signal on the cell surface. Therefore, I chose to collect and analyze secreted proteins in the supernatant of activated cells. Both screens identified both known microneme resident and new proteins. I then selected the most promising novel candidates (akratin and concavin) for further characterization.

Concavin is localized on the cell surface of ookinetes and sporozoites and gene deletion of this protein resulted in deformed sporozoites. During maturation of *concavin(-)* sporozoites they round up from the posterior end of the cell due to detachment of the inner membrane complex from the parasite membrane. This structural aberration limits the efficiency of parasite transmission from the mosquito to the host during an infectious bite. Therefore, the role of concavin emerged as pivotal in ensuring the proper form and function of sporozoites, ultimately impacting the successful conclusion of the malaria parasite's life cycle.

In-depth analyses of parasites lacking akratin revealed a dual function of the protein, both in microgametes and ookinetes. Specifically, a mutation of a putative tyrosine-containing motif

within the C-terminus showed an exclusive function during ookinete to oocyst transition, distinct from its role during gametogenesis. I also discovered two similar tyrosine containing motifs in the C- terminus of the previously characterized pantothenic acid transporter PAT which was shown to play a role in microgametes and sporozoites. Remarkably, both motifs in the C-terminus of PAT are indispensable for ookinetes but not important for gametocytes, mirroring the findings observed with akratin. Stage-specific expression of the respective mutants further underscores the significance of the C-terminus in sporozoites. Interestingly, in the case of sporozoites, only one of the two motifs is important, presenting a nuanced difference compared to ookinetes.

High resolution imaging is important for investigating the small malaria parasite. Yet STED imaging was restricted to non-hemozoin containing life cycle stages due to the high light absorbing capacity of the hemozoin crystals leading to cell damage. I developed a novel method to facilitate *Plasmodium* blood stage whole cell STED nanoscopy. Using CUBIC-P I was able to elute hemozoin from the parasites enabling STED of whole cells without restrictions. This opens up new possibilities for more detailed investigations at the nanoscale level within *Plasmodium*-infected red blood cells and potentially enables to a deeper understanding of the cellular dynamics during *Plasmodium* blood stage development.

ZUSAMMENFASSUNG

Malaria, eine lebensbedrohliche Krankheit, die durch *Plasmodium*-Parasiten verursacht wird, stellt eine große Herausforderung für die globale Gesundheit dar. Trotz der Bemühungen, die Malaria durch Prävention, Diagnose und Behandlung zu bekämpfen, fordert sie nach wie vor zahlreiche Todesopfer, insbesondere in gefährdeten Bevölkerungsgruppen wie Kleinkindern und schwangeren Frauen.

Die Beweglichkeit der Ookineten und Sporozoiten von *Plasmodium* sowohl im Mückenvektor als auch im Säugetierwirt ist ein entscheidender Aspekt des Lebenszyklus des Parasiten. Die Ookineten spielen eine entscheidende Rolle bei der Etablierung einer Infektion in der Mücke. Dank ihrer Motilität können diese Parasitenformen das Epithel des Mitteldarms durchqueren, ein wichtiger Schritt während der Entwicklung des Parasiten. Sporozoiten müssen beweglich sein, um aus Oozysten auszutreten, in Speicheldrüsen einzudringen und während der Übertragung auf den Säugetierwirt. Bei einem infektiösen Mückenstich zeigen die Sporozoiten eine bemerkenswerte Beweglichkeit, die es ihnen ermöglicht, durch die Haut zu wandern, in Blutgefäße einzudringen und die Leber zu erreichen.

Das Verständnis der Mechanismen, die der Motilität der Parasiten zugrunde liegen, ist von entscheidender Bedeutung für die Entwicklung wirksamer Strategien zur Bekämpfung und Unterbrechung ihres Lebenszyklus, was letztlich zur Kontrolle und Ausrottung der Krankheit beiträgt.

Die Motilität von Parasiten beruht auf der Sekretion spezialisierter sekretorischer Vesikel (Mikroneme) an der apikalen Seite der Zelle, um Proteine auf der Zelloberfläche zu präsentieren. Diese werden für die Interaktion mit den Rezeptoren der Wirtszelle benötigt. In meiner Dissertation konzentrierte ich mich zunächst auf die Identifizierung neuartiger Proteine, die sich in den sekretorischen Vesikeln von Ookinetes und Sporozoiten befinden, indem ich zwei verschiedene Proteomics-Ansätze verwendete. Bei Ookineten habe ich den Proteingehalt von Mikronemen mit Hilfe der Apex2-Näherungsmarkierung bestimmt. Ein ähnlicher Ansatz bei Sporozoiten erwies sich jedoch aufgrund eines hohen Hintergrundsignals auf der Zelloberfläche als erfolglos. Daher entschied ich mich, die sezernierten Proteine im Überstand aktivierter Zellen zu sammeln und zu analysieren. Bei beiden Untersuchungen wurden sowohl bekannte als auch neue Proteine identifiziert aus denen ich schließlich die zwei vielversprechendsten Kandidaten (Akratin und Concavin) zur weiteren Charakterisierung auswählte.

Concavin ist auf der Zelloberfläche von Ookineten und Sporozoiten lokalisiert, und die Entfernung dieses Proteins führte zu deformierten Sporozoiten. Während der Reifung von *Concavin(-)*-Sporozoiten runden sie sich am hinteren Ende der Zelle ab, da sich der innere

Membrankomplex von der Parasitenmembran ablöst. Diese strukturelle Abweichung schränkt die Effizienz der Parasitenübertragung von der Stechmücke auf den Wirt während eines infektiösen Insektenbisses ein. Daher hat sich die Rolle von Concavin als entscheidend für die Gewährleistung der richtigen Form und Funktion von Sporozoiten erwiesen, was sich letztlich auf den erfolgreichen Abschluss des Lebenszyklus des Malariaparasiten auswirkt.

Eingehende Analysen von Parasiten, denen Akratin fehlt, ergaben eine Doppelfunktion des Proteins, sowohl in Mikrogameten als auch in Ookineten. Insbesondere zeigte eine Mutation eines tyrosinhaltigen Motivs im C-Terminus eine ausschließliche Funktion während des Übergangs von Ookineten zu Oozysten. Zwei ähnliche Tyrosin-haltige Motive entdeckte ich auch im C-Terminus des bereits charakterisierten Pantothensäure-Transporters PAT. PAT spielt eine wichtige Rolle in Mikrogameten und Sporozoiten. Bemerkenswerterweise sind beide Motive im C-Terminus von PAT für Ookineten, jedoch nicht für Gametozyten, unverzichtbar, was den Ergebnissen mit Akratin entspricht. Die stadienspezifische Expression der jeweiligen Mutanten unterstreicht die Bedeutung des C-Terminus in Sporozoiten. Interessanterweise ist im Fall von Sporozoiten nur eines der beiden Motive wichtig, was einen kleinen Unterschied zu Ookineten darstellt.

Diese Entdeckungen fügen ein wertvolles Puzzlestück zu den laufenden Bemühungen hinzu, den Austritt, die Beweglichkeit und die Übertragung des Parasiten zu verstehen. Das Verständnis der komplexen Funktionen von Akratin, PAT und Concavin in verschiedenen Stadien des Parasitenlebenszyklus trägt nicht nur zum grundlegenden Wissen über die Malaria-Biologie bei, sondern hat auch potenzielle Auswirkungen auf die Entwicklung gezielter Interventionen gegen die Krankheit.

Hochauflösende Mikroskopie wie STED ist wichtig um detaillierte Strukturen innerhalb des winzigen Malariaparasiten zu erforschen. Bislang war STED Mikroskopie allerdings auf Lebenszyklusstadien ohne Hemozoin beschränkt. Die hohe Lichtabsorptionsfähigkeit der Hemozoin-Kristalle in Verbindung mit den energiereichen Lasern wie sie für STED Mikroskopie verwendet werden führt zu Zellschäden. Unter Verwendung von CUBIC-P konnte ich Hemozoin aus den Parasiten entfernen, was nun STED von kompletten Zellen ohne Einschränkungen ermöglicht. Dies eröffnet neue Möglichkeiten für detailliertere Untersuchungen auf nanoskaliger Ebene innerhalb von *Plasmodium*-infizierten roten Blutkörperchen und trägt möglicherweise zu einem tieferen Verständnis der komplexen zellulären Dynamik während der Entwicklung von *Plasmodium*-Blutstadien in der Zukunft bei.

ACKNOWLEDGEMENTS

First, I want to thank my supervisors Friedrich Frischknecht and Michael Lanzer, without whom this thesis would not have been possible. Your expertise, dedication, and commitment to excellence have been instrumental in shaping my research and academic development.

Freddy—A big THANK YOU for believing in me and not giving up pushing me writing this thesis. Thanks for your oversight and support during the course of my PhD studies. I appreciate your availability for occasional discussions and your general guidance throughout the process.

THANKS to Michael Lanzer who made all this possible. Your enthusiasm and support have greatly contributed to my intellectual growth. Thanks for the opportunity to enhance my research skills in your lab.

I also want to thank Matthias Mack and Nina Papavasiliou for readily agreeing to be in my PhD Defense committee.

I cannot thank enough the students I have had the privilege of supervising. You have not only been valuable collaborators but some of you also became friends. Your dedication, enthusiasm, and friendship have greatly enriched my research journey. Thanks to Dominik Ricken, Leanne Strauss, Danny Baltissen, Emma Pietsch, Julia Heinze and Chris Lance. Your contributions to parts of this theses have been crucial in shedding light on the research questions and generating meaningful insights.

Thanks to all the students contributing to other projects. Simon Kracht, Romina Augustin, Konstantin Fischer, Christian Simon, Bastian Löhning, Friedrich Braumann, Joshua Leutiger, Lennard Kleemann and David Eckey. I want to express my appreciation for the trust you placed in me as your supervisor and for allowing me to be part of your academic and personal growth. Witnessing your progress, achievements, and future endeavors fills me with great pride and joy.

A special thanks goes to Emma Pietsch, Simon Kracht and AG Ripp, Johanna Ripp but also Xani Smyrnakou. Thank you for your friendship, kindness, and the laughter we have shared along the way. Your presence has made the research process not only intellectually stimulating but also enjoyable. The countless hours we spent discussing ideas and celebrating milestones together have created lasting memories. I wouldn’t want to miss all the cake, sparkling wine, and ice-cream.

Additionally, I would like to express my appreciation to all colleagues and friends I couldn’t mention personally who have provided support, valuable insights, and stimulating discussions throughout my PhD journey. Your intellectual exchange has been invaluable.

Thanks to Rogerio Amino and Pauline Formaglio from the Pasteur Institut for the collaboration on the “concavin” project. Your “*in vivo*” imaging of my mutant sporozoites gave important additional insights to better understand transmission of these parasites.

Thanks to Charlotta Funaya and Sebastian Weber from the Electron Microscopy Core Facility for experimental support and performing the 3D SEM of concavin(-) sporozoites.

Last but not least I want to thank Carrie Anderson, Johanna Ripp, Simone Lepper and Carolina Agop- Nersesian for proofreading parts of this theses. Your comments and corrections helped a lot to improve this thesis.

Parts of this theses have been published in the following scientific journals:

Kehrer J. Heinze J, Pietsch E, Spielmann T, Frischknecht F; *Clearing of hemozoin in Malaria parasites enables whole cell STED Microscopy.* (2023) Journal of Cell Science 136:jcs260399, https://doi.org/10.1242/jcs.260399

Kehrer J. Formaglio P, Muthinja M, Weber S, Baltissen D, Lance C, Ripp J, Grech J, Meissner M, Funaya C, Amino R, Frischknecht F; *Plasmodium sporozoite disintegration during skin passage limits malaria parasite transmission*. (2022) EMBO reports 23:e54719, https://doi.org/10.15252/embr.202254719

Kimmel K*, **Kehrer J*.** Frischknecht F, Spielmann T; *Proximity-dependent biotinylation approaches to study apicomplexan biology.* (2021) Molecular Microbiology 117:553-568, https://doi.org/10.1111/mmi.14815 (Review)

Kehrer J. Ricken D, Strauss L, Pietsch E, Heinze J, Frischknecht F; *Apex- based proximity labeling of micronemes in ookinetes identifies a protein with dual function during Mosquito transmission.* (2020) BioRxiv https://doi.org/10.1101/2020.09.29.318857

In preparation:

Kehrer J. Pietsch E, Ricken D, Baltissen D, Frischknecht F; *The C- terminus of PAT determines protein function in ookinetes and sporozoites.* (in preparation)

Additional publications:

Braumann F, Klug D, **Kehrer J.** Lu C, Springer TA and Frischknecht F; *Conformational change of the Plasmodium TRAP I domain is essential for sporozoite migration and transmission of malaria.* (2023) EMBO Reports, 24:e57064, https://doi.org/10.15252/embr.202357064

Haag M*, **Kehrer J***, Sanchez C, Deponte M and Lanzer M; *Physiological jump in erythrocyte redox potential during Plasmodium falciparum development occurs independent of sickle cell trait.* (2022) Redox Biology 58:102536, https://doi.org/10.1016/j.redox.2022.102536.

Ripp J, **Kehrer J.** Smyrnakou X, Tisch N, Rogerio A, Travares J, Ruiz de Almodovar C, Frischknecht F, *Environmental elasticity impacts parasite migration during transmission of malaria.* (2021) EMBO Molecular Medicine, 13:e13933, doi.org/10.15252/emmm.202113933

Egarter S, Santos JM, **Kehrer J.** Sattler J, Frischknecht F, Mair GR; *Gliding motility protein LIMP promotes optimal mosquito midgut traversal and infection by Plasmodium berghei.* (2020) Molecular & Biochemical Parasitology 241:111347, https://doi.org/10.1016/j.molbiopara.2020.111347

Klug D, Goellner S, **Kehrer J.** Sattler J, Strauß L, Singer M, Lu C, Springer TA and Frischknecht F; *Evolutionarily distant I domains can functionally replace the essential ligand-binding domain of Plasmodium TRAP.* (2020) eLife 9:e57572, https://doi.org/10.7554/eLife.57572

de Niz M, **Kehrer J.** Branucci NMB, Moalli F, Reynaud EG, Stein JV, Frischknecht F; *3D imaging of undissected optically cleared Anopheles stephensi mosquitoes infected with Plasmodium parasites*. (2020) PloS One 15:e0238134. https://doi.org/10.1371/journal.pone.0238134

CONTENT

1 INTRODUCTION

1.1. Malaria

Malaria[1] is one of the ancient diseases of the world. It most likely originated as a zoonotic disease from African apes and coevolved with its human host (Carlton, 2018; Hayakawa et al., 2008; Liu et al., 2010). The current statistics of malaria is still alarming. There are 247 million cases of the disease per year, leading to 619000 deaths globally. Particularly concerning is the fact that 95% of cases and 96% of the death occur in Sub-Saharan Africa, highlighting the disproportionate burden faced by this region. Children bear a significant portion of the malaria burden, being at the highest risk of infection, with one child dying every 2 min (World Health Organization, 2021b).

The infection is caused by a unicellular parasite of the genus *Plasmodium* and is spread by a mosquito vector of the *Anopheles* species. *Plasmodium* spp. belong to the phylum of Apicomplexa, a huge cluster of protists. Parasites within this group are characterized by an apical complex at the front of the cell. Essential components of this complex are secretory organelles such as micronemes and rhoptries necessary for cell migration, as well as host cell traversal and invasion. Apart from malaria, well known human diseases caused by apicomplexan parasites include Babesiosis (*Babesia*); Cryptosporidiosis (*Cryptosporidium*) and Toxoplasmosis (*Toxoplasma gondii*).

Symptoms of a classic malaria infection involve fatigue, fever, sweating, body aches, headache and occasionally vomiting. Diagnosis of an infection is performed via thin or thick blood smears, a rapid diagnostic test or PCR-based methods. While the latter is the most expensive and time-consuming diagnostic method, it is considered to be the most sensitive method. In humans, six *Plasmodium* species are able to cause an infection – *P. falciparum, P. vivax, P. malariae, P. knowlesi, P. ovale curtisi* and *P. ovale wallikeri,* of which *P. falciparum* is the most virulent.

Research on the molecular and cellular biology of *Plasmodium* dates back to 1880, when Charles Laveran discovered the parasite in the blood. Subsequently in 1897/1898 Ronald Ross showed that the transmission of the disease between hosts occurs through a mosquito bite. While Ronald Ross made his findings in bird malaria, Giovanni Battista Grassi first demonstrated the

[1] The word malaria comes from the Italian words “mal aria” for “bad air”.

transmission between *Anopheles* and humans. Although it had been hypothesized in 1900 that the parasite does not directly infect red blood cells, Henry Shortt and Cyril Garnham identified the liver stage as the last missing piece of the complete parasite life cycle only in 1948 (Shortt & Garnham, 1948).

Despite massive eradication efforts since 1955 (WHO), malaria remains a vast health problem. Major obstacles, which currently prevent global malaria eradication, consist of parasite resistance to antimalarial drugs, mosquito resistance to insecticides, and the non-existence of effective vaccines (Blasco et al., 2017; Heppner, 2013; Matuschewski, 2017) . The development of a malaria vaccine is a huge challenge for the malaria community. After extensive years of research the first malaria vaccine named RTS,S or Mosquirix™ was only approved in October 2021 and targets the transmission stage of the human parasite *P. falciparum* (Laurens, 2019; World Health Organization, 2021a). A second malaria vaccine, R21 is based on the same protein, circumsporozoite protein and cheaper to manufacture. Compared to RTS,S, which demonstrates around 50% vaccine efficacy, R21 achieves an impressive efficacy rate of up to 75% during the first year (Datoo et al., 2024; RTS, S Clinical Trials Partnership, 2015). While the approval of Mosquirix™ and R21 represents a crucial step forward, ongoing efforts are essential to enhance their effectiveness, address limitations, and develop additional vaccines to combat different *Plasmodium* species and stages in the malaria life cycle. Nevertheless, the introduction of a malaria vaccine is a promising development, offering hope in the global endeavor to reduce the immense burden of this deadly disease.

1.2. *Plasmodium berghei* as a rodent malaria model

Besides humans, *Plasmodium spp*. can infect reptiles, birds and mammals. Their life cycle is largely analogous to the species infecting humans. Especially, the rodent infecting species – *P. berghei*, *P. yoelii, P. vinckei and P. chabaudi* – are adapted as model organisms in many laboratories to study the molecular details of the parasite. *P. berghei* has been identified and was isolated from wild tree-dwelling rats in Central Africa by Ignace Vincke and Marcel Lips in 1948 (Vincke & Lips, 1948). Laboratory research to study the life cycle of *P. berghei* parasites is advantageous to using other species due to the safer handling of *P. berghei* infected mosquito stages, and the fast and efficient techniques to modify the *P. berghei* genome. Furthermore, experiments in humans e.g. to study liver stages or sequestration of the parasite in different tissues have both ethical and practical limitations. Many discoveries from rodents could be transferred to human *Plasmodium* species, yet one needs to keep in mind that there are restrictions e.g. towards the development of an effective vaccine (Manwell et al., 1979; Wykes & Good, 2009).

1.3. The *Plasmodium berghei* life cycle

During its complex life cycle the malaria parasite *Plasmodium* alternates between its vertebrate and insect hosts. Whereas rodents serve as an intermediate host for the parasite to replicate, sexual reproduction exclusively occurs in the mosquito vector. Out of more than 3000 different mosquito species only 41 are known to transmit human malaria parasites (Sinka et al., 2012). Thus, most of the existing species cannot handle parasite development or eliminate the parasite completely through their immune system.

Parasite development in the host

The journey of the parasite in the mammalian host begins during an infectious bite of a female *Anopheles* mosquito. While the mosquito probes for blood it ejects saliva containing highly motile sporozoites into the skin. The amount of sporozoites deposited into the skin varies from insect to insect and from bite to bite. On average about 10 to 100 sporozoites are transmitted from the mosquito to the host (Frischknecht et al., 2004). Once in the skin sporozoites actively move at very high speed to leave the bite site in search of a blood capillary to invade. From the capillary, they are transported through the bloodstream to the liver (Amino et al., 2006; Douglas et al., 2015). Only about half of the transmitted parasites successfully enter the bloodstream. The residual cells either remain in the dermis or end up in lymph nodes (Gueirard et al., 2010). Non-motile genetically modified sporozoites remain noninfectious when transmitted by mosquitoes highlighting the importance of motility in the skin (Montagna et al., 2012). In the liver sporozoites cross the liver sinusoid and traverse several hepatocytes before they settle in their final liver cell (Mota et al., 2001). In the clinically silent liver stage, a single sporozoite develops into thousands of merozoites which are subsequently discharged into the bloodstream through the budding of merosomes (Sturm et al., 2006). The time between sporozoite injection into the skin until the first blood-stage parasite appears, is called the prepatency period and takes about 3- 4 days for *P. berghei*. As soon as the liver-derived merosomes arrive in the blood, merozoites are most likely released in the lung microvasculature and are ready to invade red blood cells (RBCs) (Baer et al., 2007). During RBC invasion of merozoites the parasitophorous vacuole (PV) is formed around the parasite before replication takes place (Matz et al., 2020). The asexual replication in RBCs includes the maturation from merozoite to ring stage and subsequently the trophozoite and the schizont stages. Mature schizonts contain fully developed merozoites which are again released to infect more RBCs. This burst of RBCs ultimately causes the malaria symptoms as it releases fever inducing factors and reduces the capacity of oxygen transport (Cowman et al., 2017). Differentiation of a small percentage of parasites into male and female gametocytes, known as

sexual commitment, is regulated by the transcription factor AP2-G (Figure 1.1) (Kafsack et al., 2014; Sinha et al., 2014).

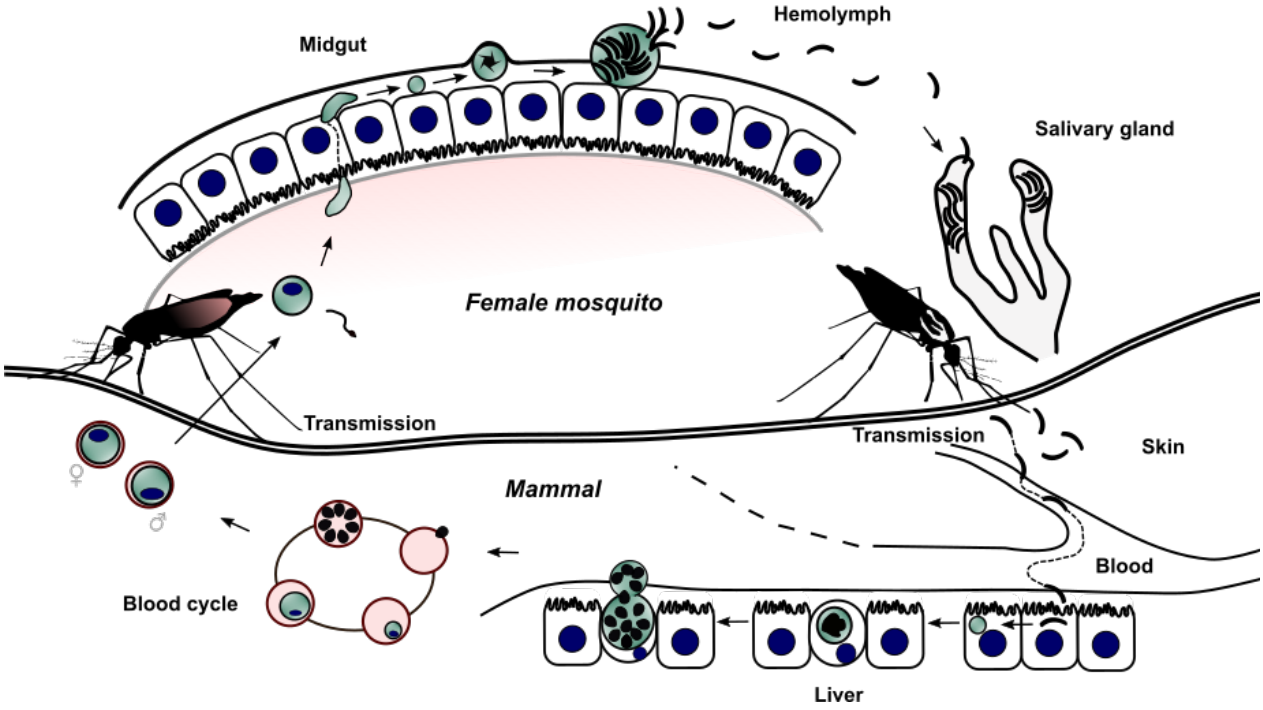

Figure 1.1 The life cycle of *Plasmodium* spp.

During the infectious bite of a female *Anopheles* mosquito sporozoites are injected into the skin of the host from where they migrate to invade blood capillaries. With the bloodstream they are transported to the liver where they invade hepatocytes and form thousands of merozoites which are released back into the blood. Merozoites invade red blood cells and most of them develop into merozoite containing schizonts or gametocytes. During a second bite gametocytes are taken up by the mosquito. In the insect gut they become activated, fertilize and form a motile ookinete traversing the midgut epithelium to establish an infection at the gut wall. Here they transform into oocysts to enable sporozoite formation. Once they are fully formed, oocysts rupture and sporozoites enter the hemolymph of the mosquito to gain access to the salivary glands waiting for the next chance to be transmitted back into the host.

Parasite development in the mosquito

The formation of infectious sporozoites in the insect vector requires several developmental steps. Of the blood-stage parasites taken up from an infected host during a bite only gametocytes can survive.

In the mosquito midgut, gametocytes instantly mature into female macrogametes (egg) and male microgametes (sperm) initiated by a change of environmental conditions such as a drop of temperature, xanthurenic acid and an increase of pH (Billker et al., 1998; Carter & Nijhout, 1977; Sinden & Croll, 1975). To allow fertilization, gametogenesis furthermore depends on the secretion of secretory vesicles to lyse the parasitophorous vacuole membrane (PVM) and the red blood cell membrane (RBCM). This process follows an inside out mechanism. While osmiophilic bodies are

released first to dissolve the PVM, disintegration of the RBCM needs the discharge of a second set of egress vesicles (Flieger et al., 2018; Sologub et al., 2011). Microgametogenesis (exflagellation) includes 3 rounds of rapid DNA replication followed by the formation of 8 motile/ beating flagella. Theses flagella ultimately detach from the residual body to fertilize a female. Vesicle secretion is thus a prerequisite for egress and fertilization (Kehrer, Singer, et al., 2016).

Within 20-24 hours, the resulting diploid zygote transforms into a motile ookinete. Subsequently, the ookinete traverses the midgut epithelium, establishing an infection beneath the basal lamina at the gut wall (Freyvogel, 1966). While thousands of ookinetes are formed, only a small proportion can escape the mosquito immune response to further develop into an oocyst (Fraiture et al., 2009; R. C. Smith et al., 2014). Within 14 days most of the oocysts are filled with sporozoites, which actively move to enter the circulatory system—the hemolymph—of the mosquito (Klug & Frischknecht, 2017). The hemolymph flow transports the sporozoites to the salivary glands which they invade. In the salivary cavities they further mature and wait to be ejected during the next mosquito bite (Frischknecht & Matuschewski, 2017; Touray et al., 1992) (Figure 1.1).

1.4. Hemozoin - The malaria pigment

Parasite development relies on the uptake of nutrients from the host. There is only limited knowledge about the nutrient source for sporozoite development in the mosquito. Based on the evidence that infected mosquitoes contain less amino acids in the hemolymph compared to noninfected insects, the circulatory fluid is thought to be the main source of nutrients (Mack et al., 1979; Mack & Vanderberg, 1978).

In the blood, parasites obtain required amino acids from host cell hemoglobin through cytostome-derived vesicles (Rudzinska et al., 1965; Sherman, 1977). During parasite maturation nearly 80% of host cell hemoglobin is taken up by the parasite in order to extract amino acids, to increase red blood cell space and reduce osmotic pressure which otherwise would lead to host cell lysis (Esposito et al., 2008).

Hemoglobin degradation occurs in the food vacuole (FV) of the parasite (Goldberg et al., 1990) and includes the formation of heme. Since heme is toxic for the cell, it is immediately converted and stored as hemozoin crystals. The food vacuole and in particular the formation of hemozoin crystals is therefore a promising target for anti-malarial drugs e.g. chloroquine. Yet one drawback is the development of resistance against these drugs due to their extensive usage. Point mutations in the chloroquine resistance transporter (CRT) which is localized in the membrane of

the food vacuole leads to transport of chloroquine from the FV back into the cytoplasm of the parasite.

When observed under a light microscope hemozoin crystals appear as black structures. They are highly light absorbent, which can be problematic when exposing the cells with high laser power as needed for STED imaging (Schloetel et al., 2019).

The possibility to observe proteins associated with the FV at high resolution would allow further studies related to drug resistance. It would furthermore allow imaging of proteins distributed throughout the entire cell such as egress vesicle in gametocytes.

1.5. Cell motility and the magic of movement

Motility or movement of single cells and multicellular organisms is a fundamental process in life. It is defined as the ability to move spontaneously and independently (www.thefreedictionary.com/motility). In eukaryotic cells forward locomotion can either be tubulin or actin dependent. Tubulin based movement was probably the first type of movement observed by Antony van Leeuwenhoek in 1676 with the aid of his own custom-built single lens microscopes. This depends on the motor protein dynein and drives motility of cells with cilia or flagella (Haimo & Rosenbaum, 1981; Sanchez et al., 2011). While some cells develop only one flagellum, such as human sperm, others can have multiple ones (Malo et al., 2006).

Cells dependent on tubulin-based movement are usually propelled forward through swimming, cells moving on solid substrates in contrast rely on an actin-myosin based motor (Alberts et al., 2015). Several types of actin-based movements exist and most eukaryotic cells change their location exhibiting mesenchymal cell migration or amoeboid movement which is the most common and best studied mode of motion (Fukui, 2002; Gręobecki, 1994). For example, *Dictyostelium*, amoeba, leukocytes, lymphocytes, dendritic and cancer cells use amoeboid movement. These cells form polarized pseudopods in the direction of movement and undergo a dramatic change of shape on their way forward.

However, *Plasmodium* ookinetes and sporozoites move actively without changing their shape by a mechanism not involving flagella, cilia or pseudopods. This special type of movement is termed gliding motility and will be introduced in more detail below. Gliding motility is also characteristic for some Diatom species and bacteria not containing flagella such as *M. xanthus* (McBride, 2001; Stanley A. Cohn & Roy E. Weitzell Jr., 1996).

Gametocyte activation and tubulin-based movement of microgametes

The observation of beating microgametes termed exflagellation led to the discovery of *Plasmodium* spp. by Laveran. Already shortly after, Maccallum found that the observed movement was the male gamete needed for sexual reproduction (Maccallum, 1897). The flagella of microgametes contain microtubules enabling the *Plasmodium* sperm to swim towards the female counterpart within the blood bolus of the mosquito midgut.

Gametogenesis is an extremely rapid process and exclusively takes place in the mosquito vector, where an increase of intracellular Ca^{2+} occurs within the first 20 s (Billker et al., 2004). The release of Ca^{2+} is triggered by a drop of temperature, an increase of pH and the presence of Xanthurenic acid (Billker et al., 1998). Xanthurenic acid mediates the interaction of GEP1 (gametogenesis essential protein 1) and the guanyl cyclase GCα initiating cGMP synthesis (Jiang et al., 2020). The increased cGMP level in turn activates PKG (protein kinase G), either leading to a phospholipase mediated opening of channels or phosphorylation of ICM1 to discharge intracellular Ca^{2+} reservoirs (Brochet et al., 2014; McRobert et al., 2008; Taylor et al., 2008). The increased cytoplasmic Ca^{2+} level subsequently leads to the activation of a signaling cascade involving calcium dependent kinases needed to initiate endomitosis and axoneme assembly of microgametes (Figure 1.2).

Disintegration of the PVM and RBCM is mediated by protein discharge of at least two distinct types of stage specific secretory vesicles—osmiophilic bodies (OB) and egress vesicles (EV) (Figure 1.2). While the release of OBs is Ca^{2+} independent, secretion of EVs requires Ca^{2+} (Sologub et al., 2011). Known proteins necessary for membrane dissolution are: g377, MDV/ PEG3 (male development-1/ protein of early gametocyte 3), GEST (gamete egress and sporozoite traversal), PAT (pantothenic acid transporter), SUB1 (subtilisin-like serine protease 1), SUB2 (subtilisin-like serine protease 2), DPAP2 (dipeptidyl aminopeptidase 2), PSOP12, GEP (gametogenesis essential protein), MiGS (microgametocyte surface protein), mTRAP (merozoite TRAP-like protein) and PPLP2 (perforin-like protein 2) (Andreadaki et al., 2020; De Koning-Ward et al., 2008; Deligianni et al., 2013; Kehrer, Frischknecht, et al., 2016; Lal, Delves, et al., 2009; Pace et al., 2019; Ponzi et al., 2009; Sala et al., 2015; Tachibana et al., 2018; Talman et al., 2011; Tanaka et al., 2013; Wirth et al., 2014) (Figure 1.2). Vesicle secretion has been shown to rely on the pantothenic acid transporter PAT (Kehrer, Singer, et al., 2016). PAT is studied as part of this thesis and will be described in more detail in section 1.7.

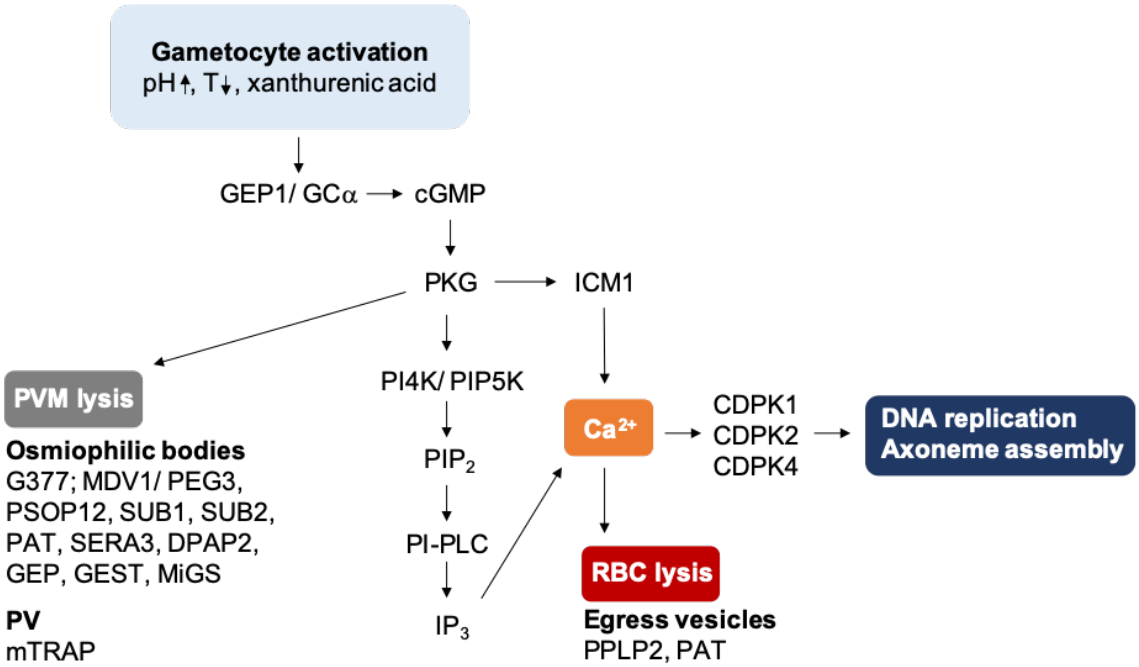

Figure 1.2 Schematic overview of the signaling events underlying gametocyte activation

Gametocyte activation is triggered by an increase of temperature and the presence of xanthurenic acid. Xanthurenic acid induces a conformational change of GEP1 important for its interaction with GCα needed to initiate cGMP synthesis. Increased cGMP levels activate PKG leading to PVM lysis and the release of intracellular Ca^{2+} via two distinct mechanisms. Free Ca^{2+} mediates RBC lyses and the activation of CDPKs needed for microgametogenesis. GEP1 (gametogenesis essential protein 1); GCα (Guanylyl Cyclase alpha); ICM1 (Important for Ca2+ mobilization; cGMP (cyclic guanosine monophosphate); PVM (parasitophorous vacuole membrane); PKG (Protein Kinase G); 1); PLC (Phospholipase C); PIP2 (phosphatidylinositol (4,5)-bi-phosphate); IP3 (Inositol-(1,4,5)-trisphosphate); CDPK (calcium-dependent protein kinases); RBC (red blood cell); g377, MDV/ PEG3 (male development-1/ protein of early gametocyte 3), GEST (gamete egress and sporozoite traversal), PAT (pantothenic acid transporter), SUB1 (subtilisin-like serine protease 1), SUB2 (subtilisin-like serine protease 2), DPAP2 (dipeptidyl aminopeptidase 2), PSOP12, MiGS (microgametocyte surface protein), mTRAP (merozoite TRAP-like protein) and PPLP2 (perforin-like protein 2).

The formation of motile microgametes necessitates three cycles of DNA replication, taking around 15 minutes to complete. While the replication machinery is already available at an earlier stage, DNA synthesis only commences upon gametocyte activation (Matthews et al., 2022). Following the aforementioned signaling cascade, the bipartite microtubule organizing center (MTOC) generates eight distinct kinetosomes or basal bodies. At the same time, DNA is replicated, and individual axonemes are assembled (Sinden et al., 1976) (Figure 1.3 A). Although axoneme assembly and exflagellation can occur independently of DNA replication, it remains unclear whether impaired DNA replication results in microgametes without a nucleus or with a partial genome (Matthews et al., 2022). Unlike cilia and flagella formation in most eukaryotes, the

Plasmodium microgamete is directly assembled in the parasite cytoplasm, which lacks the complete machinery for intra-flagellar transport. (Briggs et al., 2004).

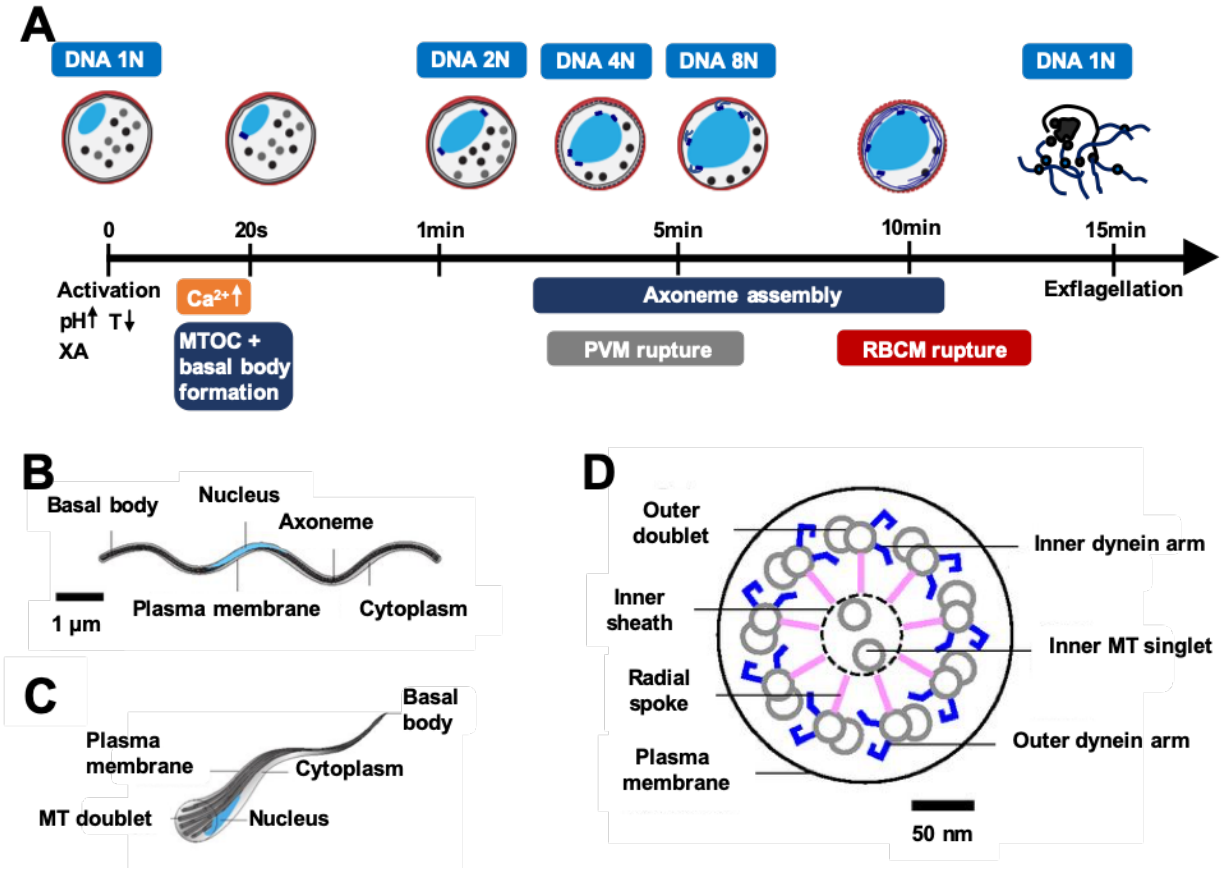

Figure 1.3 Microgametogenesis and the architecture of the *Plasmodium* microgamete

(A) Schematic timescale of microgametogenesis. Microgametogenesis is induced in the mosquito gut where the cells are able to sense environmental changes and is complete after 15 min. Microgametes subsequently undergo 3 rapid rounds of DNA replication and forms 8 individual flagella which are ultimately released into the blood bolus to fertilize a macrogamete. **(B)** Longitudinal cross-section highlighting the basic structure of a *P. berghei* microgamete. It consists of the basal body, the nucleus, the axoneme, the plasma membrane and the cytoplasm. Scale bar: 1 µm. **(C)** Angled cross-section highlighting the basic structure of a *P. berghei* microgamete. Shown are the basal body, the nucleus, the microtubule (MT) doublet, the plasma membrane and the cytoplasm. **(D)** Cartoon showing the typical structure of a 9+2 cross section of an axoneme surrounded by the plasma membrane. (Wilson et al., 2013).

The fully assembled microgamete comprises only the most fundamental components, including a nucleus, an axoneme, a basal body, and a small amount of cytoplasm, all enclosed by the plasma membrane (see Figure 1.3 B). The microgamete proteome is made up of 615 proteins within the cell. The axoneme is typically arranged in a classic 9+2 pattern, consisting of two central single microtubules (MT) surrounded by nine MT doublets, which are conserved across various species (Linck et al., 2014; Talman et al., 2014; Wilson et al., 2013) (Figure 1.3 C,D). However,

in approximately 2% of microgametes, the axoneme's composition differs and appears as either 9+1 or 9+0 (Straschil et al., 2010).

Active movement of microgametes is short lived, typically lasting around 40-60 min and is powered by glycolysis (Talman et al., 2014; Wass et al., 2012). The force driving the microgamete's motion is generated by dynein movements along microtubule filaments, which is regulated through the central apparatus and calcium (E. F. Smith, 2002; E. F. Smith & Lefebvre, 1997). Swimming microgametes exhibit three different types of movement: fast, slow, and immotile. Fast-swimming cells average about five waves per second, while slow-swimming cells reduce their movement to one wave per second. Individual microgametes can switch between fast and slow movement (Talman et al., 2014). Importantly, unlike most other flagellated cells or sperms, *Plasmodium* microgametes swim in an ambidextrous fashion (Wilson et al., 2013).

Actin-based movement of ookinetes and sporozoites

The motility of ookinetes and sporozoites is essential for tissue traversal and host cell invasion (Singer & Frischknecht, 2023). It is in particular fascinating, since the cells are able to move at very high speed without changing their shape. The gliding behavior of sporozoites for instance allows them to travel 10 times faster than the fastest cell in our human body, a neutrophil. The core gliding machinery is called the glideosome and conserved within Apicomplexa (Baum et al. 2006). The core of the glideosome and thus the engine of the parasite is an actin-myosin motor located at the periphery of the cell. The ability to move at such high pace requires the fast turnover of dynamic actin filaments. In contrast to mammalian cells that form actin fibers longer than 1 µm, *Plasmodium* sporozoites only form short and unstable filaments which are difficult to visualize (Schüler & Matuschewski, 2006). The turnover of actin filaments is regulated by actin binding proteins such as profilin (monomer binding), coronin (filament binding), formin (nucleation) and cofilin (filament breaking). Modifications or deletion of actin binding proteins or actin itself leads to an aberrant movement behavior of the sporozoite (Pollard 2016; Douglas et al. 2018; Bane et al. 2016; Moreau et al. 2017).

Actin filaments are assembled at the apical side and moved backwards by Myosin A, resulting in forward movement. The motor is anchored to the inner membrane complex (IMC), a Golgi-derived double membrane located around 25 nm beneath the plasma membrane (PM). The IMC is not only needed to localize the motor, but is also connected to the subpellicular network (SPN), which fixes the motor and microtubules (Harding & Frischknecht, 2020). Both SPN and MTs are essential for the stability and shape maintenance of the parasite. The distance of the IMC to the PM is determined by glideosome associated proteins (GAPs), which bridge the two membranes (Frénal et al., 2010). Furthermore, actin filaments are linked to the substrate via the

glideosome associated connector (GAC) and membrane-spanning surface adhesins (Jacot et al., 2016). Adhesins are initially resident in secretory vesicles called micronemes. Once the parasite is activated by an external signal, micronemes release their protein content in a calcium dependent manner into the plasma membrane at the front of the cell. At the plasma membrane the proteins then form distinct adhesion sites and are translocated to the back of the parasite. The proteins are then eventually cleaved and deposited on the substrate resulting in forward locomotion and retrograde flow (Figure 1.4) (Carruthers & Sibley, 1999; Frénal et al., 2010; Münter et al., 2009; Spaccapelo et al., 1997; Steward & Vanderberg, 1991). Hence, adhesins transmit the forces generated by the actin-myosin motor to the extracellular substrate (Quadt et al., 2016). Parasites unable to secrete their microneme contents do not efficiently attach to the substrate and are thus immobile (Kehrer, Singer, et al., 2016). It is not clear, whether there are some proteins recycled at the back of *Plasmodium* ookinetes and sporozoites as recently shown for *Toxoplasma gondii* (Gras et al., 2019).

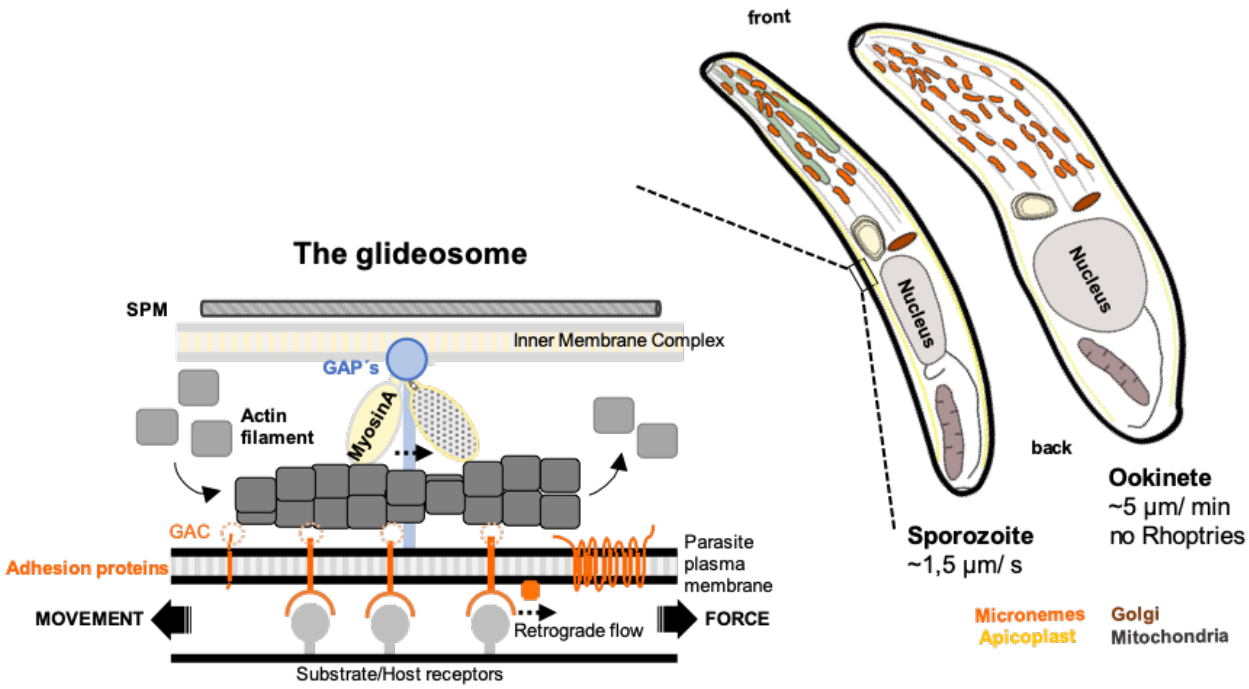

Figure 1.4 Cartoon of the gliding machinery in ookinetes and sporozoites

The glideosome of the parasite, needed for forward locomotion, depends on the power of the actin-myosin motor which is located between the inner membrane complex (IMC) and the parasite membrane (PM). Glideosome Associated Proteins (GAPs) anchor the complex in the IMC but also serve as spacer between both membranes. Short actin filaments are then linked to the substrate via surface adhesins. The force generated by the motor is opposed to the direction of movement. Subpellicular microtubules (SPM) function to stabilize the entire cell. Sporozoites and ookinetes inhabit a similar set of organelles. Sporozoites have rhoptries as additional organelles, needed for cell invasion and PVM formation (right).

Ookinetes are fully formed in the blood bolus within the mosquito midgut one day after the insect has taken up parasites during a bite. To establish an infection, ookinetes actively traverse the chitin holding peritrophic membrane and the midgut epithelium to reach the basal lamina where they ultimately arrest and form an oocyst. It has been shown that traversal of the peritrophic membrane is mediated by chitinase. Parasites lacking the gene are unable to reach the basal lamina and thus show reduced parasite infectivity (Dessens et al., 2001; Tsai et al., 2001). Interestingly, traversal of the epithelium happens without the formation of a PVM (Torii et al., 1992). Within the host cell, the parasite induces rearrangement of the actin network leading to apoptosis and elimination of the host cell from the epithelial sheet (Han & Barillas-Mury, 2002; Zieler & Dvorak, 2000). How this is initiated by the parasite is still unknown.

The ookinete stage is considered as one of the major bottlenecks during the life of a *Plasmodium* parasite. Only 10% of ingested female gametes develop into ookinetes of which only 1% manage to escape from the mosquito immune system to reach the oocysts stage, although these numbers may vary depending on parasite and mosquito species. Parasite numbers nevertheless remain lowest between the gametocyte to oocyst transition (R. C. Smith et al., 2014). Epithelial nitration marks the parasites for killing and mediates mosquito anti-plasmodial immunity (Oliveira et al., 2012). Most of the ookinetes are then destroyed at the basal side close to the hemocoel in a TEP1 mediated way, leading to lysis or melanization (Fraiture et al., 2009).

Transformation of the ookinete into an oocyst is thought to be triggered by the interaction with laminin (Arrighi & Hurd, 2002; Nacer et al., 2008). Yet recent studies in our lab also suggest that stiffness of the environment plays a role (Ripp et al., 2021). Oocyst formation at the basal lamina is the only extracellular parasite stage during the life cycle. Several ookinete proteins are supposed to be involved during the journey through the midgut lumen. Yet only little is known about their function and how they potentially interact with each other (Armistead et al., 2018; Currà et al., 2019; Dessens et al., 1999, 2003; Ecker et al., 2007; Kariu et al., 2006; Tomas et al., 2001; Vega-Rodríguez et al., 2014; Yuda et al., 2001).

A single ookinete develops within two weeks into hundreds of sporozoites. Once midgut sporozoites are fully formed, a combination of proteases and active motility are required in order for the sporozoite to exit into the hemolymph of the mosquito which transports them passively to the salivary glands (Aly & Matuschewski, 2005; Klug & Frischknecht, 2017). Entry into salivary glands relies on the presence of adhesins on the sporozoite surface and a functional actin- myosin motor. How sporozoites finally enter the secretory cells has not yet been fully described. One hypothesis is that the adhesin TRAP interacts with the surface receptor saglin (Ghosh et al., 2009). However, in mosquitoes lacking saglin the protein was shown to influence mosquito infection

rather than salivary gland invasion (Klug et al., 2023). In the cavities of the mosquito salivary gland the sporozoites await the next blood meal to be injected back into the skin of the host.

Motility of isolated sporozoites is activated by serum albumin, which induces attachment to the substrate leading to continuous circular movement on flat substrates or helical movement in three-dimensional environments (Kebaier & Vanderberg, 2010; Vanderberg, 1974; Yoeli, 1964). In the skin motility is the most important feature which aids the sporozoite to reach and enter a blood capillary. The curvature of the banana shaped sporozoite is likely adapted to match the shape of the capillaries to ease their invasion (M. J. Muthinja et al., 2017). In *P. berghei* sporozoites shape and invasion relies on 16 microtubules located underneath the IMC. A change in microtubule number and length by modifying α-tubulin strongly influences their formation, motility and infectivity (Spreng et al., 2019). Proteins with a significant impact on gliding motility of sporozoites include for example TLP, S6, PAT, GEST, HSP20, LIMP and TRP1 (Combe et al., 2009; Kehrer, Singer, et al., 2016; Klug & Frischknecht, 2017; Montagna et al., 2012; Santos et al., 2017; Talman et al., 2011).

Intense research is still needed to gain a better understanding regarding active movement of the parasite and to better characterize differences and similarities between ookinetes and sporozoites.

1.6. The TRAP- family of adhesins

The protein TRAP has been the first protein described to have a key function during sporozoite motility and thus salivary gland invasion (Sultan et al., 1997). It is characterized by the presence of a signal peptide (SP), a transmembrane domain (TMD), a thrombospondin type-I repeat (TSR) domain and a von Willebrand factor (vWF)-like A domain at its extracellular portion and an acidic cytoplasmic tail domain (CTD) with a sub-terminal tryptophan residue. The N-terminal SP guides the protein towards its final location, the secretory pathway, whereas the C-terminal TMD embeds the protein into the membrane of micronemes and ultimately the plasma membrane. At the plasma membrane the A domain and TSR domain allow the protein to interact with the substrate for ligand binding.

All proteins containing similar features are grouped into the TRAP- family of adhesins and are differently expressed depending on the life cycle stage. It includes: TRAP, TLP and S6, which are expressed in the sporozoite, CTRP in the ookinete and the protein mTRAP which was until recently considered to be merozoite specific. While TRAP, TLP and CTRP have at least one of the above described domains, mTRAP and S6 are missing an A- domain. MIC2 is the *T. gondii* ortholog of TRAP (Morahan et al., 2009) (Figure 1.5).

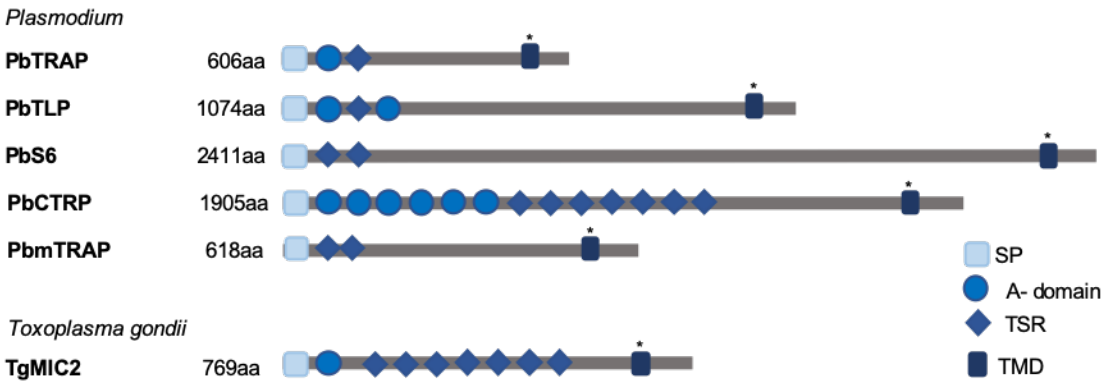

Figure 1.5 The TRAP family of adhesins

Schematic cartoon of the *Plasmodium* TRAP family of adhesins plus its *Toxoplasma gondii* ortholog. Illustrated is the protein length including the different domains within the individual sequences. SP: Signal peptide; TSR: Thrombospondin type-I repeat; TMD: Transmembrane domain. The figure is modified from (Morahan, Wang, and Coppel 2009; Klug and Frischknecht 2017). * indicates rhomboid cleavage side.

The Thrombospondin-related anonymous protein (TRAP)

Within the family, TRAP is the most studied protein. It has been identified in *P. falciparum*, and is conserved among all *Plasmodium* species (Templeton & Kaslow, 1997). The protein is localized in micronemes of the sporozoite and released into the plasma membrane while the parasite moves forward. Along the way, TRAP is translocated to the back and cleaved within its transmembrane domain by a rhomboid protease, which in turn releases parts of the protein onto the substrate (Baker et al., 2006; Ejigiri et al., 2012). Deletion of the complete protein or the modification of the A domain or cytoplasmic tail results in a failure of sporozoites to adhere and thus to invade salivary glands, leading to an interruption of the parasite life cycle (Kappe et al., 1999; Klug et al., 2020; Matuschewski et al., 2002; Sultan et al., 1997; Wengelnik et al., 1999).

TRAP features an acidic CTD which contains a YXXϕ motif at the end of the TMD (Y: tyrosine; X: any amino acid and ϕ: hydrophobic amino acid). In mammalian cells it has been shown that this motif targets proteins to various organelles. In *Plasmodium* the motif is needed to traffic the TRAP protein from the trans Golgi network to micronemes. In parasites having a mutated motif within the C- terminus of TRAP, the protein failed to localize to micronemes resulting in less motile sporozoites (Bhanot et al., 2003; Marks et al., 1997). Exchange of the TRAP C-terminus by the TgMIC2 C-terminus, leaving the suggested sorting motif intact, resulted in motile sporozoites, although a deletion of the respective part showed reduced salivary gland invasion (Kappe et al., 1999).

Besides its importance for salivary gland invasion, TRAP is also needed for liver cell infection. The TSR and the A-domains were shown to particularly interact with heparin sulphate proteoglycans on the hepatocyte surface (McCormick et al., 1999; Müller et al., 1993; Pradel et al., 2002).

The TRAP- like protein (TLP)

Besides a SP and a rhomboid cleavage side containing TMD, TLP possesses one TSR domain and two A- domains. Sporozoites lacking the gene are still motile and productively invade salivary glands of the mosquito. Yet transmission back into naïve mice resulted in a delayed prepatency due to a decreased capacity of sporozoites to traverse and infect hepatocytes (Heiss et al., 2008; Moreira et al., 2008), suggesting a role of the protein for ligand interaction.

The sporozoite protein 6 (S6) or TRAP related protein (TREP)

The protein S6 was identified in a screen in *P. yoelii* parasites with the aim to identify novel sporozoite specific proteins (Kaiser et al., 2004). With its 2411aa it is significantly longer than all other proteins belonging to the Trap family. It lacks an A-domain but contains a SP, 2 TSR domains and a TMD (Morahan et al., 2009). Expression of S6 is highest in midgut oocyst and is reduced in mature salivary gland sporozoites. Parasites lacking the protein execute mainly non-productive motility and are unable to efficiently invade salivary glands. Based on its phenotype and the close relation to TRAP it is also referred to as TRAP related protein (Combe et al., 2009; Steinbuechel & Matuschewski, 2009).

The circumsporozoite- and TRAP-related protein (CTRP)

CTRP is the TRAP family protein which is expressed in ookinetes. Similar to TRAP it contains one SP and one TMD, but 6 A-domains and 7 TSR domains. Immuno- EM localized CTRP in micronemes of ookinetes as well as outside the cell upon midgut traversal, suggesting the release of the protein due to cleavage at its rhomboid cleavage side (Baker et al., 2006; Limviroj et al., 2002; Morahan et al., 2009). Gene disruption resulted in a complete block of parasite transmission to mosquitoes due to immotile ookinetes. While TSR domains are redundant, deletion of only the A-domains mimics the gene deletion phenotype. Injecting ookinetes lacking CTRP into the hemocoel of the mosquito resulted in the formation of infectious sporozoites. (Dessens et al., 1999; Nacer et al., 2008; Ramakrishnan et al., 2011; Templeton et al., 2000; Yuda et al., 1999). Replacement of CTRP by TRAP expressed under a synthetic promoter active in ookinetes and sporozoites resulted in motile ookinetes on glass which were unable to infect mosquitoes (Klug et al., 2018).

The merozoite TRAP-like protein (mTRAP)

mTRAP is the second protein which lacks an A- domain. As S6 it contains a SP, 2 TSR domains and a TMD (Morahan et al., 2009). Studies in *P. falciparum* initially suggested the protein to be essential in blood stages, rendering it impossible to study the gene deletion phenotype in other stages. It localizes to micronemes of merozoites and similar to TRAP in sporozoites is released to the cell surface prior invasion of red blood cells. Moreover, mTRAP contains a rhomboid cleavage side in the transmembrane domain (Baker et al., 2006; Baum et al., 2006).

Surprisingly, in *P. berghei* parasites the protein was identified in a proteomic analysis of the gametocyte egressome and in contrast to *P. falciparum* the generation of a parasite line lacking mTRAP was readily possible. Research has shown that mutant parasites developed normally in the blood, however during gametogenesis both sexes remained trapped inside the RBC und thus life cycle progression into the mosquito was interrupted (Kehrer, Frischknecht, et al., 2016). Bargieri et al confirmed the phenotype in *P. berghei* and also successfully reattempted the gene deletion in *P. falciparum* parasites, illustrating once more the challenges behind generating *P. falciparum* mutant lines. Interestingly, mTRAP did not colocalize with g377 or MDV/ PEG3, known to localize to osmiophilc bodies and secretion of PPLP2 also appeared normal in parasites lacking mTRAP (Bargieri et al., 2016). Whether mTRAP also plays a role in sporozoites will be addressed in future experiments.

The *Toxoplasma gondii* protein MIC2

The gliding motor as described above for *Plasmodium* is conserved across apicomplexan parasites (Baum et al., 2006; Kappe et al., 1999). Among Apicomplexa *T. gondii* is the most widely studied model organism (Kim & Weiss, 2004). The protein TgMIC2 is the ortholog of TRAP and fulfills comparable functions. TgMIC2 contains a SP, one A-domain, 7 TSR domains and one TMD (Morahan et al., 2009). Similar to TRAP, MIC2 is secreted into the plasma membrane of the motile tachyzoite past microneme secretion, translocated to the back and released onto the substrate through cleavage by a rhomboid protease (Brossier et al., 2005). Two unusual tyrosine-containing motifs shortly after the TMD at the C- terminus of the protein are essential for trafficking MIC2 to micronemes (Di Cristina et al., 2000).

1.7. The pantothenic acid transporter PAT

The pantothenic acid transporter (PAT) in *Plasmodium* was initially suggested to be responsible for the uptake of pantothenic acid, also known as vitamin B5, which is an essential nutrient required for the synthesis of coenzyme A (CoA). The protein PAT belongs to the major facilitator superfamily, a group of transporters for solutes such as sugars, protons and small metabolites and characterized through the presence of 10 - 14 TMD (Rédei, 2008). In *Plasmodium,* PAT was identified as one of the proteins downregulated in liver-stage like forms colonizing salivary glands. This suggested the possibility for PAT to play a key role during motility of the parasite or liver cell invasion (Gomes-Santos et al., 2011).

In *P. falciparum* the protein was refractory to deletion while in *P. berghei* it could be deleted and was shown to be essential for parasite transmission into the mosquito. Moreover, in a yeast system PyPAT was able to restore the function of a pantothenic acid transporter and was consequently named PAT (Augagneur et al., 2013; Hart et al., 2014; Kehrer, Singer, et al., 2016; Kenthirapalan et al., 2016). Closer analyses of PAT revealed a dual function of the protein within the life cycle. It is essential for gametocyte egress and sporozoite invasion into salivary glands (Kehrer, Singer, et al., 2016).

In gametocytes PAT colocalizes with the osmiophilic body protein g377 and the protein PPLP2 which is localized in a second subset of egress vesicles. Parasites lacking the protein developed normally in the RBC but failed to establish an infection in the mosquito. Upon activation, micro- and macrogametes were unable to dissolve the PVM and RBCM leading to non-fertile gametes. While osmiophilic bodies and egress vesicles are still formed in this mutant, the parasites failed to secrete their protein content (Kehrer, Singer, et al., 2016).

In sporozoites, PAT concentrates at the apical part of the cell and the parasite plasma membrane and colocalizes with the micronemal protein TRAP. Gametocyte and ookinete specific expression of PAT under the CCP promoter—to overcome gametocyte-egress deficiency—resulted in the formation of sporozoite-filled oocysts. These sporozoites were released into the hemocoel but were unable to efficiently invade salivary glands, reminiscent to the phenotype of parasites lacking TRAP. Indeed, analog to the phenotype in gametocytes, sporozoites were unable to secrete micronemal proteins leading to the lack of TRAP on the parasite surface which is essential for adhesion and thus invasion (Kehrer, Singer, et al., 2016).

Whether PAT also plays a role in ookinetes still remains elusive and will be part of this thesis. In addition, I will functionally characterize the protein in more detail, since it possesses an acidic C- terminus harboring a potential micronemal targeting motif similar to TRAP or MIC2 (Di Cristina et al., 2000).

1.8. Proximity labeling in living cells (BioID)

Immunoprecipitation is commonly used to identify the contents of organellar proteins and protein-protein interactions. However, this method is not effective for detecting proteins with weak interactions, which poses a challenge for understanding complex biological processes. To overcome this limitation, proximity labeling (BioID) can be used to identify cellular components and potential protein interactions. In proximity labeling, a protein or targeting motif that localizes to a specific cell compartment is fused to an enzyme that catalyzes the labeling of proteins in the surrounding area with biotin. This process takes place in living cells. The biotinylated proteins can then be enriched using streptavidin-coated beads and analyzed by mass spectrometry (Roux et al., 2012). Proximity labeling can be mediated by either a biotin ligase (BirA*) or peroxidase (Apex), depending on the experimental design (Lam et al., 2014; Roux et al., 2012). This approach offers a promising alternative to immunoprecipitation for identifying proteins with weak interactions and for gaining insights into complex biological processes.

The promiscuous biotin ligase BirA* from *E. coli* selectively biotinylates free amino groups, such as those found in lysines, at an optimal temperature of 37°C and accumulates biotinylated proteins over 24 hours (Roux et al., 2012). To improve the efficiency of labeling, newer versions of BirA* have been developed, including TurboID, miniTurbo, and MicroID2 (Branon et al., 2018; Johnson et al., 2022). Compared to the original BirA*, TurboID, miniTurbo, and MicroID2 allow for faster proximity labeling within 10 minutes and are active at room temperature. Moreover, miniTurbo and MicroID2 are smaller than BirA* and TurboID, which minimizes interference with bait protein function and localization (Branon et al., 2018; Johnson et al., 2022; Roux et al., 2012).

The peroxidase Apex, isolated from soybean, labels electron-rich amino acids such as tyrosine at a broad range of temperatures. Unlike BirA*, the reaction requires biotin-phenol and activation with H_2O_2, which can be toxic for the cell. The labeling radius is determined by the stability of intermediate products in the reaction. Yet, Apex acts quickly, providing a snapshot of potential protein interactions within 1 minute. In addition to proximity labeling, Apex can be used for localization-specific osmium tetroxide staining and EM imaging in fixed cells. Live cell imaging of the respective protein is possible after adding AmplexRed (Lam et al., 2014; Roux et al., 2012).

For *Plasmodium*, BirA*-mediated BioID was established in our lab to discern the protein composition of egress vesicles in gametocytes. Subsequently, this method has been employed by other researchers to uncover novel components of the parasitophorous vacuolar membrane, the inner membrane complex, the apicoplast, rhoptries, mitochondria, SBP1 mediated protein export, Kelch13, Maurers clefts interaction partners of blood stage parasites, schizogony and the nuclear

pore complex (Ambekar et al., 2022; Anaguano et al., 2023; Birnbaum et al., 2020; Boucher et al., 2018; Geiger et al., 2020; Kehrer, Frischknecht, et al., 2016; Khosh-Naucke et al., 2018; Kimmel et al., 2022; Lamb et al., 2022; Machado et al., 2023; Qian et al., 2022; Sassmannshausen et al., 2023; Schnider et al., 2018; Soares et al., 2021; Wichers et al., 2021) (Figure 1.6). Since the establishment of the classic BirA* system in ookinetes was unsuccessful due to time restrictions of ookinete development and environmental factors, in this thesis Apex mediated biotinylation is used to define the vesicle content of ookinete micronemes.

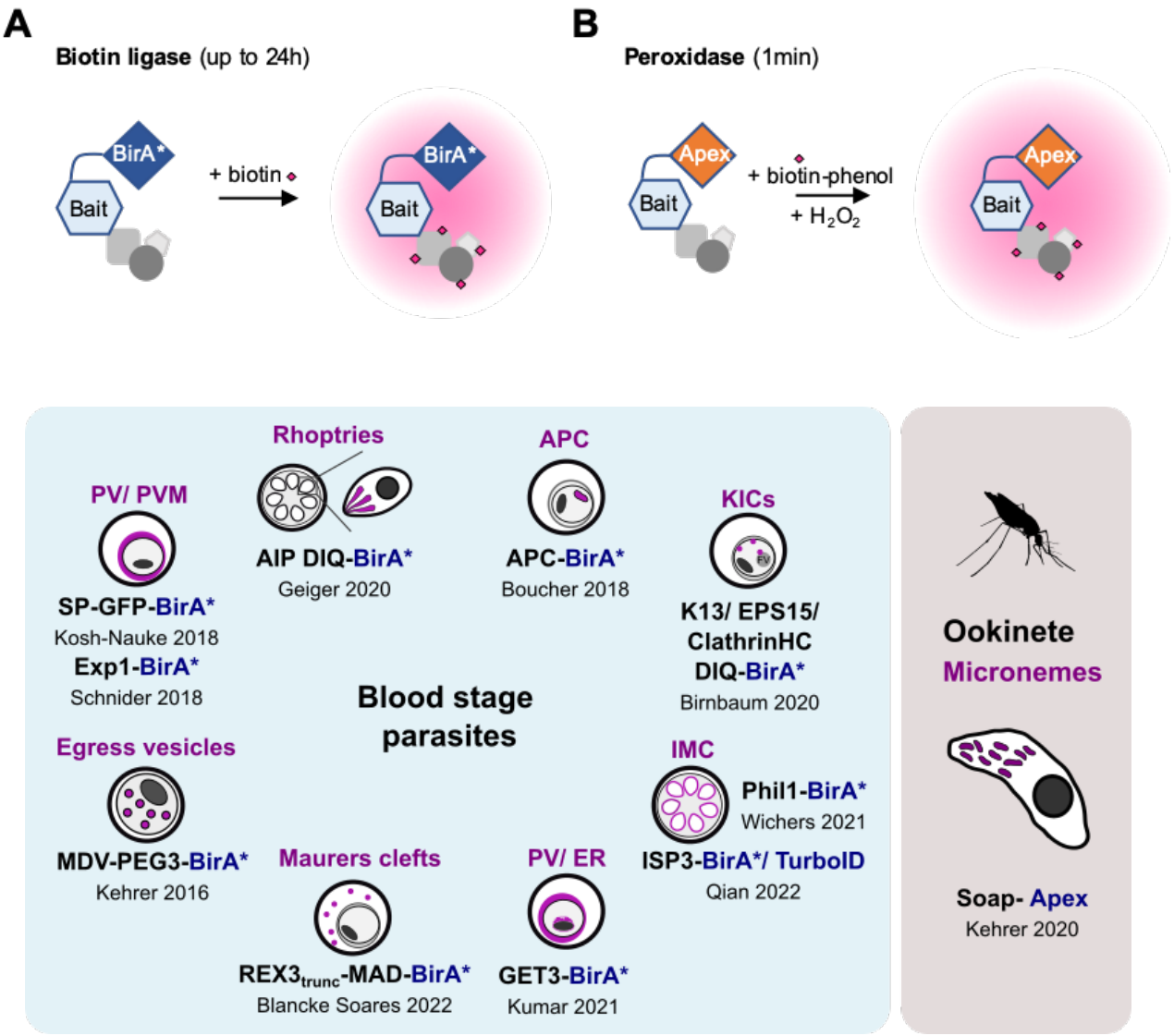

Figure 1.6 BioID approaches in *Plasmodium*

(A) Schematic illustration of biotin ligase-based proximity labeling before and after biotinylation of neighboring proteins. Biotinylation of proteins requires the presence of biotin during a period of up to 24h. **(B)** Schematic illustration of peroxidase-based proximity labeling before and after biotinylation of neighboring proteins. Biotinylation of proteins takes place within 1 min upon the activation of biotin phenol with hydrogen peroxide (H_2O_2). **(C)** Shown is an overview of biotinylation approaches in *Plasmodium* blood-stage parasites (left) as well as ookinetes (right). Respective organelles are highlighted in magenta. This figure is partly taken from (Kimmel et al., 2022).

2 AIMS OF THE THESES

Life cycle progression of the malaria parasite *Plasmodium* spp. relies on the gliding motility of two motile stages, ookinetes and sporozoites. Ookinetes require motility to penetrate the midgut epithelium, where they initiate an infection at the gut wall, leading to the development of numerous sporozoites. Sporozoites, in turn, depend on motility to exit oocysts, infiltrate mosquito salivary glands, and to actively move through the skin of the host to locate a blood vessel. For movement inside the mosquito as well as the host, the parasite possesses a unique type of locomotion, based on an actin-myosin motor which is connected to the substrate via surface adhesins. Substrate adhesion and motility rely on the discharge of proteins at the apical end from specialized organelles called micronemes.

The aim of my theses was to identify and characterize hitherto unknown proteins resident in micronemes to get a better understanding how the parasite is able to achieve forward movement at a speed 10x times faster than the fastest cell in the human body. To define the content of secretory organelles I have used proximity-dependent biotinylation within micronemes of ookinetes and collection of secreted proteins of sporozoites followed by mass spectrometry analyses using the rodent infecting parasite *Plasmodium berghei*. From both proteomic screens I then selected the most promising candidates (akratin and concavin) for further characterization. Detailed analyses of akratin showed a dual function of the protein in gametocytes and ookinetes based on a C- terminal tyrosin containing motif. I also found a similar motif in the C- terminus of the pantothenic acid transporter PAT which then led to a further characterization of PAT.
In an additional project, I also aimed on developing a method to enable *Plasmodium* blood stage whole cell STED nanoscopy, which was shown to be challenging due to the high light absorbing capacity of the hemozoin crystals leading to cell damage.

-

3 RESULTS

3.1. Identification of unknown micronemal proteins

Proximity labeling (BioID) of micronemes in Ookinetes

The discharge of proteins from specialized secretory vesicles called micronemes is essential for life cycle progression of *plasmodium* parasites through the mosquito vector (Carruthers & Sibley, 1999; Kehrer, Singer, et al., 2016). In ookinetes and sporozoites micronemes accumulate at the apical side of the cell and contribute to adhesion and motility. To identify hitherto unknown proteins localized within micronemes of ookinetes, I used the well characterized microneme resident protein SOAP (Secreted Ookinete Adhesive Protein) as bait for proximity labeling of neighboring proteins. SOAP (PBANKA_1113400) consists of 166 amino acids with a molecular weight of around 21 kDa and is important for ookinete to oocyst transition in the mosquito midgut (Dessens et al., 2003).

Ookinetes mature at a temperature of around 21°C and biotinylation of proteins is restricted to a short period of time, since they only need 20- 24 hours to fully develop. Optimal conditions for BirA* mediated proximity labeling however requires 37°C over a period of around 24 h and therefore I generated a parasite line containing the faster acting peroxidase Apex2, instead of BirA* (Lam et al., 2014).

The experimental approach was done in analogy to our previous BioID screen in gametocytes (Kehrer, Frischknecht, et al., 2016). In short, a plasmid containing SOAP fused to a '3x myc' tag and Apex2 at the C-terminus together with a resistance cassette, was integrated into the endogenous locus of wild type *P. berghei* (strain Anka) parasites via single homologous recombination. Successful transfection was tested by PCR probing for correct 5`and 3` integration (see section 5.3, Material and Methods). Using the resulting SOAP-Apex2-myc parasites in parallel to wild type, I first incubated fully mature and purified ookinetes with biotin-phenol (182 µg/ ml) for 30 min at room temperature. I next split the cell suspension into two separate populations and initiated biotinylation with a final concentration of 10 mM H_2O_2 in one vial, while the second vial served as control. Biotinylation was terminated after 1 min by the addition of a quencher solution containing sodium ascorbate and trolox. Lastly, I enriched biotinylated proteins with streptavidin coated agarose beads and tested for successful labeling of proteins by western blot and mass-spectrometry analyses (Figure 3.1.1 A). In western blot analyses, before (input) and

after enrichment (IP) of proteins, I observed a strong signal for biotinylated proteins in SOAP-Apex2-myc parasites in the presence of H_2O_2, while the control sample remained negative. The protein HSP70 served as loading control for mutant and wt parasites and an anti-myc antibody was used to confirm the presence of Soap-Apex2-myc. Both signals were detected at around 70 and 50 kDa respectively. Since HSP70 is not localized to micronemes and thus not biotinylated the signal is absent after enrichment (Figure 3.1.1 B).

To obtain high ookinete numbers with little blood-stage contamination, as needed for efficient enrichment of biotinylated proteins, blood-stage parasites are generally grown in mice treated with phenylhydrazin and sulfadiazine prior ookinete culture. However, this generates a high background autofluorescence signal within the cells, caused by the drugs, when observed under the microscope. Due to this and the fact that immunolabeling of ookinetes with the anti-myc antibody appeared challenging I additionally generated a parasite line with SOAP fused to mCherry in analogy to the generation of SOAP-Apex2-myc parasites (see section 5.3, Material and Methods). The protein size of mCherry is comparable to APEX2 and allows easier observation of the correct localization of SOAP when expressed as a fusion protein. As expected, the expression of SOAP-mCherry resulted in a vesicular staining within the ookinete, as described previously (Figure 3.1.1 C) (Dessens et al., 2003).

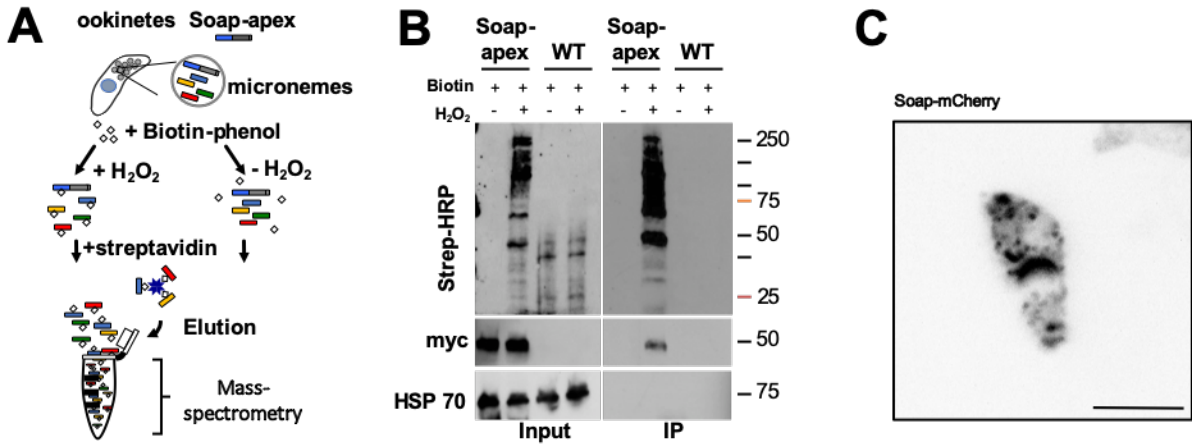

Figure 3.1.1 Apex2 based proximity labeling in ookinetes

(A) Cartoon of the experimental approach to identify micronemal proteins using APEX2 based proximity labeling. Purified ookinetes were incubated with biotin- phenol and biotinylation was initiated with H_2O_2. Biotinylated proteins were enriched using streptavidin coated beads and analyzed via Mass- spectrometry. **(B)** Western blot showing successful protein labeling with biotin of Soap-Apex2 parasites compared to WT in the presence and absence of H_2O_2 (left) and the successful enrichment of biotinylated proteins with streptavidin coated beads (right). Anti-myc and anti HSP70 detection was used as loading control. **(C)** Ookinete expressing Soap-mCherry showing vesicular localization of the protein despite the tag. Figure modified from (Kehrer et al., 2020).

In two separate experiments, I successfully identified a total of 143 proteins. Among these, 78 proteins were consistently detected in both experiments. (Figure 3.1.2 A and Appendix for complete list). Notably, 62 proteins of the 143 hits are likely not micronemal, such as the cytoskeletal proteins actin and tubulin. Furthermore, ribosomal and Golgi resident proteins as well as proteins belonging to the secretory pathway are possible contaminants. This yielded a list of 81 likely microneme-resident proteins of ookinetes for which at least 2 peptides were found in the two mass-spectrometry runs (Figure 3.1.2 B).

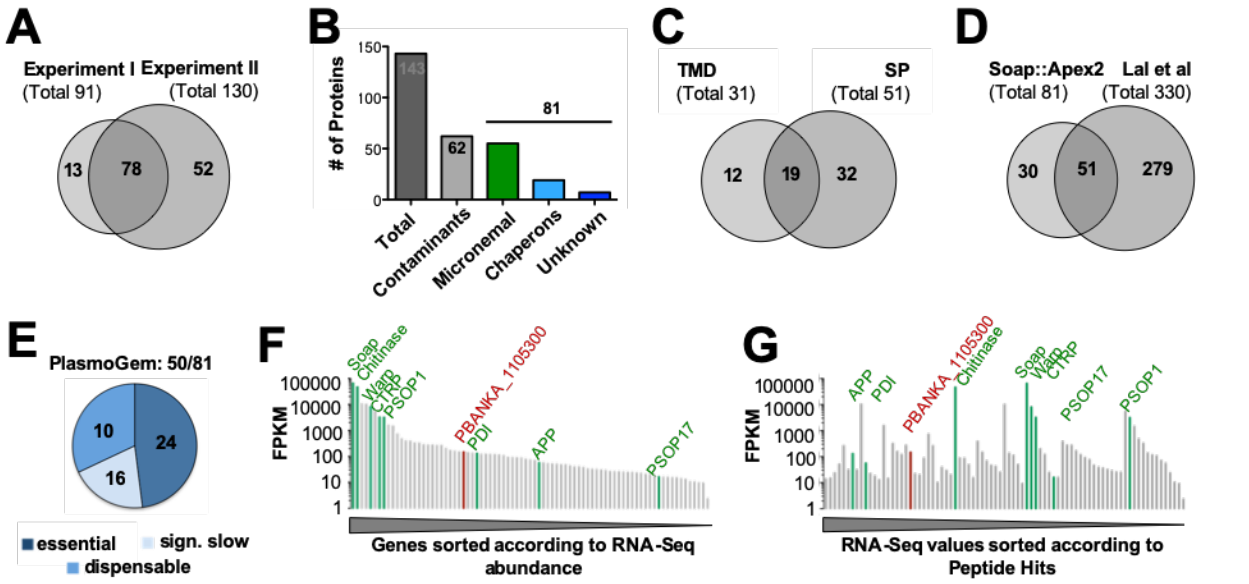

Figure 3.1.2 Analyses of identified proteins within the BioID screen

(A) Comparison of identified proteins in 2 independent mass- spec experiments. **(B)** 143 identified total proteins classified into contaminant, micronemal proteins, chaperons and proteins with unknown function. **(C)** Detected potential micronemal proteins containing either a TMD or SP or both. **(D)** Comparison of the detected proteins with the previous study by Lal et al. **(E)** Proteins sorted according to their growth rates in the PlasmoGem screen. **(F)** Genes sorted according to their RNA- Seq abundance. Known proteins are highlighted in green. Most promising candidate in red. **(G)** RNA- Seq data sorted according to peptide hits. Known proteins are highlighted in green. Most promising candidate in red. Figure modified from (Kehrer et al., 2020).

Among these proteins I could successfully detect the previously described micronemal proteins CTRP, WARP, SOAP, Chitinase, PSOP17, PSOP1, aminopeptidase (APP) and protein disulfide isomerase (PDI) (Dessens et al., 1999, 2001, 2003; Ecker et al., 2008; Lal, Prieto, et al., 2009; Yuda et al., 1999). I furthermore identified 19 chaperones and 7 conserved *Plasmodium* proteins with unknown function, which I include into the category of probable micronemal candidates (Figure 3.1.2 B).

Detected proteins with more than 20 peptide hits I considered as the highest scoring candidates. These 20 proteins include 15 known micronemal proteins, 4 chaperones and only one potential contaminant (alpha tubulin 2). For the three most abundant proteins (CCp1, CCp3, CCp5), I identified 99, 104, and 135 peptide hits, respectively. Intriguingly, all top three hits belong to the LCCL domain-containing protein family (CCp/Lap). (Saeed et al., 2010). Detected proteins with 5 to 20 peptide hits contained 54 proteins. However, this group already includes 52% of likely false positive candidates and 4 chaperones. 69 proteins counted only 2-4 peptide hits. Within this group I counted a similar amount of contaminants (48%), however the number of chaperones increased to 11. Yet, even in this fraction I detected known or likely micronemal proteins such as PSOP1 (Ecker et al., 2008) and the ookinete surface protein p25 (Tomas et al., 2001).

Excluding probable contaminants, 51 of 81 proteins contained an N- terminal signal peptide (SP), 31 had at least one transmembrane domain (TMD) and 19 proteins featured both. Only 18 proteins do not have any detectable domain (Figure 3.1.2 C). Comparing the group of 81 proteins with previous data presented by Lal et al. (330 proteins in total; but many of these were obvious contaminants) I found 51 already identified proteins but also 30 novel candidates (Figure 3.1.2 D).

Searching for proteins present in the PlasmoGem database ((Schwach et al., 2015); plasmogem.org) I found information for 50 of the 81 proteins. Of those, 24 proteins are reported to be essential for blood stage development. 16 of the proteins are reported to grow significantly slower, while 10 are reported to be dispensable (Figure 3.1.2 E). Comparing the list of candidates to the published total sporozoite and sporozoite surface proteins (Lindner, Swearingen, et al., 2013) shows that 49 of the 81 potential ookinete micronemal proteins are also present in sporozoites and hence eventually have a potential dual function in ookinetes as well as sporozoites. Furthermore, I obtained ookinete RNA Seq data of the 81 probable micronemal candidate proteins (Otto et al., 2014) and sorted them according to the number of peptide hits per protein or total RNA- Seq abundance. Known micronemal proteins are highlighted in green and contaminants are shown in grey (Figure 3.1.2 F,G). Although CTRP, SOAP, WARP, Chitinase, and PSOP1 are identified as the most abundant proteins based on RNA-Seq data, it's surprising that these proteins do not emerge as top candidates when sorted according to the number of peptide hits.

Among the identified candidates I selected PbANKA_1105300 (highlighted in red) as the top candidate for further characterization as part of this theses. The protein contains a SP and 4 TMD and is thus a promising candidate to probe for motility.

Proximity labeling does not work in sporozoites

In parallel to the identification of the microneme content in ookinetes I also attempted a similar approach in sporozoites. Since the protein Soap is only expressed in ookinetes, for sporozoites I have used the micronemal protein TRAP as bait. I have used two different parasite lines, TRAP fused to BirA*-myc (SS-BirA*-myc-TRAP) and TRAP fused to APEX2-myc (SS-APEX2-myc-TRAP) with the tags inserted at the N- terminus after the signal peptide. This site was chosen, as the insertion of a GFP after the signal peptide of TRAP has already been shown to work (Kehrer, Singer, et al., 2016). While SS-BirA*-myc-TRAP parasites have been kindly provided by Gunnar Mair (unpublished data), SS-APEX2-myc-TRAP parasites were generated as part of this theses (see section 5.3, Material and Methods). In case of SS-BirA*-myc-TRAP, biotin was supplied in salt and sugar pads used to feed the mosquitoes while for SS-APEX2-myc-TRAP parasites, mature salivary gland sporozoites were isolated and incubated on ice in PBS containing biotin-phenol. Biotinylation was initiated as described above, by adding H_2O_2 for 1min. Western blot analysis of 100 000 sporozoites to probe for biotinylated proteins of both parasite lines showed an identical band pattern in wt and the control (data not shown). Therefore, I concluded that either the fusion protein is not functional or biotinylation is not successful. To test for the correct expression and protein abundance I then stained isolated sporozoites expressing SS-BirA*-myc-TRAP with an anti-myc antibody and fluorescent streptavidin. While the anti-myc signal showed correct labeling as seen for anti-TRAP stainings (Kehrer, Singer, et al., 2016; Klug et al., 2020), it surprisingly resulted in readily stained sporozoites with streptavidin even in wt parasites not expressing biotin ligase (Figure 3.1.3). To this end proximity labeling in sporozoites is difficult due to the high unspecific background staining.

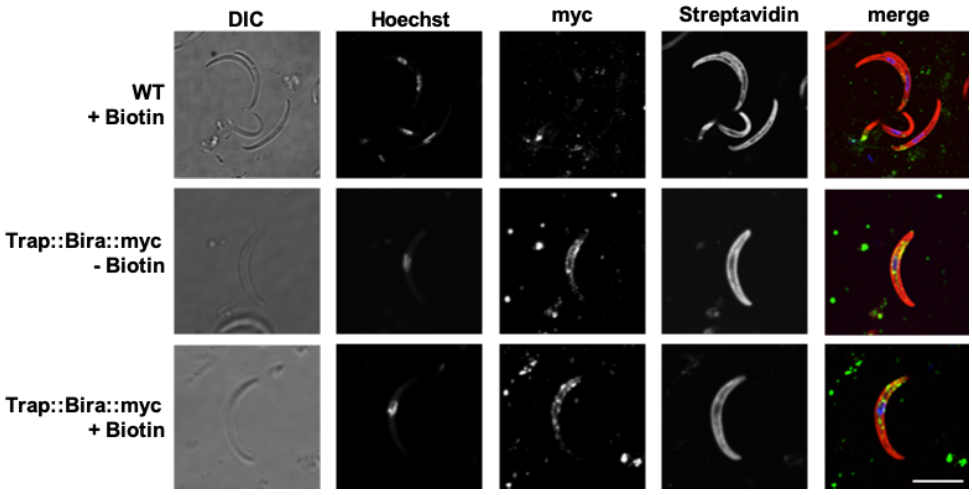

Figure 3.1.3 BioID does not work in sporozoites

Exemplary images of wt and SS-BirA*-myc-TRAP sporozoites in the presence and absence of biotin. In wt sporozoites (top row) the myc signal is absent however an unspecific signal of fluorescent streptavidin is visible. In SS-BirA*-myc-TRAP there is a clear myc signal reminiscent of the localization of TRAP and a Streptavidin signal could be detected irrespective of the presence of biotin.

The sporozoite secretome

As an alternative to identifying micronemal proteins using BioID I attempted to detect secreted proteins by the sporozoite. The motility of sporozoites is typically activated by albumin which triggers a calcium-dependent activation of the gliding machinery and the release of microneme contents such as TRAP (Carey et al., 2014; Carruthers & Sibley, 1999; Vanderberg, 1974). However, excessive amounts of albumin would make it impossible to detect low levels of secreted proteins in the supernatant. Therefore, I implemented a gliding assay to quantify sporozoite movement using pluronic acid (PA), known to stimulate calcium influx into cells (Granados, Soriano, and Saavedra-Molina 1997). Sporozoites activated with a concentration of 0.1% PA in RPMI medium at room temperature already showed around 30% of moving cells. Yet, after the activation with 0.5% PA/ RPMI, approximately 50% of sporozoites exhibited productive movement on glass (Figure 3.1.4 A). Although it was slightly lower than the movement observed in the presence of 3% BSA in RPMI, I considered it sufficient enough to proceed to the next step. To test for secreted proteins, I collected 100 000 sporozoites expressing SS-GFP-Trap as a marker, in a 1,5 ml tube and activated them with PA. After 30 min of activation, I pelleted the parasites and collected the supernatant. Successful protein secretion was assessed by performing a western blot using an anti-TRAP antibody. A prominent signal was detected in the activated sample compared to the non-activated control (Kehrer et al. 2016) and therefore I used the supernatant for the detection of secreted proteins via mass- spectrometry (Figure 3.1.4 B).

In MS analyses of three independent experiments I could detect a total of 161 proteins. Of these 161 proteins 36 proteins were identified in all three samples and an additional 34 proteins were present in at least two samples (Figure 3.1.5 C). Proteins detected in only one experiment were considered as potential contaminants even though I found known secreted proteins such as SERA5 and SPECT among them. Within the 70 proteins detected in at least 2 samples we identified SIAP1, TRAP, GAMA, CSP, 14-3-3, GEST and CELTOS. All known to play a role during sporozoite motility and cell traversal.

To uncover the functional significance of the identified protein hits I performed Gene Ontology (GO) term analyses using plasmodb.org. This analysis aimed to gain further insights into the enriched cellular components. GO term analyses is a widely used method in bioinformatics and genomics research which involves the systematic classification and annotation of genes and gene products based on their functional attributes. Go term analyses of all 161 detected proteins revealed a total of 41 different cellular components. Among these, the most abundant group was the cytoplasm. However proteins classified as apical part of the cell, apical complex, micronemes and cell surface with a great potential to be secreted during sporozoite movement appear within the top ten enriched cellular components (Figure 3.1.4 D).

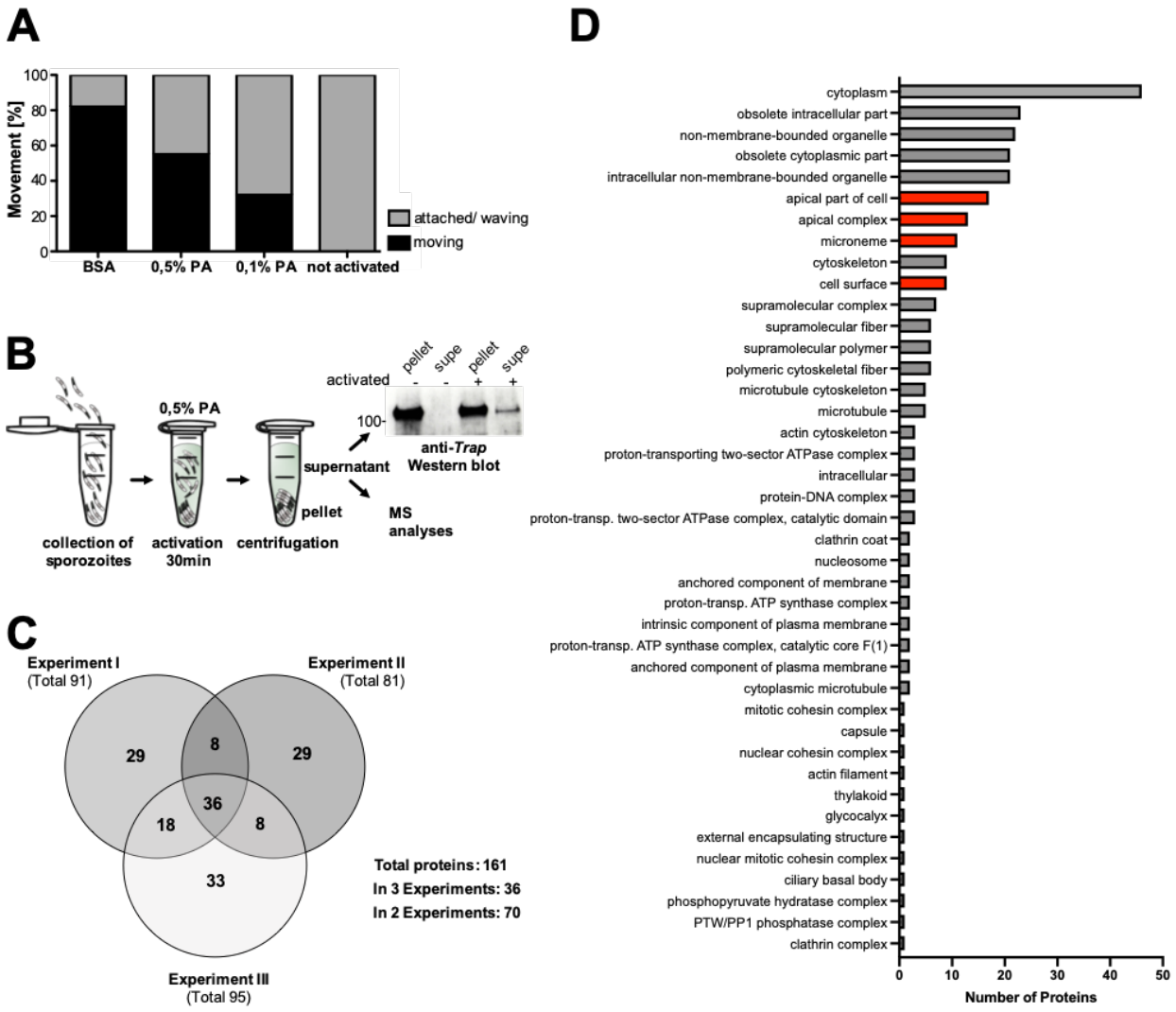

Figure 3.1.4 Sporozoite secretion in the presence of pluronic acid

(A) Motility of sporozoites on glass, activated with different concentrations of pluronic acid compared to 3% BSA in RPMI medium. **(B)** Experimental Setup for sporozoite activation and protein secretion used for MS analyses. To test for secreted proteins, parasites expressing GFP at the N- terminus of TRAP were used. **(C)** Overview of mass-spectrometry analyses. Of total of 161 identified proteins, 36 proteins were detected in 3 experiments while 70 proteins were present in 2 experiments. Yet 4 known proteins could only be detected in 1 experiment. **(D)** Go term enrichment analyses for cellular components. In red components potentially involved in motility are highlighted. A and B partly adapted from (Kehrer et al. 2016). C taken from (Kehrer et al., 2020)

Further analyses showed that 92 of the 161 total proteins identified in the secretome were also detected in the previously described *P. yoelii* total sporozoite proteome (Figure 3.1.5 B) (Lindner, Swearingen, et al., 2013). 21 proteins contain a SP and 32 proteins contain at least one TMD. Among those 11 proteins were annotated to have both (Figure 3.1.5 B). 97 proteins were present in the PlasmoGem gene deletion screen (Bushell et al., 2017). Within this screen 55 proteins were reported to be essential for blood stage development. Gene deletion of 13 candidates resulted in a significant growth defect and 29 proteins are dispensable in the blood (Figure 3.1.5 C).

I found orthologs in *P. yoelii* parasites for 160 of 161 proteins, obtained their RNA seq values in sporozoites (plasmodb.org) and plotted them according to the number of identified peptides found in our mass spec results (Table S1). Highlighted in these graphs are also the proteins known to be secreted by the parasite. Within the 36 proteins detected in all three experiments we found the known secreted proteins SIAP, TRAP, CSP, GAMA and GEST (Figure 3.1.5 D). In the dataset of proteins present in two samples we additionally found the secreted proteins AMA1, CELTOS, ROP, CRMP3, MA and PLP2 (Figure 3.1.5 E). PBANKA_1422900, here named concavin due to the observed phenotype of the deletion parasite, was the first conserved protein with unknown function with the most peptide hits (Figure 3.1.5 E highlighted in red). I detected concavin in two out of three experiments and decided to select this candidate protein for further analyses.

Even in the group of proteins detected in only one sample I found known secreted proteins such as UIS2, SERA5, PLP1 and SPECT (Figure 3.1.5 F). Like with all subcellular proteomic approaches I also detected a large number of likely false positives i.e. known or expected non-secreted proteins, e.g. ribosomal or cytoskeletal proteins.

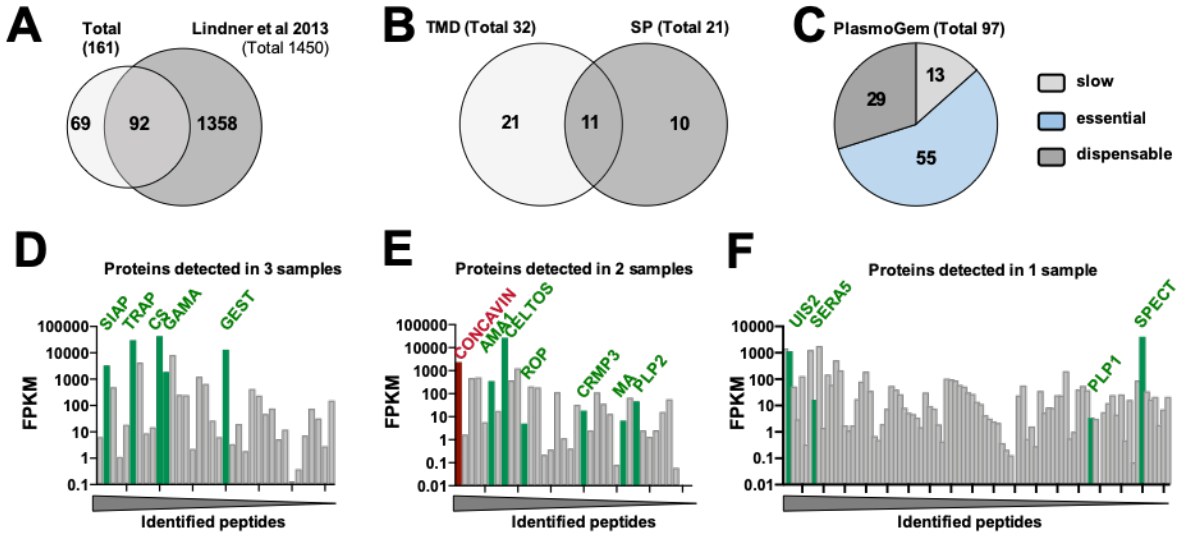

Figure 3.1.5 Mass- spec analyses of the sporozoite secretome

(A) Secretome comparison with the *P. yoelii* total sporozoite proteome. 92 of the proteins identified in the secretome were also found in the total sporozoite proteome (Lindner, Swearingen, et al., 2013). **(B)** 32 identified candidate proteins contained at least one trans-membrane domain (TMD) and 21 a signal peptide (SP), 11 contained both. **(C)** 97 candidate proteins were already investigated by the PlasmoGEM screen (Bushell et al., 2017). Within the screen 55 were classified as essential, 13 as slow growing and 29 as dispensable. **(D-F)** Identified proteins listed by RNA seq. abundance depending on their experimental appearance (Otto et al., 2014). Known micronemal/ secreted proteins are indicated in green and our top candidate in red. Figure modified from (Kehrer et al., 2020).

Discussion

I employed proximity labeling of micronemes in ookinetes using the peroxidase Apex2 fused to the protein SOAP, to define the vesicular protein content. Through mass spectrometry, I identified several widely recognized micronemal proteins such as CTRP, WARP, SOAP, Chitinase, and PSOP1, as well as previously unknown candidates. Proximity labeling is a powerful technique for identifying proteins in specific complexes or cellular compartments, including vesicles, and for identifying potential protein-protein interaction partners. However, this method has some limitations depending on the approach used. For example, BirA* is unsuitable for ookinetes since the ligase is inactive below 37°C, and the labeling speed exceeds the cell development time. In my study, I used the faster Apex2 approach, which yielded successful results. Alternatively, TurboID and miniTurbo (Branon et al., 2018) are also available, which are based on an optimized BirA* ligase.

However, unspecific labeling of proteins due to the natural presence of biotin ligases should be considered. For blood-stage parasites, this can be neglected as *Plasmodium* spp. contain only two biotin ligases and a single Acetyl-CoA carboxylase (ACC) as the only predicted biotinylated protein, which is localized to the apicoplast and essential only in liver-stage parasites (Dellibovi-Ragheb et al., 2018).

In multicellular organisms, including insects, natural biotinylation is facilitated by several biotin ligases. In mosquito-derived wild-type sporozoites, I observed strong unspecific surface labeling of sporozoites with fluorescent streptavidin in the presence of biotin. This phenomenon may be due to mosquito-derived enzymes and renders BirA*- or Apex2-based labeling quite challenging in salivary gland sporozoites (Figure 3.1.3).

The initial approach to identify proteins localized in TRAP-containing vesicles using proximity labeling did not result in any promising protein hits. Therefore, I have established an assay based on the activation of sporozoites with pluronic acid with the aim to identify secreted (potentially micronemal) proteins. To this end I collected the supernatant of stimulated sporozoites and performed proteomic analysis. This revealed most known secreted proteins such as SIAP, TRAP, CSP, GAMA and GEST AMA1, CELTOS, ROP, CRMP3, MA PLP2 UIS2, SERA5, PLP1 and SPECT, but also additional promising and likely false positive candidates (Figure 3.1.5; Appendix 9.2). Due to the experimental design, the list does not exclusively contain micronemal proteins but also proteins secreted via rhoptries and proteins shed from the membrane. Potential promising protein candidates contained in the list and will be investigated in future experiments. One of the candidates, named concavin, will be characterized in more detail in section 3.4.

3.2. Functional characterization of PbANKA_1105300

To investigate if the BioID results revealed proteins with an essential function during life cycle progression, I focused on the protein exhibiting the highest numbers of peptide hits containing a SP and four TMDs for further investigation. This protein, PbANKA_1105300, consists of 455 aa and holds a tyrosine containing motif at the C- terminus. Intriguingly, PbANKA_1105300 did not appear in my previous BioID screen from gametocytes, remained unexplored by PlasmoGEM and was absent in the study by Lal et al (Schwach et al. 2015; Lal et al. 2009; Kehrer, Frischknecht, and Mair 2016).

Using BlastP, I found PbANKA_1105300 to be conserved among *Plasmodium* spp.. It showcases an 82% identity with its ortholog in *P. yoelii*, while demonstrating only 35% and 32% with the respective orthologs in *P. falciparum* and *P. vivax*, respectively (Figure 3.2.1 A). Exploring the comparing protein features across these *Plasmodium* strains they all feature a SP. However, the count of TMDs vary. *P. berghei* and *P. falciparum* both have 4 TMDs each, whereas *P. yoelii* and *P. vivax* only have 2 (Figure 3.2.1 A). Notably, the *P. falciparum* ortholog stands out, being almost twice the length as its counterparts. Outside the *Plasmodium* spp. domain, no ortholog was discerned. The predicted protein structure for PbANKA_1105300 obtained via Alphafold2 is mainly composed of alpha helices and interspersed with short sequences of unstructured regions. The proposed localization of TMDs are illustrated in blue, the SP in light blue and the tyrosine containing motif in red (Figure 3.2.1 B).

RNA-Seq data of the protein across the lifecycle stages shows a clear peak in fully developed ookinetes in comparison to blood stage parasites and sporozoites (Figure 3.2.1 C). Further analyses of gametocyte RNA-Seq data, segregated by sex, indicates that male gametocytes exhibit approximately 50% higher expression levels (Lindner et al. 2013; Otto et al. 2014) Yeoh et al 2017) (Figure 3.2.1 D).

Predictive algorithms, such as DeepLoc (www.cbs.dtu.dk/services/DeepLoc-1.0/) play a crucial role in forecasting the subcellular localization of proteins (Almagro Armenteros et al. 2017). The model employs neural networks trained and tested on datasets sourced from Uniprot (www.uniprot.org). Utilizing DeepLoc, the protein PbANKA_1105300 is predicted to localize to membranes with a high probability of 98% (Figure 3.2.1. E) aligning well with its possession of four predicted TMDs. The suggested hierarchical tree proposes that the protein enters the secretory pathway with a probability of 58%, traversing most probably through the ER/ Golgi network with the final destination of ER membranes (Figure 3.2.1 F).

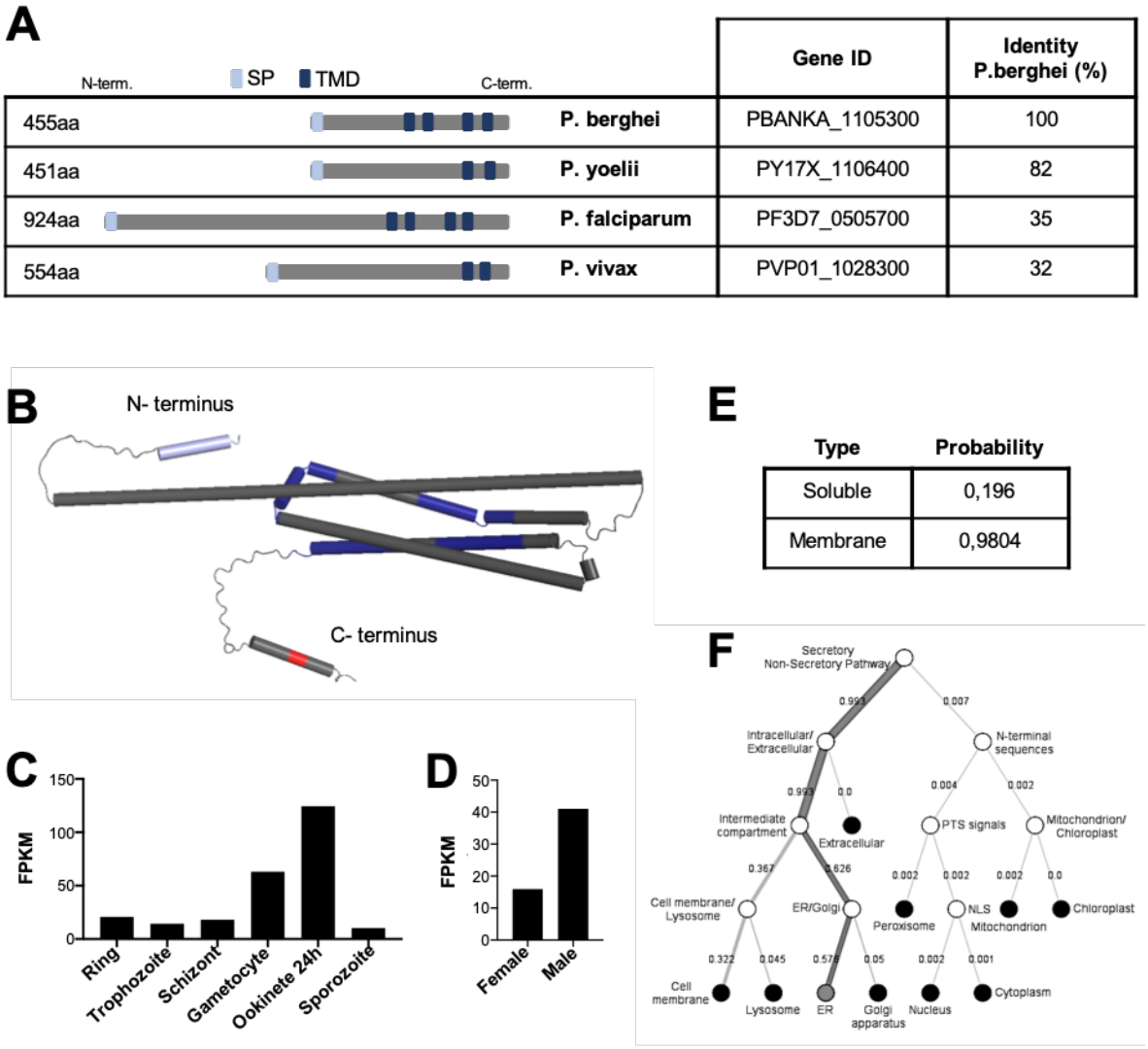

Figure 3.2.1 PBANKA_1105300 is conserved and shows peak expression in ookinetes

(A) Comparison of protein sequences from protein length to sequence identity in 4 *Plasmodium* species. Signal peptides and Transmembrane domains are shaded in blue. While Pb and Pf both have 4TMDs, Py and Pv have only 2. **(B)** Structure prediction obtained from Alphafold2 and color coded using Pymol. SP. And TMD are highlighted in blue whereas an essential motif (EYKK) is shown in red. **(C)** Transcriptome data of PBANKA_1105300 in the different life cycle stages shows peak expression in ookinetes (Otto et al 2014; Lindner et al 2013). **(D)** Gametocyte transcriptome data shows higher expression in males compared to females (Yeoh et al 2017). **(E)** Probability for the localization of the protein to membranes. **(F)** The DeepLoc decision tree proposes a localization to the ER membrane. Figure partly taken from (Kehrer et al., 2020).

PbANKA_1105300 (-) parasites fail to transmit to mosquitoes

To characterize the function of PbANKA_1105300 in detail, I generated a parasite line in the *P. berghei* background, lacking the gene by replacing the complete open reading frame (ORF) against a selection cassette containing the recyclable yFCU/ hDHFR selection cassette combined with GFP expressed under the HSP70 promoter. This not only allows the enrichment of the desired parasite line but also enables the option of fluorescent activated cell sorting (FACS) to obtain

clonal parasites (Material and Methods). The resulting PbANKA_1105300(-) parasite line showed a slightly reduced multiplication rate in the blood. While wild type parasites usually develop with a growth rate around 10, the growth rate for the mutant parasites decreased to around 7 (Figure 3.2.2 A). However more strikingly, infection of mosquitoes did not result in any oocysts. Thus transmission of the parasites from the mouse to the mosquito was completely blocked.

Closer analysis of the gene deletion phenotype showed morphologically normal gametocytes but only few exflagellating microgametes in comparison to the wild type. This slightly increased after treatment of mice with phenylhydrazin, a drug that destroys mature RBCs, leading to the production of more reticulocytes which are preferentially invaded by the parasites (Figure 3.2.2 B). Performing *in vitro* ookinete cultures therefore led to only a low amount of ookinetes. Although in the wild type we got gametocyte to ookinete conversion rates of around 40% it was reduced to 3% in our PbANKA_1105300(-) parasites (Figure 3.2.2 C). Gliding assays using these ookinetes furthermore showed a reduction in speed of about 50%. While wild type ookinetes generally moved with an average speed of 6 µm/ min the mutant showed an average speed of 3 µm/ min (Figure 3.2.2 D). Combined, these data suggested not only a function in gametocytes but also during motility of ookinetes.

For this reason, it was not surprising, that parasites lacking PbANKA_1105300 were unable to cause an efficient infection in the mosquito vector. In most of the infected midguts I did not observe any oocysts while in a small proportion of midguts I counted less than 10 oocysts (Figure 3.2.2 E). Wild type infections in contrast resulted in up to 600 oocysts per midgut (Figure 3.2.2 E).

The ortholog of *P. falciparum* is able to rescue the KO phenotype

To eliminate the possibility of a phenotype caused by off-target effects I subsequently generated two independent parasite lines complementing the deleted gene with a GFP-tagged version of *P. berghei* or the *P. falciparum* ortholog (PF3D7_0505700) before exploring the observed gene deletion phenotype in more detail.

To achieve this, I first recycled the selection cassette through negative selection with 5-FC followed by the insertion of the respective gene into the selection marker free parasites. This resulted in the creation of parasite lines Akratin(-)$^{\text{PbAkratin-GFP}}$ as well as Akratin(-)$^{\text{PfAkratin-GFP}}$ (see Methods). Both parasite lines were able to rescue the transmission block of the parasites lacking the gene. The oocyst and sporozoite numbers as well as infection rates of midgut and salivary gland sporozoites were in the wild type range (Figure 3.2.2 F-H), indicating that the observed phenotype in akratin(-) parasites is indeed due to the lack of the protein.

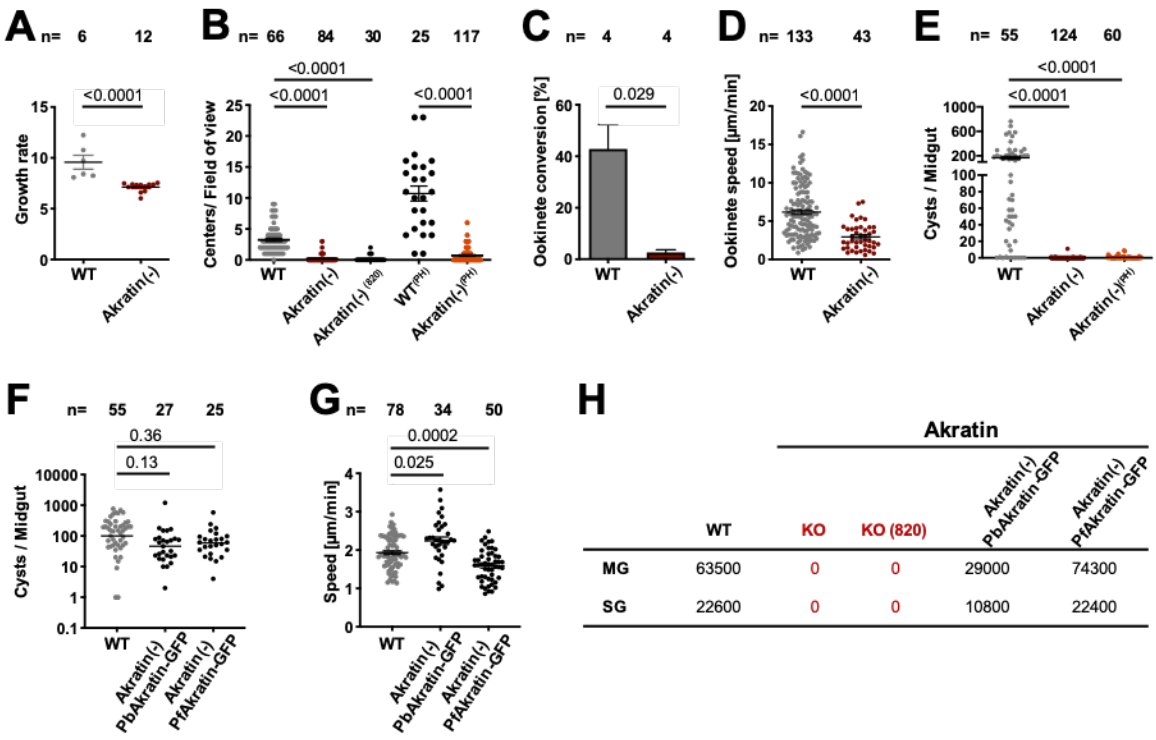

Figure 3.2.2 ***Akratin(-)* parasites are unable to establish mosquito infections.**

(A) Blood stage multiplication rate of *akratin(-)* parasites in comparison to wild type. Data points represent parasites growing in individual mice. P-values calculated by Mann Whitney test. Horizontal bars indicate mean ± SEM. **(B)** Exflagellation of microgametes in the presence and absence of phenylhydrazin (PH) is nearly absent in *akratin(-)* parasites. P-values calculated using the Kruskal Wallis Test with Dunns multiple comparison. Horizontal bars indicate mean ± SEM. **(C)** Ookinete conversion rate of *akratin(-)* parasites in comparison to wild type. P-values calculated by Mann Whitney test. **(D)** Speed of gliding *akratin(-)* and wild type (WT) ookinetes. P-values calculated by Mann Whitney test. Horizontal bars indicate mean ± SEM. **(E)** Oocysts numbers in isolated *Anopheles stephensi* mosquito midguts infected with wild type (WT) or *akratin(-)* parasites in the presence of phenylhydrazin (PH). Data points represent individual midguts observed between d12-17 post infection. P-values calculated using the Kruskal Wallis Test with Dunns multiple comparison. Horizontal bars indicate mean ± SEM. **(F)** Oocysts numbers in isolated *Anopheles stephensi* mosquito midguts infected with *Akratin(-)*$^{PbAkratin\text{-}GFP}$ *as well as Akratin(-)*$^{PfAkratin\text{-}GFP}$parasites. Data points represent individual midguts observed between d12-17 post infection. Horizontal line shows median. P-values are calculated using the Kruskal Wallis test followed by the Dunns multiple comparison test. **(G)** Speed of salivary gland sporozoites imaged with a frame rate of 3 seconds. Data points represent average speed of individual sporozoites. Shown is the mean ± SEM. P-values calculated by Kruskal Wallis test followed by Dunns multiple comparison test. **(H)** Sporozoite numbers of infected midgut (MG) and salivary glands (SG) obtained from wild type, *akratin(-)*, *Akratin(-)*$^{PbAkratin\text{-}GFP}$ *as well as Akratin(-)*$^{PfAkratin\text{-}GFP}$ counted on d17 post mosquito infection. For each counting at least 20 mosquitos were dissected. Parts of the experiments are jointly done with Dominik Ricken and Leanne Strauss. Figure modified from (Kehrer et al., 2020).

I next investigated the localization of the protein in blood stages as well as mosquito resident forms. Akratin(-)$^{PbAkratin\text{-}GFP}$ (Figure 3.2.3 A) was already detected in ring stage parasites and showed generally a stronger fluorescent signal than Akratin(-)$^{PfAkratin\text{-}GFP}$ (Figure 3.2.3 A), which was only detectable from schizonts onwards. Sporozoites isolated from oocysts or salivary glands of both parasite lines showed the same punctuated pattern reminiscent of vesicles but different to the localization of TRAP or PAT (Kehrer et al. 2016). In ookinetes Akratin(-)$^{PfAkratin\text{-}GFP}$ seemed

to be clearly punctuated/ micronemal while Akratin(-)$^{PbAkratin\text{-}GFP}$ appeared membranous. Despite having a long N-terminal extension and an overall sequence identity of only 35%, the *P. falciparum* ortholog remains functional in P. berghei. (see Appendix).

In non-activated gametocytes I could not observe any distinction between male and female gametocytes. Yet over a time course of 20 min two different populations, most likely male and females, emerged. Gametocytes were classified as male, when a clear increase of the nucleus size with a cloudy and diffuse Hoechst staining was observed. Females in contrast have a small defined nucleus. (Figure 3.2.3 C). During the entire time period, in females the protein was distributed throughout the entire cell. While in microgametes the signal was very concentrated to a small area in the parasite with additional dots at the periphery.

However western blot analyses of both parasite lines using purified ookinetes or gametocytes was unsuccessful and yielded only a protein band corresponding to the size of GFP. This suggests that, at least in parts, the GFP is cleaved off and therefore localization of the protein within the parasite needs to be taken with caution.

Subsequently, I aimed to generate similar parasite lines inserting a longer linker between the protein and the GFP. However several transfection attempts to create the respective Akratin(-)$^{PbAkratin\text{-}GFP}$ parasites were unsuccessful. On the other hand, the generation of Akratin(-)$^{PfAkratin\text{-}GFP}$ parasites with an extended linker resulted in protein localization similar to my earlier observations (Figure 3.2.3 D). Additionally, western blot analyses did not reveal any changes.

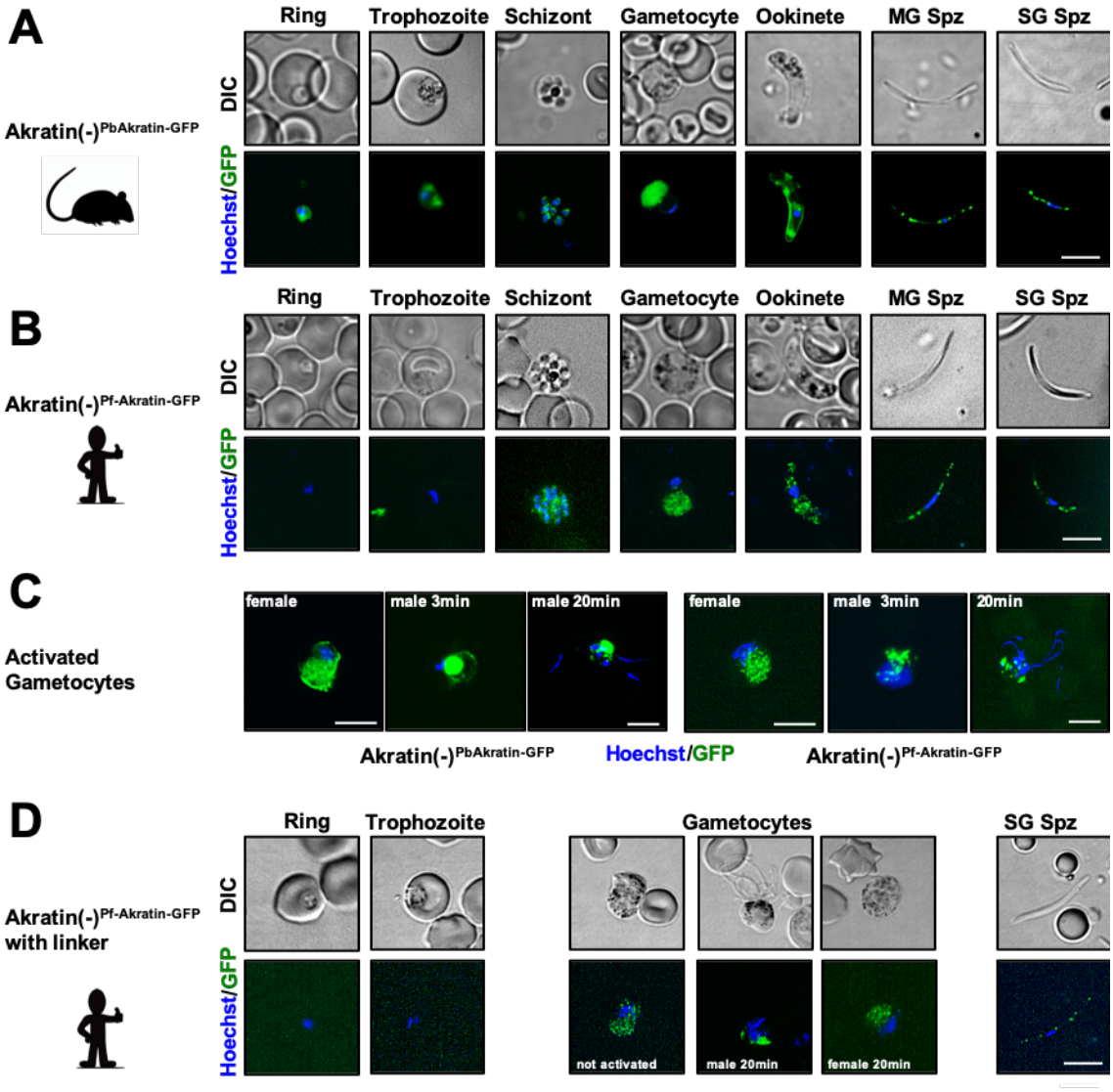

Figure 3.2.3 Akratin-GFP localization

(A) Representative images of akratin(-)$^{Pb\text{akratin-gfp}}$ localization in blood and mosquito stage parasites. Nuclei (blue) are stained with Hoechst. DIC: differential interference contrast, MG: midgut, SG: salivary gland. Scale bar: 5µm. **(B)** Representative images of akratin(-)$^{Pf\text{akratin-gfp}}$ localization in blood and mosquito stage parasites. Nuclei (blue) are stained with Hoechst. DIC: differential interference contrast, MG: midgut, SG: salivary gland. Note the weaker signal in *P. falciparum* akratin-GFP in gametocytes and the difference between the signals in ookinetes. Scale bar: 5µm. **(C)** Representative images of akratin(-)$^{Pb\text{akratin-gfp}}$ and akratin(-)$^{Pf\text{akratin-gfp}}$ localization in activated male and female gametocytes. Scale bars: 5µm. **(D)** Representative images of akratin(-)$^{Pf\text{akratin-gfp}}$ with linker. Localization in asexual blood stages as well as non- activated and activated gametocytes and salivary gland sporozoites. Nuclei (blue) are stained with Hoechst. DIC: differential interference contrast, MG: midgut, SG: salivary gland. Note the weaker signal in *P. falciparum* akratin-GFP in gametocytes and the difference between the signals in ookinetes. Scale bar: 5µm. Figure modified from (Kehrer et al., 2020).

Male gametocytes are formed but unable to generate fertile microgametes

To test for sex dependent gametocyte viability in the KO, I performed parasite-crossing experiments with a parasite line that either produces fertile male (Δp47) or fertile female (Δp48/45) gametocytes (van Dijk et al. 2010). As positive control Δp47 and Δp48/45 were crossed with each other. The control as well as KOxΔp47 crossings resulted in ookinete conversion rates of 35% and 42% respectively. While crossing of KOxΔp48/45 parasites did not produce sufficient ookinete numbers (3%). Suggesting that in the gene deletion mutant female gametocytes are still intact, while male gametocytes are impaired (Figure 3.2.4 A). In accordance with the phenotype in microgametes we named the protein akratin (from the Greek 'Akrasia': weak).

Next, I investigated whether the mutant parasite still produces male gametocytes. To address this, I have generated an additional parasite line lacking akratin in the 820cl1m1cl1 (RMgm-164) background (see Material and Methods). These selection marker-free parasites express RFP in females and GFP under the control of a male gametocyte specific promoter. Counting the ratio between both sexes in the resulting parasite line did not reveal any difference between the wild type and the KO (Figure 3.2.4 B).

Since male gametocytes are still formed I next addressed at which stage the cells arrest during microgamete formation. Therefore, I activated the cells and fixed them at certain timepoints. Male gametogenesis involves 3 round of rapid DNA replication, which is indicated by an increase of the nucleus within the first minutes. After fixation activated and non- activated cells were stained with Hoechst and the nucleus size was manually quantified using Fiji. In wild type parasites the nucleus size increased about 1,8 times after 5 min of activation. I also measured a similar increase for the mutant (Figure 3.2.4 C), indicating that microgametes are activated in general.

Analysis of the red blood cell membrane staining with an anti- Ter119 antibody in activated and non-activated male and female gametocytes still showed an intact membrane in activated microgametes of *akratin(-)* parasites. Whereas the membrane of macrogametes as well as wild type microgametes was completely dissolved (Figure 3.2.4 D). Indicating that akratin affects membrane lysis of microgametes. In addition, I also stained for microtubules since successful exflagellation also includes the formation of 8 individual axonemes. Although I did not observe fully exflagellating microgametes I observed the formation of microtubules (Figure 3.2.4 E). However, a more detailed examination at higher resolution using transmission electron microscopy (done by Marek Cyrklaff) suggests the formation of incomplete microtubules. Wild type axonemes mainly appear in a circular 9+2 structure (Figure 1.3) while in *akratin(-)* axonemes I observed an open circle with minimal inner microtubules (Figure 3.2.4 F). This indicates a potential function of the protein already during axoneme assembly.

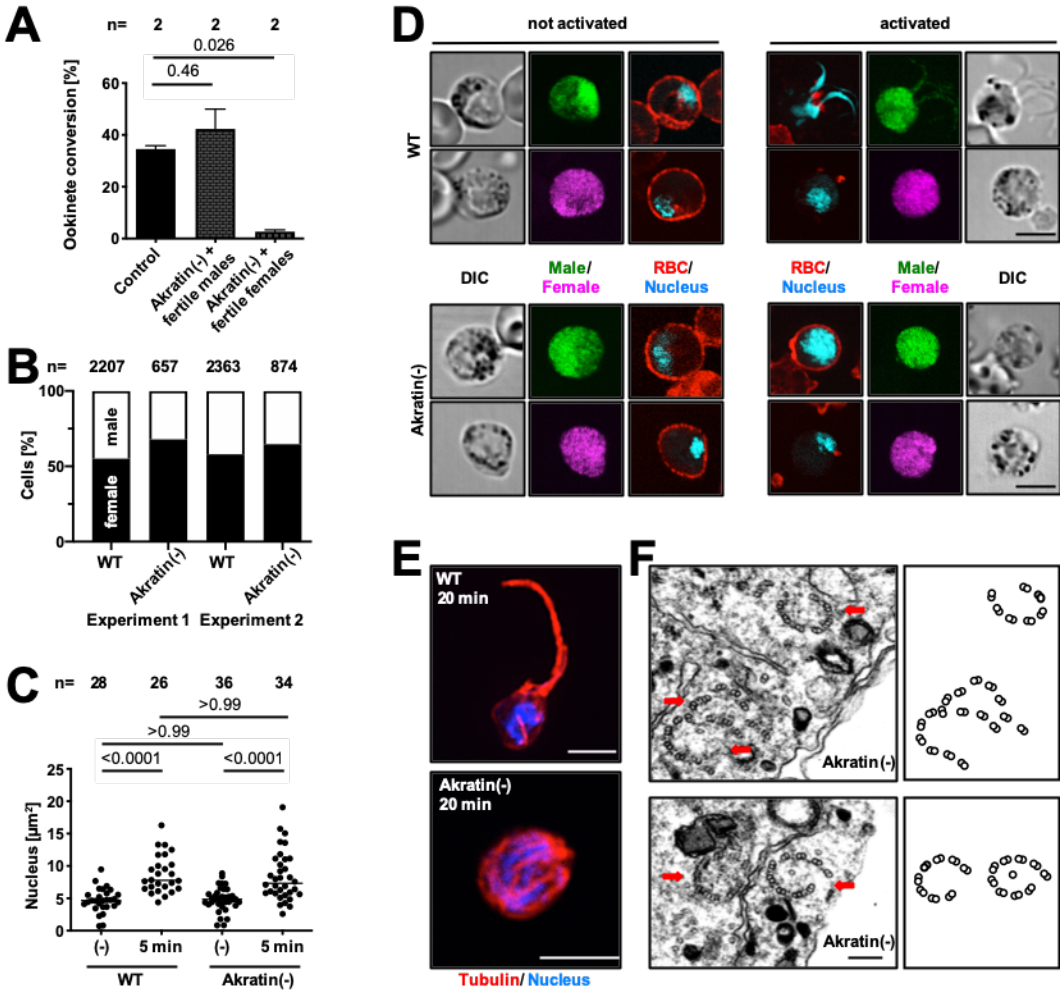

Figure 3.2.4 Male Gametocytes are formed and activated but fail to egress and to exflagellate

(A) Crossing of parasite lines deficient in either male or female gametocytes with *akratin(-)* parasite reveals that akratin functions only in males. P-value calculated by One-way Anova with Dunnetts multiple comparison test. Shown is the mean±SEM. **(B)** The same number of male and female gametocytes are formed in wild type (WT) and *akratin(-)* (KO) parasites lines. **(C)** Nuclear size determined from non-activated (-) or activated (5 min) wild type or *akratin(-)* parasites. Data points represent size of individual nuclei. P-values calculated by Kruskal Wallis Test with Dunns multiple comparison. **(D)** Activation of gametogenesis releases male and female WT gametes but only female *akratin(-)* gametes. Red blood cell (RBC) membrane is stained with Ter119 (red); male parasites are shown in green, females in pink and DNA in cyan. Scale bar: 5µm. **(E)** 20 minutes post activation *akratin(-)* parasites show microtubule staining reminiscent of assembled axonemes but not egressed gametes, while wild type parasites show the typical axonemal staining of exflagellating gametes. Scale bars: 5 µm. **(F)** TEM images taken by Marek Cyrklaff, of *akratin(-)* microgametes. Highlighted with the red arrows are axonemes which are not completely formed. This is also illustrated in the cartoon. Scale bar: 100 nm. Experiments in A and B are jointly done with Emma Pietsch. Figure modified from (Kehrer et al., 2020).

C- terminal motif uncouples protein function of Gametocytes and Ookinetes

In *Toxoplasma gondii* it was shown, that the micronemal protein MIC2 possesses c- terminal tyrosine containing motifs, essential for trafficking of the protein into secretory vesicles, to assure its function (Di Cristina et al. 2000). While in MIC2 the motif composition is rather unusual and does not reflect an order of any known motifs of mammalian cells, the identified motif in the C-terminus of TRAP is based on the sorting sequence YXXϕ (Bhanot et al. 2003) (Figure 3.2.5 A). To get a more detailed understanding of Akratin, I had a closer look at its C- terminal amino acid composition. The two motifs in MIC2 contain glutamic acid (E) and tyrosine (Y) but their amino acid composition does not display sequences of known recognition sides, while the described motif in the C- terminus of TRAP contains tyrosine as well and follows the sorting pattern YXXϕ—yet is located at the end of the TMD (Figure 3.2.5 A). Indeed, comparing the C- terminus after the last TMD of Akratin and its *P. falciparum* orthologue with the identified sequences in TgMIC2 and TRAP revealed a potential motif. In *P. berghei* the sequence order YKKL reflects the YXXϕ sorting pattern. However, since the *P. falciparum* orthologue contains a leucin instead of a tyrosine at the same position but a conserved glutamic acid prior to that I considered the sequence EYKK in *P. berghei* and ELKK in *P. falciparum* as a promising motif (Figure 3.2.5 A).

To probe a possible function of the tyrosine containing motif in gametocytes and ookinetes I generated a mutant parasite line expressing *P. berghei* Akratin-GFP with the respective motif changed into alanine's (see Material and Methods). Localization of Akratin$^{EYKK\text{-}AAAA}$-GFP in the parasite showed similar staining patterns in asexual and sexual parasite stages compared with Akratin-GFP (Figure 3.2.5 B; compare with Figure 3.2.3 E). However, in contrast to the clearly peripheral and vesicular localization in ookinetes the Akratin$^{EYKK\text{-}AAAA}$-GFP signal was more diffusely localized within the cytoplasm (Figure 3.2.5 B; compare with Figure 3.2.3 E). Yet, as described above, the localization of the GFP needs to be taken with caution since western blot analyses was unsuccessful. The difference in localization could eventually be the result of cleavage of GFP in Akratin$^{EYKK\text{-}AAAA}$-GFP. Several attempts to generate Akratin$^{EYKK\text{-}AAAA}$-GFP parasites with an extended linker between the protein and the GFP were unsuccessful.

Mutant microgametes did readily exflagellate and formed motile ookinetes similar to wild type (Figure 3.2.5 C-E). However, even though Akratin$^{EYKK\text{-}AAAA}$-GFP ookinetes were able to move *in vitro*, the parasite was unable to manifest an infection in the mosquito similar to parasites lacking the complete protein (Figure 3.2.5 F).

To investigate whether ookinetes are still able to penetrate the mosquito midgut epithelial to transform into oocysts, I isolated midguts 24 hours post infection. After a short fixation step, midguts were cut open longitudinally to wash out the remaining blood bolus, fixed again and

stained with phalloidin to visualize the actin cytoskeleton outlining the epithelial cells and the muscles fibers on the hemolymph-facing side of the midgut (Figure 3.2.5 G). In addition, the GFP signal of the ookinetes was enhanced with an anti GFP antibody staining. Observation of parasites with a fluorescent microscope resulted in the presence of ookinetes at the basal lamina in 56% of wild type infected midguts while none was found for the mutant (Figure 3.2.5 G). Suggesting a role for akratin to either cross the perithrophic membrane or the epithelial layer.

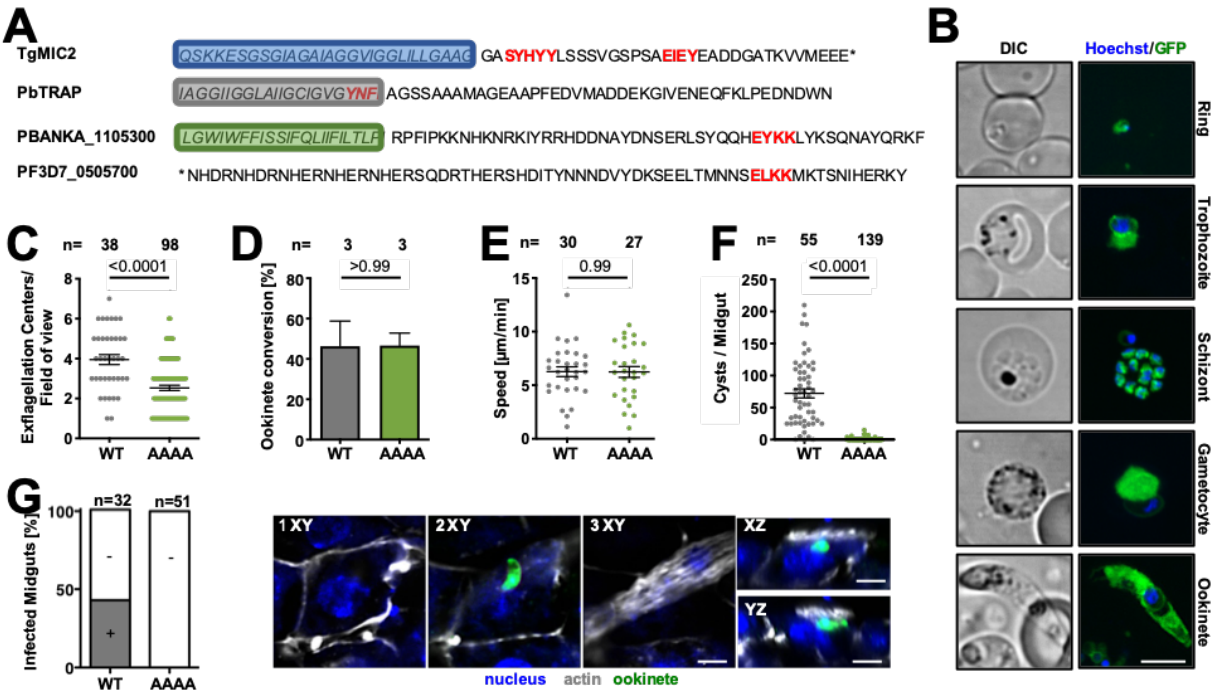

Figure 3.2.5 Mutation of C- terminal motif is sufficient to block mosquito transmission

(A) C-terminal alignment of *P. berghei* akratin, *P. falciparum* akratin, *T. gondii* MIC2 and *P. berghei* Trap highlighting the last trans-membrane domains (TMD) with its putative sorting motifs shown in red. The * indicates missing amino acids which are not shown in the figure due to space limitations. Sequences obtained from plasmodb.org. **(B)** Localization of akratin$^{EYKK/AAAA}$-GFP in the indicated *P. berghei* life cycle stages. Scale bar 5µm. **(C)** Exflagellation of akratin$^{EYKK/AAAA}$ parasites compared to wild type (WT). P- value is calculated using the Mann Whitney test. Shown is the mean ± SEM. **(D)** Ookinete conversion rate of akratin$^{EYKK/AAAA}$-GFP parasites compared to wild type (WT). P- value is calculated using the Mann Whitney test. Shown is the mean ± SEM. **(E)** Average speed of akratin$^{EYKK/AAAA}$-GFP ookinetes compared to wild type (WT). P- value is calculated using the Mann Whitney test. Shown is the mean ± SEM is comparable to wild type (WT). P- value is calculated using the Mann Whitney test. **(F)** Oocysts numbers of akratin$^{EYKK/AAAA\text{-}GFP}$ parasites compared to wild type (WT). P- value is calculated using the Mann Whitney test. Shown is the mean ± SEM. **(G)** Comparison of infected and non-infected midgut epithelia after ookinete traversal of akratin$^{EYKK/AAAA}$-GFP compared to WT (left). Representative images in the indicated views shows wild type ookinetes at different positions within the epithelial layer. Scale bar 5µm. Figure taken and modified from (Kehrer et al., 2020).

Discussion

I selected the protein akratin from a proteomic screen to identify novel micronemal proteins of ookinetes via Apex2 based proximity labeling (see section 3.1). RNA-Seq data of *akratin* obtained from plasmodb.org shows a peak expression in gametocytes (mostly microgametes) and ookinetes (Figure 3.5.1). Furthermore, the protein contains 4 transmembrane domains and a signal peptide making it a promising candidate for a protein involved in motility.

Gene deletion of *akratin* resulted in a complete block of parasite transmission into mosquitoes. In a more detailed analyses of *akratin(-)* parasites I observed that female gametocytes are still intact while microgametes showed a defect in exflagellation and red blood cell egress of male gametes, nearly abolishing gamete release and hence ookinete formation. Membrane proteins, including PAT (Kehrer, Singer, et al., 2016) and MTRAP (Bargieri et al., 2016; Kehrer, Frischknecht, et al., 2016), have been demonstrated to be involved in facilitating the exit of gametes from red blood cells. However, the precise mechanism by which they function or whether they act in concert is still unclear.

Complementation of *akratin(-)* parasites with *P. berghei* as well as *P. falciparum* akratin-GFP rescued the gene deletion phenotype. Excluding a phenotype based on off- target effects. I observed the protein to be present in all investigated stages of the life cycle, displaying distinct localization patterns. In asexual and sexual blood stages, it appeared cytosolic, while in ookinetes and sporozoites, it exhibited a more punctuated pattern. Localization of *P. falciparum* akratin-GFP was similar than *P. berghei* akratin-GFP albeit not identical. Several attempts to detect the fusion protein in western blot did only result in a band corresponding to the size of GFP. Suggesting that the GFP is most likely cleaved off. Thus localization of the protein within the cell needs to be handled with care.

Complementation of *akratin(-)* parasites with akratin containing a mutation of a putative tyrosine containing motif at the C-terminus of the protein fused to GFP did not show any effect in gametocytes and resulted in normally formed ookinetes able to move in a wild type manner when moving on glass. *In vivo* however mutant ookinetes were unable to efficiently penetrate the midgut epithelium and thus not able to develop into oocysts necessary for life cycle progression (Figure 3.2.6 G). Yet again I cannot draw any conclusion about the localization of the protein since the GFP seems to be (partly) cleaved. Thus, whether the motif plays a role in targeting the protein to micronemes needs to be investigated further e.g. by introducing a different linker between akratin and GFP.

Surprisingly mutant ookinetes were able to move on glass but not *in vivo*. There are several possible explanations for this phenomenon. One possible explanation for the observed defect in epithelial penetration of ookinetes is that the protein plays a protective role, shielding the ookinete

from host defense proteins such as TEP1 in vertebrates or mosquito defense mechanisms (Fraiture et al., 2009).

Another possibility is that mutant ookinetes fail to bind a key receptor, which prevents them from initiating the switch from migration to invasion. Alternatively, the mutant ookinetes may not generate enough force to penetrate the peritrophic matrix that forms around the blood meal during digestion or to enter the epithelium. A similar effect was observed when replacing the essential ookinete adhesin CTRP with the sporozoite adhesin TRAP (Klug et al., 2018). In this case, the TRAP-expressing ookinetes displayed normal movement on glass but failed to form oocysts, highlighting again the imperfect correlation between in vitro motility and *in vivo* migration.

Several other mutants exhibit a similar discrepancy not in ookinetes but in the behavior of sporozoites regarding their ability to move and enter salivary glands. Interestingly, sporozoites with a mutated *profilin* as well as sporozoites with a mutated *trap* display a significant impairment in gliding on glass surfaces, yet they can still enter salivary glands without any notable difficulty (Klug et al., 2020; Moreau et al., 2017). On the other hand, there are mutants that migrate almost normally but exhibit reduced efficiency in entering salivary glands (Douglas et al., 2018). These findings highlight the complex and multifaceted nature of the mechanisms involved in sporozoite entry into salivary glands, suggesting that different factors and pathways may contribute to this process.

In conclusion, I could show that *akratin* has a dual function during mosquito transmission. It plays a role during microgametogenesis and a tyrosine-containing C- terminal motif after the transmembrane domain is essential for ookinete penetration of the mosquito midgut epithelium. Further experiments can be done to investigate its function in sporozoites.

3.3. C- terminal characterization of PAT

The C- terminus of PAT is essential for ookinetes but not gametocytes

The protein PAT in *P. berghei* parasites is a membrane component of egress vesicles in gametocytes and micronemes of sporozoites (Kehrer et al., 2023; Kehrer, Singer, et al., 2016). PAT-deficient gametes fail to discharge their contents, remain intraerythrocytic and are thus unavailable for fertilization and further development in the mosquito. Furthermore, in sporozoites PAT is essential for the secretion of TRAP. Therefore sporozoites are immotile and unable to efficiently invade salivary glands (Kehrer et al. 2016). A potential function of PAT in ookinetes remains elusive because of technical limitations. In this chapter I will further characterize PAT to obtain a more detailed understanding about the protein. In analogy to akratin (see section 3.2), I investigated the C- terminus of PAT towards potential motifs after the last TMD. For akratin and TRAP, only one motif has been described to interfere with the protein function while TgMIC2 seems to require two motifs for correct trafficking (Di Cristina et al., 2000). Similar to TgMIC2, PAT contains two tyrosine containing motifs. One motif directly after the last TMD (EY) and a second one 10 bases downstream (EYKY). The precise location of both motifs is highlighted in red within the current PAT structure obtained through AlphaFold in which annotated TMDs are marked in blue (Figure 3.3.1).

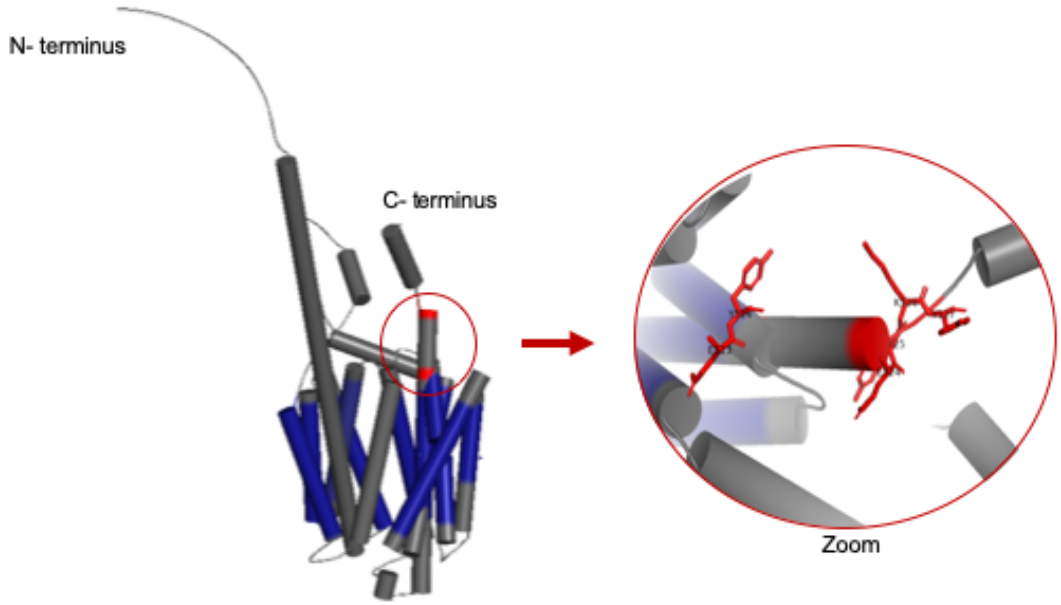

Figure 3.3.1 Predicted structure of PAT.

The structure of PAT was predicted using Alphafold2 and color coded using Pymol. Helices are shown as cylinders and transmembrane domains are highlighted in blue. The motifs EY and EYKY are shown in red and presented in more detail in the zoom.

While the first sequence YSKM follows the YXXϕ pattern—as described for sorting motifs in mammalian cells and in TRAP—the second sequence EYKY does not display any known recognition side, similar to the motifs in TgMIC2. Yet since glutamic acid seems to be present in all the described motifs and since EY is conserved among *Plasmodium* spp. I considered EY as a potential first motif instead of YSKM (Figure 3.3.2 A).

To investigate the impact of the PbPAT C-terminus and to test whether both sequences are essential for the protein I generated a parasite line via double homologous recombination of WT parasites, lacking the entire C-terminus (Δ512-541) and a parasite line leaving the first motif intact (Δ514-541) (Figure 3.3.2 A, Material and Methods). PAT$^{\Delta 512\text{-}541}$ as well as PAT$^{\Delta 514\text{-}541}$ parasites were able to form motile ookinetes in the WT range however failed to establish mosquito infections in two independent experiments each (Figure 3.3.2 B-D). Suggesting that the C-terminus is indeed crucial for the function of PAT in ookinetes but not gametocyte egress.

For more detailed investigations of the motifs I next generated a recipient parasite line replacing the entire PAT gene against the gene in marker out (GIMO) selection cassette (see Material and Methods) (Lin et al., 2011). This allows the straightforward generation of selection marker free mutants complementing the KO with modified PAT-GFP versions, leaving the endogenous locus intact. Surprisingly, while two previously generated parasite lines lacking PAT resulted in impaired gametogenesis (Kehrer, Singer, et al., 2016), PAT(-)^{GIMO} parasites in contrast did not show any phenotype in gametocytes and hence could produce motile ookinetes, yet unable to cause mosquito infections (Figure 3.3.2 B-D). To test the influence of the selection cassette regarding the observed phenotype, I next inserted a single GFP into this parasite line. Interestingly, PAT(-)^{GFP} parasites did not produce any ookinetes and reflected our previously described gene deletion phenotype (Figure 3.3.2 B-D). Suggesting an effect of the ef1a promoter downstream of the open reading frame as already described in other studies (Klug et al. 2016). I therefore continued using PAT(-)^{GIMO} parasites for the generation of further mutants, yet refer to PAT(-)^{GFP} parasites as reference.

To address an effect of the two proposed C-terminal motifs I generated the parasite lines PAT$^{EY\text{-}AA}$ and PAT$^{EYKY\text{-}AAAA}$ changing the respective motifs into alanine (Figure 3.3.2 A). Both containing an additional GFP at the C-terminus to observe the localization of the protein. Identical to the parasites lacking the complete C-terminus, PAT$^{EY\text{-}AA}$ as well as PAT$^{EYKY\text{-}AAAA}$ parasites could produce wild type numbers of motile ookinetes but failed to cause an infection of mosquitoes (Figure 3.3.2 B-D). However, both proteins still show a punctuate/vesicular localization reminiscent to PAT-GFP (Kehrer et al. 2016). The GFP signal of PAT(-)^{GFP} gametocytes in contrast is entirely cytoplasmic (Figure 3.3.2 E).

Isolated mosquito midguts 24 h post infection did not show any ookinetes traversing the epithelia cells outlining the organ. Almost 50% of mosquitoes infected with PAT-GFP parasites contained detectable ookinetes at the basal lamina whereas none of the mutants did (Figure 3.3.2 F). These data hint towards a defect of the ookinetes to interact with cell surfaces necessary to leave the blood bolus.

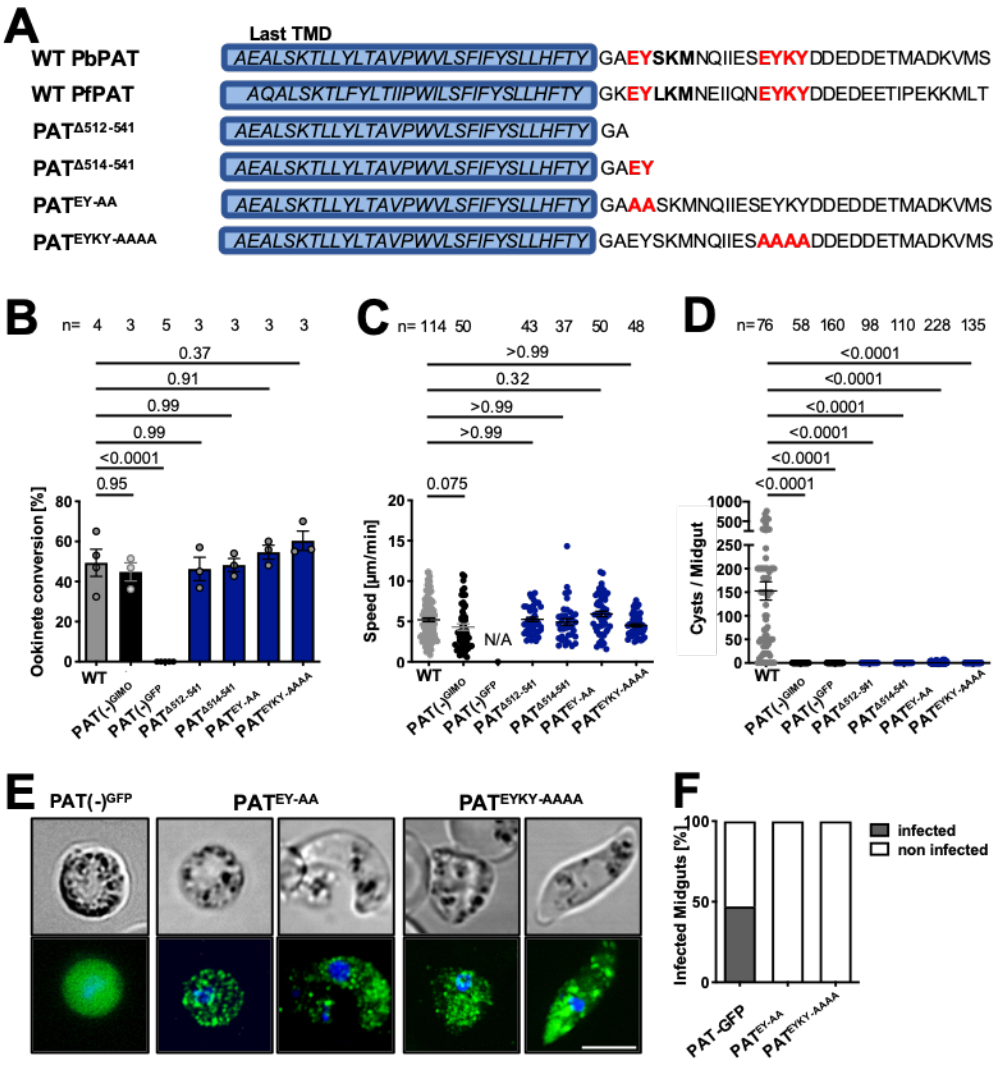

Figure 3.3.2 The C- terminus of PAT is essential for ookinete midgut traversal

(A) Terminal sequence alignment of *P. berghei* and *P. falciparum* PAT with the generated mutants. **(B)** Gametocyte to ookinete conversion of wild type parasites in comparison to mutants with C- terminal modifications. Shown is the mean +/- SEM. P-values are calculated using the Kruskal- Wallis test with Dunns multiple comparison. **(C)** Shown is the mean +/- SEM. P-values are calculated using the Kruskal- Wallis test with Dunns multiple comparison. **(D)** Oocysts numbers of mosquito midguts isolated from wild type as well as mutants with C-terminal modifications. Shown is the mean +/- SEM. P-values are calculated using the Kruskal- Wallis test with Dunns multiple comparison. **(E)** Localization of GFP in KO-GFP as well as PAT$^{EY::AA}$ and PAT$^{EYKY::AAAA}$ parasites. Scale bar: 5µm. **(F)** Quantification of ookinete midgut traversal of PAT-GFP and both motif mutation mutants. Parts of the experiments are jointly done with Dominik Ricken and Emma Pietsch.

Neither TgTFP1, nor the C- terminus of TgTFP1 or TgMIC2 can restore PAT function

PAT is conserved among Apicomplexa (Kehrer et al. 2016). The orthologue in *T. gondii* (TGGT1_216820) belongs to a group of four MFS transporters and is called transporter family protein 1 (TFP1). TgTFP1 localizes to micronemes and is essential for parasite survival(Hammoudi et al., 2018). In accordance to *P. berghei* PAT, depletion of the protein affects micronemal discharge, leading to a failure of the parasite in attachment and host cell invasion (Hammoudi et al., 2018; Sidik et al., 2016). Using BlastP TgTFP1 shares 51% sequence identity with PbPAT and 49% with its *P. falciparum* orthologue. More importantly TgTFP1 also contains a 4 base pair tyrosine containing motif in its C- terminus (Figure 3.3.3 A). In *T. gondii*, TgTFP1 fused to GFP localizes to the apical part of the cell as expected (Figure 3.3.3 B; contributed by Mirko Singer).

To test if TgTFP1 is able to complement PAT function in *P. berghei* I generated a parasite line expressing TgTFP1 fused to GFP replacing the complete endogenous PAT locus (see Material and Methods). Characterization of the mutant parasite line however reflected the phenotype of parasites lacking PAT. Expression of TgTFP1 in *P. berghei* hence lead to a complete block of the parasite in mosquito transmission. Activated gametocytes remained trapped inside the RBCM and in addition microgametes could not form 8 separated flagella (Figure 3.3.3 C). Therefore, I neither observed any ookinetes nor any midgut oocysts in mosquitoes fed on infected blood (Figure 3.3.3 D-E).

PbPAT is annotated with 12 TMDs while TgTFP1 comprises 11 TMDs only. To exclude the possibility that the observed phenotype results from an incorrect orientation of the C- terminus and to test the conservation of the motifs I subsequently exchanged the C- terminus after the last TMD of PAT against the C- terminus of TgTFP1. In parallel I also replaced the C- terminus of PbPAT against the C-terminus of TgMIC2, to investigate whether the previously described motifs are sufficient to restore PAT function (see Material and Methods). TgMIC2 contains two potential tyrosin containing motifs at the C-terminus, which have previously been demonstrated to be essential for protein trafficking to micronemes (Figure 3.3.3 A) (Di Cristina et al., 2000). Both parasite lines were unable to progress beyond the ookinete stage, which closely resembled the observed phenotype of PbPAT lacking either the complete C-terminus or expressing $PAT^{EY\text{-}AA}$ and $PAT^{EYKY\text{-}AAAA}$ respectively. I did not observe any difference in activated gametocytes compared to wild type (Figure 3.3.3 C). Although, mutant parasites were able to form ookinetes moving in a wildtype manner, transmission into mosquitoes was completely blocked (Figure 3.3.3 D-F). This suggests that the identified motifs within *T. gondii* proteins are not functionally conserved in *P. berghei*.

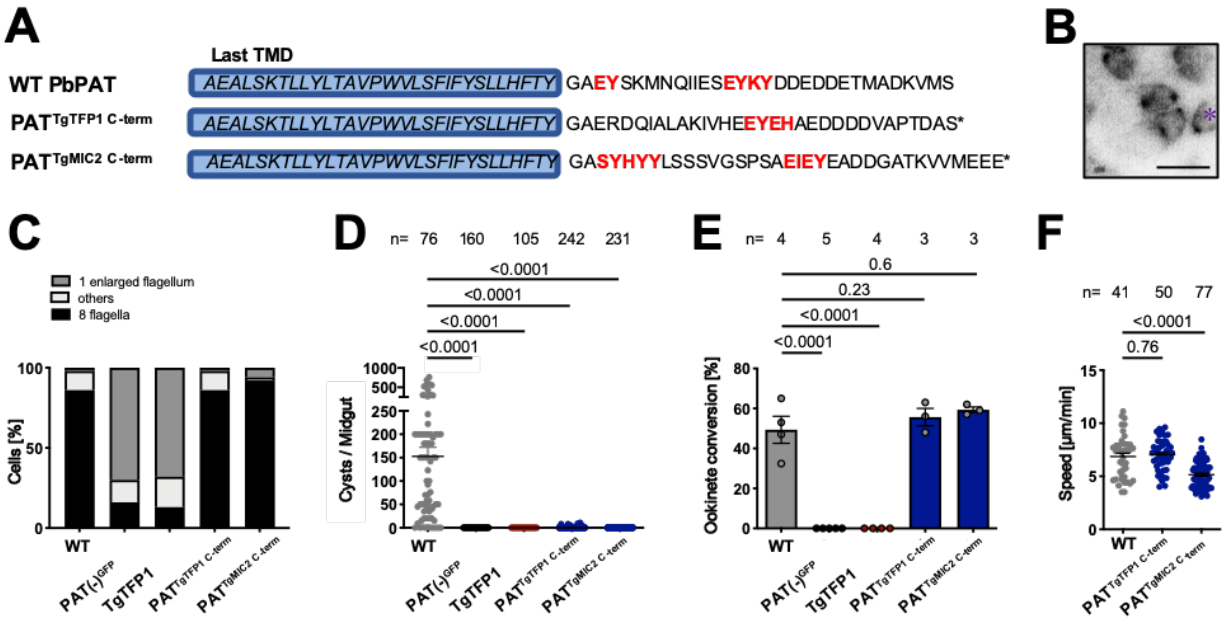

Figure 3.3.3 TgTFP1 and TgMIC2 are unable to complement PAT

(A) C-terminal alignment of PbPAT with the mutants containing either the TgTFP1 or the TgMIC2 tails. Potential functional motifs are highlighted in red. **(B)** *T. gondii* tachyzoites expressing TgTPF1-GFP. The GFP signal concentrates at the apical part of the cell reminiscent of a micronemal localization. * indicates the apical side of the tachyzoite. Scale bar: 5 µm. Image provided by Mirko Singer. **(C)** Exflagellation phenotypes of activated microgametes of WT and KO parasites in comparison to the mutants. **(D)** Oocysts numbers of isolated mosquito midguts. Shown is the mean +/- SEM. P-values are calculated using the Kruskal-Wallis test with Dunns multiple comparison. **(E)** Gametocyte to ookinete conversion of wild type parasites in comparison to the mutants. Shown is the mean +/- SEM. P-values are calculated using the one-way Anova test with Dunnetts multiple comparison. **(F)** Ookinete motility on glass. Shown is the mean +/- SEM. P-values are calculated using the Kruskal-Wallis test with Dunns multiple comparison. Parts of the experiments are jointly done with Dominik Ricken and Emma Pietsch.

PAT$^{EYKY\text{-}AAAA}$ but not PAT$^{EY\text{-}AA}$ is essential for sporozoites

Stage specific expression of wild type PAT in gametocytes and ookinetes using the CCP promoter allows sporozoite formation in the midgut but it impairs salivary gland invasion. On glass CCP-PAT sporozoites are unable to attach and thus cannot productively move forward.

To assess the impact of the identified C-terminal motifs on PAT function in sporozoites I next generated parasite lines expressing PAT under the endogenous promoter with either lacking the complete C-terminus or with the respective motifs (EY-AA or EYKY-AAAA) mutated into alanine. The parasite lines, CCP-PAT|PAT$^{C\text{-}term(-)}$, CCP-PAT|PAT$^{EY\text{-}AA}$ and CCP-PAT|PAT$^{EYKY\text{-}AAAA}$ express WT-PAT in gametocytes and ookinetes to overcome the transmission block into the mosquito but express the respective mutated PAT versions under the endogenous promoter in sporozoites. Furthermore, wild type CCP-PAT is fused to mCherry and the mutated PAT is fused to GFP (Figure 3.3.4 A). To monitor the protein abundance of the modified protein in CCP-PAT|PAT$^{C\text{-}term(-)}$, CCP-PAT|PAT$^{EY\text{-}AA}$ and CCP-PAT|PAT$^{EYKY\text{-}AAAA}$ parasites along the life cycle

and to visualize CCP promoter activity I used live cell fluorescence imaging. As expected I detected CCP-PAT in gametocytes and ookinetes but not in oocysts and sporozoites, while the mutated PAT expressed under the endogenous promoter was visible in all the parasite stages. (Figure 3.3.4 B).

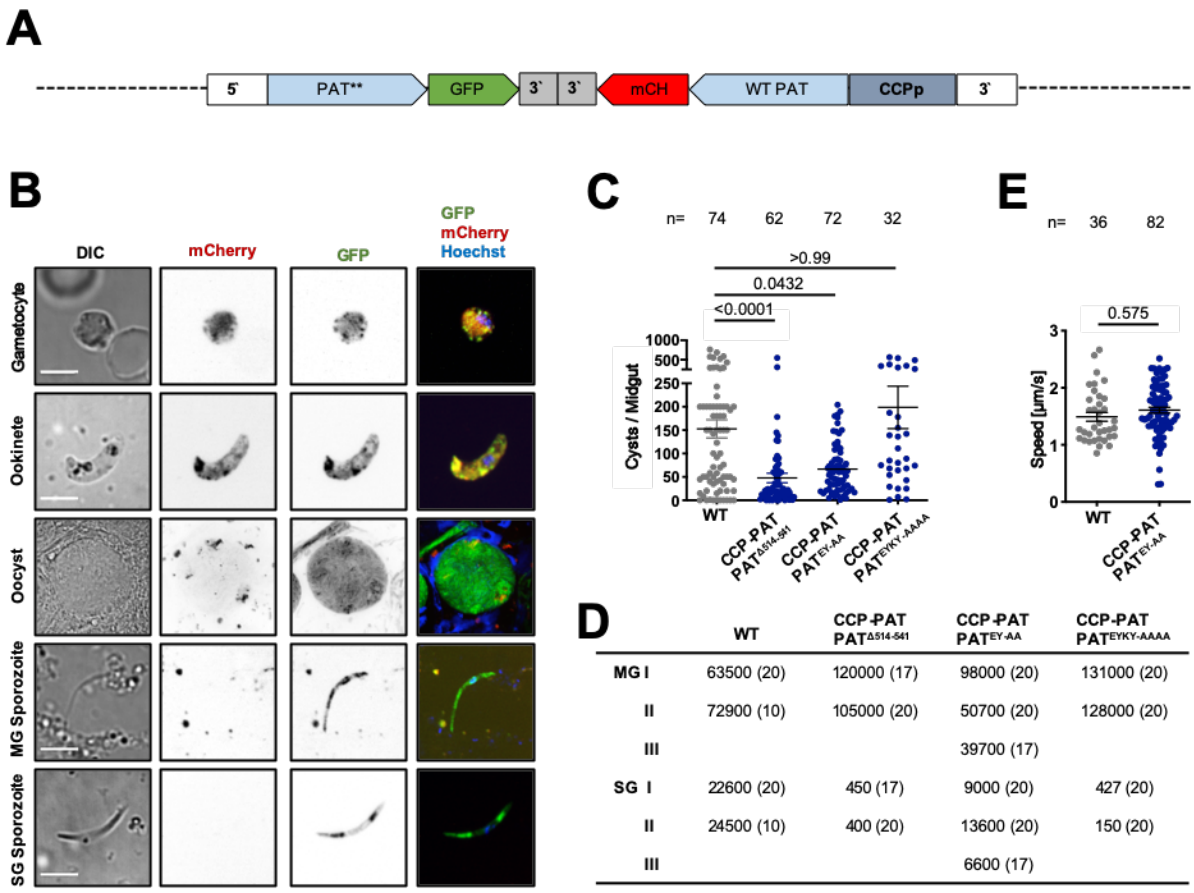

Figure 3.3.4 Stage specific expression of PAT in sporozoites

(A) Cartoon of the endogenous PAT locus complemented with CCP-PAT-mCherry and a mutated version fused to GFP (PAT**). **(B)** Representative images of PAT expression under the stage-specific CCP promoter fused to mCherry and the endogenous promoter fused to GFP in the different parasite stages. Scale bar: 5µm. **(C)** Cyst numbers of infected mosquito midguts counted after mercurochrome staining between day 12-17 post infection. P- values are calculated using the Kruskal Wallis test followed by Dunns multiple comparison. Shown is the mean +/- SEM. **(D)** Midgut and salivary gland infection rates on day 17 from at least two different cage feeds. **(E)** Speed of isolated WT and CCP-PAT|PAT$^{EY\text{-}AA}$ sporozoites on glass. P- value is calculated using the Mann Whitney test. Shown is the mean +/- SEM. Parts of the experiments are jointly done with Emma Pietsch.

Characterization of the parasite lines resulted in mosquito midgut infections comparable to WT (Figure 3.3.4 C-D). However, I observed significant differences in salivary gland invasion. CCP-PAT|PAT$^{C\text{-}term(-)}$ and CCP-PAT|PAT$^{EYKY\text{-}AAAA}$ parasites showed a drastic reduction in sporozoite invasion of salivary glands reminiscent of the phenotype observed in CCP-PAT

parasites (Kehrer et al. 2016). CCP-PAT|PAT$^{EY\text{-}AA}$ sporozoites in contrast occupy salivary glands in a WT range and further imaging of isolated sporozoites on glass resulted in motile parasites moving in circles at around 1,5 µm/s on average, similar to WT sporozoites (Figure 3.3.4 E).

These data underscore the essential role of the EYKY motif in sporozoite motility. Interestingly, the two amino acid-containing motif EY, while essential for ookinetes, does not exhibit the same level of importance in sporozoites. Therefore, the EYKY motif emerges as a crucial determinant for both ookinetes and sporozoites, whereas the EY motif is specifically required in ookinetes.

Considering the observed phenotypes, I subsequently examined the precise localization of PAT-GFP in sporozoites from all three mutant parasite lines. In CCP-PAT|PAT$^{C\text{-}term(-)}$ and CCP-PAT|PAT$^{EYKY\text{-}AAAA}$ parasites, I never observed any fluorescence at the plasma membrane but only observed an intracellular signal. (Figure 3.3.5 A-B). Conversely, in CCP-PAT|PAT$^{EY\text{-}AA}$ parasites, which did not exhibit a phenotype in salivary gland invasion, PAT was concentrated at the front of the cell reminiscent of micronemes and visible at the plasma membrane. This pattern mirrored the protein localization observed in WT PAT-GFP parasites (Kehrer et al. 2016) (Figure 3.3.5 C), suggesting a role of the C-terminus in microneme secretion but not initial trafficking of PAT to the micronemes.

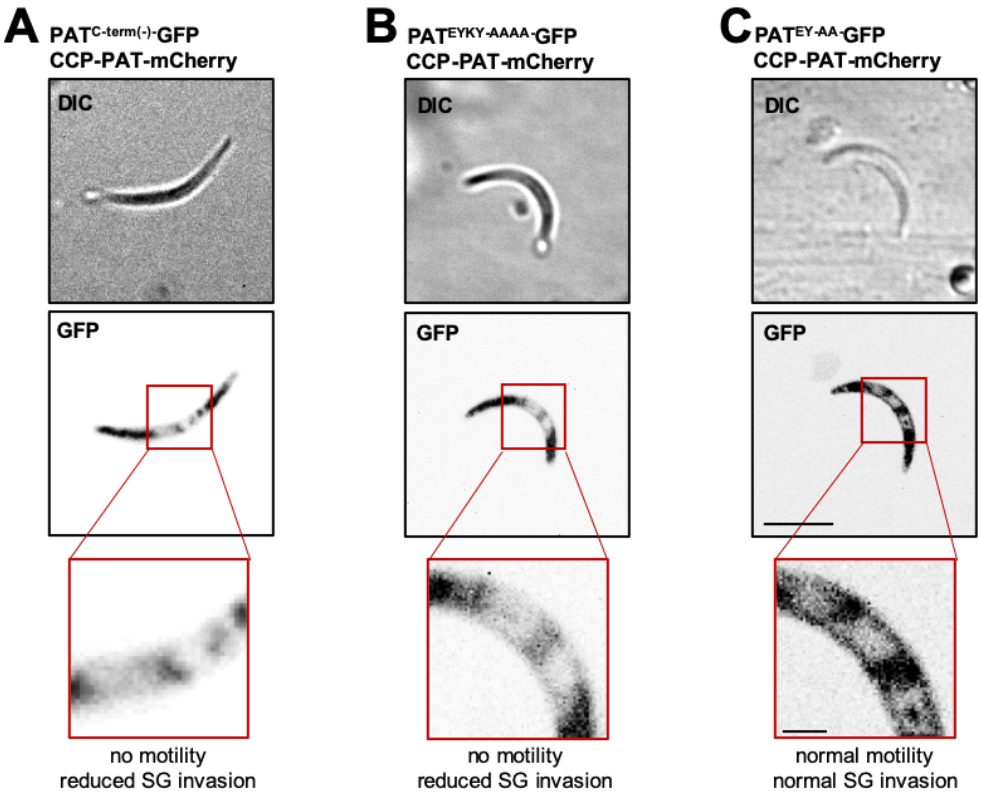

Figure 3.3.5 Modified PAT is not localized to the plasma membrane

(A) Expression and localization of CCP-PAT|PAT$^{C\text{-}term(-)}$-GFP in isolated salivary gland sporozoites. **(B)** Expression and localization of CCP-PAT|PAT$^{EYKY\text{-}AAAA}$ -GFP in isolated salivary gland sporozoites. **(C)** Expression and localization of CCP-PAT|PAT$^{EY\text{-}AA}$-GFP in isolated salivary gland sporozoites. Please note the signal at the plasma membrane compared to the other mutants. Scale bar 5µm. Scale bar zoom 1µm.

Discussion

PAT in gametocytes and ookinetes

The conserved putative pantothenate transporter PAT has been identified as an essential component in vesicle secretion of *P. berghei* gametocytes and sporozoites (Kehrer, Singer, et al., 2016). Gene deletion of PAT thus resulted in a complete block of parasite transmission into mosquitoes. In a more detailed sequence analyses of the PAT C-terminus I recognized two distinct tyrosine containing motifs (Figure 3.3.2 A) reminiscent of the described functional motifs in *P. berghei* akratin (section 3.2) and *T. gondii* MIC2 (Di Cristina et al., 2000).

Investigation of C-terminal deletion mutants as well as $PAT^{EY\text{-}AA}$ and $PAT^{EYKY\text{-}AAAA}$ parasites, resulted in healthy gametocytes and motile yet non-infectious ookinetes. Suggesting that the C-terminus indeed plays a role in ookinete infectivity while PAT function in gametocytes is most likely driven by a different part of the protein which still needs to be determined (Figure 3.3.2 and 3.3.6).

Replacement of PAT with the complete TgTFP1 as well as $PAT^{TgTFP1\ C\text{-}term}$ and $PAT^{TgMic2\ C\text{-}term}$ parasites could not complement the function of PbPAT. While $PAT(-)^{TgTFP1}$ showed the phenotype of PAT(-) parasites $PAT^{TgTFP1C\text{-}term}$ and $PAT^{TgMic2\ C\text{-}term}$ mutants resulted in motile ookinetes unable to cause an infection in mosquitoes similar to the phenotype I observed for $PAT^{EY\text{-}AA}$ and $PAT^{EYKY\text{-}AAAA}$ and the C- terminal deletions (Figure 3.3.3 and 3.3.6). While all three proteins feature tyrosine containing motifs at their C-terminus these motifs are not identical and are situated at different distances from the last TMD. This might have consequences on their function. For example, shifting the sorting or tyrosine containing motif of the lysosomal protein LAMP-1 by one or five amino acids has been shown to already influence its function (Rohrer et al., 1996). Furthermore, TgTFP1 only contains one motif instead of two in PAT (EY (…) EYKY). Indicating that the motif information coded in TgPAT and TgMIC2 C-termini is not recognized by *P. berghei* and thus the protein content of *T. gondii* cannot just easily be transferred to *Plasmodium*. The different composition of the motifs in Plasmodium PAT versus the motif in TgTFP1 which again is different from the motifs SYHYY (…) EXEY/FE in TgMIC2, might affect the function of the protein. This could explain why $PAT(-)^{TgPAT}$ and $PAT(-)^{TgMIC2}$ are unable to exert their function.

The phenotype might also be caused by differences in the protein structure. In addition, the TgPAT C-terminus and the TgMIC2 C-terminus are longer than the endogenous PAT C-terminus. Their folding might block PAT interaction sites or interfere with PAT function as a transporter. In contrast to this hypothesis, PAT^{TgPAT}/ PAT^{TgMIC2} localization in gametocytes and ookinetes appeared normal (Figure 5) indicating that protein trafficking is not impaired. However, in order to make a reliable statement about the conservation of targeting motifs, the micronemal targeting

motifs EEYE of TgPAT or SYHYY (…) EXEY/FE of TgMIC2 could be introduced into PAT replacing the putative *P. berghei* targeting motifs EY (…) EYKY.

In conclusion, I found that the PAT C-terminus containing two tyrosine containing motifs is essential for the infectivity of ookinetes but not important during gametogenesis. This is similar to akratin (see section 3.2). Detailed characterization of akratin resulted in an identical pattern showing that a C-terminal tyrosine containing motif uncouples protein function in gametocytes and ookinetes. Whether there are more proteins along this line still needs to be addressed bioinformatically.

PAT in sporozoites

In sporozoites, PAT localizes to TRAP-positive micronemes and remains associated with the plasma membrane after secretion. Stage specific expression of PAT in gametocytes under the CCP promoter showed an additional function of the protein during salivary gland invasion. Caused by a failure of sporozoite attachment and thus impaired motility (Kehrer, Singer, et al., 2016).

Expression of the complete PAT protein under the CCP promoter together with modified PAT versions under the endogenous promoter allowed characterization of the C- terminus in sporozoites. CCP-PAT|PAT$^{C\text{-}term(-)}$ and CCP-PAT|PAT$^{EYKY\text{-}AAAA}$ sporozoites were unable to efficiently colonize mosquito salivary glands similar to sporozoites lacking PAT. CCP-PAT|PAT$^{EY\text{-}AA}$ parasites in contrast were able to progress through the insect in a wild type manner. Suggesting that in the sporozoite only the EYKY motif plays an essential role while the first EY motif is dispensable Figure 3.3.5 and 3.3.6).

Furthermore, alterations in the putative targeting motifs could potentially impact posttranslational modifications (PTM) of PAT. The amino acid residues within these putative targeting motifs—namely, glutamic acid (E), tyrosine (Y), and lysine (K)—can undergo diverse modifications. Glutamic acid, for instance, has been documented to undergo acetylation, glycosylation, or phosphorylation. Similarly, lysine residues are often subject to acetylation, methylation, or ubiquitination, while tyrosine residues are recognized as classical phosphorylation sites. Of particular significance, phosphorylation has been demonstrated to play a pivotal role in governing protein dynamics. It achieves this by inducing conformational changes or furnishing binding sites for other proteins (Alberts et al., 2002). Phosphorylation is a key mechanism influencing the activity, structure, and cellular localization of numerous proteins within eukaryotic cells (Alberts et al., 2002). Introducing mutations in the motifs at crucial residues of PAT could potentially disrupt the post-translational modifications of the protein, thereby impacting its dynamics, functionality, or its ability to interact with binding partners. Nevertheless, currently there is no evidence of post-translational modifications of PAT (plasmodb.org).

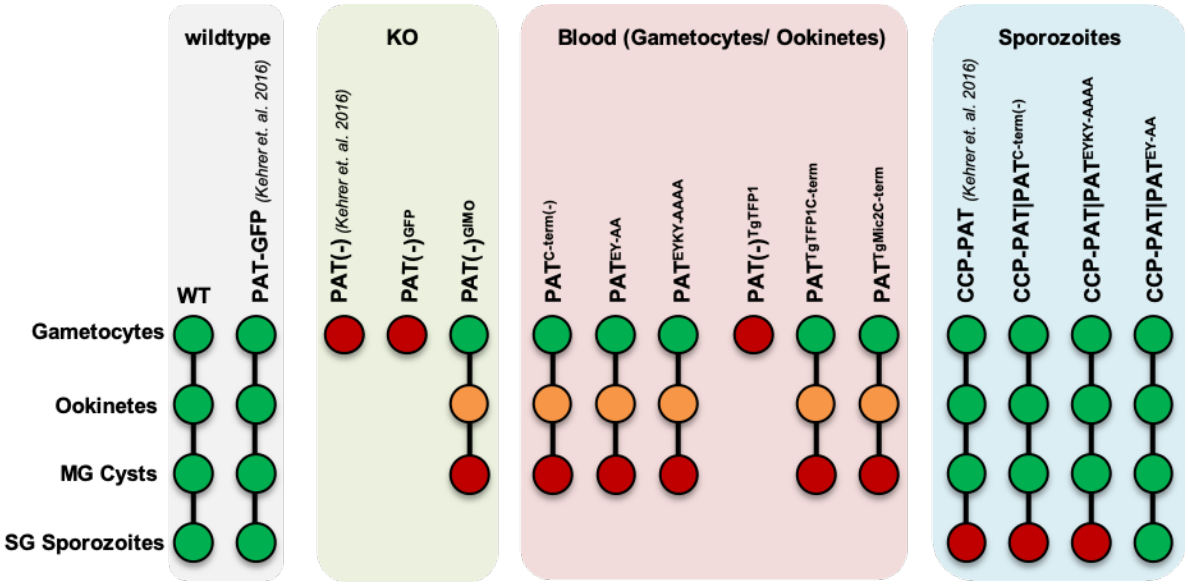

Figure 3.3.6 Phenotypic summary of PAT mutants

Cartoon summarizing all the generated PAT mutants with their respective phenotypes in gametocytes, ookinetes, cysts and sporozoites. For better visualization, mutants are classified according to their expression in the blood and in sporozoites as well as wildtype and complete gene deletion (KO). Green - no phenotype; orange- impaired; red – completely blocked.

PAT localization and vesicle secretion

Comparing the localization of wild-type PAT-GFP (Kehrer, Singer, et al., 2016) with the localization of $PAT^{EY\text{-}AA}$ and $PAT^{EYKY\text{-}AAAA}$ in gametocytes and ookinetes as well as salivary gland sporozoites, revealed no significant differences in protein localization patterns in gametocytes and ookinetes. I still observed a speckled pattern similar to egress vesicles in gametocytes and micronemes in ookinetes while PAT(-) parasites expressing only GFP under the endogenous promoter appeared purely cytoplasmic (Figure 3.3.2 E). Therefore, the C-terminal motifs are essential for PAT function in ookinetes but not per se important for protein trafficking to the vesicles as described for *T. gondii* Mic2 (Di Cristina et al., 2000).

Sporozoites expressing CCP-PAT|$PAT^{C\text{-}term(-)}$ and CCP-PAT|$PAT^{EYKY\text{-}AAAA}$ were unable to efficiently colonize salivary glands. Crucially, in both mutants, the GFP signal was localized to micronemes but absent on the plasma membrane of sporozoites (Figure 3.3.5). This absence on the plasma membrane indicates a disruption in microneme secretion. Consequently, this indicates a failure of the sporozoite to attach, move and invade. On the other hand, CCP-PAT|$PAT^{EY\text{-}AA}$ sporozoites, which were able to invade salivary glands, displayed a signal in micronemes as well as on the plasma membrane.

Given that PAT is anchored in the membrane of micronemes with the C-terminus facing the cytoplasm of sporozoites, (Kehrer, Singer, et al., 2016) these results strongly suggest that the PAT C-terminus is involved in protein interactions crucial for microneme secretion. Therefore, these results propose that the PAT C- terminus might play a role in protein interactions required for microneme secretion. In *T. gondii* tachyzoites DOC2.1 facilitates membrane fusion of micronemes as the absence of DOC2.1 resulted in a failure of microneme secretion (Farrell et al., 2012). Interestingly, downregulation of DOC2.1 in *P. falciparum* blood stage parasites showed a strong effect on merozoite invasion but not merozoite egress (Farrell et al., 2012). This might explain our observed differences between gametocyte egress and the function in ookinetes and sporozoites. Alternatively, the PAT C-terminus could also be involved in recruiting proteins needed for vesicle fusion to micronemes as shown for the *T. gondii* orthologue TgTFP1 (Hammoudi et al., 2018).

Generation and phenotype of PAT(-)^{GIMO} parasites

The creation of the receiver line PAT(-)^{GIMO}, using the same homology regions employed for the generation of the previously described PAT(-) parasites (Kehrer, Singer, et al., 2016), has yielded a surprisingly distinct phenotype. While PAT(-) parasites showed a phenotype during gametogenesis PAT(-)^{GIMO} parasites efficiently formed ookinetes which were, however, unable to cause mosquito infections. Replacing the GIMO selection cassette with GFP in contrast showed again a phenotype in gametocytes not leading to the formation of ookinetes.

Another existing study deleting *P. berghei* PAT as part of a screen to assess the function of a group of orphan membrane transporters confirms the protein to play a role during gametogenesis (Kenthirapalan et al., 2016). Deletion of PAT in *P. yoelii* parasites however lead to the formation of ookinetes not able to cause mosquito infections reflecting the phenotype of PAT(-)^{GIMO} parasites (Hart et al., 2014). Notably, deletion of PAT in *P. falciparum* parasites was unsuccessful (Augagneur et al., 2013).

Closer examination of the generation process for the various parasite lines suggests a potential influence of the selection cassette on the phenotype during gametogenesis. PAT(-) parasites feature a selection cassette comprising TgDHFR/TS driven by the PbDHFR/TS promoter. Notably, PAT(-)^{GIMO} parasites and *P. yoelii* parasites lacking PAT both incorporate hDHFR, propelled by the bi-directional ef1a promoter, inserted in the opposite direction to the endogenous gene. In contrast, PAT(-)^{GFP} parasites do not carry any selection cassette. The bidirectionality of the ef1a promoter raises the possibility of an impact on transcription on adjacent regions of the inserted locus, a phenomenon previously observed when inserting a sequence into a silent chromosome 12 locus (Klug et al., 2016). Yet how the ef1a promoter exactly influences the PAT locus still needs to be determined.

3.4. Functional characterization of concavin

PBANKA_1422900 (later named concavin), was identified as part of the sporozoite secretome (see section 3.1). Using BlastP, I found that PBANKA_1422900 is conserved among *Plasmodium* spp.. It shares 96% identity with its ortholog in *P. yoelii* and 76% and 80% with its orthologs in *P. falciparum* and *P. vivax*, respectively (Figure 3.4.1 A). The protein consists of 393 aa and does not contain any annotated motifs such as signal peptide (SP) or transmembrane domains (TMD). However, the protein contains an N-terminal cysteine which could eventually be post translational modified, for example via palmitoylation (Figure 3.4.1 B). RNAseq data obtained through plasmodb.org shows a peak expression in ookinetes and sporozoites (Figure 3.4.1 C). Using the DeepLoc Algorithm (www.cbs.dtu.dk/services/DeepLoc-1.0/) the protein is predicted to be soluble with a probability of 86% (Figure 3.4.1 D). The proposed hierarchical tree envisages that the protein enters the non- secretory pathway, localizing within the cytoplasm (Figure 3.4.1E).

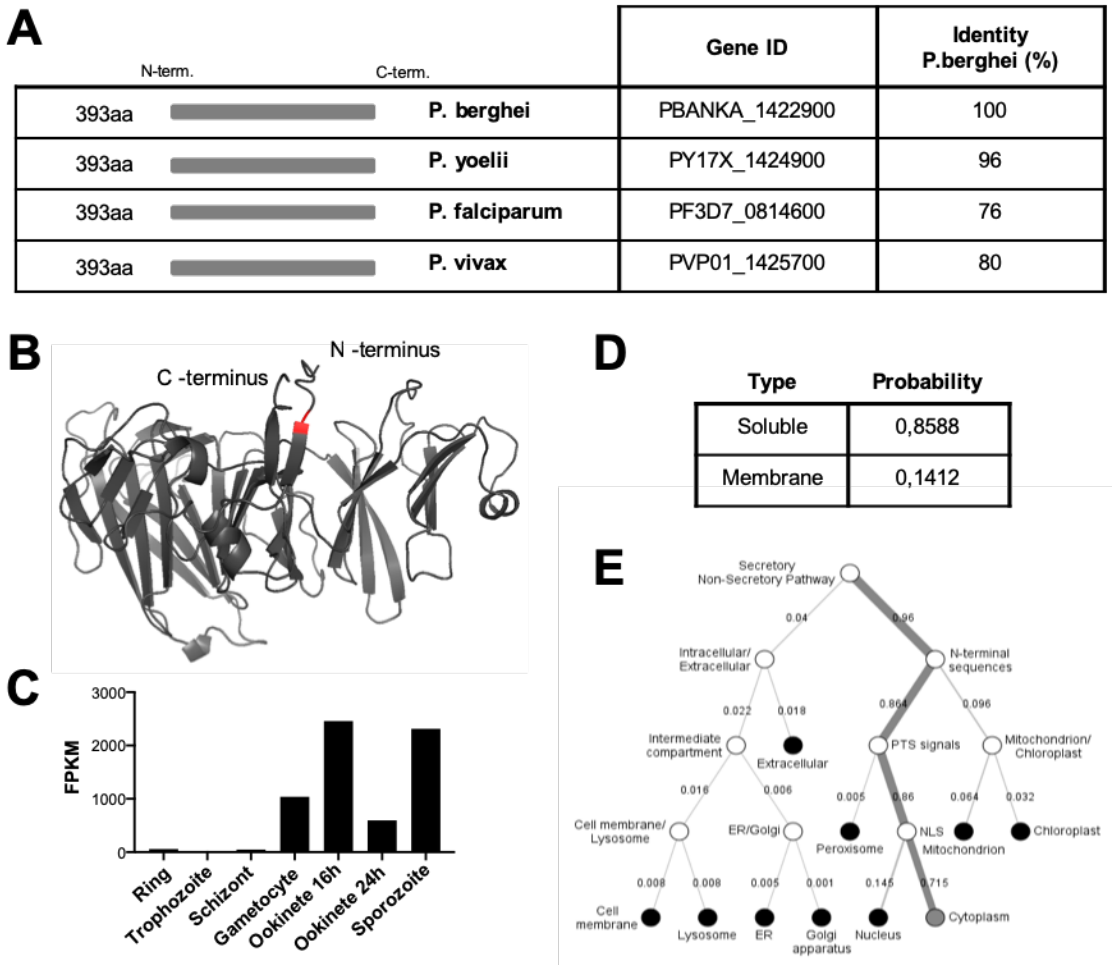

Figure 3.4.1 Concavin is conserved among Plasmodium species

(A) Protein sequences of Concavin within *Plasmodium* spp. from protein length to sequence identity. **(B)** Alphafold2 structure prediction of concavin. The N-terminal cysteine is highlighted in red. **(C)** Transcriptome data of the different PBANKA_1105300 life cycle stages shows peak expression in ookinetes (Otto et al 2014; Lindner et al 2013). **(D)** Localization probability to membranes. **(E)** The DeepLoc decision tree proposes a localization in the cytoplasm. Figure modified from (Kehrer et al., 2022).

PbANKA_1422900 (-) sporozoites are deformed

To characterize the function of PbANKA_1422900 in more detail, I generated a *P. berghei* parasite line lacking the gene by replacing its open reading frame (ORF) against a standard yfcu/ hDHFR containing selection cassette via double homologous recombination (see Material and Methods). This allowed for positive selection of the parasites with pyrimethamine and subsequent negative selection with 5-fluorocytosine to recycle the selection cassette needed for follow up modifications of the locus.

The obtained isogenic parasites developed normally in the blood. Wild type as well as mutant parasites grew with a multiplication rate of around 10 (Figure 3.4.2A). Furthermore, gametocyte to ookinete conversion as well as ookinete morphology and speed did not show any significant differences to wild type. As a result, parasites lacking the gene were able to cause regular infections in *Anopheles stephensi* mosquito midguts (Figure 3.4.2B-E).

In isolated salivary glands I observed a significant proportion of deformed sporozoites. While some sporozoites retained their characteristic “banana- shape” others seemed to round up from the back of the cell until they became completely round (Figure 3.4.2F). A more detailed quantification of the sporozoites' cell shapes between day 12 and 28 post mosquito infection revealed a decrease of normally shaped cells over time while the amount of deformed and round cells increased during sporozoite maturation. At least 80% of sporozoites isolated from midguts on day 12 and 14 and hemolymph on day 16 were normally shaped, but more than 50% of salivary gland sporozoites isolated on day 28 appeared completely round (Figure 3.4.2G). Due to the phenotype of the mutant parasites we named the protein concavin (as the concave-convex polarity of the parasite was lost). Hence concavin, instead of PbANKA_1422900, will be used from here onwards.

For further characterization, I next activated isolated salivary gland sporozoites lacking concavin with 3% BSA in RPMI medium to observe their motility. Sporozoites lacking concavin imaged over a period of 3 min with a frame rate of 3 s, were still able to move. Whereas normally formed sporozoites moved in a circular manner with a speed similar to wild type sporozoites, deformed sporozoites moved significantly slower and possessed an irregular movement pattern (Figure 3.4.2H-I). Completely rounded sporozoites showed no movement at all.

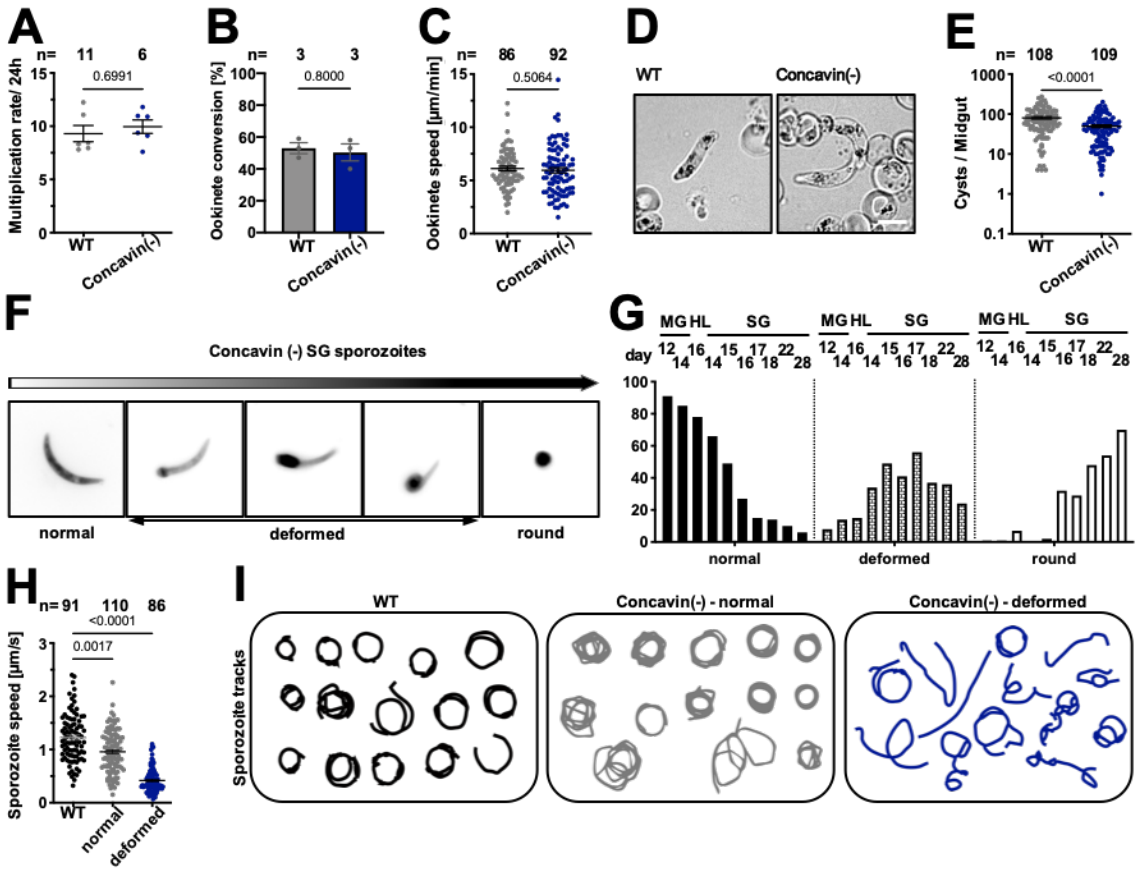

Figure 3.4.2 Deletion of concavin leads to deformed salivary gland sporozoites

(A) Multiplication rate of *concavin(-)* parasites and wild type in the blood. Data points represent parasites growing in individual mice. P-value is calculated using the Mann Whitney test. Shown is the mean +/- SEM. **(B)** Gametocyte to ookinete conversion of *concavin(-)* and wild type parasites. P-value is calculated using the Mann Whitney test. Shown is the mean +/- SEM. **(C)** Ookinete speed of concavin(-) parasites and wild type ookinetes. P-value is calculated using the Mann Whitney test. Shown is the mean +/- SEM. Each data point represents the speed of an individual ookinete from 3 independent experiments. **(D)** Ookinete shape of wild type and *concavin(-)* parasites. Scale bar: 5µm. **(E)** Oocyst development between d12-17 post infection. Data points represent individual midguts. P-value is calculated using the Mann Whitney test. Shown is the mean +/- SEM. **(F)** Images of sporozoites rounding up over time. **(G)** Quantification of sporozoite rounding up over time in the midgut, hemolymph and salivary gland. Sporozoites were classified as either normal, deformed or round. **(H)** Speed of salivary gland sporozoites imaged with a frame rate of 3 s. Data points represent individual sporozoites. P-values are calculated using the Kruskal Wallis test followed by Dunns multiple comparison. **(I)** Selected trajectories of manually tracked sporozoites. Experiments jointly done with Danny Baltissen. Figure taken from (Kehrer et al., 2022).

Surprisingly, infection of *A. gambiae* mosquitoes with *concavin(-)* parasites showed a significant difference in oocyst numbers compared to wild type. Quantification of the sporozoite shape of parasites isolated from *A. gambiae* mosquitoes however showed the same phenotype. In sporozoites isolated from midguts nearly 100% of sporozoites were normally shaped while in sporozoite populations isolated from salivary glands on day 15 and 17 I clearly detected deformed as well as round parasite forms (Figure 3.4.3 A).

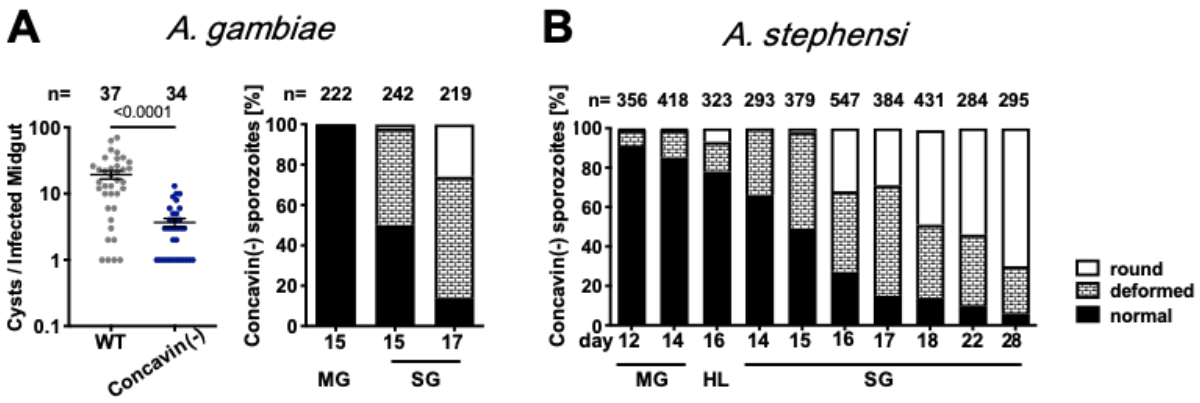

Figure 3.4.3 Reduced infection of *Anopheles gambiae* mosquitoes

(A) Oocyst development of wild type and *concavin(-)* parasites in *A. gambiae* mosquitoes. Data points represent individual midguts observed between d12-17 post infection (left). Quantification of sporozoite forms in the midgut and the salivary gland at indicated time points. **(B)** Quantification of sporozoite forms in the midgut, the hemolymph and the salivary gland at indicated time points in *A. stephensi* infections. Please note that this are the same data points as shown in Figure 3.4.2 G. Figure taken from (Kehrer et al., 2022).

Concavin is located at the periphery of sporozoites

To determine the localization of concavin and to rescue the phenotype observed after gene deletion to exclude any off-target effects I generated two additional parasite lines expressing *P. berghei* concavin as well as the *P. falciparum* orthologue fused to GFP. To achieve this, I initially utilized negative selection to recycle the resistance cassette in *concavin(-)* parasites (Braks et al., 2006). Subsequently, I reintroduced the corresponding sequences, as outlined in the materials and methods section, leading to the generation of the parasite lines *concavin(-)*$^{Pbconcavin\text{-}gfp}$ and *concavin(-)*$^{Pf3D7concavin\text{-}gfp}$. Both parasites lines completed the life cycle similar to wild type, indicating that both parasite lines with restored proteins are fully functional (Figure 3.4.4 A-C).

I detected concavin-GFP in gametocytes, ookinetes, sporozoites, and liver stages, but it was absent in asexual blood-stage parasites (Figure 3.4.4 D-E). In gametocytes, the protein showed a cytoplasmic localization (3.4.4 D). However, in ookinetes and salivary gland-derived sporozoites, concavin-GFP localized to the periphery. A localization of the protein towards the periphery of the parasite could possibly localize to either the sub-pellicular network, the IMC, the supra-alveolar space or the plasma membrane (Bane et al., 2016; Khater et al., 2004). For a more precise understanding of concavin-GFP localization, I next fixed concavin(-)$^{Pbconcavin\text{-}gfp}$ sporozoites on glass slides and labelled them with anti-GFP antibodies with or without membrane permeabilization. In case of a GFP localization at the surface of the plasma membrane we would already detect a fluorescence signal without the need of permeabilization. Yet, detection of

concavin-GFP occurred solely after permeabilization, indicating an internal protein localization (Figure 3.4.4 F).

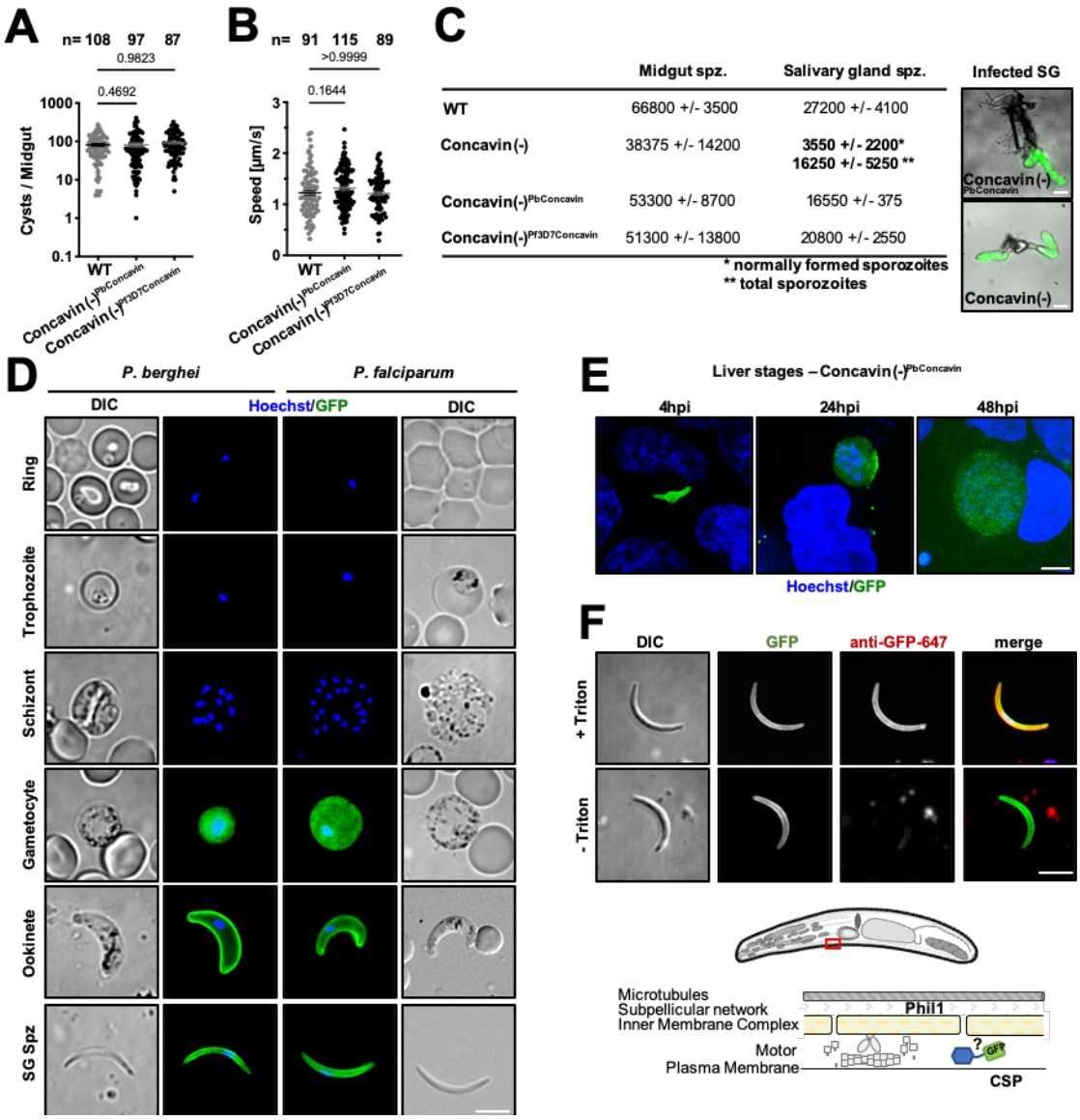

Figure 3.4.4 Concavin-GFP localizes to the periphery of ookinetes and sporozoites

(A) Oocyst development of *concavin(-)*$^{Pbconcavin\text{-}gfp}$ and *concavin(-)*$^{Pf3D7concavin\text{-}gfp}$ parasites. Data points represent individual midguts observed between d12-17 post infection. Shown is the mean with SEM. P-values are calculated using the Kruskal Wallis test followed by the Dunns multiple comparison test. (B) Average speed of salivary gland sporozoites imaged with a frame rate of 3 s. Data points represent individual sporozoites. Shown is the mean with SEM. P-values are calculated using the Kruskal Wallis test followed by the Dunns multiple comparison test. **(C)** Sum table of Mosquito infections of wild type, *concavin(-)*, *concavin(-)*$^{Pbconcavin\text{-}gfp}$ and *concavin(-)*$^{Pf3D7concavin\text{-}gfp}$ counted on d17 post mosquito infection. For each counting at least 20 mosquitos were dissected. Please note for *concavin(-)* parasites only normally shaped sporozoites were counted. **(D)** *concavin(-)*$^{Pbconcavin\text{-}gfp}$ and *concavin(-)*$^{Pf3D7concavin\text{-}gfp}$ localization in blood and mosquito stages. Nuclei (blue) are stained with Hoechst. Scale bar 5µm. **(E)** Localization of *concavin(-)*$^{Pbconcavin\text{-}gfp}$ in liver stages. Nuclei (blue) are stained with Hoechst. Scale bar 5µm. **(F)** Immunofluorescence images of permeabilized and unpermeabilized concavin-GFP salivary gland sporozoites stained with an anti-GFP antibody. A GFP signal could only be detected after permeabilization, excluding concaving localization on the parasite surface. Scale bar 5µm. Figure taken from (Kehrer et al., 2022).

Concavin-GFP is mobile and associated with CSP at the plasma membrane

To test if concavin-GFP is associated with the inner membrane complex (IMC) or the mobile plasma membrane (PM), I photo- bleached the GFP signal and monitored the recovery of the signal over time (FRAP). To this end, I bleached the fluorescence signal of moving concavin-GFP sporozoites imaged with a frame rate of 1 s at a defined spot with 100% laser power of a 405 nm laser. Manual quantification of the GFP signal before and after photo-bleaching showed a clear recovery of the fluorescence, hinting towards a localisation reminiscent to the plasma membrane associated protein CSP. Most proteins connected with the IMC in contrast do not recover (Kehrer et al., 2022).

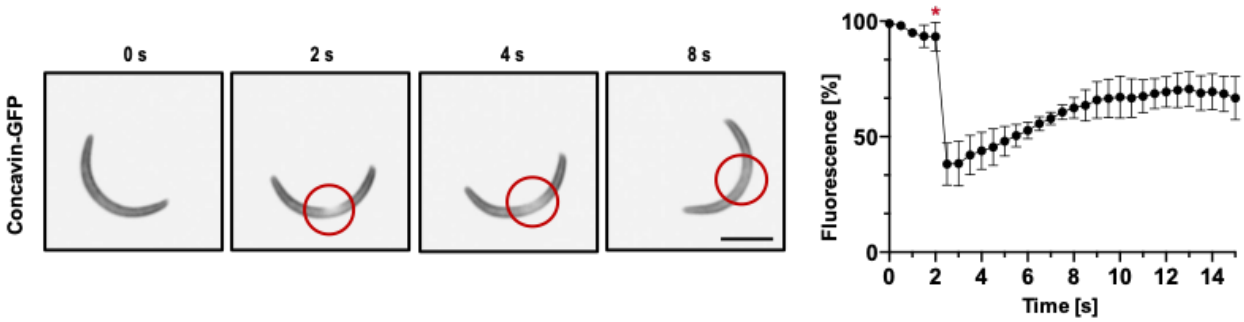

Figure 3.4.5 Concavin-GFP recovers after photo- bleaching

Time series of moving concavin-GFP sporozoites before and after bleaching. The fluorescence signal of three independent sporozoites was quantified over time. Shown is the mean ± SEM. * indicates time of bleaching. Scale bar: 5µm. Experiment jointly done with Chris Lance. Figure taken from (Kehrer et al., 2022).

To confirm this hypothesis, I next implemented super-resolution STED microscopy to explore and quantify the distance between the IMC protein PHIL1 fused to GFP and the plasma membrane protein CSP as well as concavin- GFP and CSP. I made use of a PHIL1-GFP parasite line generated by Mendi Muthinja during the course of her PhD project (J. M. Muthinja, 2017) and performed antibody staining's using anti-GFP combined with anti- rabbit Atto 594 and anti CSP antibodies combined with anti-mouse Atto 647 respectively. In parallel, I performed the same experimental setup using concavin- GFP sporozoites.

As control and to exclude bleed through of Atto 594 into the Atto 647 channel I also stained PHIL1-GFP as well as concavin- GFP with the two different colours within the same parasite. This led to overlays that showed very little difference in distance between the two channels (Figure 3.4.6 A-B). In contrast, I observed a clear separation in signals between the anti-GFP staining for PHIL1-GFP and CSP-specific antibodies. Conversely, the concavin-GFP and CSP signals co-localized, hinting that concavin-GFP is situated closer to CSP than the PHIL1 (Figure 3.4.6 C).

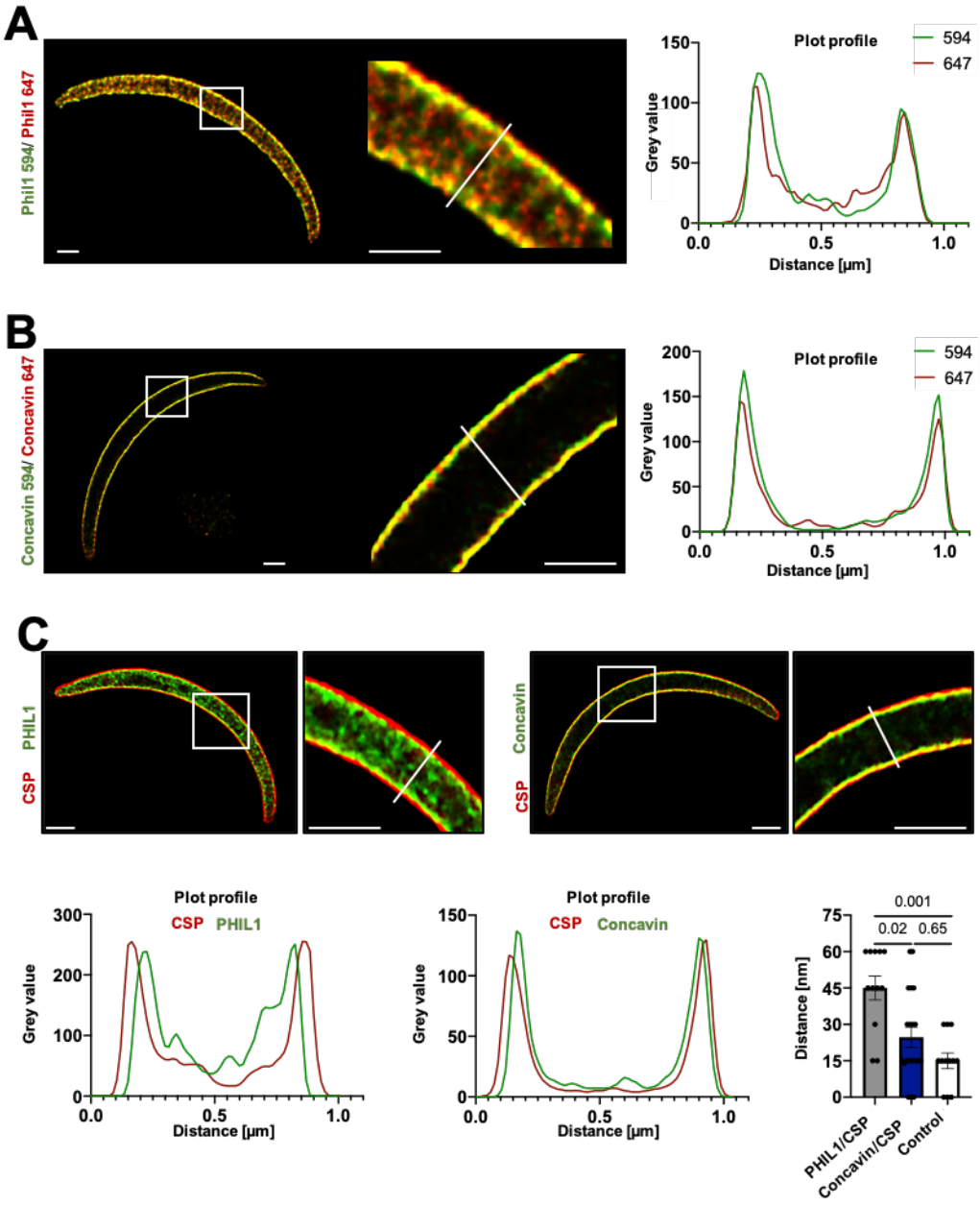

Figure 3.4.6 Concavin-GFP is associated with CSP at the plasma membrane

(A) STED image of a sporozoite expressing Phil1-GFP labelled with an anti GFP antibody in combination with Atto-594 (green) and Atto-647 (red) as control for the quantification of distances and bleed through. Images were deconvolved using the Richardson-Lucy algorithm. The distance between the 2 signals was quantified using the plot profile of the respective channels in Fiji. Measurements and plot profiles are taken at the center of the cell as indicated with the white line. Scale bar: 1 µm. **(B)** STED image of a sporozoite expressing concavin-GFP labelled with an anti GFP antibody in combination with Atto 594 (green) and Atto 647 (red) as control for the quantification of distances and bleed through. Images were deconvolved using the Richardson-Lucy algorithm. The distance between the 2 signals was quantified using the plot profile of the respective channels in Fiji. Measurements and plot profiles are taken at the center of the cell as indicated with the white line. Scale bar: 1 µm. **(C)** STED imaging of PhiL1-GFP and CSP as well as concavin-GFP and CSP. Cells were stained with an anti-GFP antibody in combination with Atto-594 (green) in addition to an anti-CSP staining in combination with Atto-647. Images were deconvolved using the Richardson-Lucy algorithm. The distance between the 2 signal peaks was measured using the plot profile of the respective channels in Fiji. Data points represent distance in individual sporozoites at the center of the cell. P-values are calculated using the Kruskal Wallis test followed by the Dunns multiple comparison test. Scale bar: 1 µm. Figure taken from (Kehrer et al., 2022).

Subsequently, I generated a non-clonal parasite line expressing PHIL1-GFP in the *concavin*(-) parasite via single homologous recombination to further explore the subpellicular network in these parasites (see Material and Methods). PHIL1-GFP localization in this parasite was akin to that of PHIL1-GFP in wild-type blood stage parasites (Kehrer et al., 2022). However, in sporozoites, PHIL1-GFP appeared to be mis-localized due to the altered shape of the sporozoite (Figure 3.4.7). The GFP expression unveiled unexpected signal accumulations. The labeling of microtubules with SiR tubulin and the staining of CSP with anti-CSP antibodies in contrast showed that microtubules as well as the plasma membrane are largely intact and similar to wild type (Figure 3.4.7).

For, a closer inspection of the PHIL1-GFP signal to gain a higher resolution of the deformed sporozoites, I scrutinized sporozoite-containing salivary glands using transmission and scanning electron microscopy. I fixed intact salivary glands isolated from infected mosquitoes in 4% PFA whereas the complete sample preparation as well as the imaging was performed by Charlotta Funaya and Sebastian Weber. The analysis showed that the IMC was still subtending the plasma membrane in wild-type sporozoites (Figure 3.4.8 A). In deformed *concavin(-)* sporozoites however, the IMC was partially detached from the plasma membrane and extended into the sporozoite cytoplasm Figure 3.4.8 B/ C).

Using array tomography (as described in (Araki et al., 2020; Horstmann et al., 2012)), we reconstructed the serial sections of an entire rounded *concavin(-)* sporozoite. This revealed a tube-like 'rolled up' structure separating the IMC from the remaining plasma membrane (Figure 3.4.9 A,B). Hence, the IMC remained intact but detached from the underlying plasma membrane.

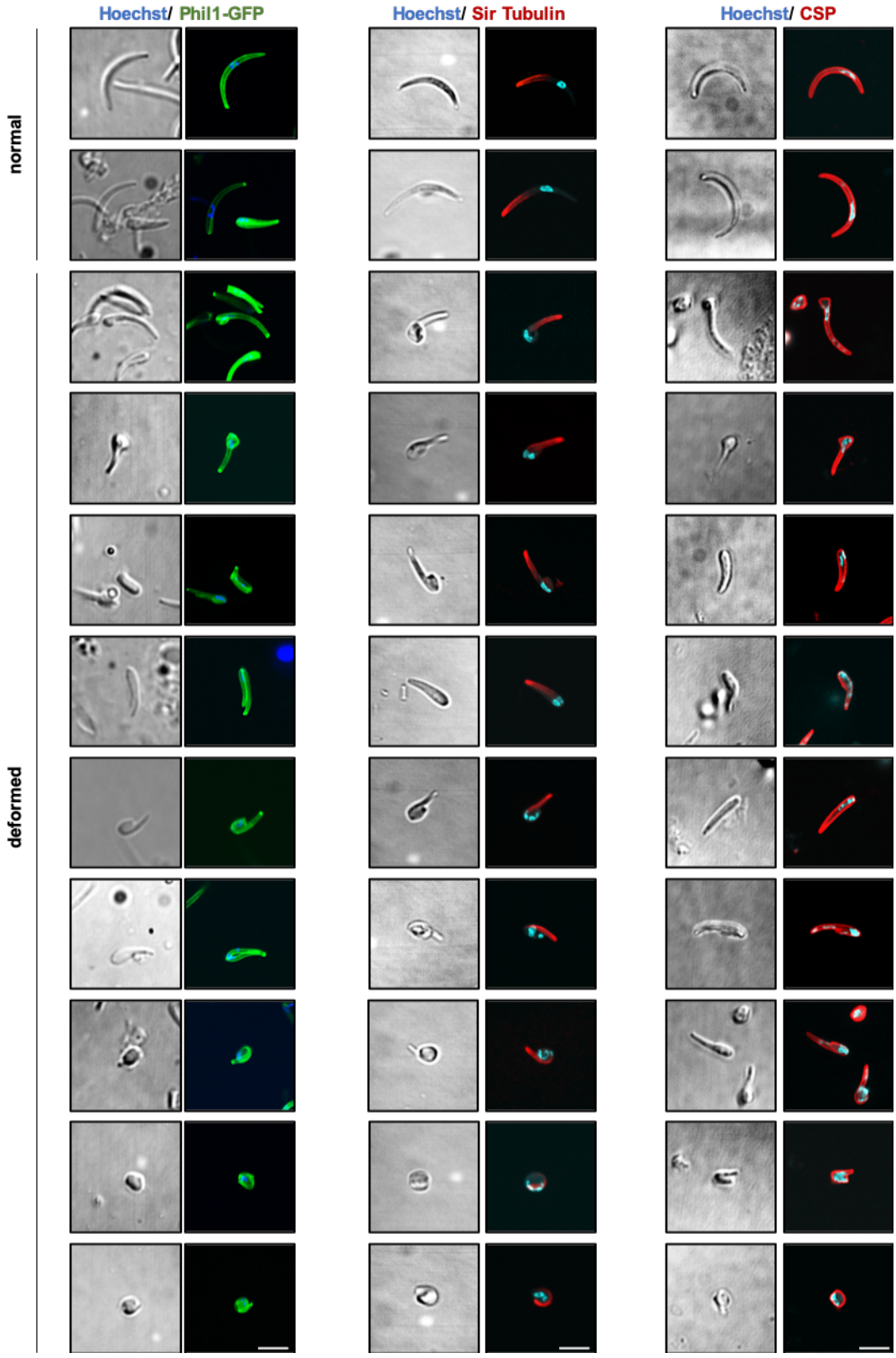

Figure 3.4.7 Image gallery of *concavin(-)* parasites stained with Phil1-GFP, Sir Tubulin and CSP.

Exemplary images taken with a spinning disc confocal microscope of normal and deformed *concavin(-)* sporozoites stained with hoechst in combination with Phil1-GFP (left), Hoechst with Sir Tubulin (middle) and Hoechst with anti CSP (right). Scale bar: 5µm. Figure taken from (Kehrer et al., 2022).

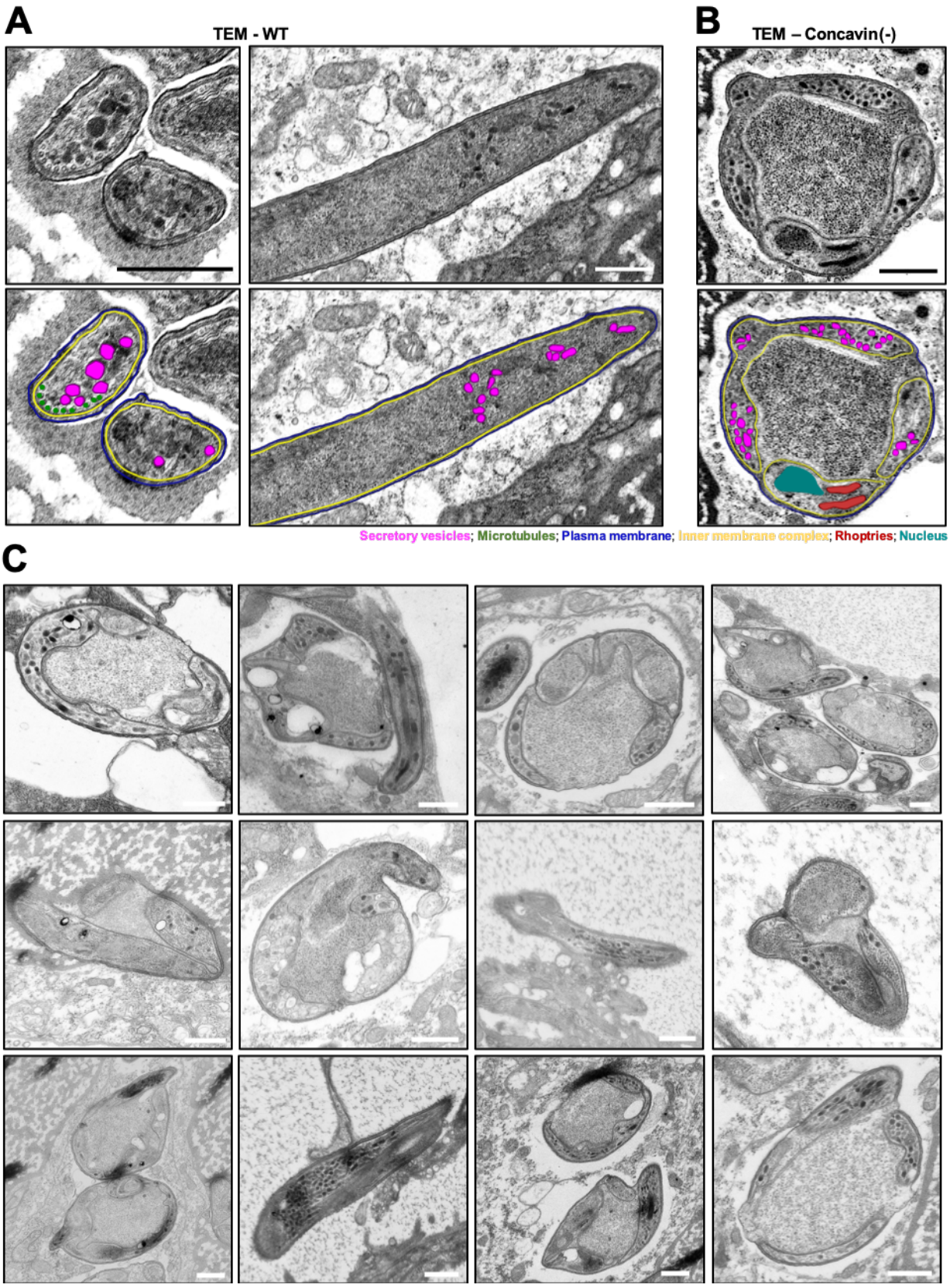

Figure 3.4.8 Cytoplasmic IMC extensions in concavin(-) sporozoites.

(A) Transmission electron micrographs of wild type sporozoites with secretory organelles in magenta, IMC in yellow and plasma membrane in blue. **(B)** Transmission electron microscopy of *concavin(-)* sporozoites with secretory organelles in magenta, IMC in yellow, plasma membrane in blue, rhoptries in red and nucleus in turqoise. **(C)** 700nm serial section of normal (right) and deformed (left) *concavin(-)* sporozoites. Scale bars: 500nm. Electron microscopy was done by Charlotta Funaya and Sebastian Weber. Images taken from (Kehrer et al., 2022).

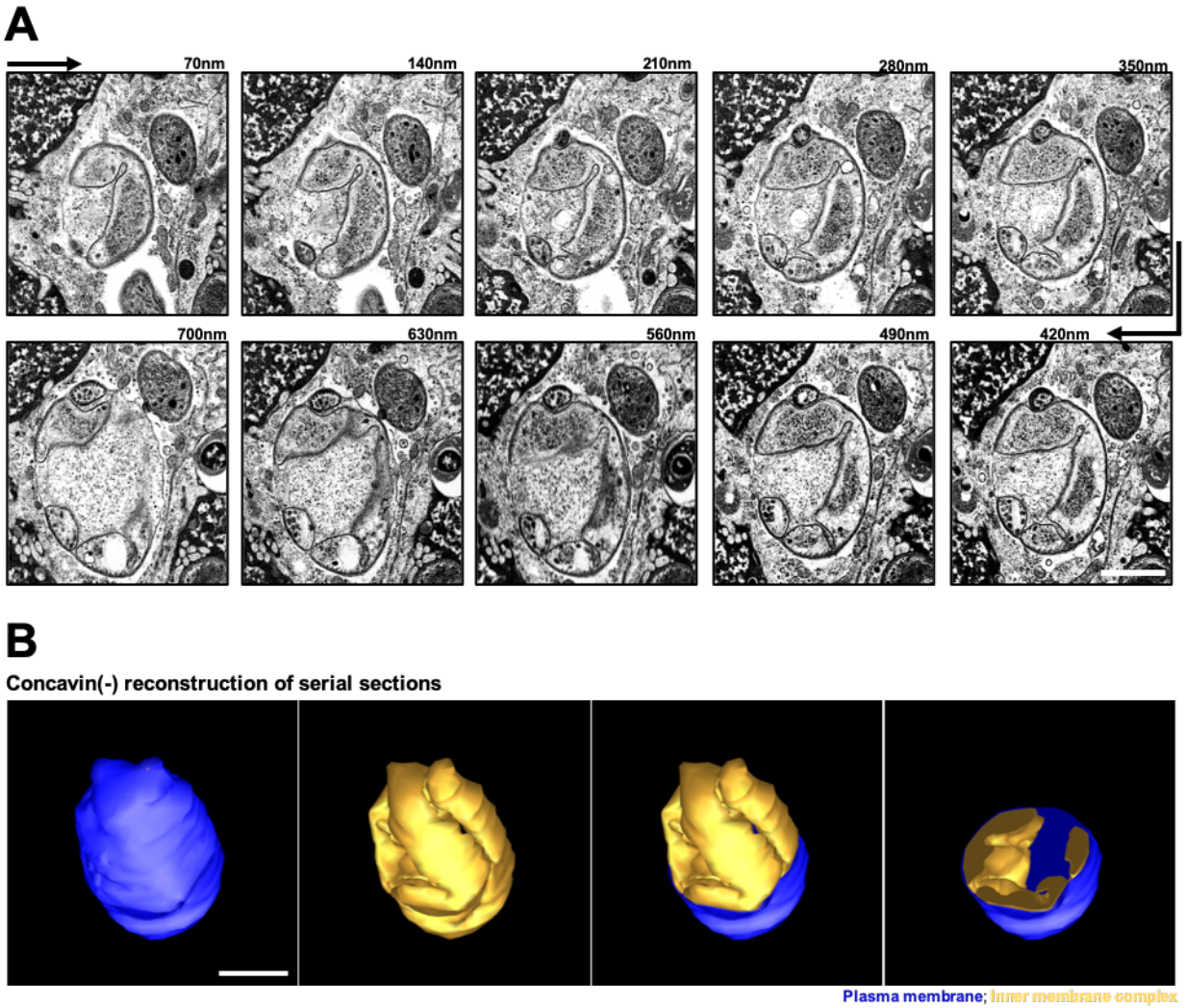

Figure 3.4.9 Cytoplasmic IMC extensions in *concavin(-)* sporozoites.

(A) Exemplary SEM serial sections of a deformed sporozoite. Scale bar 500nm. **(B)** Reconstruction of SEM serial sections of a complete rounded up *concavin(-)* sporozoite; plasma membrane is shown in blue and IMC in yellow. Scale bar 1µm. Electron microscopy was done by Charlotta Funaya and Sebastian Weber. Figure taken from (Kehrer et al., 2022).

Mutation of a potential palmitoylation site at the N-terminus does not fully complement the KO

Palmitoylation is a type of protein post-translational modification that involves the addition of a palmitoyl group to cysteine residues. This modification increases the hydrophobicity of proteins, enabling them to associate more strongly with cellular membranes.

In the case of concavin, sequence analysis revealed the presence of a cysteine residue at position 7 of the protein's N-terminus (see Appendix), a location that is commonly associated with palmitoylation. In order to explore the potential role of palmitoylation in concavin function, I generated a complemented parasite line expressing a mutated version of concavin, concavin$^{C7A\text{-}GFP}$ (see Material and Methods). In this mutant, the cysteine residue at position 7 was replaced with alanine, preventing palmitoylation (Figure 3.4.10 A). I found that concavin$^{C7A\text{-}GFP}$ displayed a cytoplasmic signal in gametocytes and was absent in asexual stages similar to wild type concavin-GFP parasites (Figure 3.4.10 B). The parasite line produced oocyst numbers comparable to wild type infections (Figure 3.4.10 C). However, oocyst and salivary gland derived sporozoites quantified between day 13 and 22 post mosquito infection showed that over 80% of sporozoites maintained their normal shape (Figure 3.4.10 D). Only a small number of sporozoites were completely rounded, while 5-20% of sporozoites showed a rounded proximal end or rounded off around the nucleus. The normally shaped sporozoites moved in a wild type manner, while deformed sporozoites moved at a reduced speed (Figure 3.4.10 E).

These results suggest that palmitoylation is not essential for concavin function only, but most likely contributes to it. Furthermore, concavin$^{C7A\text{-}GFP}$ showed a peripheral localization in both normally shaped and slightly rounded sporozoites, indicating that the mutation did not affect its localization (Figure 3.4.10 F). Interestingly, the GFP signal in this line resembled the signal obtained by anti-CSP antibodies in concavin(-) sporozoites, suggesting once more that concavin$^{C7A\text{-}GFP}$ localizes to the plasma membrane rather than the IMC.

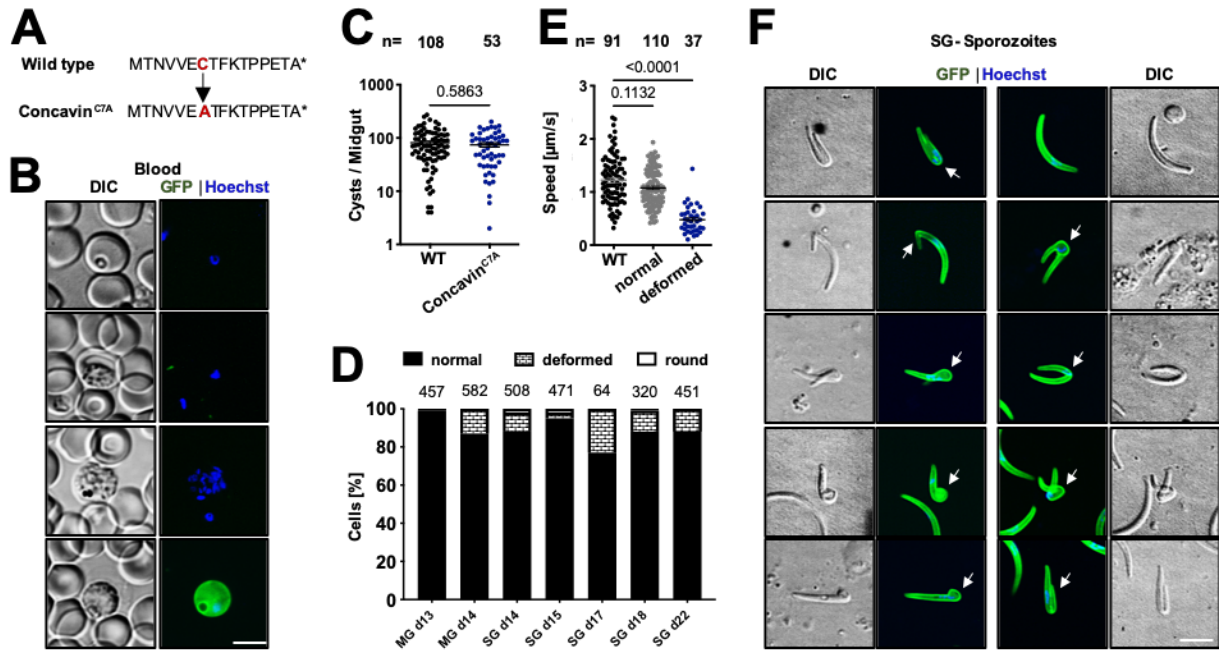

Figure 3.4.10 Impact of potential palmitoylation site in concavin^{C7A} parasites

(A) Cysteine 7 is predicted to be palmitoylated and was changed into alanine in the concavin^{C7A}-GFP mutant. **(B)** Expression and localization of concavin^{C7A} in blood stage parasites. **(C)** Oocysts number in infected mosquitoes. Data points represent individual midguts observed between d12-17 post infection. Shown is the mean ± SEM. P-values is calculated using the Mann Whitney test. **(D)** Quantification of concavin_C7A-GFP sporozoite cell shapes at the indicated days from midguts (MG) or salivary glands (SG). Numbers above bars indicate investigated sporozoites. (E) Average speed of salivary gland sporozoites. Data points represent individual sporozoites. Shown is the mean ± SEM. P-values are calculated using the Kruskal Wallis test with the Dunns multiple comparison test. **(F)** Localization of concavin^{C7A}-GFP in normal and deformed sporozoites. Scale bar: 5 µm. Figure taken from (Kehrer et al., 2022).

Concavin is essential for parasite transmission but not liver-stage development

To assess whether the deformed sporozoites could still transmit malaria to mice, a group of ten *A. stephensi* mosquitoes infected with either wild-type or *concavin(-)* parasites were allowed to bite C57BL/6 mice, which are highly susceptible to *P. berghei* infections. All control mice bitten by wild-type infected mosquitoes developed a blood stage infection starting three days post infection (Figure 3.4.11 A,B). However, only eight out of twelve mice bitten by mosquitoes infected with *concavin(-)* parasites became infected, and the development of the blood stage infection was delayed by over one day compared to wild-type controls, resulting in a 90% loss of infectivity (Figure 3.4.11 A,B). Notably, mice infected with 10,000 *concavin(-)* sporozoites via intravenous injection did not show any differences compared to the wild-type (Figure 3.4.11 A,B).

To investigate whether the deformed sporozoites could still invade host cells, an infection experiment was performed using cultured HeLa cells, which are as susceptible to *P. berghei* infection as hepatocytes. Although the first three independent experiments showed that wild-type

parasites had a higher percentage of cell invasion than *concavin(-)* parasites, a fourth experiment lowered the level of statistical confidence. Nevertheless, it was found that the deformed parasites could enter host cells, although the *concavin(-)* parasites likely entered at an overall lower rate than wild-type parasites (Figure 3.4.11 C). Liver-stage development of *concavin(-)* parasites did not differ from wild-type parasites (Figure 3.4.11 D).

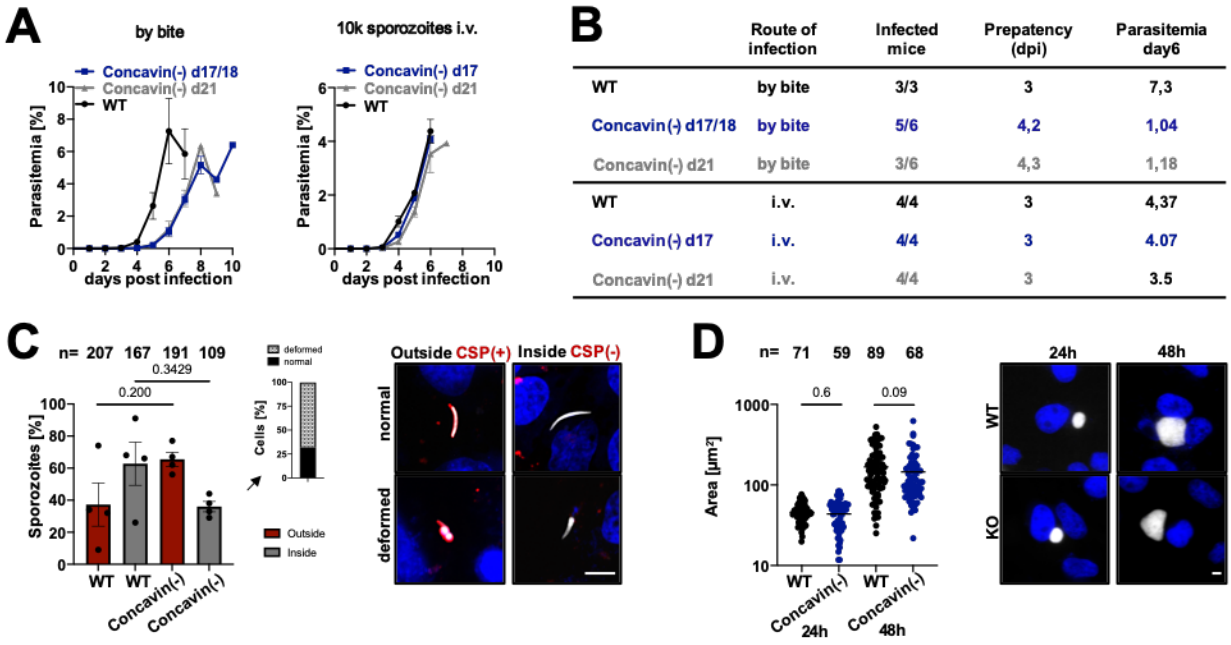

	Route of infection	Infected mice	Prepatency (dpi)	Parasitemia day6
WT	by bite	3/3	3	7,3
Concavin(-) d17/18	by bite	5/6	4,2	1,04
Concavin(-) d21	by bite	3/6	4,3	1,18
WT	i.v.	4/4	3	4,37
Concavin(-) d17	i.v.	4/4	3	4.07
Concavin(-) d21	i.v.	4/4	3	3.5

Figure 3.4.11 Concavin is essential for efficient transmission between mosquito and host

(A) Growth curve of parasites in C57BL6 mice infected by the bite of 10 mosquitoes within 15.min. Shown is the mean with SEM. **(B)** Sum table of infected mice with respective pre-patency period and parasitemia on day 6. **(C)** Liver cell invasion assay of concavin-gfp and *concavin(-)* parasites. Parasites are positively stained for CSP in case they remain extracellular. Both, normal and deformed parasites were detected intracellular. Quantification of CSP positive (red) and negative (grey) sporozoites is shown in the graph. Data points represent individual experiments. Shown is the mean with SEM. P- values are calculated using the Mann Whitney test. Scale bar 5µm. **(D)** Liver stage development of wildtype CS-mCherry (WT) and concavin(-) HSP70-GFP (KO) parasites 24h and 48h post invasion. Shown is the mean with SEM. P-values are calculated using the Mann Whitney test. Scale bar: 5µm. Figure taken from (Kehrer et al., 2022).

To investigate the ability of deformed *concavin(-)* sporozoites to enter the narrow salivary ducts of mosquitoes during a bite needed for efficient parasite transmission into the skin, Friedrich Frischknecht and I observed salivating mosquitoes. To do so *concavin(-)* infected mosquitoes were immobilized with super glue on glass slides, and the ejection of sporozoites was observed to directly monitor their shape. The ejection of sporozoites was irregular, but the majority of sporozoites showed a normal crescent shape, thus rounded sporozoites could most likely not efficiently enter and pass through the salivary canals (Figure 3.4.12 A).

To mimic sporozoite movement in the skin intact salivary glands isolated from infected mosquitoes were squeeze between a glass slide and a polyacrylamide gel by Johanna Ripp to test whether sporozoites could migrate through confined spaces. The results showed that deformed sporozoites could not cross the dense matrix of the gel, indicating that they probably could not enter and move through confined spaces such as the salivary canals and the skin (Figure 3.4.12 B).

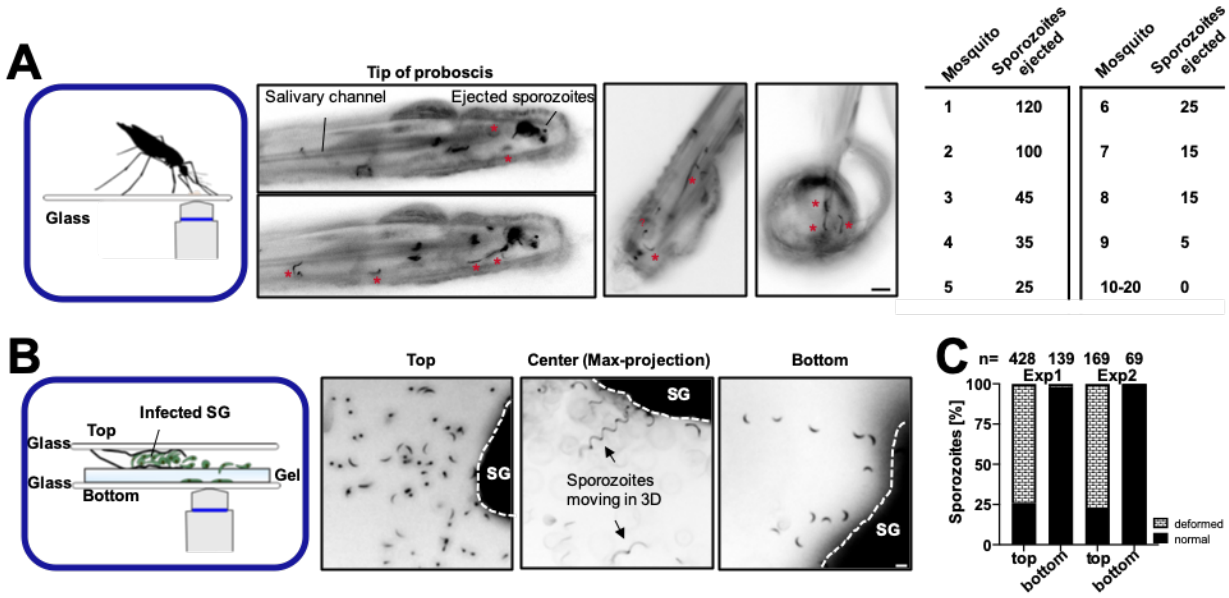

Figure 3.4.12 Concavin is essential for efficient transmission between mosquito and host

(A) Sporozoite ejection of immobilized *concavin(-)* infected mosquitoes on glass slides and quantification of sporozoite numbers. **(B-C)** *Concavin(-)* sporozoites moving on polyacrylamide gels in 3D. In 2 individual experiments only the normal shaped sporozoites were able to migrate through the gel, which mimics the skin phase of infection. Experiments in panel A were performed together with F. Frischknecht and experiments in panels B and C with J. Ripp. Figure taken from (Kehrer et al., 2022).

Disintegration of sporozoites migrating in the skin

To directly test how *concavin(-)* sporozoites migrate in the skin "in vivo" I sent the parasites to the lab of Rogerio Amino at the Institut Pasteur. To investigate parasite transmission and the ability of *concavin(-)* sporozoites to traverse the skin, Pauline Formaglio performed live cell spinning disk microscopy of *concavin(-)*$^{HSP70\text{-}GFP}$ and HSP70-GFP expressing wild type sporozoites transmitted by bite of an infected mosquito into a mouse ear. Mosquitoes were less successful in transmitting concavin(-) than wild type sporozoites. More specifically, fewer mosquitoes transmitted *concavin(-)* sporozoites and at lower numbers. Although precise quantification appeared difficult due to a lower level of fluorescence in the *concavin(-)* sporozoites, it was intriguing to note that 80% of the 90 *concavin(-)* sporozoites observed over 13 different bite sites

appeared to have a normal morphology. This again suggests that fewer abnormal sporozoites pass through the mosquito proboscis during a bite.

Around 20% of *concavin(-)* sporozoites were abnormally shaped from the beginning of the recording, with some being only half as long as normal sporozoites and exhibiting a completely roundish or rounded posterior end. Further analysis of time-lapse series showed that fewer migrating mutant sporozoites progressed through the skin, but they moved at the same speed as wild type parasites. Additionally, fewer blood vessel invasion events were observed in motile micro-syringe inoculated *concavin(-)* sporozoites.

Remarkably, some sporozoites formed a bulky dot at their rear during migration, mostly associated with passing through a narrow stricture. This was indicated by their body constriction and decrease in speed. This round posterior structure sometimes detached as the parasites kept moving forward, resulting in the loss of body integrity or disintegration. Of the 57 migrating *concavin(-)* sporozoites, 32% disintegrated, while 7% exhibited posterior deformation only. Conversely, only 4% of the 54 wild type sporozoites showed disintegration.

This proposes that in their effort to migrate in the skin, around 30-40% of *concavin(-)* sporozoites lose their shape or cellular integrity. Most of those sporozoites stop migrating, while some appear to suffer no impairment for the duration of imaging. Furthermore, around 10% lose their viability as evidenced by the loss of GFP fluorescence. Disintegration most frequently occurred when sporozoites were gliding inside hair follicles, in the upper part of the dermis, or after sustained circular gliding, which is usually associated with cell traversal. This implies that sporozoite disintegration is a consequence of tight interactions between migrating parasites and host cells, either because the sporozoites squeeze themselves between or through cells.

Taken together, our data strongly suggest that normally formed *concavin(-)* sporozoites fail to maintain their shape once transmitted into the skin. This hinders their migration into the salivary ducts and leads to lower levels of transmission. Furthermore, a significant proportion of the transmitted sporozoites lose their cellular integrity and cannot migrate efficiently in the skin, thereby explaining the reduced transmission to the mammalian host.

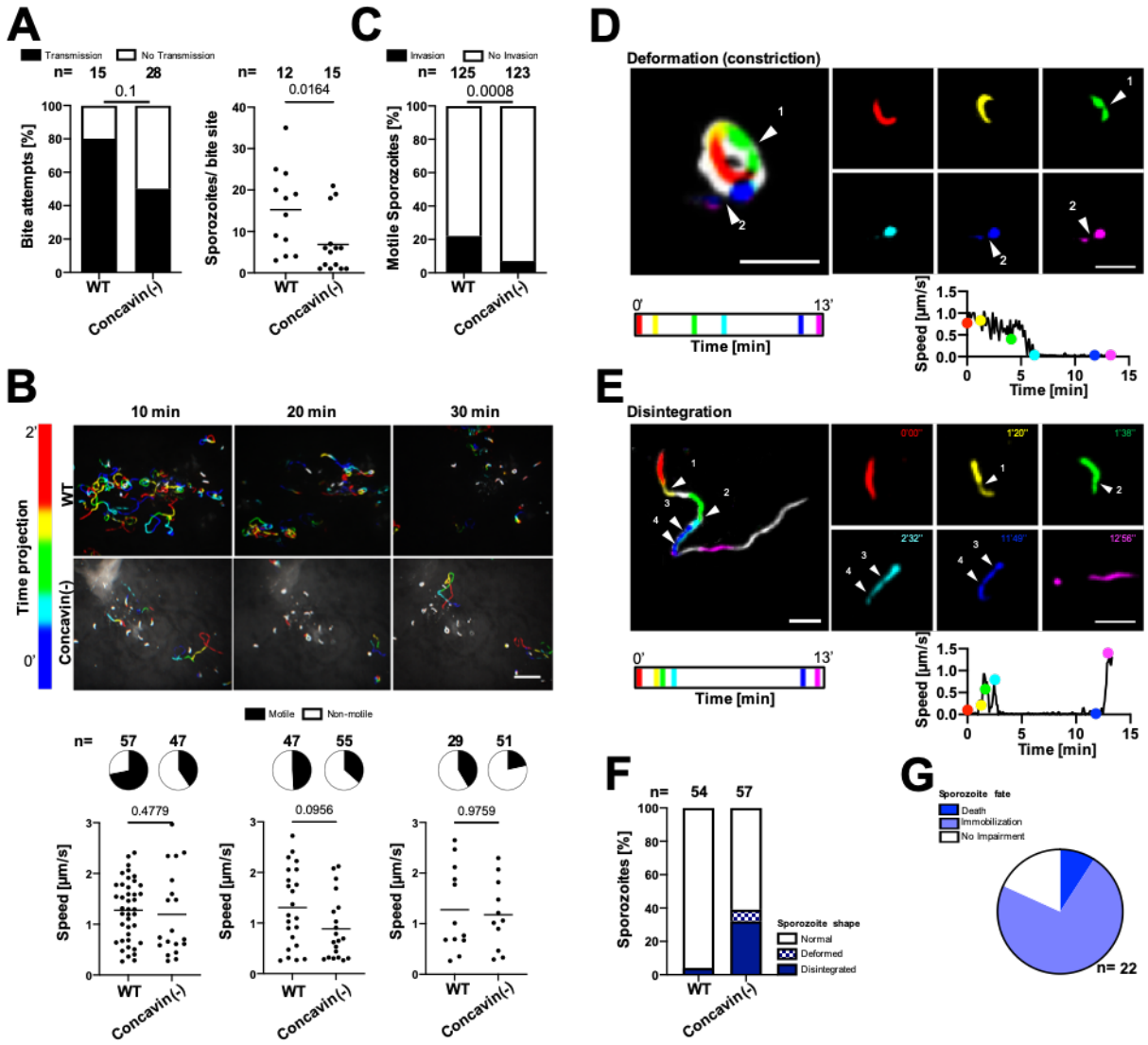

Figure 3.4.13 Migrating *concavin(-)* sporozoites lose their cellular integrity

(A) Percentage of mosquitoes depositing WT or *concavin(-)* sporozoites in the skin of a mouse during a bite (left) and sporozoites deposited during a mosquito bite (right). . P-values are calculated using the Fishers exact test (left) and the Mann Whitney test (right). **(B)** Maximum fluorescence intensity projections encoded by color for time from movies showing migrating sporozoites after mosquito-bite transmission. Graphs and camembert diagrams below show fraction of motile and immotile sporozoites after 10, 20 and 30 minutes of recording, numbers analysed as well as sporozoite speed. Pooled data from 4-5 WT or 5-8 *concavin (-)* bite sites per time point. Scale bar: 50 µm. P-values are calculated using the Mann Whitney test. **(C)** Motile WT or *concavin(-)* sporozoites entering blood vessels during the first hour following micro-injection. Number above bars shows numbers of sporozoites observed. Pooled data from four WT or five *concavin(-)* experiments. P-values are calculated using the Fishers exact test. **(D)** Deformation and **(E)** disintegration of *concavin(-)* sporozoites migrating in the skin. Individual images corresponding to the frames shown on the right are indicated in distinct colors in the maximum projection (left) of 13-min movies. Arrowheads indicate constrictions of the parasites. Graphs below time-lapse show that deformation and disintegration are preceded by a decrease in speed. Color of dots correspond to the time-points displayed in the time-lapse images. Scale bars: 10 µm. **(F)** Percentage of deformation and disintegration events observed in 54 WT and 57 *concavin(-)* sporozoites that were tracked for at least 10 min. Pooled data from 5 WT or 10 *concavin(-)* bite sites. **(G)** Consequence of deformation and disintegration from the 22 sporozoites in F include immobilization and parasite death. Experiments performed and analyzed by P. Formaglio (Institut Pasteur). Figure taken from (Kehrer et al., 2022).

Discussion

Concavin was detected in a proteomic screen of potentially secreted sporozoite proteins and I could show that concavin is expressed in gametocytes, ookinetes and sporozoites. While in gametocytes there is a cytoplasmic signal, in ookinetes and sporozoites the protein clearly localizes to the periphery, reminiscent of CSP.

Concavin(-) parasites round up from their posterior end during sporozoite maturation in the insect vector. While I could already observe a noticeable change in the midgut and the hemolymph of infected mosquitoes, the phenotype becomes significantly more pronounced after salivary gland entry (Figure 3.4.2). This underscores the critical role played by concavin in maintaining the correct shape of sporozoites, which in turn contributes to the efficient transmission of the parasite from the mosquito to the mammalian host.

The deformation of the cells inhibits sporozoite ejection from the narrow salivary canal and reduces their efficient deposition in the skin. However, a small proportion of sporozoites able to keep their shape can still be ejected and transmitted during a bite (Figure 3.4.11 and 3.4.12). Although they are still able to move in the skin similar to wild type parasites they experience more frequent loss of cellular integrity when squeezing through narrow spaces. While moving in the skin the absence of concavin leads to blebbing of the plasma membrane and thus damage of the sporozoites (Figure 3.4.13). The blebbing is most likely caused by external physical forces exerted by the skin. A similar loss of cellular integrity is observed during sporozoite migration in the presence of antibodies targeting the circumsporozoite protein (CSP) (Aliprandini et al., 2018). This similarity suggests that the skin environment poses a threat to migrating sporozoites and implies a potential link between the absence of concavin and CSP crosslinking by antibodies in compromising the parasite's structural stability.

I did not observe any significant differences during liver stage invasion and development compared to wild type infections after intra venous injection of sporozoites into mice (Figure 3.4.11). Highlighting again the importance of the skin barrier during transmission. When sporozoites invade liver cells, they round up and thus actively change their shape. This process is mediated by newly translated proteins. Sporozoites lacking the RNA binding protein pumilio-2 round up after several days in the salivary glands in a way reminiscent to liver stage parasites (Gomes-Santos et al., 2011; Lindner, Mikolajczak, et al., 2013). The absence of concavin however resulted in early rounding after salivary gland invasion. Furthermore, the rounding of liver stages is initiated at the center of the parasite while the deformation of sporozoites is induced at the back of the cell hinting towards two distinct mechanisms.

Closer analyses of deformed *concavin(-)* sporozoites by transmission electron microscopy revealed invaginations of the inner membrane complex (IMC) and irregular spacing to the plasma

membrane (Figure 3.4.8 and 3.4.9). The observed invaginations are comparable to invaginations observed in *T. gondii* tachyzoites lacking the gliding- associated- protein 45 (GAP45). In *T. gondii* GAP45 localizes to the periphery and functions in spanning the IMC and the plasma membrane to keep their defined distance of 25 nm (Frénal et al., 2010). Thus, concavin is eventually an additional component that contributes to securing the plasma membrane to the underlying IMC. Similar to concavin, GAP45 does not contain any annotated motifs such as signal peptide, transmembrane domain or GPI anchor. However, it has been shown that GAP45 is anchored to the IMC as well as the plasma membrane via post translational lipid modifications (Frénal et al., 2010). Interestingly, mutation of a predicted palmitoylation site at the N- terminus of concavin leads to only a mild phenotypic difference, suggesting that palmitoylation alone is not solely responsible for protein localization and function and indicates the involvement of other protein-protein interactions essential for concavin localization and functionality, as well as sporozoite shape maintenance. The partial impact of palmitoylation again parallels findings in *T. gondii*, where disruption of myosin light chain palmitoylation results in partial disassembly of the gliding motor complex without significantly affecting protein localization and motility (Rompikuntal et al., 2020). Based on the potential palmitoylation site located at the N-terminus of concavin, and considering its ability to recover after FRAP (Figure 3.4.5), it is more likely that the protein is incorporated into the plasma membrane rather than the IMC. Moreover, the observation that both normal and deformed sporozoites remain motile suggests that concavin is unlikely to be involved in glideosome formation. Therefore, concavin might play a role in organizing the PM and IMC directly or through transient interactions with GAP45.

In ookinetes, deletion of the phosphodiesterase PDEδ, responsible for cyclic nucleotide breakdown, yields a phenotype remarkably similar to concavin deletion in sporozoites. PDEδ-deficient ookinetes show progressively rounded shapes and fail to migrate across the midgut epithelium, resulting in reduced mosquito infection rates. Pdeδ(-) parasites successfully developed normally shaped ookinetes initially. However, these ookinetes gradually rounded up and were unable to migrate across the midgut epithelium. Consequently, the pdeδ(-) parasites faced significant challenges in establishing an infection within mosquitoes (Moon et al., 2009). Transmission electron microscopy analysis revealed a partial absence of the inner membrane complex (IMC) in these parasites. Suprisingly, I did not observe any significant impact of concavin in ookinetes during *A. stephensi* infections.

3.5. STED nanoscopy of *Plasmodium* parasites

Super-resolution microscopy techniques, such as stimulated emission depletion (STED), structured illumination microscopy (SIM), photo-activated localization microscopy (PALM), and stochastic optical reconstruction microscopy (STORM), have gained increasing attention for providing deeper insights into the cellular biology. STED is capable of rapidly imaging cells at a resolution as high as 30-50 nm (Hell SW et al, 1994), while SIM is limited to approximately 100 nm (Gustafsson, M.G. et al, 2000). On the other hand, PALM and STORM can achieve similar resolution to STED but are more time-consuming and require complex image analysis workflows (Betzig et al, 2006).

For *Plasmodium* spp. parasites, whole cell STED nanoscopy has been used to image merozoites, sporozoites and liver stages (Prado et al., 2015; Volz et al., 2016; Kehrer et al., 2022). However, imaging of hemozoin-containing blood-stage parasites such as trophozoites, schizonts and gametocytes as well as early mosquito stages such as ookinetes, is limited. The high light-absorbing capacity of the hemozoin crystals in combination with the powerful STED laser leads to immediate cell destruction once hemozoin is hit by the laser. Hence, imaging of blood-stage parasites is so far only possible on Abberior instruments containing adaptive optics such as RESCue STED or guided STED (Mehnert et al., 2019; Schloetel et al., 2019). Both methods turn off the laser in response to hemozoin to avoid cell damage and thus restricts imaging to hemozoin free areas of the cell. Excluding hemozoin from the imaging setup using adaptive optics is in particular challenging when hemozoin crystals are distributed in small vesicles towards the entire cell (e.g. in *P. berghei* parasites), while in the most virulent human-infecting parasite *P. falciparum* it is only one distinct dot located inside a single digestive vacuole (DV) (Figure 3.5.1 A).

CUBIC- P elutes hemozoin and enables STED imaging

Clearing of tissues to reduce light scattering during microscopy was initially developed for 3D imaging of whole organs and is mostly solvent based (Dodt et al., 2007; Spalteholz, 1914; Tian et al., 2021; Tuchin, 1997). For *Plasmodium* parasites, clearing has so far only been used to image infected *Anopheles stephensi* mosquitoes (de Niz et al., 2020; Mori et al., 2019).

In a recent screen of 1600 hydrophilic chemicals for their clearing abilities, CUBIC-P (TCI Chemicals) has been shown to be the most effective for decolorization of red blood cells (RBCs) (Tainaka et al 2018). To test the effect of CUBIC-P on RBCs and its ability to elute hemozoin from the parasite I used fixed *P. berghei* infected blood-stage parasites. To determine the necessary CUBIC-P concentration I incubated the cells with 10, 50 and 100% CUBIC- P at 37°C over night and on the following day cells were washed and observed under a microscope.

Using a widefield microscope with standard GFP, mCherry and Hoechst settings I observed swelling of RBCs and an increase of background fluorescence in the CUBIP-P treated cells. Compared to untreated RBCs, RBCs incubated with 50% CUBIC-P resulted in slightly higher background fluorescence then parasites incubated with 10% CUBIC-P. Furthermore, RBCs treated with either 10, 50, or 100% CUBIC-P resulted in an increase of 1,5 nearly 2 and almost 3 fold in size respectively, compared to non-treated control cells (Figure 3.5.1 A,B). Same was true using *P. falciparum* parasites incubated with 10, 50 and 100% CUBIC-P. Please also note, that human RBCs are generally bigger compared to mouse RBCs (Figure 3.5.1 C). Strikingly, in all infected RBCs none of the parasite stages (trophozoites, schizonts, gametocytes and ookinetes) in both *Plasmodium* strains showed any remaining hemozoin crystals (Figure 3.5.1 D,E). The absence of hemozoin crystals I could also confirm using transmission electron microscopy of cleared and non-cleared *P. berghei* and *P. falciparum* infected RBCs (Figure 3.5.1 F).

I furthermore assessed the removal of hemozoin in ookinetes and early oocysts within intact isolated mosquito midguts infected with *Plasmodium berghei* parasites expressing HSP70-GFP, one day after a blood meal. In infected midguts treated with CUBIC-P, I observed the complete absence of any remaining hemozoin crystals, whereas non-cleared midguts clearly exhibited the presence of these crystals (Figure 3.5.2 A,B).

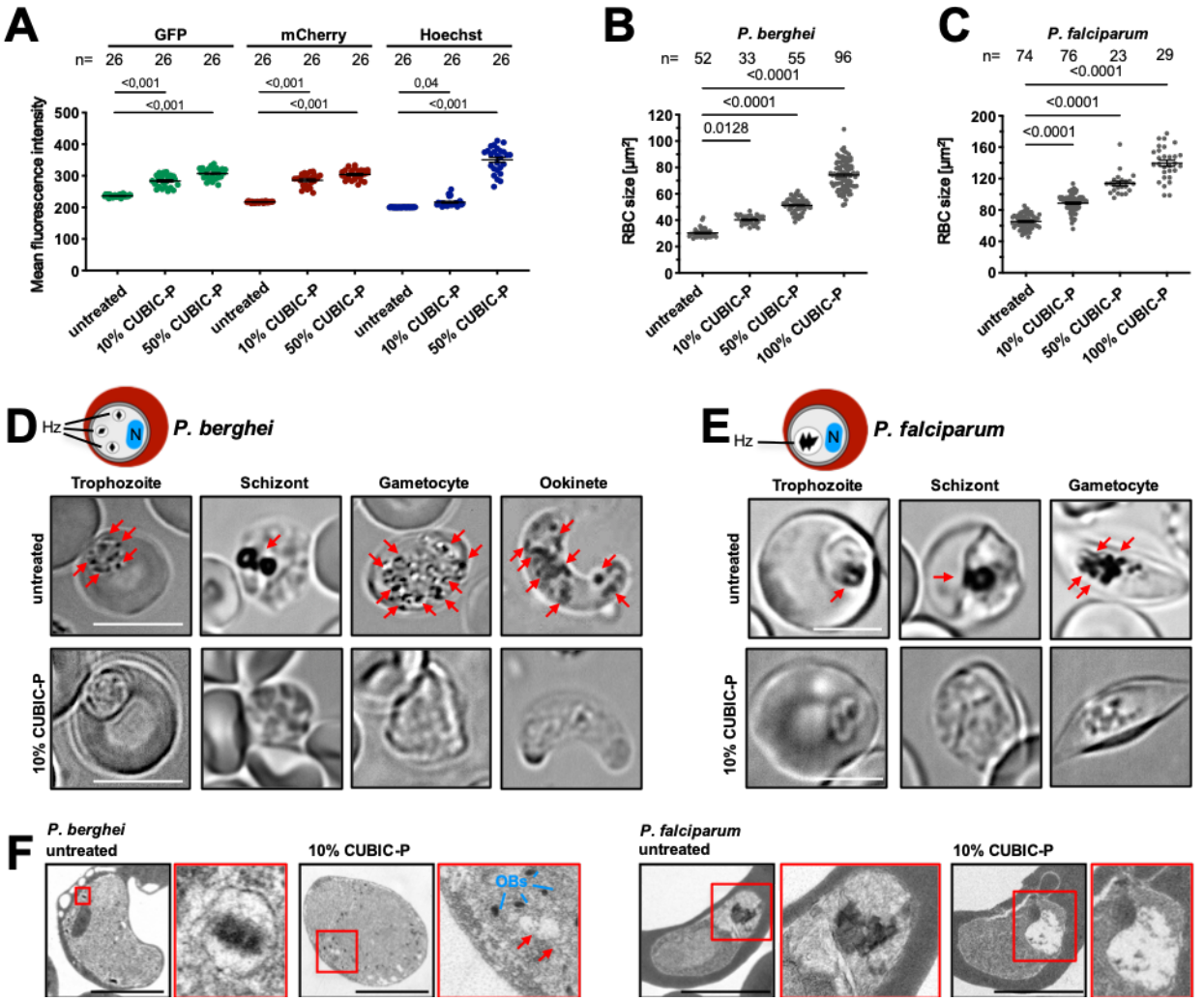

Figure 3.5.1 CUBIC-P treatment elutes hemozoin

(A) Quantification of RBC auto- fluorescence in GFP, mCherry and Hoechst settings in non- treated cells and cells treated with 10% as well as 50% CUBIC-P. P- values are calculated using one-way Anova with Dunnetts multiple comparison. Shown is the mean +/- SEM. **(B)** Quantification *P. berghei* RBC sizes in non-treated cells and cells treated with 10%, 50% as well as 100% CUBIC-P. P- values are calculated using one-way Anova with Dunnetts multiple comparison. Shown is the mean +/- SEM. **(C)** Quantification *P. falciparum* RBC sizes in non-treated cells and cells treated with 10%, 50% as well as 100% CUBIC-P. P- values are calculated using one-way Anova with Dunnetts multiple comparison. Shown is the mean +/- SEM. **(D)** Representative images of *P. berghei* blood- stage parasites and ookinetes with and without hemozoin crystals. Red arrows indicate hemozoin in untreated cells. Scale bars 5 µm. **(E)** Representative images of *P. falciparum* blood- stage parasites with and without hemozoin crystals. Red arrows indicate hemozoin in untreated cells. Scale bars 5 µm. **(F)** TEM images of non-treated and CUBIC-P treated *P. berghei* and *P. falciparum* parasites. Scale bars: 2 µm. Experiments jointly performed with Emma Pietsch an Julia Heinze. Figure modified from (Kehrer et al., 2023).

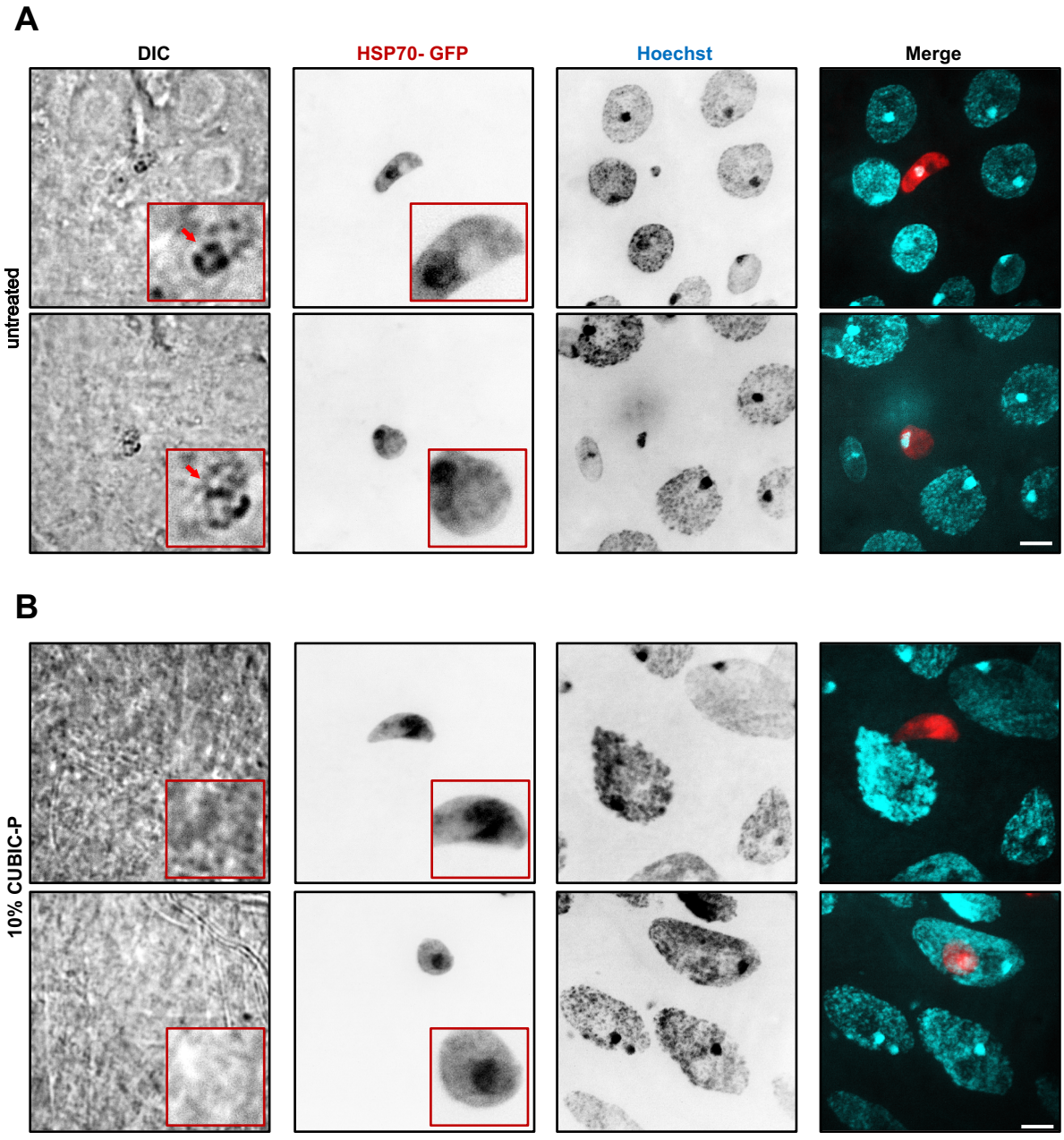

Figure 3.5.2 Clearing and imaging of ookinetes and early oocysts in isolated mosquito midguts.

(A) Spinning disc confocal microscopy images of ookinetes (top row) and early oocysts (bottom row) expressing HSP70-GFP. Hemozoin crystals are indicated with the red arrow on the DIC image. Nuclei are stained with Hoechst. The merge shows an overlay of HSP70- GFP (red) and the nucleus (cyan). The red boxes show a 2,5x zoom to better visualize the hemozoin. Scale bar: 5 µm. **(B)** Spinning disc confocal microscopy images of ookinetes (top row) and early oocysts (bottom row) expressing HSP70-GFP. Midguts were treated with 10% CUBIC-P overnight. Please note the absence of hemozoin crystals on the DIC image. Nuclei are stained with Hoechst. The merge shows an overlay of HSP70-GFP (red) and the nucleus (cyan). The red boxes show a 2,5x zoom to better visualize the hemozoin. Scale bar: 5 µm. Figure taken from (Kehrer et al., 2023).

I next tested whether the cleared *P. berghei* infected RBCs can withstand the powerful STED laser without any cell damage. To do so, I used blood- stage parasites treated with 10% CUBIC-P, since this concentration has been sufficient for hemozoin removal. I imaged a drop of cell suspension on a microscope slide covered with a cover glass on an Abberior STED Microscope. Since the transparent infected red blood cells are difficult to find I have used Hoechst to locate them in confocal mode. To test STED robustness, I made use of the RBC auto-fluorescence. While non-cleared parasites immediately burst upon contact with the laser, the cleared parasites were resistant to even up to 100% laser power (Figure 3.5.3), which enables STED based super-resolution imaging of blood-stage parasites in future experiments.

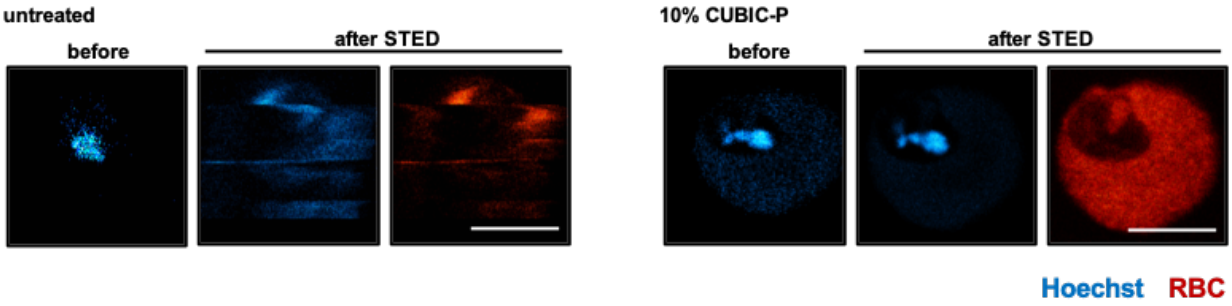

Figure 3.5.3 CUBIC-P treatment enables STED nanoscopy

Confocal images of *P. berghei* infected RBCs of non-treated and CUBIC-P treated parasites before and after imaging with the STED laser. Scale bars 5 µm. Figure modified from (Kehrer et al., 2023).

CUBIC-P treatment preserves fluorescence and allows antibody staining

In order to determine if CUBIC-P treatment could facilitate the staining of specific organelles and structures within infected red blood cells (RBCs) using standard immunofluorescence protocols, I conducted a series of tests. First, I treated infected RBCs with 10% CUBIC-P and subsequently performed immunofluorescence staining using standard protocols and compared them to untreated cells. To visualize secretory organelles in segmented schizonts I employed NHS-ester staining, which is known to effectively highlight rhoptries due to their high protein density (Liffner et al., 2021 BioRxiv). Remarkably, I did not observe any significant differences between treated and non- treated cells, indicating that treatment with CUBIC-P does not adversely affect rhoptries. In both scenarios, we consistently observed distinct staining at the apical region of the cells (Figure 3.5.2 A).

In *P. berghei* parasites, gametocytes have the highest amount of hemozoin localized in distinct clusters throughout the cell. To test if epitopes in parasites treated with CUBIC-P are still

accessible for immunolabeling with antibodies needed for STED imaging, I have used our previously described PAT-GFP|g377-mCherry parasite line. PAT-GFP as well as g377-mCherry localize to secretory vesicles in gametocytes and are distributed within the parasite (Kehrer, Singer, et al., 2016). To do so, I fixed gametocyte-containing blood with 4% PFA and treated the cells with 10% CUBIC-P at 37°C over, followed by an immunofluorescence staining against GFP or mCherry in combination with the STED-compatible secondary antibody Atto 647N. On a conventional spinning disc microscope, I observed, that both, the PAT-GFP and the g377-mCherry signal were preserved after parasite clearing. CUBIC-P treatment of the parasites did not negatively influence the fluorescent proteins and thus imaging was still possible (Figure 3.5.2 B). Furthermore, single antibody staining against GFP or mCherry resulted in the same localization pattern than the endogenous signal, showing that cells are still accessible for antibodies (Figure 3.5.2 B). Imaging of PAT-GFP in gametocytes as well as ookinetes, stained with an anti-GFP antibody combined with ATTO 647, using the STED microscope was possible without any cell damage (Figure 3.5.2 C,D). Therefore, clearing of *Plasmodium* parasites leading to the removal of hemozoin crystals enables the visualization of individual secretory vesicles, essential to better understand parasite transmission into mosquitoes.

Using PAT-GFP|pplp2-mCherry as well as PAT-GFP|g377-mCherry parasites I next stained for GFP and mCherry in the same gametocyte. Similar to g377, the perforin like protein2 (pplp2) localizes to egress vesicles in the gametocyte and colocalizes with PAT-GFP (Kehrer, Singer, et al., 2016). Whole cell STED microscopy of both parasite lines stained with anti-mCherry Atto 594 and anti- GFP Atto 647 resulted in colocalization of PAT with g377 and PAT with pplp2. Thus, confirming our previous observations (Kehrer, Singer, et al., 2016). Quantification of colocalization of PAT with g377 in 19 gametocytes resulted in an R-value of around 0,8 whereas colocalization of PAT with pplp2 in 12 gametocytes was slightly lower but still resulted in an R-value of around 0,7. Colocalization of the two fluorescent signals was quantified using the Pearson's correlation coefficient where a value of one stands for perfect correlation and zero for no correlation (Figure 3.5.2 E).

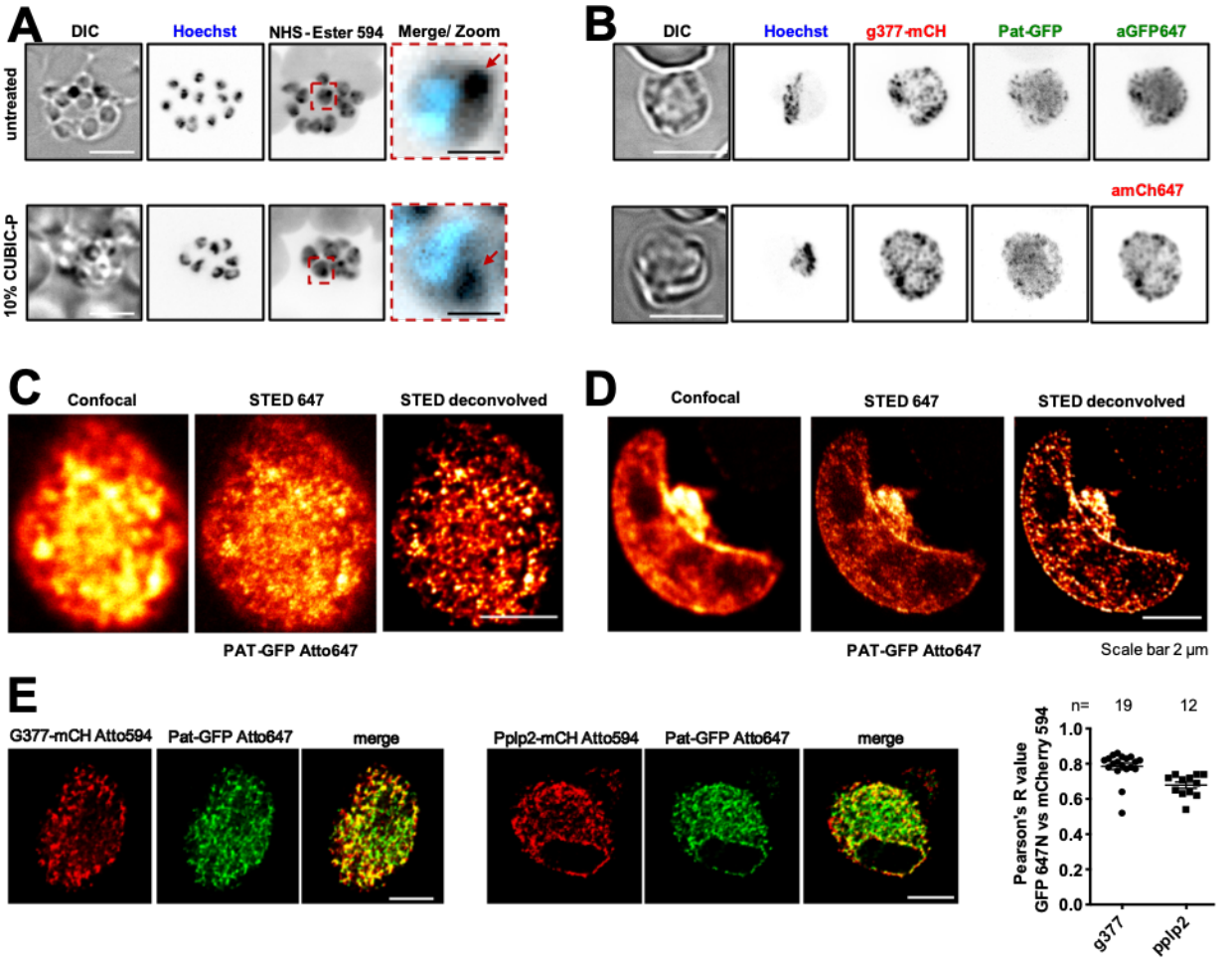

Figure 3.5.4 CUBIC- P treated cells are susceptible to antibody staining

(A) Spinning disc confocal microscopy images of *P. berghei* schizonts/ merozoites stained with NHS- Ester Atto594. Untreated cells (top row) show a prominent apical concentration of proteins highlighting rhoptries. A similar staining was observed in cells treated with 10% CUBIC-P. The merge/ zoom shows an overlay of the nucleus (blue) with the NHS- Ester (grey). Scale bars: 5 µm (DIC) and 1 µm (zoom). **(B)** Spinning disc confocal microscopy images of cleared *P. berghei* gametocytes expressing the egress vesicle resident proteins PAT-GFP and g377-mCherry stained with either a rabbit anti-GFP antibody (top row) or rabbit anti-mCherry (bottom row) and anti-rabbit Atto 647N. Hoechst as nuclear DNA stain. Scale bars: 5 µm. **(C)** Cleared *P. berghei* PAT-GFP|g377-mCh gametocyte stained with rabbit anti-GFP and anti-rabbit Atto 647N and imaged as indicated. Scale bar: 3 µm. **(D)** Cleared *P. berghei* PAT-GFP ookinete stained with rabbit anti-GFP and anti-rabbit Atto 647N and imaged as indicated. Scale bar: 3 µm. **(E)** Dual color STED imaging of cleared PAT-GFP|g377-mCh or PAT-GFP|pplp2-mCh parasites. Staining with rabbit anti-GFP and anti-rabbit Atto 647N antibody. Additional staining with rabbit anti-mCherry Atto 594 antibody. Scale bar: 2 µm. **(F)** Quantification of colocalization of 647N (GFP) and 594 (mCherry) signal from D expressed as Pearson's R value. n indicates the number of cells investigated. Shown is the mean +/- SEM. Experiments B-F jointly performed with Emma Pietsch. Figure modified from (Kehrer et al., 2023).

3D STED is possible at the food vacuole

To demonstrate the power of the method for imaging at or close to the DV I selected the *P. berghei* chloroquine resistance transporter (PbCRT). This furthermore allows the detailed visualization of the DV in the rodent strain. I first generated a parasite line with PbCRT fused to GFP via single cross over integration. Successful integration of the plasmid was confirmed by analytical PCR (see Material and Methods).

Spinning disc microscopy of PbCRT-GFP parasites showed a clear overlap of the GFP signal with the black hemozoin crystals (Figure 3.5.3 A). As expected and in contrast to *P. falciparum* parasites the fluorescence signal was localized to separate spots within the parasite.

STED imaging of cleared PbCRT-GFP parasites stained with an anti- GFP antibody (rabbit) followed by an anti- rabbit Atto647N antibody suitable for STED confirmed the vesicular pattern observed by confocal microscopy. Quantification and direct comparison of the fluorescence signal via line plots highlights the defined lumen of the observed vesicles in the STED image (Figure 3.5.3 B).

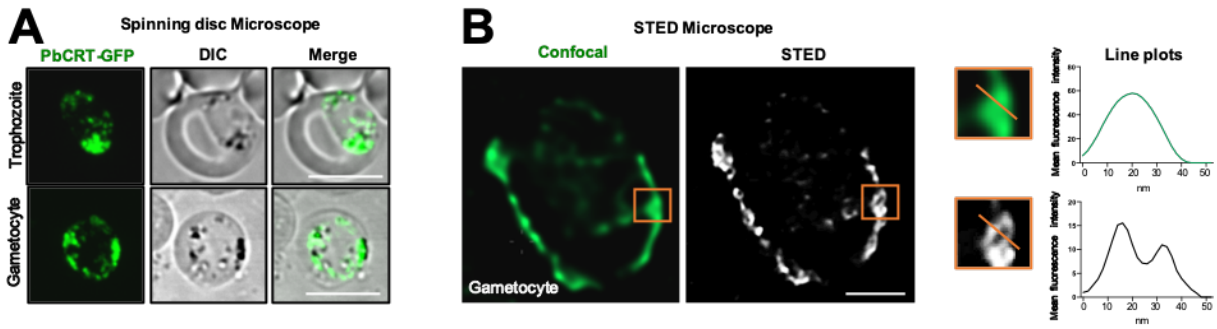

Figure 3.5.5 STED of PbCRT is possible at the food vacuole

(A) Spinning disc images of a trophozoite (top) and a gametocyte (bottom) expressing PbCRT-GFP. Note the GFP signal surrounding the black hemozoin dots. Scale bar: 5 µm. **(B)** Confocal and STED image of a cleared gametocyte expressing PbCRT-GFP. Line plots clearly indicate CRT in a vesicular structure. Note that the lumen of the vesicle is only visible in STED. Scale bar: 2µm. Figure taken from (Kehrer et al., 2023).

Discussion

The presence of hemozoin in blood-stage parasites limits whole cell STED imaging. In this section, I have established a protocol to elute hemozoin crystals from *P. berghei* blood-stage parasites and ookinetes as well as *P. falciparum* blood-stage parasites, using the hydrophilic clearing reagent CUBIC-P (Tainaka et al., 2018). Cells treated with CUBIC-P were still accessible for fluorescence staining and thus successful STED imaging of egress vesicles of *P. berghei* gametocytes and the chloroquine resistance transporter CRT as part of the DV demonstrates the potential of the method. Especially in *P. berghei* as well as in other human infecting parasites except *P. falciparum* it is challenging to only image hemozoin- free areas using Rescue STED, since the crystals are distributed in many small digestive vacuoles compared to *P. falciparum*. Using our newly established method, overcomes this difficulty and suggests that CUBIC-P treatment can be effectively incorporated into standard immunofluorescence techniques for visualizing specific organelles and structures in infected RBCs and early mosquito stage parasites. One major drawback however is the unfeasibility of the protocol for live cell imaging.

Vesicular structures in cleared parasites most likely remain intact and unaltered due to the fluorescence signal of egress vesicles observed. Nevertheless, I observed that clearing interfered with Osmium tetroxide contrasting of membranes due to de-lipidation of the samples. Therefore, I was unable to draw any conclusion about the complete organelle integrity. Despite encountering these challenges, I was able to successfully identify and recognize osmiophilic bodies in gametocytes and the quality of the transmission electron microscopy (TEM) images obtained was satisfactory to confirm the absence of hemozoin.

After treatment with CUBIC-P, RBCs slightly increased in size (Figure 3.5.1 B,C), reminiscent of expansion microscopy. For expansion microscopy cells are embedded into a swellable hydrogel able to expand the cells (Chen et al., 2015) leading to a physical increase of small structures to improve magnification on conventional microscopes. CUBIC-P contains 5% Triton X-100, 5% 1- Methylimidazol and 10% N- Butyldiethanolamine (Tainaka et al., 2018). Indeed, 20% 1- Methylimidazol (CUBIC-X1) has been used to develop an expansion microscopy protocol based on aqueous chemicals without the need of embedding the tissue in a hydrogel (Murakami et al., 2018). A combination of CUBIC-X1 with CUBIC-P, as an alternative to the classic expansion microscopy protocol, or just the treatment of parasites with higher concentrations of CUBIC-P might be worth a try, to increase resolution even further, not only for hemozoin- containing life cycle stages but also sporozoites and parasites developing in the liver.

Clearing of hemozoin will enable STED nanoscopy of *Plasmodium* blood-stage parasites, important to better understand the life cycle stage, which causes clinical symptoms. This tool might not only be helpful for *Plasmodium spp.* but also for other blood feeding parasites.

4 CONCLUSION

In vitro, cell migration is based on the movement of the cell on a solid surface. However forward locomotion *in vivo* also requires the ability to interact with the environment e.g. degradation of extracellular matrix, invasion/ traversal of cells, cooperation with surface proteins. These general statements also apply to malaria parasites.

In this thesis, I first established a new assay for rapid biotinylation of proteins based on Apex2, to profile proteins resident in ookinete micronemes. This approach together with the identified sporozoite secretome not only generated a comprehensive list of putative micronemal and secreted proteins of the respective parasite stages but also unveiled potential new candidates (see Appendix) for life cycle interventions. The findings presented in this thesis pave the way for future investigations and underscore the importance of innovative techniques in advancing our knowledge of ookinete and sporozoite biology. The use of Apex2 based BioID together with other existing rapid BioID approaches such as TurboID or miniTurboID provides an important tool for further discoveries along the complex *Plasmodium* life cycle.

The application of two proteomic approaches has yielded valuable insights into the characterization of the proteins akratin (ookinete BioID) and concavin (sporozoite secretome). Building on the promising results obtained for akratin, I further continued to characterized the previously described protein PAT. While full-length akratin and PAT play an essential role during microgametogenesis a tyrosine-containing motif within their C- termini plays a more specific function during ookinete migration through the mosquito midgut. Additionally, one of the two motifs in the C-terminus of PAT is important for efficient salivary gland invasion and colonization (Figure 4.1).

Concavin(-) parasites exhibit normal progression through the mosquito midgut. However, a significant phenotype emerges upon reaching the salivary gland, where a large proportion of these parasites undergo deformation. When the remaining normally shaped sporozoites are transmitted into the skin they disintegrate while they move forward to find and reach a blood vessel (Figure 4.1).

In conclusion, my discoveries add valuable pieces to the puzzle of ongoing efforts to comprehend parasite egress, motility, and transmission. Understanding the intricate functions of akratin, PAT and concavin in the different stages of the parasite life cycle not only contributes to the fundamental knowledge of malaria biology but also holds potential implications for the development of targeted interventions against the disease.

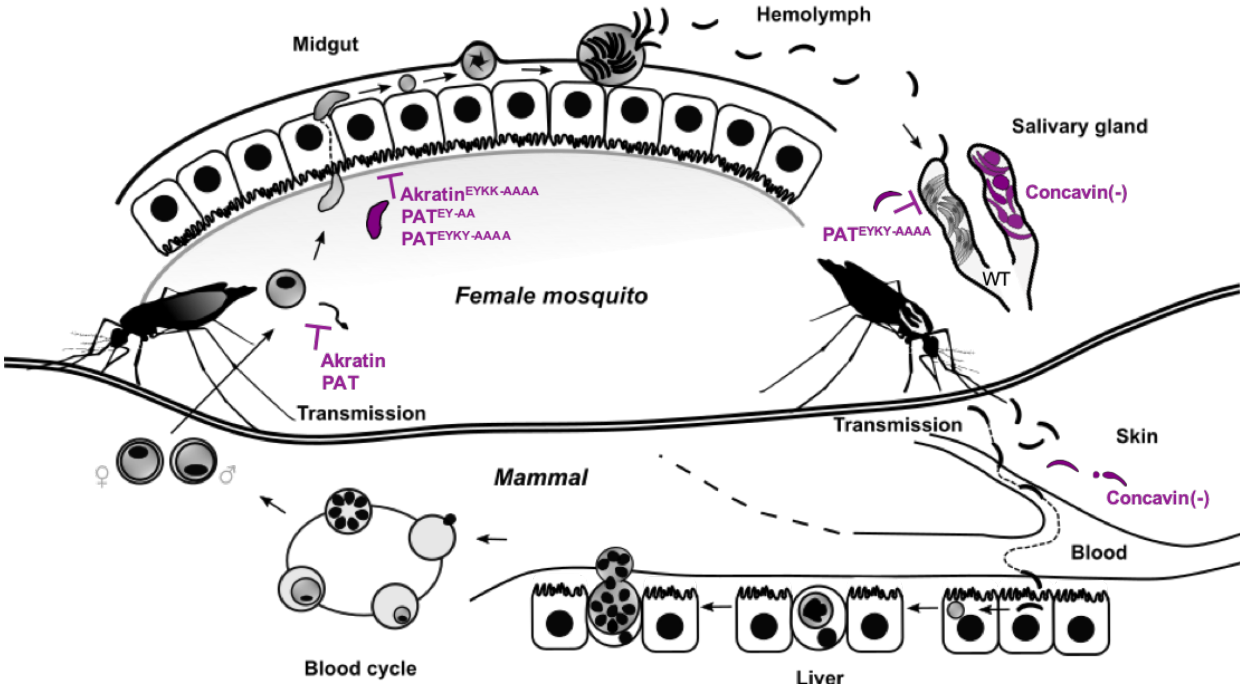

Figure 4.1 Summary cartoon of main findings

Life cycle of *P. berghei* parasites highlighting the main findings of this thesis in magenta. *Akratin(-)* and *PAT(-)* parasites both block microgametogenesis while parasites with a mutated motif in the C- terminus form ookinetes unable to penetrate the midgut epithelium. $PAT^{EYKY\text{-}AAAA}$ sporozoites are furthermore unable to efficiently invade salivary glands. *Concavin(-)* parasites progress normally through the mosquito midgut but deform once in the salivary gland. Plus, normally formed sporozoites transmitted into the host disintegrate while moving in the skin.

5 MATERIAL AND METHODS

5.1. Material

Standard lab- equipment such as pipets, centrifuges, incubators, heating blocks, thermocycler etc. are not separately listed. Stock consumables such as plasticware, chemicals and enzymes were generally bought from the following companies: Carl Roth (Karlsruhe/ Germany), VWR (Darmstadt/ Germany), SIGMA (Munich/ Germany), Roche (Basel/ Switzerland), Thermo Fisher Scientific (Waltham/ USA), New England Biolabs (Ipswitch/ USA).

Microscopes

Instrument	Specifications
Zeiss Axiostar Plus	Upright brightfield Microscope Objectives: 100x Oil (NA 1,25); 40x Air (NA 0,65); 10x Air (NA 0,25)
Nikon Eclipse E100	Upright brightfield Microscope Objectives: 100x Oil (NA 1,25); 40x Air (NA 0,65); 10x Air (NA 0,25)
Nikon SMZ 1500	Binocular Zoom: 0,75- 11,25
Zeiss AxioObserver	Inverted Widefield Microscope Objectives: 63x Oil (NA 1,4); 25x Water (NA 0,8); 10x Air (NA 0,25) Photometrics Prime BSI camera; Zen Blue Software
Nikon TiE PerkinElmer UltraVIEW VoX spinning disc	Inverted Spinning disc confocal Microscope with environmental control and FRAP modul Objectives: 100x Oil (NA 1,4), 60x Oil (NA 1,4) 40x Oil (NA 1,3); Perkin Elmer Ultraview Modul; Hamamatsu Orca Flash camera; Volocity Software

Abberior STED Microscope	Super-resolution Microscope Objective: 100x (NA 1,4) Imspector Software

Kits

Kit	Company
Amaxa Human T Cell Nucleofector Kit	Lonza, Köln, Germany
DNeasy Blood and Tissue Kit	Qiagen, Hilden, Germany
QIAprep Spin Miniprep Kit	Qiagen, Hilden, Germany
High Pure PCR Purification Kit	Roche, Basel, Switzerland
Gibson Assembly Master Mix	New England Biolabs, Ipswich, USA

Chemicals and reagents

Chemical	Company
1kb ladder	New England Biolabs, Ipswich, USA
5- Fluorocytosine (5-FC)	Sigma, München, Germany
Agarose Research grade	Carl Roth, Karlsruhe, Germany
Biotin Phenol	Sigma, München, Germany
Cubic- P	TCI Chemicals, Japan
Heparin Sodium 25000U	Ratiopharm, Ulm, Germany
Ketamin hydrochloride solution	Sigma, München, Germany
Mercurochrome NF XII	Sigma, München, Germany
Midori Green Advanced	Nippon Genetics Europe, Düren, Gernamy
Nonidet P40	AppliChem, Darmstadt, Germany
Nycodenz	Axis-shield, Heidelberg, Germany
Paraformaldehyde (PFA)	Sigma, München, Germany
PBS tablets	Gibco Thermo Fisher, Waltham, USA
Phusion polymerase	New England Biolabs, Ipswich, USA
Restriction Enzymes	New England Biolabs, Ipswich, USA
Saponin	Sigma, München, Germany
Streptavidin coated beads	Thermo Scientific, Waltham, USA
Trolox	Sigma, München, Germany
Xanthurenic acid	Sigma, München, Germany

Xylazine hypochloride solution	Sigma, München, Germany
Hypoxanthine	Sigma, München, Germany
Pyrimethamine	Sigma, München, Germany
Giemsa	VWR, Darmstadt, Germany
Immersol 518F; n= 1,518	Carl Zeiss, Jena, Germany
Immersol W; n= 1,334	Carl Zeiss, Jena, Germany

Antibodies and dyes

Antibody/ Dye	Dilution	Company
Anti alpha- Tubulin	1/ 500	Sigma, München, Germany
Anti CS (mouse)	1/ 3000	(Yoshida et al., 1980)
Anti GFP (mouse) for WB	1/ 1000	Roche
Anti GFP (rabbit) for IFA	1/ 40	Abfinity
Anti HSP70 (mouse) for IFA and WB	1/ 500	(Wiser & Plitt, 1987)
Anti mouse HRP	1/ 10000	GE Healthcare
Anti Myc (mouse) for IFA and WB	1/ 500 (IFA); 1/ 1000 (WB)	Bio-Rad
Anti rabbit Alexa 488/ 546/ 594	1/ 500	Invitrogen
Anti rabbit Atto 647N for STED	1/ 200	Sigma, München, Germany
Anti mouse Atto 594.for STED	1/ 200	Sigma, München, Germany
Anti rabbit HRP	1/ 10000	Bio-Rad
Anti mouse Alexa 488/ 546/ 594	1/ 500	Invitrogen
Anti Ter-119 (Alexa 488)	1/ 500	Biolegend
Anti Trap (rabbit)	1/ 500	(Ejigiri et al., 2012)
Hoechst 33342 (10mg/ml)	1/ 500	Sigma, München, Germany
Streptavidin- 594	1/ 1000	Sigma, München, Germany

Software

Software	Company
chatGPT 3.0	OpenAI
FIJI	Schindelin et al 2012
GraphPad Prism 9	GraphPad Software (San Diego, USA)
Huygens	Scientific Volume Imaging (Amsterdam, NL)
Imspector	Abberior (Göttingen, Germany)
Mendeley	Elsevier (Amsterdam, NL)
Pymol	DeLano Scientific LLC, Schrödinger Inc.
Snapgene	Snapgene (Chicago, USA)
Volocity	Perkin Elmer (Waltham, USA)
ZenBlue	Zeiss, Jena, Germany

Buffer and solutions

Buffer/ Solution	Incredients
Freezing solution	10% (v/v) Glycerol in Alsever's solution
KX	10% (v/v) Ketamine 2% (v/v) Xylazine In PBS
LB- medium	10 g/ L NaCl 10 g/ L Bacto-Tryptone 5 g/ L Bacto-Yeast Extract Ampicillin 100 µg/ ml or Kanamycin 50 µg/ ml
Nycodenz stock 100%	0.394 g Tris/ HCl 0.112 g KCL 0.056 g Na_2EDTA 138 g Nycodenz add ddH_2O to 500 ml (pH 7.5)
Ookinete Medium	250 ml RPMI + HEPES + Glutamine 12.5 mg Hypoxanthine 2.5 ml Pen/Strep 0.5 g $NaHCO_3$ 100 µm Xanthurenic acid (5.12 mg); pH 7,8-8

PBS	137 mM NaCl 2.7 mM KCl 8 mM Na_2HPO_4 1.8 mM KH_2PO_4 in ddH_2O (pH 7,4)
PBS "rich"	20 mM HEPES 20 mM Glucose 4 mM $NaHCO_3$ 0.1% BSA add ddH_2O to 500 mL
TAE buffer 50x	242 g Trisbase 57.1 mL Acetic acid 100 mL 0.5 M EDTA add ddH_2O to 1 L
Transfection- medium	60 ml RPMI 22,5 µl Gentamycin 15 ml FCS US origin
BioID elution buffer	30 mM Biotin 2% SDS 160 mM NaCl 6 M Urea
2x Quencher solution for BioID	20 mM Sodiumascorbate 20 mM Trolox 10 mM NaN3
RIPA buffer	50 mM Tris pH 8 1% NP40 0,5% Na deoxycholate 0,1% SDS 150 mM NaCl 2 mM EDTA
Giemsa staining buffer	2,541g KH_2PO_4 per 5 liter 0,5507 g Na_2HPO_4 x 2 H_2O per 5 liter pH 7.2 with NaOH
Giemsa staining solution	10% Giemsa in Giemsa staining buffer

Overview of final plasmids/ parasite lines

All parasite lines were generated in the *P. berghei* ANKA background.

Internal ID	Parasite line
pL 7	SP- APEX2- TRAP
pL 8	SOAP- APEX2
pL 12	PAT (-) for GIMO
pL 15	PAT $^{\Delta 512\text{-}541}$
pL 16	PAT $^{\Delta 514\text{-}541}$
pL 24	PbANKA_1422900 (-)
pL 24 NS	PbANKA_1422900 (-) negative selected
pL 28	PbANKA_1105300 (-)
pL 28 NS	PbANKA_1105300 (-) negative selected
pL 40	PAT(-)$^{TgTFP1\text{-}GFP}$
pL 45	PAT$^{\Delta 514\text{-}541}$- GFP
pL 46	PAT$^{EYKY\text{-}AAAA}$- GFP
pL 47	PAT(-)- GFP
pL 59	PbANKA_1105300 (-) $^{PbANKA\_1105300\text{-}GFP}$
pL 67	PAT$^{TgTFP1(C\text{-}term)}$
pL 71	PAT$^{\Delta 512\text{-}541}$-GFP|CCP-PAT-mCherry
pL 73	PAT$^{EYKY\text{-}AAAA}$-GFP|CCP-PAT-mCherry
pL 75	PbANKA_1105300 (-) $^{PF3D7\_0505700\text{-}GFP}$
pL 79	PbANKA_1422900 (-) $^{PbANKA\_1422900\text{-}GFP}$
pL 82	PbANKA_1422900 (-) $^{Pf3D7\_0814600\text{-}GFP}$
pL 84	PbANKA_1105300^{AAAA}
pL 85	PAT$^{EY\text{-}AA}$
pL 91	PAT$^{TgMic2(C\text{-}term)}$
pL 95	PAT$^{EY\text{-}AA}$-GFP|CCP-PAT-mCherry
pL 104	PbCRT- GFP
pL 120	PbANKA_1422900 (-) ^{C7A}
	PbANKA_1422900 (-)$^{Phil1\text{-}GFP}$

Oligonucleotides

Oligonucleotides were generally ordered from Thermofisher or Sigma.

Internal ID	Sequence
JK 6	AAAGGATCCGTGCATTTCGGTCTTAATAAAAG
JK 7	AAATCTAGAATGGAAGAATATTCATGGG
JK 8	AAACCGCGGCACACATTGGCATTATATAGAAATTG
JK 10	AAAGATATCATGGAAGAATATTCATGGG
JK 11	AAATCTAGTGAAAAAATATATGAATAATCTAG
JK 12	TACCAATTGATTGTATTTATAAC
JK 13	AAAGGATCCGCTTGCATGCCTGC
JK 14	AAAATCGATACTAGATATATTACGAATTGACACC
JK 15	AAAATCGATATGGAAGAATATTCATGGG
JK 16	GGCTCACCAAAAGCTTTCC
JK 17	GCATGGATCCGGAAAGTC
JK 18	GCTTTAACAGATCCTCTTC
JK 19B	CGAAACATATGGGAAAGTCTTACCCAACTG
JK 20B	AAAGGCGCCGAGCTTTAACAGATCCTCTTC
JK 21	GGATCTATATACATGTCTATAAAGC
JK 22	CCTCTGAGCTTCTTCTTCG
JK 23	CGTAAAATTACTAATTAATTATTGCG
JK 24	AAAAAGCTTTACCCATCGAAATTGAAGG
JK 25	AAAGAATTCGTTCCAGATTATGCATAAGGGC
JK 26	AAAGAATTCTGCAGCCCAGCTTAATTC
JK 27	CGCAAGCTTCGAAATTGAAGGAAAAAACATC
JK 28	AAACATATGAATATTGAAAAAGCTGAAGCG
JK 29	AAACCGCGGCTGGCATTTTCCTCCTTAACG
JK 30	AAAGGATCCACAAAGACGACATAAAGCG
JK 31	AAAGGTACCGATTCCCCATAAAGCTTAATTAGC
JK 32	AAAGGATCCCCTATATATATATTCAATGCTTGCTAC
JK 33	AAATTAATTAAACAAAACGTGGGAAATAAATTAAAAAAAC
JK 34	AAACCGCGGCAATTTATTGCATCCTTGAATGATC
JK 35	AAAGATATCGCTTTGATCCCGTTTTTCTTAC
JK 36	ACCAAGCTTCGAAATTGAAGGAAAAAACATC
JK 37	AAAGGTACCTGGAAGGAAGTATAATTGACGG
JK 38	AAAGATATCTTATGCTCCATAAGTAAAATGAAG
JK 39	AAAGATATCTTAATATTCTGCTCCATAAGTAAAATGA
JK 40	ATTCTCTTCTTCATTTTACTTATGGAGCATAAGATATCGCTTTGATCCCGTTTTTCTTACTTATA
JK 41	TATATAAGTAAGAAAAACGGGATCAAAGCGATATCTTATGCTCCATAAGTAAAATGAAGAAG
JK 42	TATATAAGTAAGAAAAACGGGATCAAAGCGATATCTTAATATTCTGCTCCATAAGTAAAATGAAG
JK 43	TTCTTCATTTTACTTATGGAGCAGAATATTAAGATATCGCTTTGATCCCGTTTTTCTTACTTATA

JK 44	AAATCTAGATTATTTGTATAGTTCATCCATGCC
JK 45	AAAGAATTCGTTAATAATAGTATTTTATCGCCTAG
JK 46	AAAGGATCCAAATTTTCTTTGATATGCATTTTGAC
JK 47	AAAGATATCGCTATCAATTTATGTAGCTCTTTTATTAG
JK 48B	AAAGGATCCTAATTCGTCTTTTCCGGATGAAATATCTTCA
JK 49	CAAATGACTGGACGTACGTAATAATACTAAACAAACTTTAC
JK 50	GTAAAGTTTGTTTAGTATTATTACGTACGTCCAGTCATTTG
JK 51	AAAGGATCCACCAATGACAAAGTGACTTTTG
JK 52	AAAGATATCGTAGATTTAAATGGTGATTGTAAAGC
JK 53	AAATGAATTCAGATCTGTTAACGTCT
JK 54	AAAGCGGCCGCCGTTTTTCTTACTTATATATTTATACCAA
JK 55	AAAGGTACCCGCATATCCTCATATATAATAAATTACCA
JK 56	TTATCATAAAAGCTTGGCTGTCTT
JK 57	AAAGCGGCCGCAACAAACAAATCTTCATGTTTGT
JK 58	AAACCGCGGTGATATATGTACTCTTTTGTGTTCC
JK 65	AAAAAGCTTTTTAAAAAAAAAAAATCAAATAAAGTAAACTAAAATAAAATCG
JK 66	AAAGGTACCCAACATTATTCGCATATAAAGATATGTT
JK 67	AAAGCGGCCGCATTATTTCATCGAGTTGTAGTGTG
JK 68	AAACCGCGGGTTTATCCATGCACATGGACTA
JK 69	AAAAAGCTTGTTATTATTATTGGGAAAATGTTGTATAG
JK 70	AAAGGTACCTGGAGAATAAGCATATGCTATATTTATAGG
JK 71	AAAGTCGACATGAAATTTTATAGCATTTTTGCAATTG
JK 72	AAACCGCGGATCAACAACAGTAGTGTTTTCATCA
JK 73	AAACCGCGGCTTTATTTTAAGCGCCTTTTATTTATAC
JK 74	AAAGCGGCCGCCTTTTTTTTATGAAACCAAATGGGAAT
JK 75	ACTAAGCTTTGGTTTTTTCTTTATTTTTATATTATTATTCTTTTATTAAATCC
JK 76	AAAGGTACCATACACGTTAAGAGGTATTAACATTAG
JK 77	AAAGCGGCCGCACAAAAACTAAAACTATAACTAATTAAC
JK 78	AAACCGCGGGTATGAAATTGACGAAACATATGAAT
JK 79	AAAGGTACCATTCATATTTACATAAATATGTGTCCC
JK 80	AAAAAGCTTATTTCCTACTTATATACCACTACTACT
JK 81	AAAGGATCCTTTAGTTAATTTGACATATTTCGTATAAACAC
JK 82	AAAGAATTCAGGAGCTTTAACATTAGCATATACC
JK 83	AAAGAATTCGAAAATGGGCATAAATATAGATGTGCA
JK 84	AAAGGATCCTAATAcATTTTTATCTTCATCGGTATAAGG
JK 85	AAAGAATTCGTGAACGTAAATTAATGAGTGTAATTGTA
JK 86	AAAGGATCCTTGTGTCTTTAATTTTTGACCATATCCAA
JK 87	AAAGATATCTAGATATTGATAATATTGTAGCTGAGCC
JK 88	AAAGGATCCTAATAATTCAATGCTTTCTGGATATTTTTTTTGTG
JK 89	AAACCGCGGctcGTCGACACTAGATATATTACGAATTGACACC

JK 90	GATTTCACTTTTCTTTTCAGAAAGCATGTCGACACTAGATATATTACGAATTGACACCATT
JK 91	TGGTGTCAATTCGTAATATATCTAGTGTCGACATGCTTTCTGAAAAGAAAAGTGAAATC
JK 92	AAAGGTACCTCCATATTTTATATTACAAGTCATATAACTTG
JK 93	AAACCGCGGGTCGAGTTTCATCAATGGAATGGATTAA
JK 94	ATGTCGTAATACTGGAGCTACTATT
JK 95	GCATCATGCATCACATGAGTAAACGA
JK 96	CCAAATGCTCAAATGCAAAATCGAAG
JK 97	CGCAGTAAGGGATAAATTATATTACATACG
JK 98	AAAAAGCTTATGGCGAGTGAGCCGTTCATTG
JK 99	AAACTGCAGGATCCCGCCACTCTCCGATGTGTTTCA
JK 100	AAAGAATTCTTATTTGTATAGTTCATCCATGCCATG
JK 101	GATATCACAAACATGGAACATAATTC
JK 102	GATGGCATATTTGTTCACATTAATTATC
JK 103	GGTTAAACCCAGAGATCCATGGGTA
JK 104	TAACTCACAAGCCCCTTTATTA
JK 105	TACAAGCTTGGGGCATAAAACATAACTAGTACTATATCA
JK 106	AAAGGTACCAACAATGTGCTCATTGCCCCATAT
JK 107	GTTCGGATATATTTTGGGAGGGAA
JK 108	GCATAATTTGAGAGAATTATCTTCCCATC
JK 109	GACAAATGATACTAGCGGAAATGAA
JK 110	GCCTGAATAGTATCGTCATATAACTG
JK 111	AACACCAGTCTGACACCAATTC
JK 112	CCAGATCCAGTATTTTATACCATAGATG
JK 113	GTATGCGCATAAGTATATATAGGCAC
JK 114	ATTTCGCTACTTCATTTCGCCAC
JK 115	TATGCACACATGCATGTGCGT
JK 116	ACTACCCTTAACATATTTATTGTTTTGTC
JK 117	AAAGCGGCCGCCGATGTATCTCGAAAATAGTGTAT
JK 118	AAACCGCGGTTACATATAATCTTCCTCATTAAAATCGTCG
JK 119	GAAAAGAAAGCTTCATTAAATTTTAATTTAATATC
JK 120	AAAGGTACCATGTGTGTGCAAATAAGCGTATG
JK 121	AAAACATATAAACACAAATGATGTTTTTTCCTTCAATTTCGACAAAGACGACATAAAGCGATATACATA ATTTTATATTATAG
JK 122	CAAGCTCGAAATTAACCCTCACTAAAGGGAACAAAAGCTGGTACCATGTGTGTGCAAATAAGCGTATGA TATATTTATAAAG
JK 123	CATCAATAGTAATTGGAGTTTTAGTGG
JK 124	AGTAAAACAAGTTTAGTGAAAATATCCAT
JK 125	ACATAAGTAAATCGGGAGCTAAC
JK 126	CAATTTTCTTGATCACTACATACACA
JK 127	TAATGGAATTGATATGGCTGTAAAG
JK 128	CTTTTTCATAATTTAATAACCCCCCA

JK 129	GTATTTTGTTCTGTAAAACATTGCATATAC
JK 130	AAAAAGCTTATGAATGCTGATTCCTATACCC
JK 131	AAAGGATCCTGCTCCATAAGTAAAATGAAGAAG
JK 132	AAAGGATCCATATTCTGCTCCATAAGTAAAATGAAGAAG
JK 133B	AAAGGATCCTGACATAACTTTATCTGCCATAGTTTCATCATCTTCATCATCTGCTGCGGCTGCTGATTCAAT TATTTGGTTCATTTTTGAATATTC
JK 134	AAAGCGGCCGCTTTGATTAATATAAATACAAAAAAGGGTATATATATAAGAG
JK 135	AAAGCGCGCTCTGCCAGGAATTATGATGATAATTCT
JK 136	AAAGCGGCCGCTTGTGTTTTGCTTTGTATTTAAAATAGATTATATTTC
JK 137	AAAGCGCGCCACCATTCCATTATAAATATATATACCACTTC
JK 138	AAACATATGAAATTAGGGAAAGTCTGGATTTTC
JK 139	AAACCGCGGTTAAAATTTTCTTTGATATGCATTTTGAC
JK 140	AAAAAGCTTATGGCTAAAAACCAGTATATGGAGGATAG
JK 141	AAAACCGGTTGTTAACATTTTTTTTTCTGGAATGGTTTC
JK 142	AAAGCGGCCGCATGGCCATCATCAAGGAGTTC
JK 143	AAAGCGGCCGCTGTTAACATTTTTTTTTCTGGAATGGTTTC
JK 144	AAAGTCGACCTTAAGATCGCTGATATTTATGAGTATTCCATGTTTC
JK 147	GATAAAGATAATATATATTAAAAATTAGGAAAAATGGCTAAAAACCAGTATATGGAGGATAGAAA TATTAGAGAACCT
JK 148	CTATCCTCCATATACTGGTTTTTAGCCATTTTTCCTAATTTTTAATATATATATTATCTTTATCCTTTACA GCCATATCAATTCC
JK 149	GCGGCCGCTTGTTAACATTTTTTTTTCTGGAATGGTTTC
JK 149B	AAAGCGGCCGCTTGTTAACATTTTTTTTTCTGGAATGGTTTC
JK 150	AAAGGTACCTCTAGATATATTTATTCGTACAGCTATAATTAAATATTTACC
JK 151	AAAAAGCTTTATATATGTATTTATCTATCTATCTATCTATCTATCTATC
JK 152	AAACATATGAAATTTTCTTTGATATGCATTTTGAC
JK 153	TACAAAATGAGCATATTCACACGG
JK 154	AAAGCGGCCGCCGAAATTGAAGGAAAAAACATCATTTG
JK 155	AAAGTCGACATGGCTAAAAACCAGTATATGGAGGATAG
JK 156	AAAGTCGACTTTTCCTAATTTTTAATATATATATTATCTTTATCCTTTACAG
JK 157	AAACCGCGGCTTAAGATCGCTGATATTTATGAGTATTCCATGTTTC
JK 158	AAAAGCGGCCGCTTGACATAACTTTATCTGCCATAGTTTC
JK 159	AAAGTCGACATGAATGCTGATTCCTATACCC
JK 160	AAAGTCGACTTGAAAAAATATATGAATAATCTAGATTAATATAATTC
JK 161	AAACTTAAGGTATCTCGAAAATAGTGTATTTAATATTATAC
JK 162	AAAAAGCTTATATATTTATTCGTACAGCTATAATTAAATATTTACC
JK 163	AAAACCGGTTGCTCCATAAGTAAAATGAAGAAG
JK 164	AAAACCGGTTGACATAACTTTATCTGCCATAGTTTCATCATCTTCATCATCTGCTGCGGCTGCTGATTC AATTATTTGGTTCATTTTTGAATATTC
JK 165	AAACATATGAATGCTGATTCCTATACCC
JK 166	AAACCGCGGGCGGCCGCTGACATAACTTTATCTGCCATAGTTTC
JK 166-2	AAACCGCGGGCGGCCGCATGACATAACTTTATCTGCCATAGTTTC

JK 167	AAACCGCGGCTTAAGGTATCTCGAAAATAGTGTATTTAATATTATAC
JK 168	AAAGGTACCCTCGAGTATATATTTATTCGTACAGCTATAATTAAATATTTACC
JK 169	AAAACCGGTTGCTCCATAAGTAAAATGAAGAAG
JK 170	AAAACCGGTTGACATAACTTTATCTGCCATAGTTTCATCATCTTCATCATCTGCTGCGGCTGCTGATTCAAT TATTTGGTTCATTTTTGAATATTC
JK 171	TTTAAGCTTATGAAATTAACTTGTTACTGTATTATGTTTTTATTTATTC
JK 172	AAACATATGATATTTTCTCTCGTGTATATTTGAAGTTTTC
JK 173	AAAGCGGCCGCGAAGTCATAAAACAATGGCACATG
JK 174	AAACCGCGGAAATACGTATTTTCATTTAATTAATCAACACAAAAAAAAAAAAAAATATGTATATTCCT
JK 175	ATGAAATTAGGGAAAGTCTGGATTTTC
JK 176	GCAGCATTTTCTACTGGATAAGACAG
JK 177	AAATTCGAAATGACAAACATTATAGAATGTACGTTCAAG
JK 178	GGTTCCTTGTCCAATGGATATGACAAAG
JK 179	AAATTCGAATTTGGAATATAACAAAAAAATATATCTCGTAATATATTATTAAAAAAAAAATATATGC
JK 180	CATAAGCTTATAATTAATTAAAAATGTGATCAAAT
JK 181	AAAGGTACCGAAGTCATAAAACAATGGCACATG
JK 182	AAAGCGGCCGCAAATACGTAATGAAAACACATATTACTACTTATTTATATATATATATAATCTTTC
JK 183	AAACCGCGGCCCTACTAGCATCTGTTTCATTTAC
JK 184	TTTGCCAACATTCTTTTTGGGATTG
JK 185	AAAGCGGCCGCCTGTGTAATAAAAAAAAATTATCATTTATATAATACCG
JK 186	TTTGTATATTGCTTGTTCAGAAAATTTATG
JK 187	AAAGCGGCCGCGTTCGTATAATAATTTAACTACTCCCG
JK 188	TTTTAAAACAGTAAAATTCCTTTTTGTTATTTTATATTTTTAGC
JK 189	AAAGCGGCCGCGGCACTCATAAATATAACTATATATAATATATAAATTTTG
JK 190	CACATGGCATGGATGAACTATACAAATAAGTAGCTAAAAGGTGTGCAAGCCCG
JK 191	TCCATTATTGTCCTATTTTTAAAGTTTTAGCGAAATTGAAGGAAAAAACATCATTTGTGTTTATATGT
JK 192	CTGCTACCTCTCTTAAATTGTATAC
JK 193	GAACTGTTTGGATGACCTCATG
JK 195	AAACTCGAGCTATATTTATTCGTACAGCTATAATTAAATATTTACC
JK 196	TAAGCATAAAGAGCTCGAAAAGAATTAAGCTGGGCTGCAGTAGCTAAAAGGTGTGCAAGCCCGT
JK 197	
JK 198	CAGTTTTACTCATTTGAGATATGCAC
JK 199	AAACATATGACCACCACCATCCATTTCAAAGAACATTCTTTTTATTTCTG
JK 200	AAAGCGGCCGCGCAAATTCAACAAATGGTCAACTTC
JK 201	AAACTCGAGAATATATATACTGATTTTTATTTTAACCTACGTTATAC
JK 202	AAACCCATGGTTTATTTCAAAAGTTAAAGGAG
JK 203	TACAATCAATTGGTATAAATATATAAGTAAGAAAAACGGCGGCCGCGTATATTTATAATTCTAGTTATTTGTT CTATCTTTGAGATACTAT
JK 204	TCTCCTTTACTCACAGACATCGTCTATTTTACAGTTTTTTGTGATTTAGCTATTAGT
JK 205	CAAAAAACTGTAAAATAGACGATGTCTGTGAGTAAAGGAGAAGAACTT
JK 206	TTTATTTTATCATCCTCCATGGCGCCTTTGTATAGTTCATCCATG

JK 207	ATGAACTATACAAAGGCGCCATGGAGGATGATAAAATAAAGTCAAACAGTATCTCT
JK 208	GTAATACGACTCACTATAGGGCGAATTGGAGCTCCACCGCGGCATATTTTCAAAATCACTAGAATCGCTCAATTCAGT
JK 209	AAAAAGCTTCTAACAGTTATATTATTATATGGGTAAATGTTC
JK 210	AAAGGTACCGTACTATATATATGGAATCATAATAACCAAGTTATG
JK 211	TACAATCAATTGGTATAAATATATAAGTAAGAAAAACGGCGGCACTCATAAATATAACTATATATAATATATAAATTTTGTAATAAAAA
JK 212	CAGACTTTCCCTAATTTCATTTTTAAAACAGTAAAATTCCTTTTTGTTATTTTATATTTTTAGCAGT
JK 213	GGAATTTTACTGTTTTAAAAATGAAATTAGGGAAAGTCTGGATTTTCATAGC
JK 214	GTAATACGACTCACTATAGGGCGAATTGGAGCTCCACCGCGGTTAAAATTTTCTTTGATATGCATTTTGACTTTTGTATAATTTTTTGT
JK 215	TAAGCATAAAGAGCTCGAAAAGAATTAAGCTGGGCTGCAGTAGCTAAAAGGTGTGCAAGCCCGTTTAAGGATTATTAAATG
JK 211B	CAATTGGTATAAATATATAAGTAAGAAAAACGGCGGCACTCATAAATATAACTATATATAATATATAAATTTTGTAATAAAAAAAATGAAAATAATA
JK 212B	AAATATAATAATACTGCTAAAAATATAAAATAACAAAAAGGAATTTTACTGTTTTAAAAATGAAATTAGGGAAAGTCTGGATTTTCATAGC
JK 213B	CAAAAAGGAATTTTACTGTTTTAAAAATGAAATTAGGGAAAGTCTGGATTTTCATAGCTTTAGTATATGTAG
JK 214B	CATGAATACAAAAAATTATACAAAAGTCAAAATGCATATCAAAGAAAATTTTAACCGCGGTGGAGCTCCAATTCGCCCTATAGTGAGTCGTATTAC
JK 215	CACCCATTGAAAATATGCCATTTTC
JK 216	CTAAACTGGGTACATGCTTGTATATGG
JK 217	GAACGGATTTATCTTATTTCCCATTTATAC
JK 218	GAATATTTAGGAGATGACTATCCATGG
JK 219	AAAGCGGCCGCCACTCATAAATATAACTATATATAATATATAAATTTTGTAATAAAAAAAATG
JK 220	ATTAACAAATTATTACATATGTTTTGTATGAC
JK 221	AAAAACCGCGGGGGGTTAAATGGAAATATACGTATG
JK 222	AAAGAATTCCTTATTACTATAGCCGTTGTAGAAAC
JK 223	AAAGGATCCTGCCCTTGATGTTTCTATAGAAG
JK 222B	AAAGAATTCGCATTCATTATACTTATTACTATAGCCGTTGTAGAAAC
JK 223B	AAAGGATCCTGCCCTTGATGTTTCTATAGAAGTTAATTCTGC
JK 224	CACATTCTTTTATCTTTCTATGTGCTTC
JK 225	CACAGACATATGATATTTTCTCTCGTGTATATTTGAAGTTTTCATTGCTGCGGCTGCTGAATTATTC
JK 226	AAAAAGCTTATGAAATTAACTTGTTACTGTATTATGTTTTTATTTATTCATATAATAAAATATG
JK 227	CACAGACATATGATATTTTCTCTCGTGTATATTTGAAGTTTTCATTGCTGCGGCTGCTGAATTATTCATTGTTAATTCTTCAGATTTATC
JK 228	TATCCCAATAAATTACAATTACAATTATTTATGAAAAGTTTTAAGAACAAAAATACTTTGAGGAGAAAGAAG
JK 229	TGAAAAGTTCTTCTCCTTTACTCACAGACATATGCATATGACCACAGCATCCTCTTTTCTTCT
JK 230	AAAACCGGTCAATATTAACCATTCTAATATAAAGAGGAG
JK 231	GGAGGAGGAAACCACAGCATCCTCTTTTCTTCTTTTTC
JK 232	GCTTAAATGTAAAGGACAAATAAAAGGGATAC
JK 233	ATGAAAAGTTTTAAGAACAAAAATACTTTGAGG
JK 234	AAAAAGCTTGAGGAGGAACCACAGCATCCTCTTTTCTTCTTTTTC

JK 235	AAATTCGAAATGACAAACATTATAGAAGCTACGTTCAAG
JK 236	ATGACAAATGTTGTAGAAGCTACTTTTAAAACC
JK 237	CTAGGATCCTTAGGCGCCTTTGTATAGTTCATCCATGCCATGTG
P 136	CGCAATTTGTTGTACATAAAATAGGC
P 176	CTAGACAGCCATCTCCATCTGG
P 177	ATGCATAAACCGGTGTGTCTGG
P 210	TTAACATCACCATCTAATTCAACAAG
P 322	CCCCGTTGTCTGAGAAGG
P 587	CTTTGGTGACAGATACTAC
P 668	TGATTAGCATAGTTAAATAAAAAAAGTTG
P 862	TCCAGTGAAAAGTTCTTCTCCT
P 961	ATCCTCTGGTAATTTTTCG
P 963	TAAGCAGTCGACCTACACAATCATGCATACTATGCC
P 969	TAAGCAGAATTCCCCTTCCGAACAAATTTACGCC
P 970	ATGGATCCACCACCACCACCACCACCACCACCCATATTATCTTTAGGGCATTCTTGATC
P 1446	CAGCTGCTGGGATTACACATG

5.2. Methods

Animal handling

Mice

Experiments were approved by the Federal State Authority (Regierungspräsidium Karlsruhe) and performed according to FELASA (Federation of European Laboratory Animal Science Association) guidelines. Experiments were performed using either NMRI, Swiss CD1 or C57Bl6 mice (25g, 6-8 weeks old) obtained from the companies Charles River or Janvier. Three of four mice were kept in each cage depending on their body weight and provided with *ad libitum* food and water.

Infection of mice

Naïve mice were infected by injecting parasites intraperitoneal (frozen parasite aliquots) or intravenously (infected blood- stages and sporozoites) or by bite of an infected mosquito to probe for parasite transmission.

Mosquitoes

The majority of experiments conducted as part of this theses were performed with *Anopheles stephensi* mosquitoes. However, it is important to note that experiments presented in Figure 3.4.3 A were conducted with *Anopheles gambiae mosquitoes* (kind gift from the lab of Victoria Ingham). Generally, mosquitoes were fed with 1% salt/water solution and 10% sucrose/water solution containing 0.05% Para- aminobenzoic acid (PABA). Naïve mosquitoes were kept at 28°C and 80% humidity and subsequently transferred into a 21°C incubator after infection.

Molecular biology and cloning

Genotyping of mutant parasites

Successful integration of the plasmids into the genome was monitored by PCR using *Taq* polymerase. Respective Primer combinations are indicated separate for each parasite line.

Reaction Mix (25µl):	10x Taq buffer	2,5µl
	dNTPs (10mM)	2,5µl
	gDNA	2µl
	Primer (100µM)	0,5µl each
	Polymerase	0,5µl
	ddH_2O	17,5µl

PCR amplification for cloning

PCR reactions to obtain fragments for cloning were usually done with Phusion polymerase and genomic DNA of *P. berghei* or *P. falciparum* as template.

Reaction Mix (50µl):	5x GC buffer	10µl
	dNTPs (10mM)	5µl
	Template	2µl
	Primer (100µM)	0,5µl each
	Polymerase	0,5µl
	ddH_2O	31,5µl

For challenging PCRs 1,5 µl of ddH_2O was replaced against the same amount of DMSO.
PCR products were separated and visualized on a 0,8% Agarose Gel. Fragments were cut from the Gel and purified using the PCR product purification kit according to the manufacturers protocol. Elution was done in 44 µl ddH_2O.

Restriction Digest

PCR fragments (insert) for cloning were digested in a total volume of 50 µl. Meaning to the purified 44 µl of product 5 µl of 10x Cutsmart buffer and 0,5 µl of each Enzyme was added. Vectors were digest in a volume of 20 µl. 17 µl of plasmid was added to 2µl of 10x Cutsmart buffer and 0,5 µl of the respective enzyme. Both, insert and vector were digested at 37°C over night and purified using the PCR purification kit (Roche) according to the manufacturer protocol.

Ligation and Transformation

Ligation of Insert and Vector was done in a total Volume of 10 µl. 7 µl of digested and purified insert, 1µl of backbone plasmid together with 1µl of T4 DNA Ligase and 1µl 10x ligase buffer was mixed and incubated for a minimum of 30 minutes at room temperature. For transformation into *E. coli* the complete Ligation mix was resuspended with 35 µl of bacteria and stored for 10 min on ice. Heat shock was done at 42 °C for 90 seconds, followed by 5 minutes on ice before being plated on LB agar plates containing the respective antibiotics. Agar plates were left at 37°C over night and 1 colony was used to inoculate 6 ml of liquid culture.

Plasmid Isolation

All plasmids were grown and multiplied in Xl1 blue DH5- alpha chemical competent *E. coli* bacteria (New England Biolabs, Ipswich, USA). Plasmids were generally isolated from 4-6 ml of bacteria culture grown in LB- Medium supplemented with Ampicillin or Kanamycin using the QIAprep Spin Miniprep Kit according to the manufacturer protocol.

Isolation of genomic DNA

For isolation of genomic DNA parasite containing blood was harvested from one mouse via cardiac puncture. The isolated blood was transferred into a 2 ml reaction tube containing 1 ml of PBS. RBCs were lyses by adding 150 µl of 1% Saponin. After inverting the tube a few times, the whole mixture was centrifuges for 1 min at full speed and the pellet was washed with 1ml of PBS. The resulting pellet was then resuspended in 200 µl of PBS to proceed with gDNA isolation using the Blood and Tissue kit (Qiagen) following the manufacturers protocol.

Plasmodium specific methods

Workflow for the generation of mutant parasites

Excluding plasmid preparation, the generation of a clonal parasite line takes about 3-4 weeks (Figure 5.2.1). It starts with the transfection of the linearized plasmid into purified schizonts using electroporation. Once mice become positive, parasites are harvested and successful transfection is determined by genotyping PCR. Subsequently the mixed parasite population in the blood is used to generate a clonal parasite line with limiting dilution.

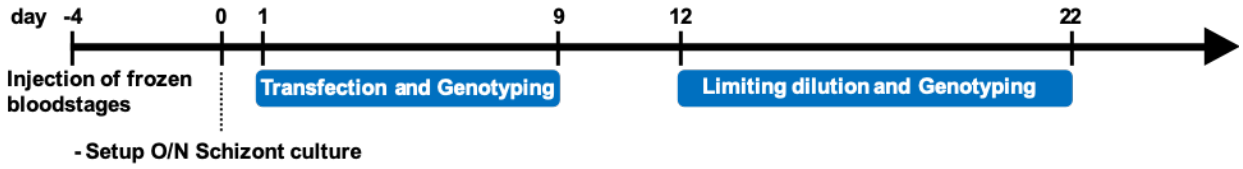

Figure 5.2.1 Schematic timeline for the generation of mutant parasite lines.

Purified schizonts are transfected with the respective plasmid via electroporation using the Amaxa kit. Mice infected with successfully transfected parasites become positive around d9 post transfection and the mixed population can subsequently be used for the generation of a clonal line via limiting dilution.

Parasite transfection

Transfection of linearized plasmids was performed as previously described (Janse et al. 2006). In short, schizonts obtained through in vitro overnight culture of blood stage parasites were purified with a 55% Nycodenz density gradient. After their subsequent electroporation followed by injection into a naïve mouse positive selection was done using Pyrimethamine (70 µg/ ml) while for negative selection or to recycle the selection cassette 5-FC (2 mg/ ml) was used. Both drugs were administered oral via the drinking water.

Generation of clonal parasite lines with limiting dilution

To generate a clonal parasite line from a mixed parental population after transfection a limiting dilution was performed. Blood of the donor mouse with a maximum of 1% parasitemia was harvested and diluted in PBS to obtain 0.9 parasites in 100 µl PBS. Subsequently, 10 mice were injected intravenously. Parasitemia was monitored using Giemsa stained blood smears. Blood of positive mice was harvested, parasites were isolated and the gDNA of the parasites was genotyped.

Generation of clonal parasite lines with FACS

For the generation of isogenic *akratin*(-) parasites (Kehrer et al., 2020) two drops of blood were collected from the tail vein of a mouse with a parasitemia of up to 0.3%. The blood was diluted in 1.5 ml of RPMI medium. Before analyses, the sample was drained using a 40 µm cell strainer. For detection, a 488 nm laser with a 527/32 nm filter for the GFP signal was used. Sorting was carried out in purity mode with the lowest flow rate at room temperature, using PBS as the sheath fluid. The sorted cells (hundred positive events) were immediately injected intravenously into naive Swiss CD1 or NMRI mice.

Workflow for the characterization of mutant parasite lines

Analyses of every mutant through the entire life cycle can take up to 4 weeks (not including transmission from the mosquito back into the host). Time intervals for each developmental stage are indicated below and each step is explained in detail in the following section.

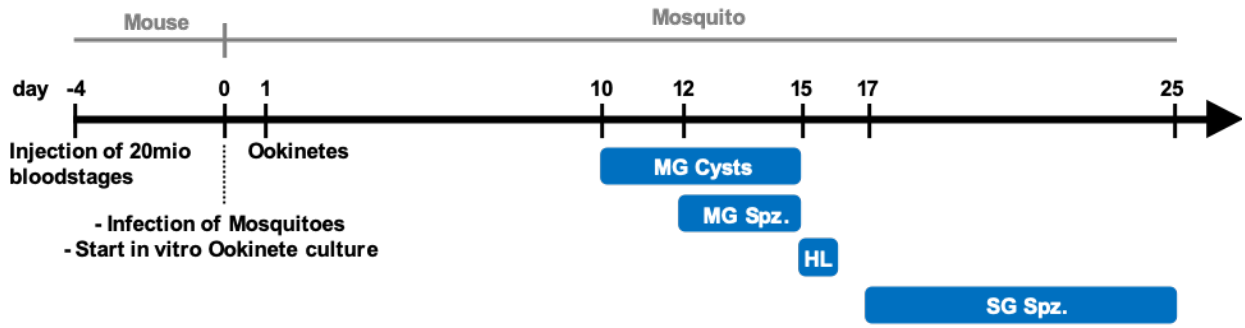

Figure 5.2.2 Schematic timeline for the analyses of mutant parasite lines

The characterization of newly generated parasite lines starts with the initial infection of a mouse with the respective parasite line. 4 days post infection the mouse is used for the infection of naïve mosquitoes or the setup of an in vitro ookinete culture. Between day 10 and 15 after mosquito infection oocysts can be analysed, followed by hemolymph sporozoites on day 15 and 16 and the characterization of fully formed salivary gland sporozoites from day 17 onwards.

Gametocyte activation and exflagellation

"Mice were injected i.p. with 20 million blood stage parasites. 3- 4 days post infection the infected blood was harvested.

For gametocyte activation, either 1 droplet of blood from the tail tip was placed on a glass slide, covered with a cover glass and incubated for 10 min at RT before observation and quantification of exflagellation events under the microscope, or 100 µl of blood was added to 500 µl of ookinete medium at 19°C and fixed with PFA after certain timepoints to use for immunostainings" (Kehrer et al., 2020).

Infection of mosquitoes

Mice used for mosquito infections were infected with 20 million blood-stage parasites i.p. 4 days before feeding. Sugar and salt pads were removed at least 4h prior the feed. Two mice containing exflagellating microgametes in the blood were anesthetized with ketamin (87,5mg/ kg) and xylazin (12,5 mg/ kg) in a volume of 100µl of PBS and placed on top of about 200 female mosquitoes for 20min. While every 5 min mice were turned around to allow the maximum number of mosquitos to bite. Subsequently mice were killed by cervical dislocation and mosquitoes were stored at 21°C with regular change of salt and sugar pads until further use.

Parasite isolation from infected mosquitoes

Generally, mosquitoes were dissected using a SMZ 1500 binocular microscope (Nikon) and two dissection needles. To remove intact midguts, the last two abdominal segments were cut off and the remaining abdomen was detached from the thorax to expose the midgut, which was subsequently transferred into a reaction tube containing/filled with 100 µl phosphate buffered saline (PBS). Salivary glands were obtained by carefully decapitating the mosquito with a pulling movement in a way that left the salivary glands attached to the head. Subsequently the salivary glands were separated from the head and transferred to a reaction tube supplied with 100 µl PBS. To collect haemolymph sporozoites, the last two abdominal segments of the mosquito were cut off and the thorax pierced with a finely drawn pasteur pipette filled with PBS. The mosquito was gently flushed with PBS and the drops forming at the abdominal opening were collected on a piece of Parafilm. Drops were then transferred into an empty reaction tube using a pipette.

in vitro ookinete culture

"Either 20 million blood stage parasites were injected i.p. or 6 million blood stage parasites were injected i.v. into a naïve NMRI/ CD1 mouse treated with Phenylhydrazin. 3 days post infection the drinking water was supplemented with Sulfadiazin (20 mg/ L; needs to be added before 8am)

to reduce asexual blood stages. 4 days post infection the blood was harvested by cardiac puncture to set up ookinete cultures. The blood of one mouse was added to 10 ml of Ookinete Medium (RPMI containing 25 mM Hepes and 300 mg l−1, l-glutamine, 10 mg l−1hypoxanthine, 50 000 units l−1penicillin, 50 mg l−1streptomycin, 2 g l−1NaHCO3, 20.48 mg l−1xanthurenic acid, 20% FCS; pH 7.8) @19 °C and incubated for 21h. Fully developed ookinetes were purified via 63% Nycodenz cushion and remaining RBCs were lysed with 170 mM NH4CL for 5min on ice (for proximity labeling only)" (Kehrer et al., 2020). Please note, neither Phenylhydrazin nor Sulphadiazin was used when ookinetes where used for fluorescence microscopy due to the high background signal after drug treatment.

Ookinete motility

Imaging of moving ookinetes was performed on a Zeiss AxioObserver microscope with either a 20x or 63x objective. For the observation of motile ookinetes, a single drop of cell suspension was placed onto a microscope slide and covered with a thin cover glass to create a confined environment. Movies were recorded with a frame rate of 20 frames per second for a duration of 10 minutes. In each experiment, multiple movies were recorded. The microscope slide was replaced after every two recordings to maintain experimental consistency. speed of ookinetes was subsequently analyzed using the manual tracking plugin in ImageJ.

Ookinete midgut traversal

"20 million blood stage parasites were injected i.p. into a naive Swiss CD1 mouse treated with phenylhydrazin 24 h prior transfer. 4 days post transfer about 20 female *anopheles* mosquitoes were allowed to feed for about 15min. Blood filled midguts were isolated after 24h as described previously (Han et al., 2000). Midguts were fixed in cold 4% Paraformaldehyde (PFA) for 45s and washed with cold PBS. The epithelial cell layer was then opened longitudinally using two needles to carefully remove the blood bolus followed by a second fixation with 4% PFA over night (Kehrer et al., 2020). To better visualize traversed ookinetes an additional IFA was performed. To do so cells were permeabilized with 0,5% Triton for 30min, incubated with an anti GFP antibody (abfinity) for 2h and a 2h incubation with an anti-rabbit 488 secondary antibody plus the addition of Phalloidin TRIC and Hoechst. Midguts were transferred onto a microscope slide and images were taken on a Nikon spinning disc Microscope using either a 40x or 60x objective" (Kehrer et al., 2020).

Apex- based proximity labeling in ookinetes

"Apex based labelling of proteins was performed as described in (Kehrer et al., 2020). Cells were washed once with PBS and resuspended in 1ml of ookinete medium containing biotin phenol (182 µg/ml). After incubation for 30 min at RT cells were split into 2 tubes. One was used as control and in one biotinylation was activated by adding 5µl of 100 mM H_2O_2. After 90 s the reaction was inactivated by adding 500 of 2x quencher solution (20 mM Sodiumascorbate, 20 mM Trolox, 1 0mM NaN3 in PBS). After washing the cells two times with 1x quencher solution samples were then lysed with RIPA buffer (50 mM Tris pH8, 1% Nonidet P-40, 0.5% Na-deoxycholate, 0.1% SDS, 150 mM NaCl, 2 mM EDTA). 20% of the lysate was kept as input control and biotinylated proteins were enriched using streptavidin coated beads at 4 °C overnight as described. Elution of proteins was done with a buffer containing 30 mM of Biotin, 2% SDS, 160 mM NaCl and 6 M Urea followed by mass-spectrometric analysis as described above" (Kehrer et al., 2020).
Western blot was performed using the following antibodies: anti-myc antibody (Roche 0.4 mg/ml, 1/1000) followed by incubation with goat anti mouse HRP (BioRad 1/10000), Streptavidin- HRP (Sigma, 1/500) or mouse anti-HSP70 followed by incubation with goat anti mouse HRP.

Proteomics

Mass spectrometric analysis was performed at the CellNetworks Core Facility for Mass Spectrometry and Proteomics of the ZMBH (Zentrum für Molekularbiologie der Universität Heidelberg) as previously described (Kehrer, Frischknecht, and Mair 2016).

Visualization of oocysts in infected midguts

For the quantification of oocyst numbers, infected midguts were isolated between day 10- 15 as described above and transferred into a 1,5 ml reaction tube containing 200 µl PBS. For permeabilization, PBS was replaced with 200 µl of 1% NP40/ PBS and after 20 minutes, the midguts were stained with 200 µl of 0.1% mercurochrome solution for at least 30 minutes but mostly over lunch. After several washes, when the supernatant appeared clear, midguts were transferred onto a microscope slide using a glass pipette and subsequently cover with a cover glass. Cysts were counted with transmission light using a 10x Objective and a green filter.

Sporozoite motility

"To observe motile sporozoites, parasites were isolated from salivary glands between d17 and 25 post mosquito infection. 5-10 infected salivary glands were transferred into a 1,5 ml reaction tube containing 100 µl PBS. Glands were smashed using a pestil and sporozoite number were counted using a hemocytometer. 30k sporozoites were pelleted resuspended in 3% BSA/ PBS and transferred into a 96 well plate with optical bottom. Before imaging the plate was spin down for 4 min with 1500 rpm in a tissue culture centrifuge. Imaging was done at a Zeiss widefield microscope using the 25x objective with a frame rate of 3 s for 3 min" (Kehrer et al., 2020).

In vivo imaging of sporozoites in the mouse skin

In vivo experiments in the skin of a mouse were performed by P. Formaglio and R. Amino at the Institut Pasteur as described in (Kehrer et al., 2022).

Cryopreservation of blood stage parasites

To cryopreserve blood stage parasites for long- term storage, 100 µl of blood obtained via cardiac puncture was mixed with 200 µl of freezing solution (10% Glycerol in Alsevers solution) and immediately frozen. For short term storage vials were kept at -80°C while for long term storage they were transferred into liquid nitrogen.

Clearing of parasites

100 µl of infected blood was fixed with an equal volume of 4% PFA at 4°C for 48 h. For clearing, cells were washed with PBS, resuspended in 200 µl of 10 or 50% CUBIC-P in PBS and incubated 24 h at 37°C. Post incubation time, cells were washed twice with PBS and stained with respective antibodies and Hoechst. For imaging, a drop of the resuspended cells was added onto a microscope slide and immediately covered with a cover glass (Kehrer et al., 2023).

Immunofluorescence staining

For staining of parasites with antibodies, cells were first fixed with 4% PFA and permeabilized with 0.5 % Triton X-100/PBS for 15 minutes at room temperature. Primary antibodies and secondary antibodies diluted in RPMI or PBS were incubated for at least 1 h at room temperature. After each step cells were washed three times with PBS. Please see additional table above for specific antibody dilutions.

Transmission electron microscopy of parasites treated with CUBIC-P

Infected red blood cells were obtained via cardiac puncture of an infected mouse and immediately fixed in a solution containing 2% glutaraldehyde and 2% PFA in 100 mM Cacodylate buffer at 4°C overnight. After fixation, the samples were rinsed three times for 5 minutes each in 100 mM Cacodylate buffer. Subsequently, they were incubated in 1% OsO_4 in 100 mM Cacodylate buffer for 60 minutes at room temperature. Next, the samples were washed twice with Cacodylate buffer and twice with distilled water (5 minutes for each washing step). Post-contrast staining was performed using 1% uranyl acetate in distilled water at 4°C overnight, followed by two washes with distilled water for 10 minutes each at room temperature.

For dehydration of the samples, H_2O was replaced by acetone through incubations with increasing concentrations of acetone: 30%, 50%, 70%, and 90% acetone solutions for 10 minutes per step, followed by two 10-minute incubations with 100% acetone. Subsequently, samples were infiltrated with 25%, 50% and 75% Spurr for 45 minutes each, followed by an infiltration step with 100% Spurr at 4 °C overnight. Samples were then incubated at 60 °C overnight leading to polymerization of the resin. Sections of 60-70 nm were cut and contrasted with 3% uranyl-acetate and 2% lead citrate, before imaging at the transmission electron microscope JEM-1400 (JEOL). (Kehrer et al., 2023)

Transmission electron microscopy and array tomography (concavin)

For the characterization of concavin, transmission electron microscopy (TEM) as well as array tomography was performed by the Electron microscopy core facility (EMCF) of the University of Heidelberg as described in (Kehrer et al., 2022).

.

5.3. Generation of Parasite lines

Parasites for proximity labeling (Section 3.1)

Generation of SOAP-Apex2-myc parasites (pL8)

The Apex2-myc sequence flanked with the restriction sites BamHI and XbaI was ordered via geneart and after digestion with the 2 enzymes the fragment was ligated into a vector containing SOAP- BirA* (kind gift from Gunnar Mair) exchanging the bira* sequence. The resulting plasmid pL8 was linearized with HpaI prior transfection to facilitate an integration via single crossover and transfected into wild type PbANKA parasites (Kehrer et al., 2020).

Soap-Apex2 parasites are not clonal and thus still contain a tiny amount of wild type.

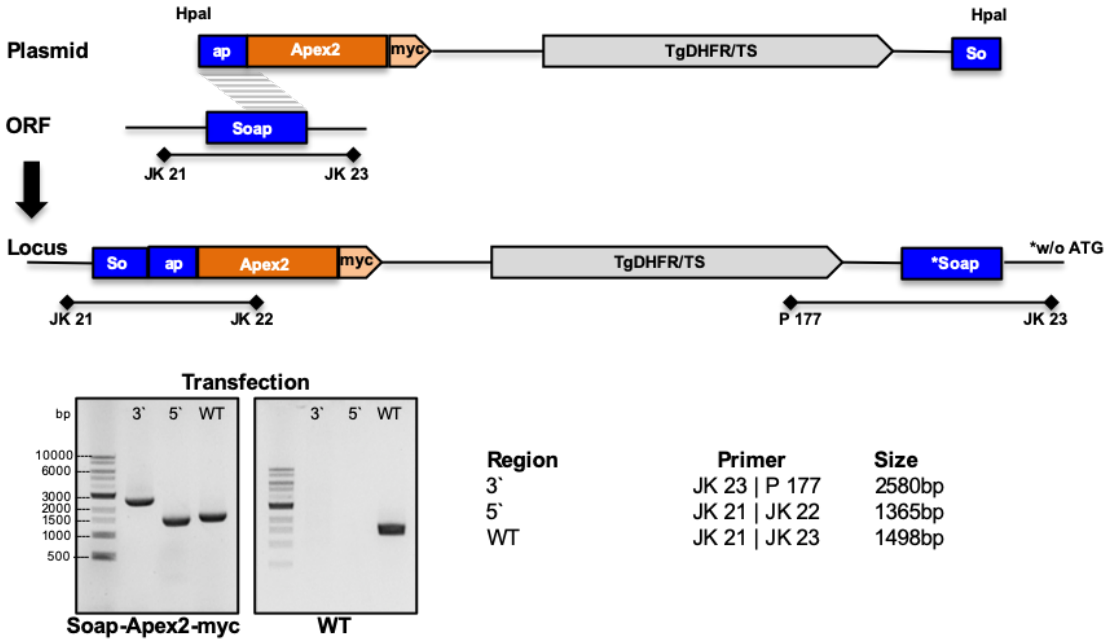

Figure 5.3.1 Generation of SOAP-APEX2-myc parasites

Generation of Soap-APEX2 parasites via single homologous recombination. The cartoon shows the integration strategy and primers used for genotyping with amplicon sizes of the resulting transgenic line indicated. For primer sequences please see Material and Methods. Plasmid contains the resistance marker dihydrofolatereductase/thymidine-synthase from Toxoplasma gondii (Tgdhfr/ts) (grey). Note that the second copy of soap lacks the ATG and should not be expressed. Figure modified from (Kehrer et al., 2020).

Generation of SOAP-mCherry parasites (pL127)

SOAP was amplified from plasmid pL7 with primers JK243 and JK244. The resulting 517 bp product was digested with EcorI and NdeI and inserted in frame with mCherry into the Spooki-mCherry plasmid (Klug et al., 2018) digested with the same enzymes. The resulting plasmid pL127 was linearized with HpaI prior transfection to facilitate an integration via single crossover and transfected into wild type PbANKA parasites.

Parasites are not clonal and thus still contain a tiny amount of wild type.

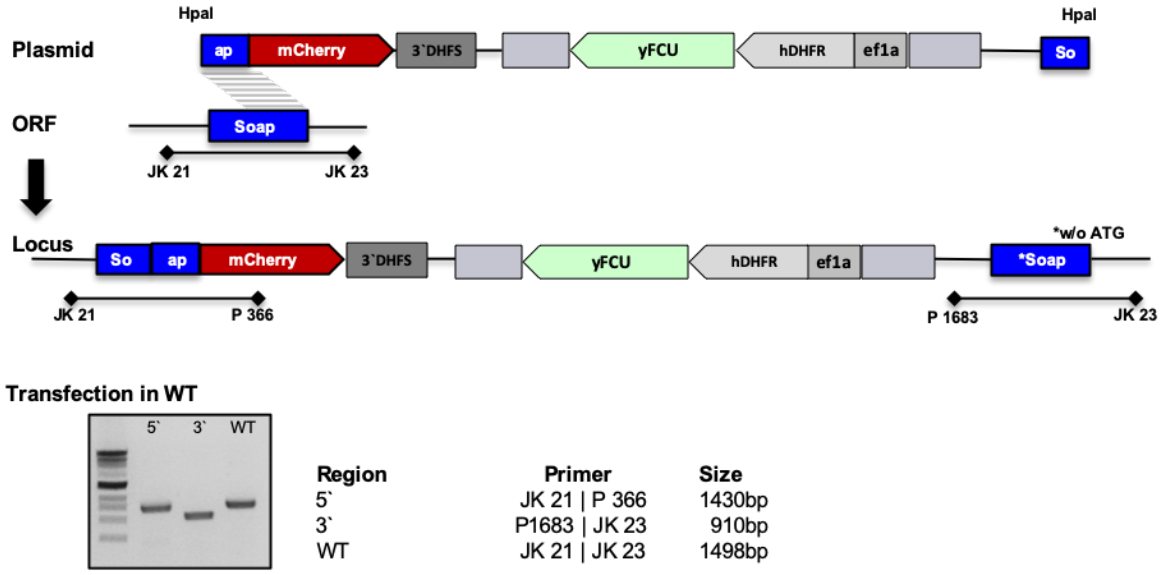

Transfection in WT

Region	Primer	Size
5`	JK 21 | P 366	1430bp
3`	P1683 | JK 23	910bp
WT	JK 21 | JK 23	1498bp

Figure 5.3.2 Generation of SOAP-mCherry parasites

Generation of Soap-mCherry parasites via single homologous recombination. The cartoon shows the integration strategy and primers used for genotyping with amplicon sizes of the resulting transgenic line indicated. For primer sequences please see Material and Methods.

Generation of SP-Apex2/myc-TRAP parasites (pL7)

The Apex2-myc sequence was ordered via geneart and amplified with primers JK17 and JK18. The resulting 878bp fragment was digested with BamHI and ligated into a vector containing SP-BirA*- Trap (kind gift from Gunnar Mair) exchanging the bira* sequence. The SP- BirA*- Trap plasmid was first digested with HindIII and respective overhangs were filled in to obtain blunt ends followed by the digestion with BamHI. The resulting plasmid pL7 was linearized with ClaI prior transfection to facilitate an integration via single crossover and transfected into wild type PbANKA parasites.

Parasites are not clonal and thus still contain a tiny amount of wild type.

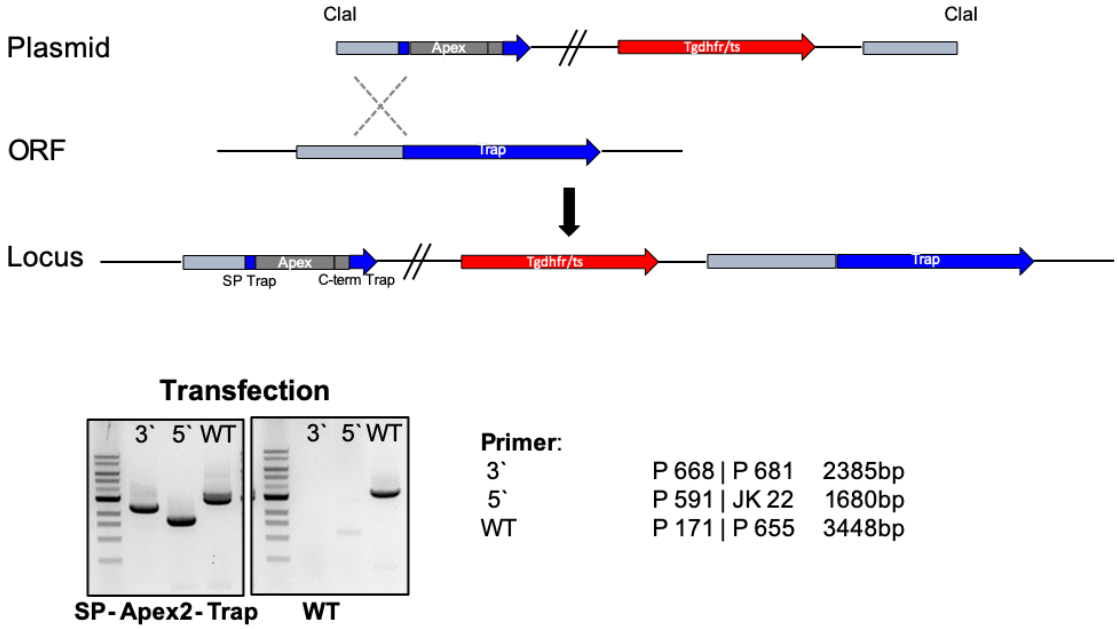

Figure 5.3.3 Generation of SP-Apex2/myc-TRAP parasites

Generation of SP-APEX2-Trap parasites via single homologous recombination. The cartoon shows the integration strategy and primers used for genotyping resulting the transgenic line indicated. For primer sequences please see Material and Methods. Plasmid contains the resistance marker dihydrofolatereductase/thymidine-synthase from Toxoplasma gondii (Tgdhfr/ts) (grey).

Parasites related to PbANKA_1105300 (Section 3.2)

Generation of PbANKA_1105300 (-) parasites (pL28)

"3`UTR of PbANKA_1105300 was amplified using primers JK67 and JK68 and inserted into a plasmid containing the recyclable yFCU/ hDHFR selection cassette and GFP expressed under the HSP70 promoter digested with NotI and SacII. The 5`UTR of PbANKA_1105300 was amplified using primers JK65 and JK66 and inserted into the plasmid using KPNI and HindIII. The resulting plasmid pL28 was linearized with NotI and SacII prior transfection to facilitate double crossover integration. Genotyping of transfected parasites is shown below. Polyclonal parasites were obtained by FACS. To generate selection marker-free parasites (KO (NS)) for complementing the locus with *P. berghei* or *P. falciparum* the drinking water of mice was supplemented with 2mg/ ml 5- FC. Leading to the survival of parasites which looped out the selection cassette. Clonal parasites were obtained by limiting dilution" (Kehrer et al., 2020).

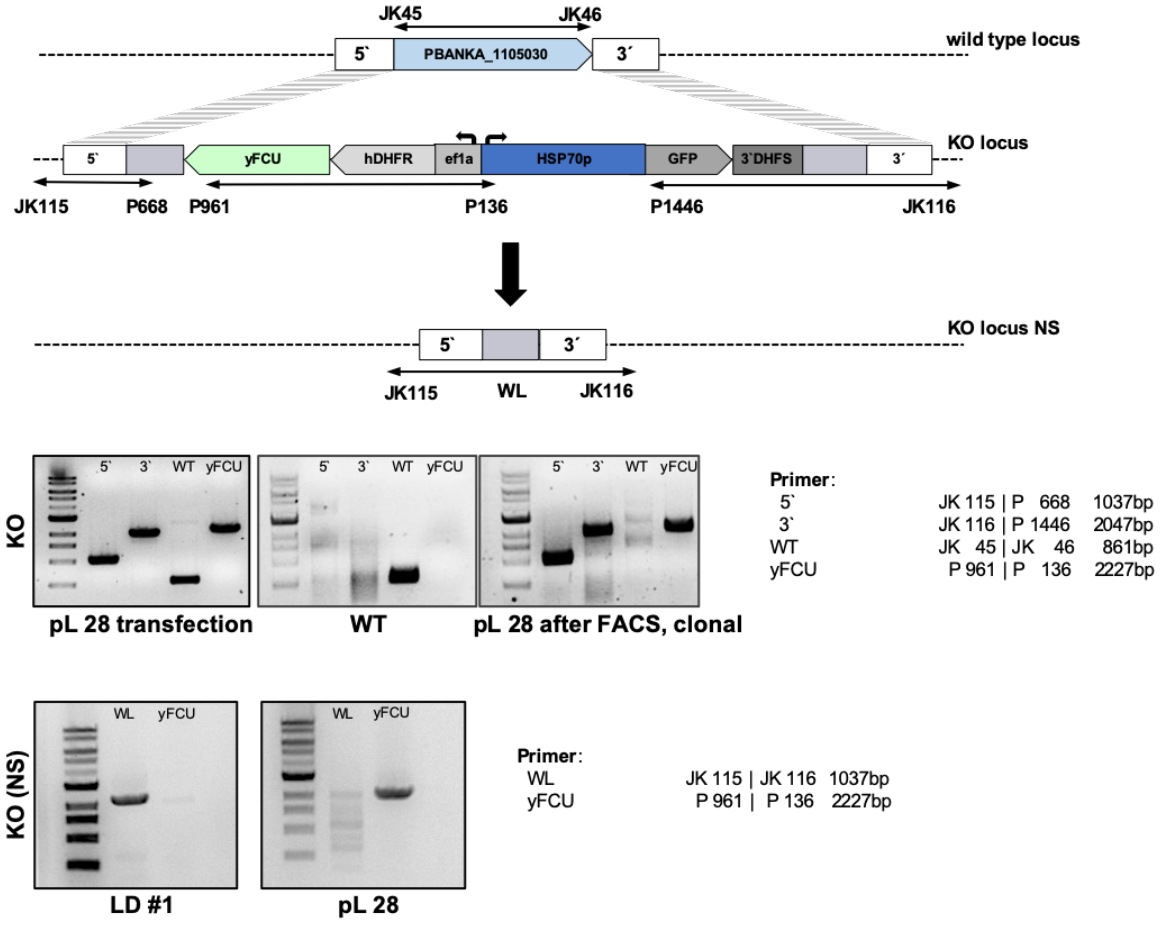

Figure 5.3.4 Generation of PBANKA_1105300 (-) and KO(NS) parasites

Generation of *akratin(-)* and *akratin(-)* negative selected parasites via double homologous recombination. The cartoon shows the integration strategy and primers used for genotyping. Note that as yFCU (Yeast cytosine deaminase-uracil phosphoribosyl transferase fusion protein) was used as a negative selection marker (see methods). Figure taken from (Kehrer et al., 2020).

Generation of akratin(-)$^{Pbakratin\text{-}gfp}$ parasites (pL59)

"The 5`UTR with the entire ORF of PbANKA_1105300 was amplified from wild type gDNA using primers JK66 and JK152 and inserted into the KO plasmid (pL28) using KpnI and NdeI replacing the selection marker. Therefore, a TgDHFR seclection cassette was amplified using primers JK153 and JK154 and inserted between the GFP and 3`UTR using NotI and EcorV resulting in plasmid pL59. For transfection of parasites via double crossover the plasmid was digested with KpnI and SacII and transfected into negative selected KO parasites" (Kehrer et al., 2020).

Generation of akratin(-)$^{Pfakratin\text{-}gfp}$ parasites (pL75)

"The ORF of PF3D7_0505700 was amplified from gDNA using primers JK171 and JK172 and inserted into the KO plasmid (pL28) downstream of the *P. berghei* 5`UTR using HindIII and NdeI replacing the selection marker. The TgDHFR selection cassette was amplified using primers JK153 and JK154 and inserted between the GFP and 3`UTR using NotI and EcorV resulting in plasmid pL 75. For transfection of parasites via double crossover the plasmid was digested with KpnI and SacII and transfected into negative selected KO parasites" (Kehrer et al., 2020).

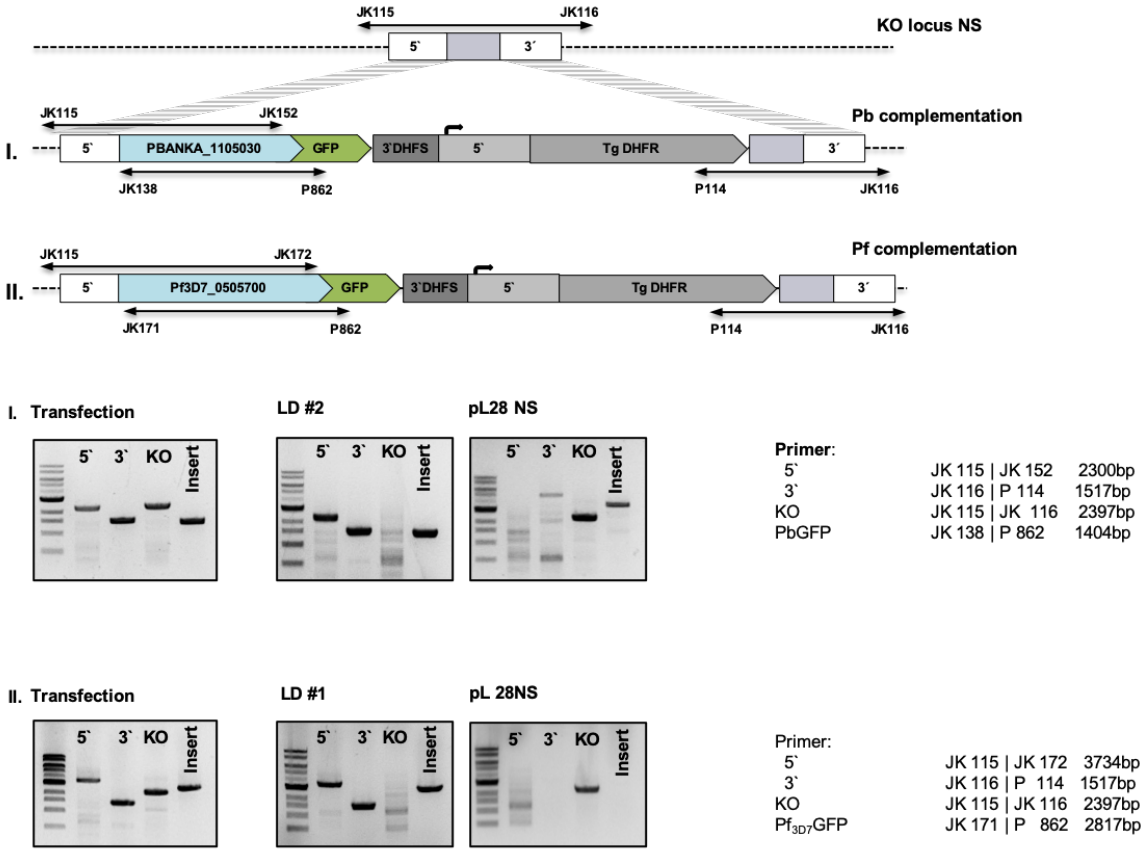

Figure 5.3.5 Generation of PBANKA_1105300(-) complementation parasites

Generation of *P. berghei* and *P. falciparum* complementation parasites via double homologous recombination. The cartoon shows the cloning strategy and primers used for genotyping. Figure taken from (Kehrer et al., 2020).

Generation of akratin$^{EYKY\text{-}AAAA}$ parasites (pL84)

"The 5`UTR together with the entire ORF was amplified from wt gDNA using primer JK66 and a reverse Primer introducing the mutations and inserted into the pL59 plasmid using KpnI and NdeI resulting in pL84. For transfection of parasites via double crossover the plasmid was digested with KpnI and SacII and transfected into negative selected KO parasites" (Kehrer et al., 2020).

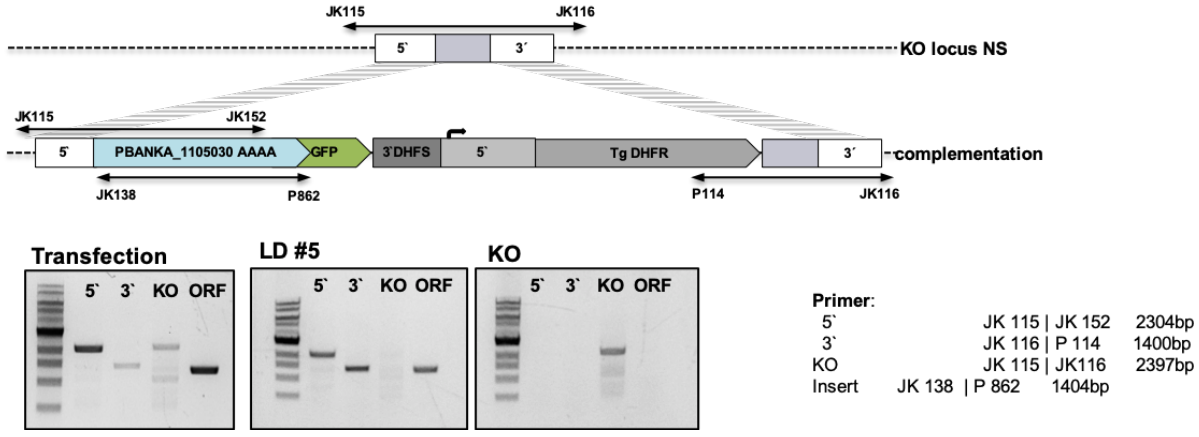

Figure 5.3.6 Generation of akratin$^{EYKY\text{-}AAAA}$ parasites

Generation of akratin$^{EYKK/AAAA}$ parasites via double homologous recombination. The cartoon shows the cloning strategy and primers used for genotyping. Agarose gel pictures show 5`integration, 3`integration as well as KO and the inserted locus as indicated. Expected amplicon sizes are indicated on the right. Figure taken from (Kehrer et al., 2020).

Parasites related to PAT (Section 3.3)

Generation of PAT(-)^{GIMO} for the gene in marker out strategy

The 2791 bp selection cassette containing the ef1a promoter, hDHFR and yFCU was amplified from the Actin replacement plasmid, provided by Ross Douglas (Douglas et al., 2018)using primers JK26 and JK27. The PCR product was digested with HindIII and EcoRI and ligated into pLIS0076 (Kehrer, Singer, et al., 2016), resulting in the final plasmid pL12 which was transfected into wild type ANKA parasites.

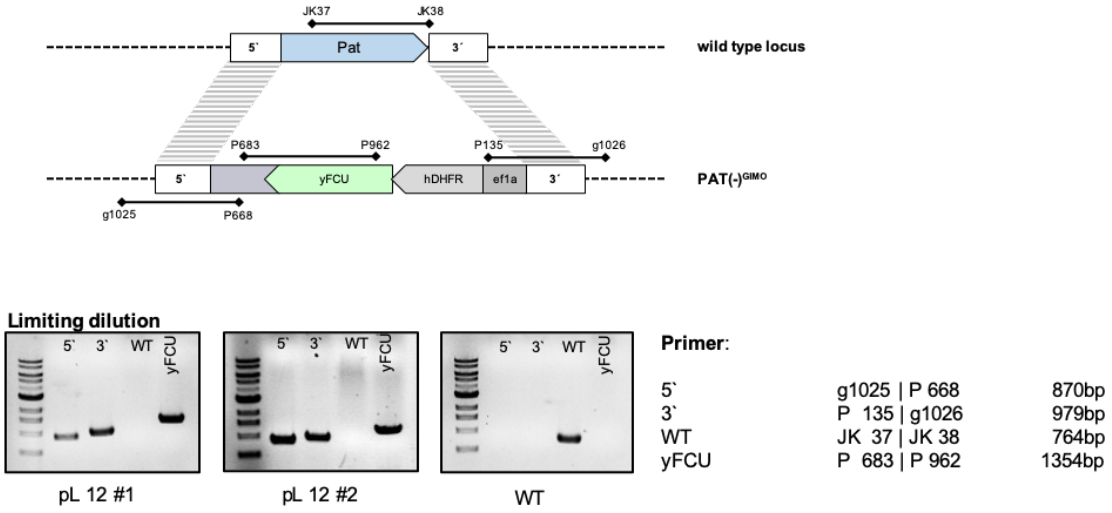

Figure 5.3.7 Generation of PAT(-)^{GIMO}

Cartoon showing the integration strategy for the generation of PAT(-)^{GIMO} parasites and primers used for genotyping. Genotyping PCRs of wild type and mutant parasites directly after transfection and after limiting dilution. Agarose gel pictures show 5`integration, 3`integration as well as wildtype and selection marker as indicated. Expected amplicon sizes are indicated on the right.

Generation of PAT$^{\Delta 512-541}$ (pL15)

The final plasmid pL15 was generated in a multistep process. First, plasmid pL12 was digested with EcoRV and HindIII and ligated with a 479 bp PCR fragment amplified with primers JK35 and JK36 from the previously published 030309|KO plasmid (Kehrer, Singer, et al., 2016)to obtain the 3' UTR of PbDHFR/ts.

Next the 785 bp of PATΔ512-541 was amplified from genomic DNA using the primers JK37 and JK38 and inserted into the same plasmid right before the 3`UTR using KpnI and EcoRV.

For the generation of the final pL15 plasmid the PATΔ512-541 sequence together with the 3' UTR of PbDHFR/ts (1252 bp) was amplified from the above intermediate plasmid with primers JK36 and JK37 digested with KpnI and HindIII and ligated into the sequence. After digestion through KpnI and HindIII, the fragment was ligated in the 030390|KO plasmid digested with the same enzymes. For transfection into wild type parasites the plasmid was linearized with KpnI and SacII.

Generation of PAT$^{\Delta 514-541}$ (pL16)

For the generation of PATΔ514-541 parasites (pL16) 791 bp of the PAT gene was amplified from genomic DNA using the primers JK37 and JK39. The resulting fragment was digested with KpnI and EcorV and ligated in front of the PbDHFR/ts 3`UTR in analogy to pL15.

For the generation of the final pL16 plasmid the PATΔ514-541 sequence together with the 3' UTR of PbDHFR/ts (1258 bp) was amplified from the above intermediate plasmid with primers JK36 and JK37 digested with KpnI and HindIII and ligated into the sequence. After digestion through KpnI and HindIII, the fragment was ligated in the 030390|KO plasmid digested with the same enzymes. For transfection into wild type parasites the plasmid was linearized with KpnI and SacII.

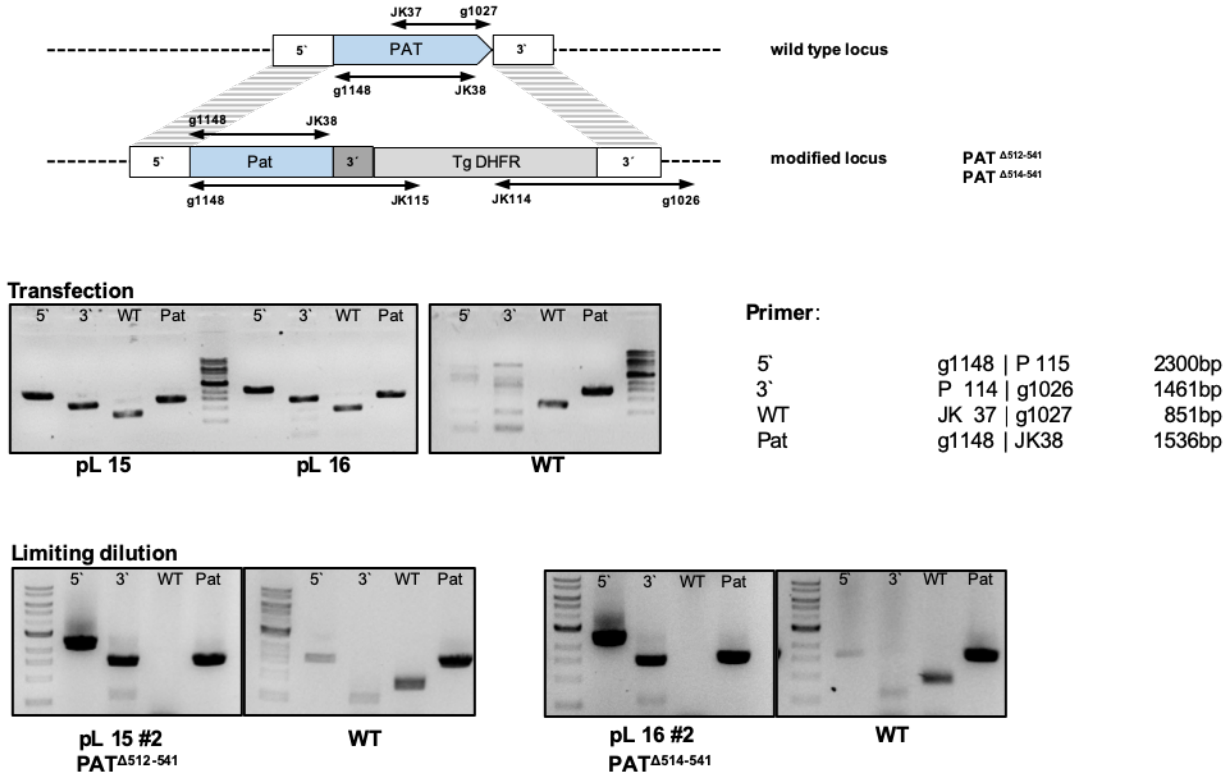

Figure 5.3.8 Generation of PAT tail deletions

Cartoon showing the integration strategy and primers used for genotyping. Genotyping PCRs of wild type and mutant parasites directly after transfection and after limiting dilution. Agarose gel pictures show 5`integration, 3`integration as well as wildtype and selection marker as indicated. Expected amplicon sizes are indicated on the right.

Generation of PAT$^{\Delta 514-541}$- GFP (pL45)

Plasmid pL40 was digested using HindIII and BamHI. The insert lacking the c- terminus was amplified with primers JK130 and JK132 from PbANKA genomic DNA. The 1560 bp PCR fragment was ligated with the same enzymes and ligated into pL40. The resulting final plasmid pL45 was digested with KpnI and SacII for transfection into PAT(-) parasites.

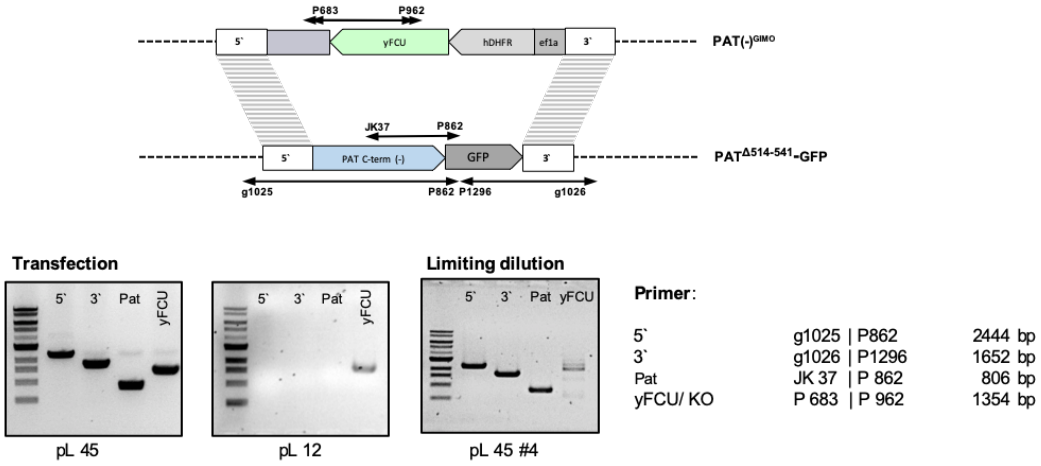

Figure 5.3.9 Generation of PAT $^{\Delta 514-541}$- GFP (pL45)

Cartoon showing the integration strategy for the generation of PAT $^{\Delta 514-541}$-GFP and primers used for genotyping (top). Genotyping PCRs of the non-clonal PAT $^{\Delta 514-541}$-GFP parasite line directly after transfection and after limiting dilution compared to the receiver line PAT(-)^{GIMO}. Agarose gel pictures show 5`integration, 3`integration as well as PAT and the yFCU selection cassette. Expected amplicon sizes are indicated on the right.

Generation of PAT(-)$^{EYKY\text{-}AAAA}$ (pL46)

PAT was amplified from genomic DNA using primers 130 and 133. Mutations were introduced with primer 133 at the c- terminus. The 1641 bp fragment was ligated with plasmid pL40 digested with the enzymes HindIII and BamHI to generate a fusion with GFP. The final plasmid pL46 was digested with KpnI and SacII for transfection into PAT(-) GIMO parasites.

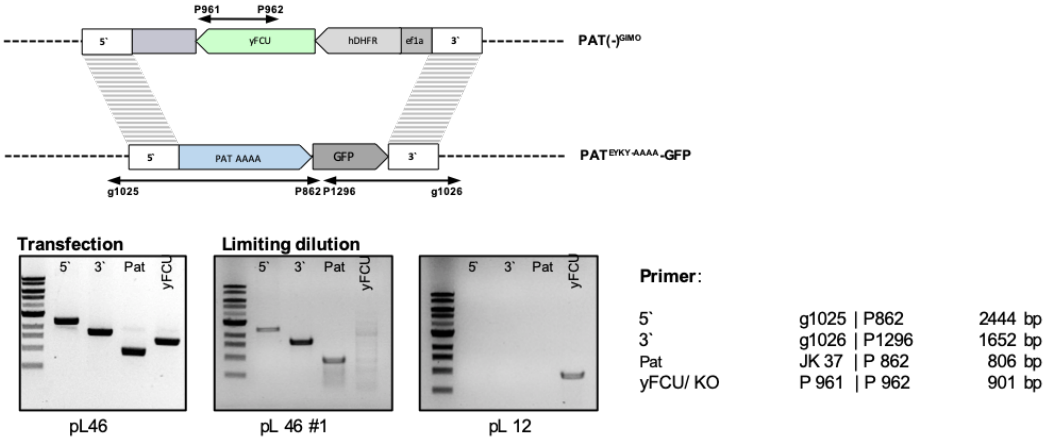

Figure 5.3.10 Generation of PAT(-)$^{EYKY\text{-}AAAA}$-GFP parasites (pL46)

Cartoon showing the integration strategy for the generation of PAT$^{EYKY\text{-}AAAA}$-GFP and primers used for genotyping (top). Genotyping PCRs of the non-clonal PAT$^{EYKY\text{-}AAAA}$-GFP parasite line directly after transfection and after limiting dilution compared to the receiver line PAT(-)^{GIMO}. Agarose gel pictures show 5`integration, 3`integration as well as PAT and the yFCU selection cassette. Expected amplicon sizes are indicated on the right.

Generation of PAT(-)- GFP (pL47)

Plasmid pL40 was digested with HindIII and BamHI and subsequently, blunt ends were generated using T4 DNA polymerase and re- ligated. The resulting plasmid was called pL47 digested with KpnI and SacII and transfected into PAT(-) parasites.

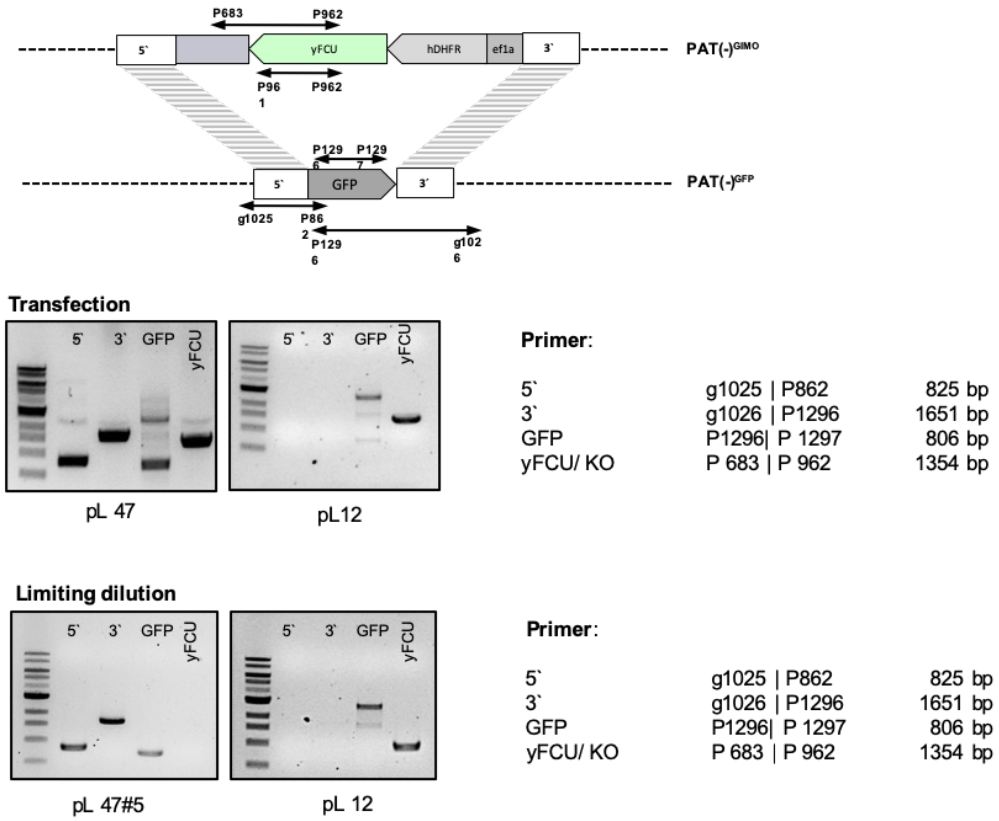

Figure 5.3.11 Generation of PAT(-)^{GFP} (pL47)

Cartoon showing the integration strategy for the generation of PAT(-)^{GFP} and primers used for genotyping (top). Genotyping PCRs of the non-clonal PAT(-)^{GFP} parasite line directly after transfection and after limiting dilution compared to the receiver line PAT(-)^{GIMO}. Agarose gel pictures show 5`integration, 3`integration as well as GFP and the yFCU selection cassette. Expected amplicon sizes are indicated on the right.

Generation of PAT(-)^{TgTFP1} (pL 40)

The 1703 bp of TGGT1_216820 were amplified from cDNA using primers JK98 and JK99, digested with HindIII and PstI and ligated into pL12 digested with the same enzymes, resulting in plasmid pL39. The 735 bp GFP sequence was amplified using the primers P1296 and JK100 digested with BamHI and EcoRI and ligated into the digested and purified pL39, resulting in plasmid pL40.

Generation of PAT$^{TgTFP1\ C\text{-}term}$ (pL 67)

A 269 bp fragment containing 62 bases of the PAT-ORF and the C-terminus of the TgTFP1 starting after the last TM domain was ordered from Geneart. Using PstI and BamHI restriction sites, it was ligated into the pL46 vector. In the resulting plasmid pL67 the PbPAT C-terminus was replaced by the TgPAT C-terminus. The resulting plasmid pL67 was transfected into PAT(-)- GFP parasites using KpnI and SacII for linearization.

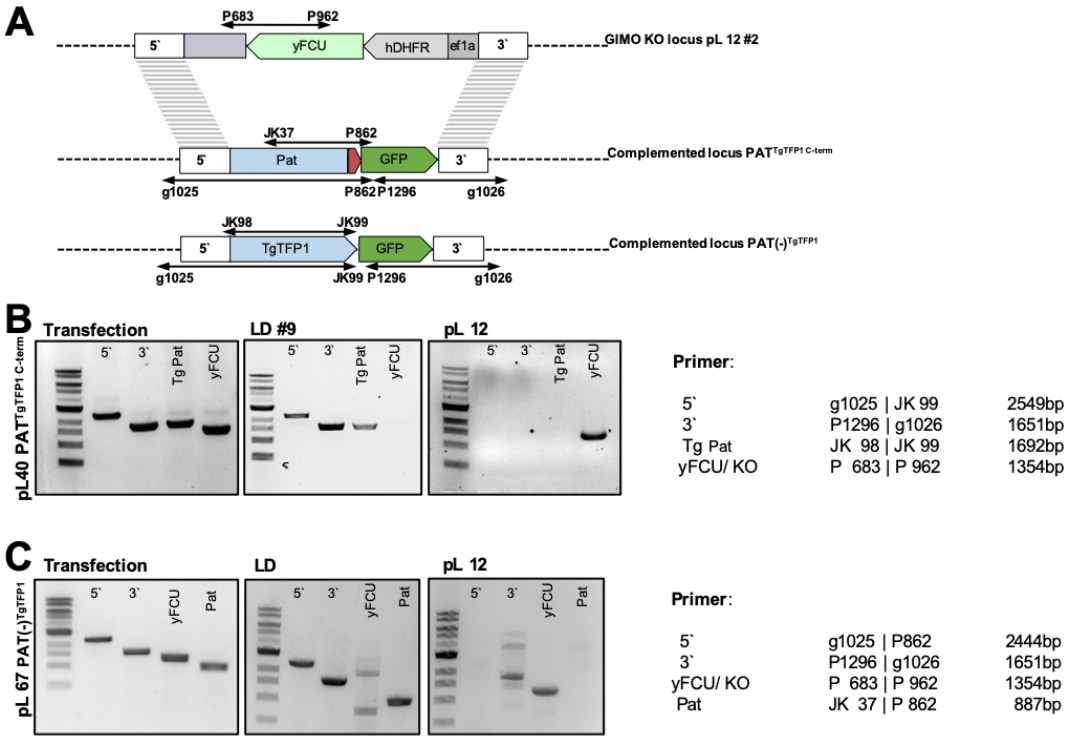

Figure 5.3.12 Generation of PAT(-)^{TgTFP1} and PAT$^{TgTFP1C\text{-}term}$

(A) Cartoon showing the integration strategy for the generation of the respective mutant and primers used for genotyping. (B) Genotyping PCRs of the non-clonal PAT$^{TgTFP1C\text{-}term}$ parasite line directly after transfection and after limiting dilution compared to the receiver line PAT(-)^{GIMO}. (C) Genotyping PCRs of the non-clonal PAT(-)^{TgTFP1} parasite line directly after transfection and after limiting dilution compared to the receiver line PAT(-)^{GIMO} (bottom). Agarose gel pictures show 5`integration, 3`integration as well as PAT and the yFCU selection cassette. Expected amplicon sizes are indicated on the right.

Generation of PAT(-)$^{EY\text{-}AA}$ (pL85)

The ORF coding for a 145-bp pat region containing the EY- AA mutation was ordered from GeneArt (ThermoFisher) and ligated into the pL67 vector (see below) after PstI and BamHI (NEB) digest. The

resulting plasmid was called pL85. For transfection pL85 was linearized using KpnI and SacII and transfected into PAT(-) GIMO parasites.

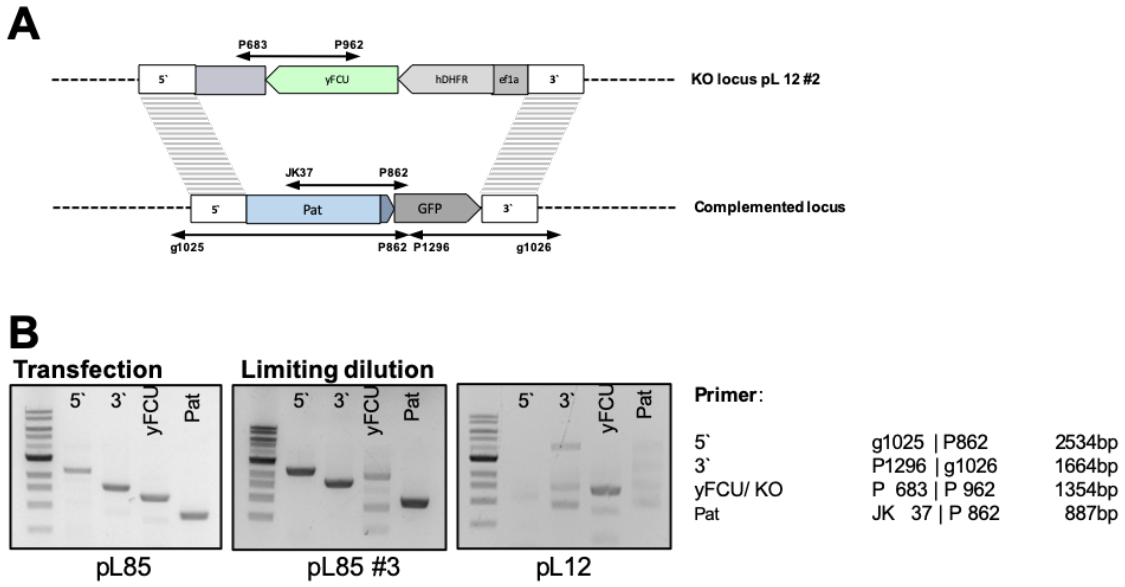

Figure 5.3.13 Generation of PAT(-)$^{EY\text{-}AA}$ parasites

(A) Cartoon showing the integration strategy and primers used for genotyping. (B) Genotyping PCRs of non-clonal parasites directly after transfection and after limiting dilution as well as KO negative control. Agarose gel pictures show 5`integration, 3`integration as well as PAT and selection marker as indicated in A. Expected amplicon sizes are indicated on the right.

Generation of PAT(-)$^{TgMIC2\ C\text{-}term}$ (pL 91)

A 234 bp fragment encompassing 62bp of the PAT-ORF and the C-terminus of the TgMIC2 protein starting after the last TM domain was synthesized by Geneart. The fragment was released from its vector using PstI and PvuII and inserted into plasmid pL46. Since PvuII creates blunt ends, pL46 was first digested with BamHI for 1 h and the overhang was filled-in by adding 1 µl dNTPs and 1 µl T4 DNA Polymerase for 15 min to catalyse 5´-3´ synthesis. Afterwards a second restriction digest using PstI was performed. Ligation resulted in plasmid pL66. Several attempts in integrating pL66 into PAT(-) GIMO parasites failed therefore we have changed our strategy.
A selection cassette was amplified from the pL75 plasmid using the primers JK190 and JK191, and assembled with the EcoRI digested plasmid pL66 using Gibson assembly. The final plasmid pL91 was linearized using KpnI and SacII and transfected into PAT(-)- GFP parasites.

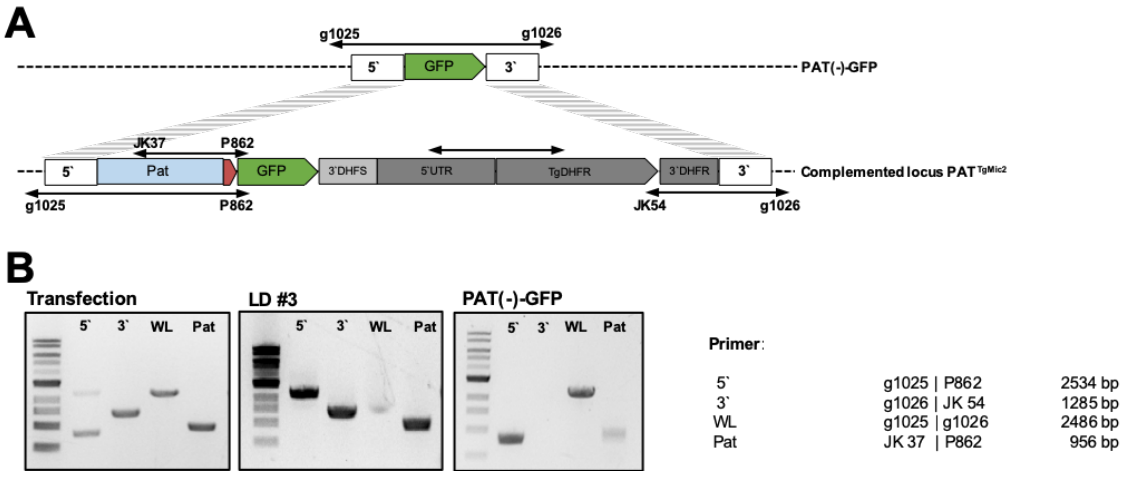

Figure 5.3.14 Generation of PAT(-)$^{TgMIC2\ C\text{-}term}$ parasites

(A) Cartoon showing the integration strategy and primers used for genotyping. (B) Genotyping PCRs of non-clonal parasites directly after transfection and after limiting dilution as well as KO negative control. Agarose gel pictures show 5`integration, 3`integration as well as amplification of the whole locus and PAT as indicated in A. Expected amplicon sizes are indicated on the right.

Generation of PAT $^{C\text{-}term\ (-)}$|CCP-PAT (pL71)

The final plasmid pL 71 was generated in multiple steps. To assemble CCP-PAT-mCherry, the PAT ORF was amplified from genomic DNA using primer JK165 and JK166. The resulting fragment was digested with NdeI and SacII and ligated into the CCP-PAT plasmid (Kehrer, Singer, et al., 2016) digested with the same enzymes leading to plasmid pL68. Next the ccp promoter region as well as the pat ORF were amplified by PCR from the pL68 plasmid using the primers JK166 and JK167, and ligated into the pL54 vector using NotI and SacII restriction sites to obtain a plasmid coding for an mCherry-tagged pat under ccp promoter expression (pL69).

To assemble PAT$^{C\text{-}term(-)}$ fused to GFP the required fragment was amplified using primers JK168 and JK169, digested with KpnI and AgeI and ligated into pL56 digested with the same enzymes leading to plasmid pL70.

For the final step to generated pL71, pL69 was digested with AflII and AgeI and recombined with pL70 digested with AflII and AgeI. For transfection into PAT(-) GIMO parasites the plasmid was digested with XhoI and SacII.

Generation of PAT $^{EYKY\text{-}AAAA}$|CCP-PAT (pL73)

First the motif mutation of PAT was created by PCR-amplification of a 2395 bp fragment with the primers JK168 and JK170 enclosing the complete ORF of PAT. The fragmentwas digested with KpnI and AgeI and inserted into pL56 resulting in the intermediate plasmid pL72.

In analogy to the generation of pL71, plasmid pL69 was digested with AflII and AgeI and recombined with pL72 digested with AflII and AgeI. For transfection into PAT(-) GIMO parasites the final plasmid was digested with XhoI and SacII.

Generation of PAT $^{EY\text{-}AA}$|CCP-PAT (pL95)

PAT $^{EY\text{-}AA}$ together with the 5`UTR was amplified from plasmid pL85 (see above), digested with XhoI and AgeI and ligated into pL73 digested with the same enzymes. For transfection into PAT(-) GIMO parasites the final plasmid was digested with XhoI and SacII.

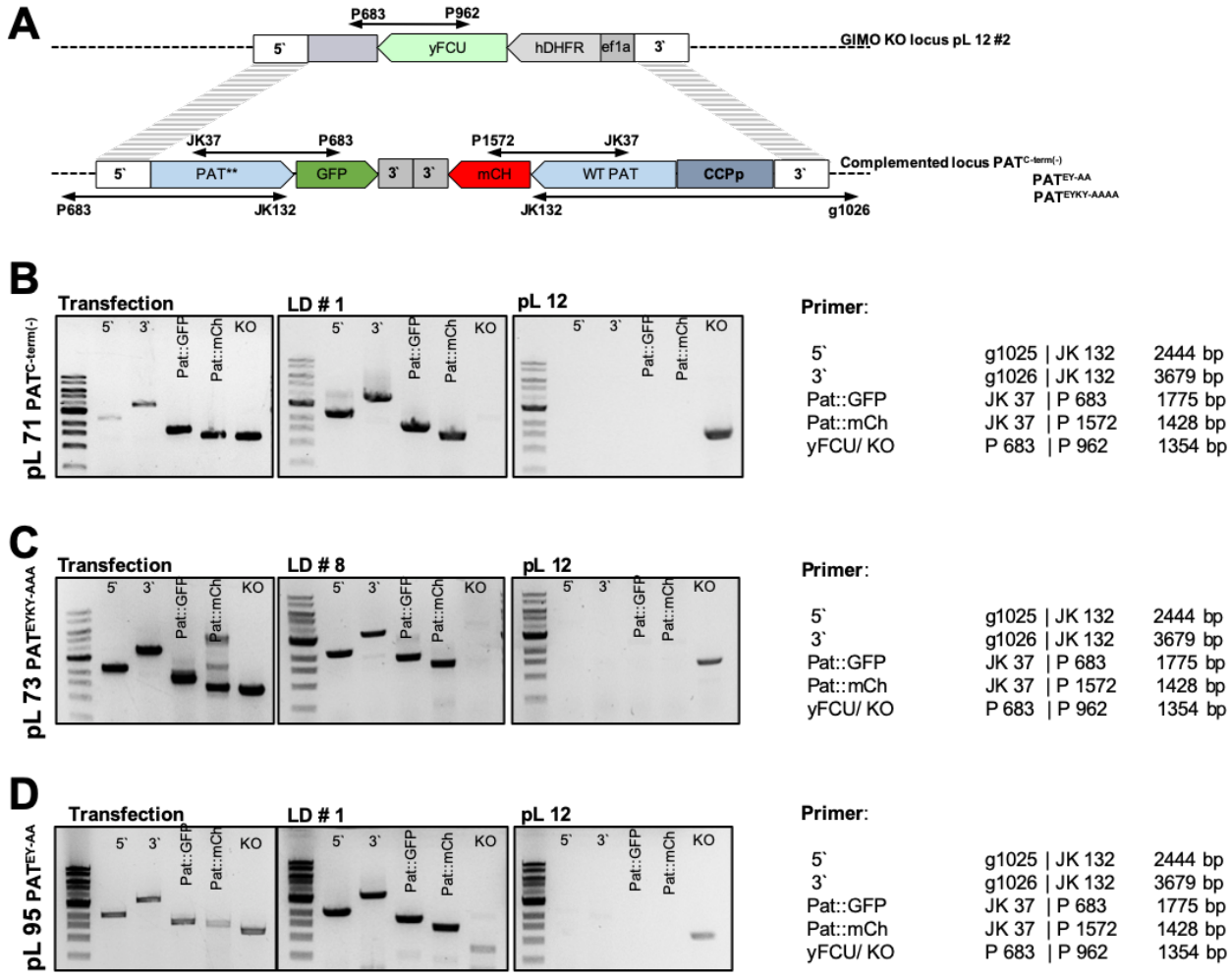

Figure 5.3.15 Generation of parasite lines for stage specific expression of modified PAT versions

(A) Cartoon showing the integration strategy and primers used for genotyping. (B) Genotyping PCRs of the non-clonal PAT$^{c\text{-}term(-)}$ parasite line directly after transfection and after limiting dilution. Agarose gel pictures show 5`integration, 3`integration as well as PAT-GFP, PAT-mCherry and wild type as indicated in A. Expected amplicon sizes are indicated on the right. (C) Genotyping PCRs of the non-clonal PAT$^{EYKY\text{-}AAAA}$ parasite line directly after transfection and after limiting dilution. Agarose gel pictures show 5`integration, 3`integration as well as PAT-GFP, PAT-mCherry and wild type as indicated in A. Expected amplicon sizes are indicated on the right. (D) Genotyping PCRs of the non-clonal PAT$^{EY\text{-}AA}$ parasite line directly after transfection and after limiting dilution. Agarose gel pictures show 5`integration, 3`integration PAT-GFP, PAT-mCherry and wild type as indicated in A. Expected amplicon sizes are indicated on the right.

Parasites related to concavin (Section 3.4)

Generation of concavin(-) parasites (pL24)

"The 3`UTR (779 bp) of PbANKA_1422900 was amplified from wild type gDNA using primers JK57 and JK58 and inserted into a plasmid (pL22) containing the recyclable yFCU/ hDHFR selection cassette and *gfp* expressed under the *hsp70* promoter digested with NotI and SacII. The 5`UTR (554 bp) was amplified using primers JK55 and JK56 and inserted into the plasmid using KpnI and HindIII. The resulting plasmid pL24 was linearized with KpnI and SacII prior transfection for double crossover integration" (Kehrer et al., 2022).

Generation of concavin(-) parasites negative selected

"The drinking water of mice infected with *concavin(-)* parasites was supplemented with 2 mg/ml 5-FC. Clonal parasites which looped out the selection cassette were obtained by limiting dilution" (Kehrer et al., 2022).

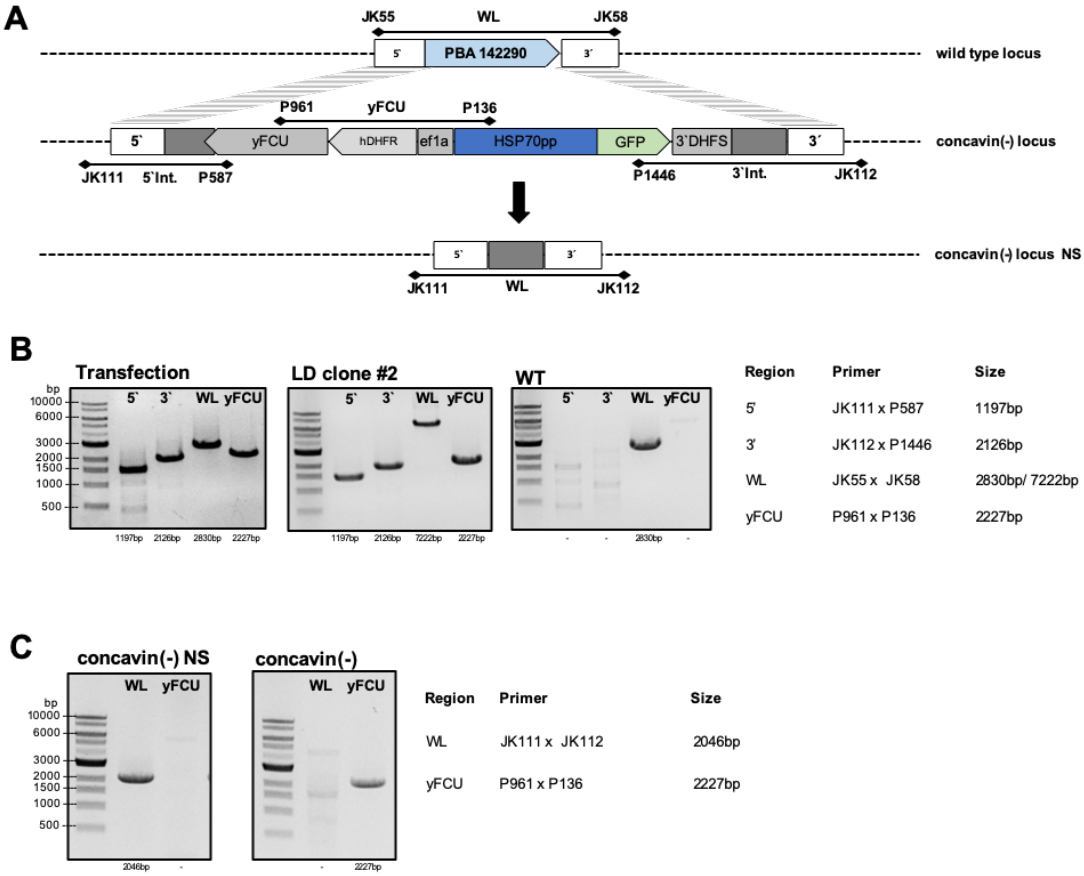

Figure 5.3.16 Generation of *concavin(-)* and *concavin(-) NS* parasites

(A) Cartoon showing the cloning strategy and primers used for genotyping. (B) Genotyping PCRs of non-clonal *concavin(-)* parasites directly after transfection and after limiting dilution. Agarose gel pictures show 5`integration, 3`integration as well as wildtype and selection marker as indicated in A. Expected amplicon sizes are indicated on the right. (C) Genotyping PCRs of *concavin(-)* parasites after looping out the selection cassette. Expected amplicon sizes are indicated on the right. Figure taken from (Kehrer et al., 2022).

Generation of Concavin(-)^{PbConcavin} (pL79)

"The 5`UTR together with the entire ORF of PbANKA_1422900 was amplified from wild type gDNA using primers JK55 and JK176 and inserted into a plasmid (pL59) containing *gfp* and the *TgDHFR* selection cassette using KpnI and NdeI. Resulting in plasmid pL79. For transfection of *concavin(-)NS* parasites via double crossover the plasmid was digested with KpnI and SacII" (Kehrer et al., 2022).

Generation of Concavin(-)^{Pf3D7Concavin} (pL82)

"The *P. berghei* 5`UTR was amplified using primers JK55 and JK179 and inserted into pL59 using KpnI and BstBI. Followed by the insertion of PF3D7_0814600 amplified with primers JK177 and JK178 from P. *falciparum* gDNA and digested with BstBI and NdeI. For transfection of *concavin(-)NS* parasites via double crossover the plasmid was digested with KpnI and SacII" (Kehrer et al., 2022).

Generation of Concavin^{C7A} (pL120)

"Concavin^{C7A} together with *gfp* was amplified from pl79 using primers JK236 and JK237. The resulting PCR product was digested with BamHI and ligated into pL82 digested with BamHI and BstBI with filled in overhangs. Leading to the final plasmid pL120. For transfection of *concavin(-)NS* parasites via double crossover the plasmid was digested with KpnI and SacII" (Kehrer et al., 2022).

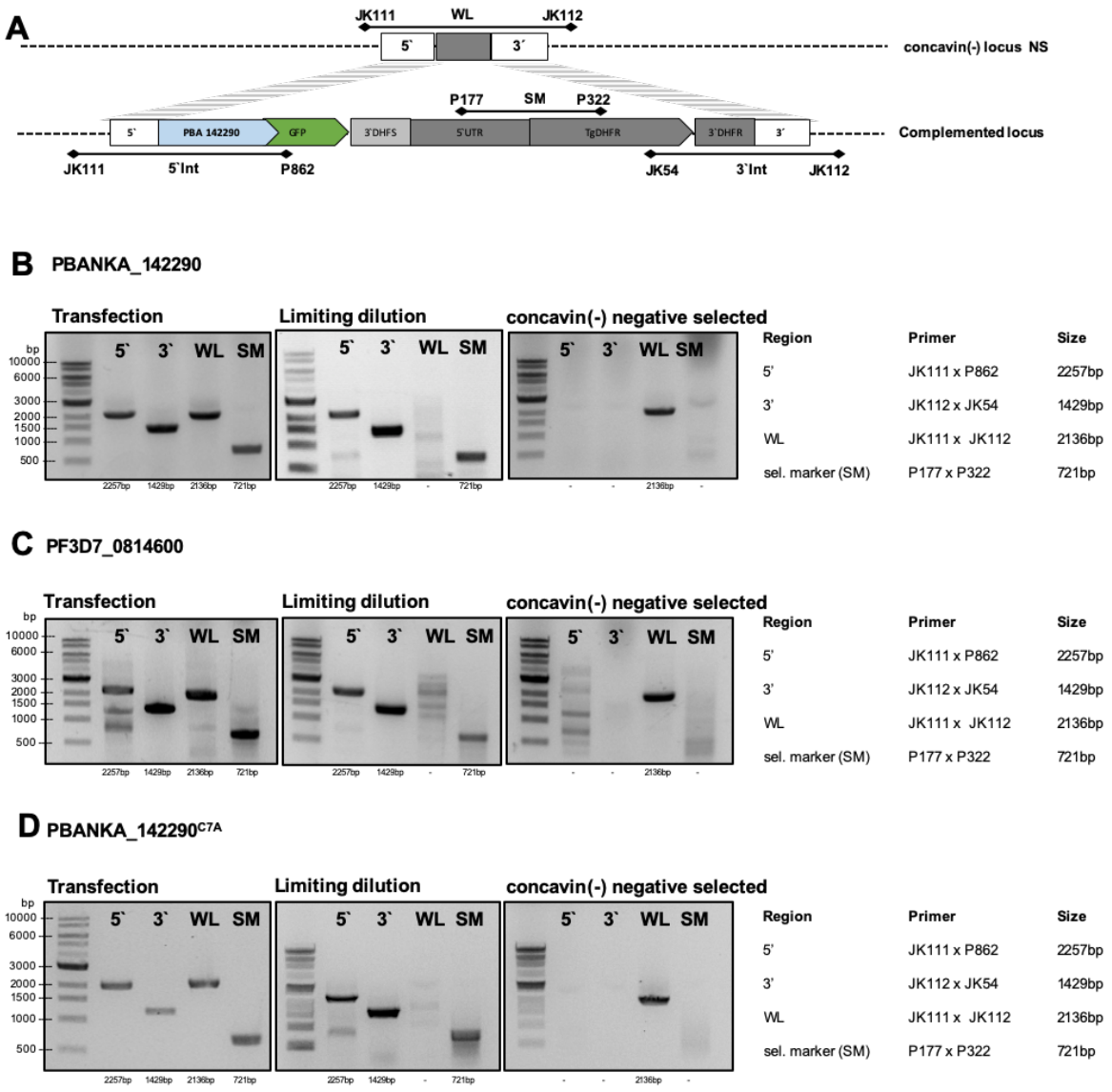

Figure 5.3.17 Generation of *concavin(-)*^{Pbconcavin}-GF*P*, *concavin(-)*^{Pfconcavin}-GFP and *concavin*^{C7A} parasites

(A) Cartoon showing the cloning strategy and primers used for genotyping. (B) Genotyping PCRs of the non-clonal *concavin(-)|P.berghei-gfp* parasite line directly after transfection and after limiting dilution. Agarose gel pictures show 5`integration, 3`integration as well as wildtype and selection marker as indicated in A. Expected amplicon sizes are indicated on the right. (C) Genotyping PCRs of the non-clonal *concavin(-)|P.falciparum-gfp* parasite line directly after transfection and after limiting dilution. Agarose gel pictures show 5`integration, 3`integration as well as wildtype and selection marker as indicated in A. Expected amplicon sizes are indicated on the right. (D) Genotyping PCRs of the non-clonal *concavin*^{C7A} parasite line directly after transfection and after limiting dilution. Agarose gel pictures show 5`integration, 3`integration as well as wildtype and selection marker as indicated in A. Expected amplicon sizes are indicated on the right. Figure taken from (Kehrer et al., 2022).

Generation of Concavin(-)$^{Phil1\text{-}GFP}$ parasites

For the generation of Concavin(-)$^{Phil1\text{-}GFP}$-parasites a plasmid provided by Mendi Muthinja was used (J. M. Muthinja, 2017) and inserted into *concavin(-)* parasites via single homologous recombination.

The plasmid contains parts of the PhIL1 gene amplified with primers P969 and P970. Starting 54 bp after the ATG and lacking the stop codon. A *TgDHFR* selection cassette was used as a positive selection marker. For transfection the final vector was linearized using BsaB1 (Kehrer et al., 2022).

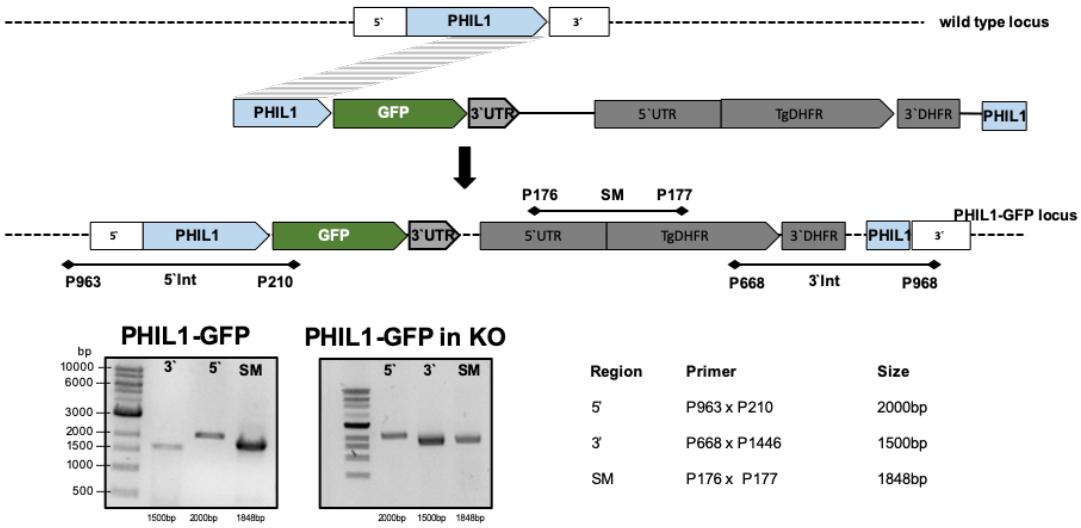

Figure 5.3.18 Generation of concavin(-)$^{Phil1\text{-}GFP}$ parasites.

Generation of concavin(-)|phil1-gfp parasites via single homologous recombination. The cartoon shows the cloning strategy and primers used for genotyping. Agarose gel pictures shows genotyping of the non-clonal parasites in the wild type as well as in the concavin(-) background. Figure taken from (Kehrer et al., 2022).

Parasites for STED (Section 3.5)

Generation of PbCRT- GFP parasites (pL104)

"1832bp of the PbCRT C- terminus was amplified from wild type ANKA gDNA with primers JK222 and JK223. The resulting PCR product was digested with EcoRI and BamHI and ligated in frame with GFP into pL18 containing the TgDHFR/TS as selection marker. For transfection the plasmid was linearized with AflII. Transfection of the linearized plasmid was performed as previously described (Janse et al., 2006). After electroporation of schizonts, positive selection was performed by adding pyrimethamine to the drinking water of mice" (Kehrer et al., 2023).

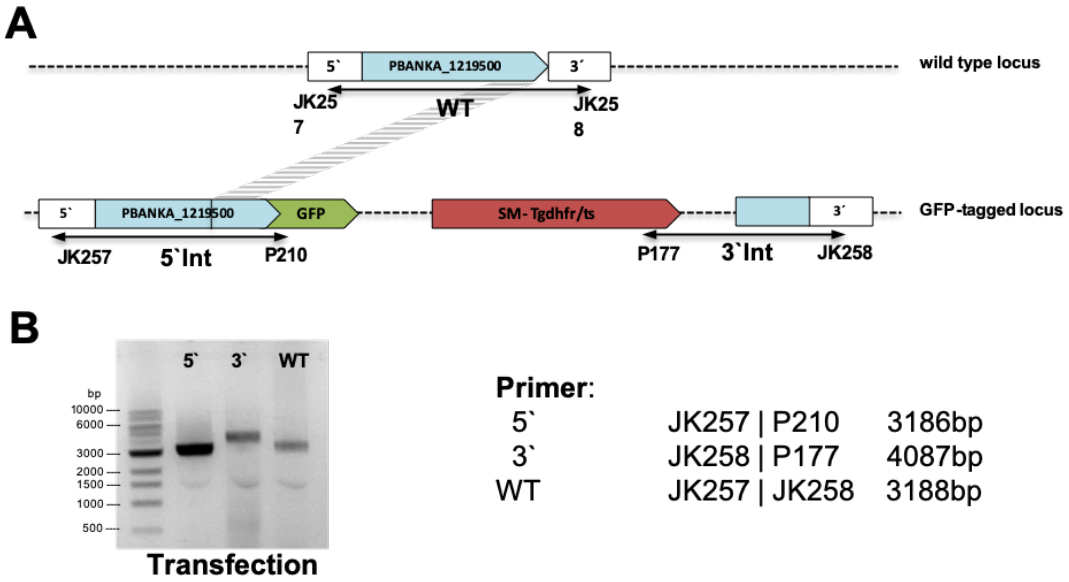

Figure 5.3.19 Generation of PbCRT- GFP parasites

(A) Cartoon showing the single integration cloning strategy and primers used for genotyping. (B) Genotyping PCRs of non-clonal *CRT-gfp* parasites directly after transfection. Agarose gel picture shows 5`integration, 3`integration and wildtype as expected for a non-clonal population of transfectants. Expected amplicon sizes are indicated on the right. (C) Primer sequences used for genotyping. Figure taken from (Kehrer et al., 2023).

6 BIBLIOGRAPHY

Alberts, B., A, J., & Lewis J. (2002). Analyzing Protein Structure and Function. *Molecular Biology of the Cell*.

Alberts, B., Johnson, A., Lewis, J., Morgan, D., Raff, M., Roberts, K., & Walter, P. (2015). Molecular biology of the cell Molecular biology of the cell / Bruce Alberts . *Molecular Biology of the Cell*, *2002*.

Aliprandini, E., Tavares, J., Panatieri, R. H., Thiberge, S., Yamamoto, M. M., Silvie, O., Ishino, T., Yuda, M., Dartevelle, S., Traincard, F., Boscardin, S. B., & Amino, R. (2018). Cytotoxic anti-circumsporozoite antibodies target malaria sporozoites in the host skin. In *Nature Microbiology*. https://doi.org/10.1038/s41564-018-0254-z

Aly, A. S. I., & Matuschewski, K. (2005). A malarial cysteine protease is necessary for Plasmodium sporozoite egress from oocysts. *Journal of Experimental Medicine*. https://doi.org/10.1084/jem.20050545

Ambekar, S. V., Beck, J. R., & Mair, G. R. (2022). TurboID Identification of Evolutionarily Divergent Components of the Nuclear Pore Complex in the Malaria Model Plasmodium berghei. *MBio*, *13*(5). https://doi.org/10.1128/mbio.01815-22

Amino, R., Thiberge, S., Martin, B., Celli, S., Shorte, S., Frischknecht, F., & Ménard, R. (2006). Quantitative imaging of Plasmodium transmission from mosquito to mammal. *Nature Medicine*. https://doi.org/10.1038/nm1350

Anaguano, D., Dedkhad, W., Brooks, C. F., Cobb, D. W., & Muralidharan, V. (2023). Time-resolved proximity biotinylation implicates a porin protein in export of transmembrane malaria parasite effectors. *Journal of Cell Science*, *136*(20), jcs260506. https://doi.org/10.1242/jcs.260506

Andreadaki, M., Pace, T., Grasso, F., Siden-Kiamos, I., Mochi, S., Picci, L., Bertuccini, L., Ponzi, M., & Currà, C. (2020). Plasmodium berghei Gamete Egress Protein is required for fertility of both genders. *MicrobiologyOpen*, *9*(7). https://doi.org/10.1002/mbo3.1038

Araki, T., Kawai, S., Kakuta, S., Kobayashi, H., Umeki, Y., Saito-Nakano, Y., Sasaki, T., Nagamune, K., Yasutomi, Y., Nozaki, T., Franke-Fayard, B., Khan, S. M., Hisaeda, H., & Annoura, T. (2020). Three-dimensional electron microscopy analysis reveals endopolygeny-like nuclear architecture segregation in Plasmodium oocyst development. *Parasitology International*, *76*, 102034. https://doi.org/https://doi.org/10.1016/j.parint.2019.102034

Armistead, J. S., Jennison, C., O'Neill, M. T., Lopaticki, S., Liehl, P., Hanson, K. K., Annoura, T., Rajasekaran, P., Erickson, S. M., Tonkin, C. J., Khan, S. M., Mota, M. M., & Boddey, J. A. (2018). Plasmodium falciparum subtilisin-like ookinete protein SOPT plays an important and conserved role during ookinete infection of the Anopheles stephensi midgut. *Molecular Microbiology*, *109*(4). https://doi.org/10.1111/mmi.13993

Arrighi, R. B. G., & Hurd, H. (2002). The role of Plasmodium berghei ookinete proteins in binding to basal lamina components and transformation into oocysts. *International Journal for Parasitology*. https://doi.org/10.1016/S0020-7519(01)00298-3

Augagneur, Y., Jaubert, L., Schiavoni, M., Pachikara, N., Garg, A., Usmani-Brown, S., Wesolowski, D., Zeller, S., Ghosal, A., Cornillot, E., Said, H. M., Kumar, P., Altman, S., & Ben Mamoun, C. (2013). Identification and functional analysis of the primary pantothenate transporter, PfPAT, of the human malaria parasite Plasmodium falciparum. *Journal of Biological Chemistry*. https://doi.org/10.1074/jbc.M113.482992

Baer, K., Klotz, C., Kappe, S. H. I., Schnieder, T., & Frevert, U. (2007). Release of hepatic Plasmodium yoelii merozoites into the pulmonary microvasculature. *PLoS Pathogens*. https://doi.org/10.1371/journal.ppat.0030171

Baker, R. P., Wijetilaka, R., & Urban, S. (2006). Two Plasmodium rhomboid proteases preferentially cleave different adhesins implicated in all invasive stages of malaria. *PLoS Pathogens*. https://doi.org/10.1371/journal.ppat.0020113

Bargieri, D. Y., Thiberge, S., Tay, C. L., Carey, A. F., Rantz, A., Hischen, F., Lorthiois, A., Straschil, U., Singh, P., Singh, S., Triglia, T., Tsuboi, T., Cowman, A., Chitnis, C., Alano, P., Baum, J., Pradel, G., Lavazec, C., & Ménard, R. (2016). Plasmodium Merozoite TRAP Family Protein Is Essential for Vacuole Membrane Disruption and Gamete Egress from Erythrocytes. *Cell Host and Microbe*. https://doi.org/10.1016/j.chom.2016.10.015

Baum, J., Richard, D., Healer, J., Rug, M., Krnajski, Z., Gilberger, T. W., Green, J. L., Holder, A. A., & Cowman, A. F. (2006). A conserved molecular motor drives cell invasion and gliding motility across malaria life cycle stages and other apicomplexan parasites. *Journal of Biological Chemistry*. https://doi.org/10.1074/jbc.M509807200

Bhanot, P., Frevert, U., Nussenzweig, V., & Persson, C. (2003). Defective sorting of the thrombospondin-related anonymous protein (TRAP) inhibits Plasmodium infectivity. *Molecular and Biochemical Parasitology*. https://doi.org/10.1016/S0166-6851(02)00295-5

Billker, O., Dechamps, S., Tewari, R., Wenig, G., Franke-Fayard, B., & Brinkmann, V. (2004). Calcium and a calcium-dependent protein kinase regulate gamete formation and mosquito transmission in a malaria parasite. *Cell*. https://doi.org/10.1016/S0092-8674(04)00449-0

Billker, O., Lindo, V., Panico, M., Etienne, A. E., Paxton, T., Dell, A., Rogers, M., Sinden, R. E., & Morris, H. (1998). Identification of xanthurenic acid as the putative inducer of malaria development in the mosquito. *Nature*. https://doi.org/10.1038/32667

Birnbaum, J., Scharf, S., Schmidt, S., Jonscher, E., Maria Hoeijmakers, W. A., Flemming, S., Toenhake, C. G., Schmitt, M., Sabitzki, R., Bergmann, B., Fröhlke, U., Mesén-Ramírez, P., Soares, A. B., Herrmann, H., Bártfai, R., & Spielmann, T. (2020). A Kelch13-defined endocytosis pathway mediates artemisinin resistance in malaria parasites. *Science*. https://doi.org/10.1126/science.aax4735

Blasco, B., Leroy, Di., & Fidock, D. A. (2017). Antimalarial drug resistance: Linking Plasmodium falciparum parasite biology to the clinic. In *Nature Medicine*. https://doi.org/10.1038/nm.4381

Boucher, M. J., Ghosh, S., Zhang, L., Lal, A., Jang, S. W., Ju, A., Zhang, S., Wang, X., Ralph, S. A., Zou, J., Elias, J. E., & Yeh, E. (2018). Integrative proteomics and bioinformatic prediction enable a high-confidence apicoplast proteome in malaria parasites. *PLoS Biology*. https://doi.org/10.1371/journal.pbio.2005895

Branon, T. C., Bosch, J. A., Sanchez, A. D., Udeshi, N. D., Svinkina, T., Carr, S. A., Feldman, J. L., Perrimon, N., & Ting, A. Y. (2018). Efficient proximity labeling in living cells and organisms with TurboID. *Nature Biotechnology*, *36*(9). https://doi.org/10.1038/nbt.4201

Briggs, L. J., Davidge, J. A., Wickstead, B., Ginger, M. L., & Gull, K. (2004). More than one way to build a flagellum: Comparative genomics of parasitic protozoa [2]. In *Current Biology* (Vol. 14, Issue 15). https://doi.org/10.1016/j.cub.2004.07.041

Brochet, M., Collins, M. O., Smith, T. K., Thompson, E., Sebastian, S., Volkmann, K., Schwach, F., Chappell, L., Gomes, A. R., Berriman, M., Rayner, J. C., Baker, D. A., Choudhary, J., & Billker, O. (2014). Phosphoinositide Metabolism Links cGMP-Dependent Protein Kinase G to Essential Ca2+ Signals at Key Decision Points in the Life Cycle of Malaria Parasites. *PLoS Biology*, *12*(3). https://doi.org/10.1371/journal.pbio.1001806

Brossier, F., Jewett, T. J., Sibley, L. D., & Urban, S. (2005). A spatially localized rhomboid protease cleaves cell surface adhesins essential for invasion by Toxoplasma. *Proceedings of the National Academy of Sciences of the United States of America*. https://doi.org/10.1073/pnas.0407918102

Bushell, E., Gomes, A. R., Sanderson, T., Anar, B., Girling, G., Herd, C., Metcalf, T., Modrzynska, K., Schwach, F., Martin, R. E., Mather, M. W., McFadden, G. I., Parts, L., Rutledge, G. G., Vaidya, A. B., Wengelnik, K., Rayner, J. C., & Billker, O. (2017). Functional Profiling of a Plasmodium Genome Reveals an Abundance of Essential Genes. *Cell*. https://doi.org/10.1016/j.cell.2017.06.030

Carey, A. F., Singer, M., Bargieri, D., Thiberge, S., Frischknecht, F., Ménard, R., & Amino, R. (2014). Calcium dynamics of Plasmodium berghei sporozoite motility. *Cellular Microbiology*. https://doi.org/10.1111/cmi.12289

Carlton, J. M. (2018). Evolution of human malaria. In *Nature Microbiology*. https://doi.org/10.1038/s41564-018-0170-2

Carruthers, V. B., & Sibley, L. D. (1999). Mobilization of intracellular calcium stimulates microneme discharge in Toxoplasma gondii. *Molecular Microbiology*. https://doi.org/10.1046/j.1365-2958.1999.01174.x

Carter, R., & Nijhout, M. M. (1977). Control of gamete formation (exflagellation) in malaria parasites. *Science*. https://doi.org/10.1126/science.12566

Chen, F., Tillberg, P. W., & Boyden, E. S. (2015). Expansion microscopy. *Science*, *347*(6221). https://doi.org/10.1126/science.1260088

Combe, A., Moreira, C. K., Ackerman, S., Thiberge, S., Templeton, T. J., & Ménard, R. (2009). TREP, a novel protein necessary for gliding motility of the malaria sporozoite. *International Journal for Parasitology*. https://doi.org/10.1016/j.ijpara.2008.10.004

Cowman, A. F., Tonkin, C. J., Tham, W. H., & Duraisingh, M. T. (2017). The Molecular Basis of Erythrocyte Invasion by Malaria Parasites. In *Cell Host and Microbe*. https://doi.org/10.1016/j.chom.2017.07.003

Currà, C., Kehrer, J., Lemgruber, L., Silva, P. A. G. C., Bertuccini, L., Superti, F., Pace, T., Ponzi, M., Frischknecht, F., Siden-Kiamos, I., & Mair, G. R. (2019). Malaria transmission through the mosquito requires the function of the OMD protein. *PLoS ONE*. https://doi.org/10.1371/journal.pone.0222226

Datoo, M. S., Dicko, A., Tinto, H., Ouédraogo, J.-B., Hamaluba, M., Olotu, A., Beaumont, E., Ramos Lopez, F., Natama, H. M., Weston, S., Chemba, M., Compaore, Y. D., Issiaka, D., Salou, D., Some, A. M., Omenda, S., Lawrie, A., Bejon, P., Rao, H., … Valea, I. (2024). Safety and efficacy of malaria vaccine candidate R21/Matrix-M in African children: a multicentre, double-blind, randomised, phase 3 trial. *The Lancet*, *403*(10426), 533–544. https://doi.org/https://doi.org/10.1016/S0140-6736(23)02511-4

De Koning-Ward, T. F., Olivieri, A., Bertuccini, L., Hood, A., Silvestrini, F., Charvalias, K., Berzosa Díaz, P., Camarda, G., McElwain, T. F., Papenfuss, T., Healer, J., Baldassarri, L., Crabb, B. S., Alano, P., & Ranford-Cartwright, L. C. (2008). The role of osmiophilic bodies and Pfg377 expression in female gametocyte emergence and mosquito infectivity in the human malaria parasite Plasmodium falciparum. *Molecular Microbiology*. https://doi.org/10.1111/j.1365-2958.2007.06039.x

de Niz, M., Kehrer, J., Brancucci, N. M. B., Moalli, F., Reynaud, E. G., Stein, J. V., & Frischknecht, F. (2020). 3D imaging of undissected optically cleared Anopheles stephensi mosquitoes and midguts infected with Plasmodium parasites. *PLoS ONE*, *15*(9 September). https://doi.org/10.1371/journal.pone.0238134

Deligianni, E., Morgan, R. N., Bertuccini, L., Wirth, C. C., Silmon de Monerri, N. C., Spanos, L., Blackman, M. J., Louis, C., Pradel, G., & Siden-Kiamos, I. (2013). A perforin-like protein mediates disruption of the erythrocyte

membrane during egress of Plasmodium berghei male gametocytes. *Cellular Microbiology*. https://doi.org/10.1111/cmi.12131

Dellibovi-Ragheb, T. A., Jhun, H., Goodman, C. D., Walters, M. S., Ragheb, D. R. T., Matthews, K. A., Rajaram, K., Mishra, S., McFadden, G. I., Sinnis, P., & Prigge, S. T. (2018). Host biotin is required for liver stage development in malaria parasites. *Proceedings of the National Academy of Sciences of the United States of America*, *115*(11). https://doi.org/10.1073/pnas.1800717115

Dessens, J. T., Beetsma, A. L., Dimopoulos, G., Wengelnik, K., Crisanti, A., Kafatos, F. C., & Sinden, R. E. (1999). CTRP is essential for mosquito infection by malaria ookinetes. *EMBO Journal*. https://doi.org/10.1093/emboj/18.22.6221

Dessens, J. T., Mendoza, J., Claudianos, C., Vinetz, J. M., Khater, E., Hassard, S., Ranawaka, G. R., & Sinden, R. E. (2001). Knockout of the rodent malaria parasite chitinase PbCHT1 reduces infectivity to mosquitoes. *Infection and Immunity*. https://doi.org/10.1128/IAI.69.6.4041-4047.2001

Dessens, J. T., Sidén-Kiamos, I., Mendoza, J., Mahairaki, V., Khater, E., Vlachou, D., Xu, X. J., Kafatos, F. C., Louis, C., Dimopoulos, G., & Sinden, R. E. (2003). Soap, a novel malaria ookinete protein involved in mosquito midgut invasion and oocyst development. *Molecular Microbiology*. https://doi.org/10.1046/j.1365-2958.2003.03566.x

Di Cristina, M., Spaccapelo, R., Soldati-Favre, D., Bistoni, F., & Crisanti, A. (2000). Two Conserved Amino Acid Motifs Mediate Protein Targeting to the Micronemes of the Apicomplexan Parasite Toxoplasma gondii. *Molecular and Cellular Biology*. https://doi.org/10.1128/mcb.20.19.7332-7341.2000

Dodt, H. U., Leischner, U., Schierloh, A., Jährling, N., Mauch, C. P., Deininger, K., Deussing, J. M., Eder, M., Zieglgänsberger, W., & Becker, K. (2007). Ultramicroscopy: Three-dimensional visualization of neuronal networks in the whole mouse brain. *Nature Methods*, *4*(4). https://doi.org/10.1038/nmeth1036

Douglas, R. G., Amino, R., Sinnis, P., & Frischknecht, F. (2015). Active migration and passive transport of malaria parasites. In *Trends in Parasitology*. https://doi.org/10.1016/j.pt.2015.04.010

Douglas, R. G., Nandekar, P., Aktories, J. E., Kumar, H., Weber, R., Sattler, J. M., Singer, M., Lepper, S., Sadiq, S. K., Wade, R. C., & Frischknecht, F. (2018). Inter-subunit interactions drive divergent dynamics in mammalian and Plasmodium actin filaments. *PLoS Biology*. https://doi.org/10.1371/journal.pbio.2005345

Ecker, A., Bushell, E. S. C., Tewari, R., & Sinden, R. E. (2008). Reverse genetics screen identifies six proteins important for malaria development in the mosquito. *Molecular Microbiology*. https://doi.org/10.1111/j.1365-2958.2008.06407.x

Ecker, A., Pinto, S. B., Baker, K. W., Kafatos, F. C., & Sinden, R. E. (2007). Plasmodium berghei: Plasmodium perforin-like protein 5 is required for mosquito midgut invasion in Anopheles stephensi. *Experimental Parasitology*, *116*(4). https://doi.org/10.1016/j.exppara.2007.01.015

Ejigiri, I., Ragheb, D. R. T., Pino, P., Coppi, A., Bennett, B. L., Soldati-Favre, D., & Sinnis, P. (2012). Shedding of TRAP by a rhomboid protease from the malaria sporozoite surface is essential for gliding motility and sporozoite infectivity. *PLoS Pathogens*. https://doi.org/10.1371/journal.ppat.1002725

Esposito, A., Tiffert, T., Mauritz, J. M. A., Schlachter, S., Bannister, L. H., Kaminski, C. F., & Lew, V. L. (2008). FRET imaging of hemoglobin concentration in Plasmodium falciparum-infected red cells. *PLoS ONE*, *3*(11). https://doi.org/10.1371/journal.pone.0003780

Farrell, A., Thirugnanam, S., Lorestani, A., Dvorin, J. D., Eidell, K. P., Ferguson, D. J. P., Anderson-White, B. R., Duraisingh, M. T., Marth, G. T., & Gubbels, M. J. (2012). A DOC2 protein identified by mutational profiling is essential for apicomplexan parasite exocytosis. *Science*, *335*(6065). https://doi.org/10.1126/science.1210829

Flieger, A., Frischknecht, F., Häcker, G., Hornef, M. W., & Pradel, G. (2018). Pathways of host cell exit by intracellular pathogens. In *Microbial Cell*. https://doi.org/10.15698/mic2018.12.659

Fraiture, M., Baxter, R. H. G., Steinert, S., Chelliah, Y., Frolet, C., Quispe-Tintaya, W., Hoffmann, J. A., Blandin, S. A., & Levashina, E. A. (2009). Two Mosquito LRR Proteins Function as Complement Control Factors in the TEP1-Mediated Killing of Plasmodium. *Cell Host and Microbe*. https://doi.org/10.1016/j.chom.2009.01.005

Frénal, K., Polonais, V., Marq, J. B., Stratmann, R., Limenitakis, J., & Soldati-Favre, D. (2010). Functional dissection of the apicomplexan glideosome molecular architecture. *Cell Host and Microbe*. https://doi.org/10.1016/j.chom.2010.09.002

Freyvogel, T. A. (1966). Shape, movement in situ and locomotion of plasmodial ookinetes. *Acta Tropica*.

Frischknecht, F., Baldacci, P., Martin, B., Zimmer, C., Thiberge, S., Olivo-Marin, J. C., Shorte, S. L., & Ménard, R. (2004). Imaging movement of malaria parasites during transmission by Anopheles mosquitoes. *Cellular Microbiology*. https://doi.org/10.1111/j.1462-5822.2004.00395.x

Frischknecht, F., & Matuschewski, K. (2017). Plasmodium sporozoite biology. *Cold Spring Harbor Perspectives in Medicine*. https://doi.org/10.1101/cshperspect.a025478

Fukui, Y. (2002). Mechanistics of amoeboid locomotion: Signal to forces. *Cell Biology International*. https://doi.org/10.1006/cbir.2002.0959

Geiger, M., Brown, C., Wichers, J. S., Strauss, J., Lill, A., Thuenauer, R., Liffner, B., Wilcke, L., Lemcke, S., Heincke, D., Pazicky, S., Bachmann, A., Löw, C., Wilson, D. W., Filarsky, M., Burda, P. C., Zhang, K., Junop, M., & Gilberger, T. W. (2020). Structural Insights Into PfARO and Characterization of its Interaction With PfAIP. *Journal of Molecular Biology*. https://doi.org/10.1016/j.jmb.2019.12.024

Ghosh, A. K., Devenport, M., Jethwaney, D., Kalume, D. E., Pandey, A., Anderson, V. E., Sultan, A. A., Kumar, N., & Jacobs-Lorena, M. (2009). Malaria parasite invasion of the mosquito salivary gland requires interaction between the Plasmodium TRAP and the Anopheles saglin proteins. *PLoS Pathogens*. https://doi.org/10.1371/journal.ppat.1000265

Goldberg, D. E., Slater, A. F. G., Cerami, A., & Henderson, G. B. (1990). Hemoglobin degradation in the malaria parasite Plasmodium falciparum: An ordered process in a unique organelle. *Proceedings of the National Academy of Sciences of the United States of America*, *87*(8). https://doi.org/10.1073/pnas.87.8.2931

Gomes-Santos, C. S. S., Braks, J., Prudêncio, M., Carret, C., Gomes, A. R., Pain, A., Feltwell, T., Khan, S. M., Waters, A., Janse, C. J., Mair, G. R., & Mota, M. M. (2011). Transition of Plasmodium sporozoites into liver stage-like forms is regulated by the RNA binding protein Pumilio. *PLoS Pathogens*, *7*(5), e1002046. https://doi.org/10.1371/journal.ppat.1002046

Gras, S., Jimenez-Ruiz, E., Klinger, C. M., Schneider, K., Klingl, A., Lemgruber, L., & Meissner, M. (2019). An endocytic-secretory cycle participates in Toxoplasma gondii in motility. *PLoS Biology*, *17*(6). https://doi.org/10.1371/journal.pbio.3000060

Gręobecki, A. (1994). Membrane and Cytoskeleton Flow in Motile Cells with Emphasis on the Contribution of Free-Living Amoebae. *International Review of Cytology*. https://doi.org/10.1016/S0074-7696(08)62405-5

Gueirard, P., Tavares, J., Thiberge, S., Bernex, F., Ishino, T., Milon, G., Franke-Fayard, B., Janse, C. J., Ménard, R., & Amino, R. (2010). Development of the malaria parasite in the skin of the mammalian host. *Proceedings of the National Academy of Sciences of the United States of America*. https://doi.org/10.1073/pnas.1009346107

Haimo, L. T., & Rosenbaum, J. L. (1981). Cilia, flagella, and microtubules. In *Journal of Cell Biology*. https://doi.org/10.1083/jcb.91.3.125s

Hammoudi, P. M., Maco, B., Dogga, S. K., Frénal, K., & Soldati-Favre, D. (2018). Toxoplasma gondii TFP1 is an essential transporter family protein critical for microneme maturation and exocytosis. *Molecular Microbiology*. https://doi.org/10.1111/mmi.13981

Han, Y. S., & Barillas-Mury, C. (2002). Implications of time bomb model of ookinete invasion of midgut cells. *Insect Biochemistry and Molecular Biology*. https://doi.org/10.1016/S0965-1748(02)00093-0

Han, Y. S., Thompson, J., Kafatos, F. C., & Barillas-Mury, C. (2000). Molecular interactions between Anopheles stephensi midgut cells and Plasmodium berghei: The time bomb theory of ookinete invasion of mosquitoes. *EMBO Journal*. https://doi.org/10.1093/emboj/19.22.6030

Harding, C. R., & Frischknecht, F. (2020). The Riveting Cellular Structures of Apicomplexan Parasites. In *Trends in Parasitology*. https://doi.org/10.1016/j.pt.2020.09.001

Hart, R. J., Lawres, L., Fritzen, E., Mamoun, C. Ben, & Aly, A. S. I. (2014). Plasmodium yoelii vitamin B5 pantothenate transporter candidate is essential for parasite transmission to the mosquito. *Scientific Reports*. https://doi.org/10.1038/srep05665

Hayakawa, T., Culleton, R., Otani, H., Horii, T., & Tanabe, K. (2008). Big bang in the evolution of extant malaria parasites. *Molecular Biology and Evolution*. https://doi.org/10.1093/molbev/msn171

Heiss, K., Nie, H., Kumar, S., Daly, T. M., Bergman, L. W., & Matuschewski, K. (2008). Functional characterization of a redundant Plasmodium TRAP family invasin, TRAP-like protein, by aldolase binding and a genetic complementation test. *Eukaryotic Cell*. https://doi.org/10.1128/EC.00089-08

Heppner, D. G. (2013). The malaria vaccine-Status quo 2013. In *Travel Medicine and Infectious Disease*. https://doi.org/10.1016/j.tmaid.2013.01.006

Horstmann, H., Körber, C., Sätzler, K., Aydin, D., & Kuner, T. (2012). Serial Section Scanning Electron Microscopy (S3EM) on Silicon Wafers for Ultra-Structural Volume Imaging of Cells and Tissues. *PLOS ONE*, *7*(4), e35172. https://doi.org/10.1371/journal.pone.0035172

Jacot, D., Tosetti, N., Pires, I., Stock, J., Graindorge, A., Hung, Y. F., Han, H., Tewari, R., Kursula, I., & Soldati-Favre, D. (2016). An Apicomplexan Actin-Binding Protein Serves as a Connector and Lipid Sensor to Coordinate Motility and Invasion. *Cell Host and Microbe*, *20*(6). https://doi.org/10.1016/j.chom.2016.10.020

Jiang, Y., Wei, J., Cui, H., Liu, C., Zhi, Y., Jiang, Z. Z., Li, Z., Li, S., Yang, Z., Wang, X., Qian, P., Zhang, C., Zhong, C., Su, X. zhuan, & Yuan, J. (2020). An intracellular membrane protein GEP1 regulates xanthurenic acid induced gametogenesis of malaria parasites. *Nature Communications*, *11*(1). https://doi.org/10.1038/s41467-020-15479-3

Johnson, B. S., Chafin, L., Farkas, D., Adair, J., Elhance, A., Farkas, L., Bednash, J. S., & Londino, J. D. (2022). MicroID2: A Novel Biotin Ligase Enables Rapid Proximity-Dependent Proteomics. *Molecular & Cellular Proteomics*, *21*(7), 100256. https://doi.org/https://doi.org/10.1016/j.mcpro.2022.100256

Kafsack, B. F. C., Rovira-Graells, N., Clark, T. G., Bancells, C., Crowley, V. M., Campino, S. G., Williams, A. E., Drought, L. G., Kwiatkowski, D. P., Baker, D. A., Cortés, A., & Llinás, M. (2014). A transcriptional switch underlies commitment to sexual development in malaria parasites. *Nature*. https://doi.org/10.1038/nature12920

Kaiser, K., Matuschewski, K., Camargo, N., Ross, J., & Kappe, S. H. I. (2004). Differential transcriptome profiling identifies Plasmodium genes encoding pre-erythrocytic stage-specific proteins. *Molecular Microbiology*. https://doi.org/10.1046/j.1365-2958.2003.03909.x

Kappe, S., Bruderer, T., Gantt, S., Fujioka, H., Nussenzweig, V., & Ménard, R. (1999). Conservation of a gliding motility and cell invasion machinery in Apicomplexan parasites. *Journal of Cell Biology*. https://doi.org/10.1083/jcb.147.5.937

Kariu, T., Ishino, T., Yano, K., Chinzei, Y., & Yuda, M. (2006). CelTOS, a novel malarial protein that mediates transmission to mosquito and vertebrate hosts. *Molecular Microbiology*. https://doi.org/10.1111/j.1365-2958.2005.05024.x

Kebaier, C., & Vanderberg, J. P. (2010). Initiation of Plasmodium sporozoite motility by albumin is associated with induction of intracellular signalling. *International Journal for Parasitology*. https://doi.org/10.1016/j.ijpara.2009.06.011

Kehrer, J., Formaglio, P., Muthinja, J. M., Weber, S., Baltissen, D., Lance, C., Ripp, J., Grech, J., Meissner, M., Funaya, C., Amino, R., & Frischknecht, F. (2022). Plasmodium sporozoite disintegration during skin passage limits malaria parasite transmission. *EMBO Reports*. https://doi.org/10.15252/embr.202254719

Kehrer, J., Frischknecht, F., & Mair, G. R. (2016). Proteomic analysis of the plasmodium berghei gametocyte egressome and vesicular bioid of osmiophilic body proteins identifies merozoite trap-like protein (MTRAP) as an essential factor for parasite transmission. *Molecular and Cellular Proteomics*. https://doi.org/10.1074/mcp.M116.058263

Kehrer, J., Pietsch, E., Heinze, J., Spielmann, T., & Frischknecht, F. (2023). Clearing of hemozoin crystals in malaria parasites enables whole-cell STED microscopy. *Journal of Cell Science*, *136*(1). https://doi.org/10.1242/jcs.260399

Kehrer, J., Ricken, D., Strauss, L., Pietsch, E., Heinze, J. M., & Frischknecht, F. (2020). APEX-based proximity labeling in Plasmodium identifies a membrane protein with dual functions during mosquito infection. *BioRxiv*. https://doi.org/10.1101/2020.09.29.318857

Kehrer, J., Singer, M., Lemgruber, L., Silva, P. A. G. C., Frischknecht, F., & Mair, G. R. (2016). A Putative Small Solute Transporter Is Responsible for the Secretion of G377 and TRAP-Containing Secretory Vesicles during Plasmodium Gamete Egress and Sporozoite Motility. *PLoS Pathogens*. https://doi.org/10.1371/journal.ppat.1005734

Kenthirapalan, S., Waters, A. P., Matuschewski, K., & Kooij, T. W. A. (2016). Functional profiles of orphan membrane transporters in the life cycle of the malaria parasite. *Nature Communications*. https://doi.org/10.1038/ncomms10519

Khosh-Naucke, M., Becker, J., Mesén-Ramírez, P., Kiani, P., Birnbaum, J., Fröhlke, U., Jonscher, E., Schlüter, H., & Spielmann, T. (2018). Identification of novel parasitophorous vacuole proteins in P. falciparum parasites using BioID. *International Journal of Medical Microbiology*. https://doi.org/10.1016/j.ijmm.2017.07.007

Kim, K., & Weiss, L. M. (2004). Toxoplasma gondii: The model apicomplexan. In *International Journal for Parasitology*. https://doi.org/10.1016/j.ijpara.2003.12.009

Kimmel, J., Kehrer, J., Frischknecht, F., & Spielmann, T. (2022). Proximity-dependent biotinylation approaches to study apicomplexan biology. *Molecular Microbiology*, *117*(3), 553–568. https://doi.org/10.1111/mmi.14815

Klug, D., & Frischknecht, F. (2017). Motility precedes egress of malaria parasites from oocysts. *ELife*. https://doi.org/10.7554/eLife.19157

Klug, D., Gautier, A., Calvo, E., Marois, E., & Blandin, S. A. (2023). The salivary protein Saglin facilitates efficient midgut colonization of Anopheles mosquitoes by malaria parasites. *PLoS Pathogens*, *19*(3). https://doi.org/10.1371/journal.ppat.1010538

Klug, D., Goellner, S., Kehrer, J., Sattler, J., Strauss, L., Singer, M., Lu, C., Springer, T. A., & Frischknecht, F. (2020). Evolutionarily distant I domains can functionally replace the essential ligandbinding domain of plasmodium trap. *ELife*, *9*, 1–27. https://doi.org/10.7554/eLife.57572

Klug, D., Kehrer, J., Frischknecht, F., & Singer, M. (2018). A synthetic promoter for multi-stage expression to probe complementary functions of Plasmodium adhesins. *Journal of Cell Science*. https://doi.org/10.1242/jcs.210971

Klug, D., Mair, G. R., Frischknecht, F., & Douglas, R. G. (2016). A small mitochondrial protein present in myzozoans is essential for malaria transmission. *Open Biology*. https://doi.org/10.1098/rsob.160034

Lal, K., Delves, M. J., Bromley, E., Wastling, J. M., Tomley, F. M., & Sinden, R. E. (2009). Plasmodium male development gene-1 (mdv-1) is important for female sexual development and identifies a polarised plasma membrane during zygote development. *International Journal for Parasitology*. https://doi.org/10.1016/j.ijpara.2008.11.008

Lal, K., Prieto, J. H., Bromley, E., Sanderson, S. J., Yates, J. R., Wastling, J. M., Tomley, F. M., & Sinden, R. E. (2009). Characterisation of Plasmodium invasive organelles; an ookinete microneme proteome. *Proteomics*. https://doi.org/10.1002/pmic.200800404

Lam, S. S., Martell, J. D., Kamer, K. J., Deerinck, T. J., Ellisman, M. H., Mootha, V. K., & Ting, A. Y. (2014). Directed evolution of APEX2 for electron microscopy and proximity labeling. *Nature Methods*. https://doi.org/10.1038/nmeth.3179

Lamb, I. M., Rios, K. T., Shukla, A., Ahiya, A. I., Morrisey, J., Mell, J. C., Lindner, S. E., Mather, M. W., & Vaidya, A. B. (2022). Mitochondrially targeted proximity biotinylation and proteomic analysis in Plasmodium falciparum. *PLoS ONE*, *17*(8 August). https://doi.org/10.1371/journal.pone.0273357

Laurens, M. B. (2019). RTS,S/AS01 vaccine (Mosquirix^{TM}): an overview. *Human Vaccines and Immunotherapeutics*. https://doi.org/10.1080/21645515.2019.1669415

Limviroj, W., Yano, K., Yuda, M., Ando, K., & Chinzei, Y. (2002). Immuno-Electron Microscopic Observation of Plasmodium berghei CTRP Localization in the Midgut of the Vector Mosquito Anopheles stephensi. *The Journal of Parasitology*. https://doi.org/10.2307/3285340

Lin, J. wen, Annoura, T., Sajid, M., Chevalley-Maurel, S., Ramesar, J., Klop, O., Franke-Fayard, B. M. D., Janse, C. J., & Khan, S. M. (2011). A novel "Gene Insertion/Marker Out" (GIMO) method for transgene expression and gene complementation in rodent malaria parasites. *PLoS ONE*, *6*(12). https://doi.org/10.1371/journal.pone.0029289

Linck, R., Fu, X., Lin, J., Ouch, C., Schefter, A., Steffen, W., Warren, P., & Nicastro, D. (2014). Insights into the structure and function of ciliary and flagellar doublet microtubules: Tektins, Ca2+-binding proteins, and stable protofilaments. *Journal of Biological Chemistry*. https://doi.org/10.1074/jbc.M114.568949

Lindner, S. E., Mikolajczak, S. A., Vaughan, A. M., Moon, W., Joyce, B. R., Sullivan, W. J., & Kappe, S. H. I. (2013). Perturbations of PlasmodiumPuf2 expression and RNA-seq of Puf2-deficient sporozoites reveal a critical role in maintaining RNA homeostasis and parasite transmissibility. *Cellular Microbiology*. https://doi.org/10.1111/cmi.12116

Lindner, S. E., Swearingen, K. E., Harupa, A., Vaughan, A. M., Sinnis, P., Moritz, R. L., & Kappe, S. H. I. (2013). Total and putative surface proteomics of malaria parasite salivary gland sporozoites. *Molecular and Cellular Proteomics*. https://doi.org/10.1074/mcp.M112.024505

Liu, W., Li, Y., Learn, G. H., Rudicell, R. S., Robertson, J. D., Keele, B. F., Ndjango, J. B. N., Sanz, C. M., Morgan, D. B., Locatelli, S., Gonder, M. K., Kranzusch, P. J., Walsh, P. D., Delaporte, E., Mpoudi-Ngole, E., Georgiev, A. V., Muller, M. N., Shaw, G. M., Peeters, M., … Hahn, B. H. (2010). Origin of the human malaria parasite Plasmodium falciparum in gorillas. *Nature*. https://doi.org/10.1038/nature09442

Maccallum, W. G. (1897). ON THE FLAGELLATED FORM OF THE MALARIAL PARASITE. *The Lancet*. https://doi.org/10.1016/S0140-6736(00)46556-6

Machado, M., Klaus, S., Klaschka, D., Guizetti, J., & Ganter, M. (2023). Plasmodium falciparum CRK4 links early mitotic events to the onset of S-phase during schizogony. *MBio*, *14*(4). https://doi.org/10.1128/mbio.00779-23

Mack, S. R., Foley, D. A., & Vanderberg, J. P. (1979). Hemolymph volume of noninfected and Plasmodium berghei-infected Anopheles stephensi. *Journal of Invertebrate Pathology*, *34*(2). https://doi.org/10.1016/0022-2011(79)90088-0

Mack, S. R., & Vanderberg, J. P. (1978). Plasmodium berghei: Energy metabolism of sporozoites. *Experimental Parasitology*, *46*(2). https://doi.org/10.1016/0014-4894(78)90144-3

Malo, A. F., Gomendio, M., Garde, J., Lang-Lenton, B., Soler, A. J., & Roldan, E. R. S. (2006). Sperm design and sperm function. *Biology Letters*. https://doi.org/10.1098/rsbl.2006.0449

Manwell, R. D., Killick-Kendrick, R., & Peters, W. (1979). Rodent Malaria. *The Journal of Parasitology*. https://doi.org/10.2307/3280306

Marks, M. S., Ohno, H., Kirchhausen, T., & Bonifacino, J. S. (1997). Protein sorting by tyrosine-based signals: Adapting to the Ys and wherefores. In *Trends in Cell Biology*. https://doi.org/10.1016/S0962-8924(96)10057-X

Matthews, H., McDonald, J., Totañes, F. I. G., & Merrick, C. J. (2022). Dynamics of DNA Replication during Male Gametogenesis in the Malaria Parasite Plasmodium Falciparum. *Cellular Microbiology*, *2022*. https://doi.org/10.1155/2022/2701868

Matuschewski, K. (2017). Vaccines against malaria—still a long way to go. In *FEBS Journal*. https://doi.org/10.1111/febs.14107

Matuschewski, K., Nunes, A. C., Nussenzweig, V., & Ménard, R. (2002). Plasmodium sporozoite invasion into insect and mammalian cells is directed by the same dual binding system. *EMBO Journal*, *21*(7). https://doi.org/10.1093/emboj/21.7.1597

Matz, J. M., Beck, J. R., & Blackman, M. J. (2020). The parasitophorous vacuole of the blood-stage malaria parasite. In *Nature Reviews Microbiology* (Vol. 18, Issue 7). https://doi.org/10.1038/s41579-019-0321-3

McBride, M. J. (2001). Bacterial Gliding Motility: Multiple Mechanisms for Cell Movement over Surfaces. *Annual Review of Microbiology*, *55*(1), 49–75. https://doi.org/10.1146/annurev.micro.55.1.49

McCormick, C. J., Tuckwell, D. S., Crisanti, A., Humphries, M. J., & Hollingdale, M. R. (1999). Identification of heparin as a ligand for the A-domain of Plasmodium falciparum thrombospondin-related adhesion protein. *Molecular and Biochemical Parasitology*. https://doi.org/10.1016/S0166-6851(99)00052-3

McRobert, L., Taylor, C. J., Deng, W., Fivelman, Q. L., Cummings, R. M., Polley, S. D., Billker, O., & Baker, D. A. (2008). Gametogenesis in malaria parasites is mediated by the cGMP-dependent protein kinase. *PLoS Biology*, *6*(6). https://doi.org/10.1371/journal.pbio.0060139

Mehnert, A. K., Simon, C. S., & Guizetti, J. (2019). Immunofluorescence staining protocol for STED nanoscopy of Plasmodium-infected red blood cells. *Molecular and Biochemical Parasitology*, *229*. https://doi.org/10.1016/j.molbiopara.2019.02.007

Montagna, G. N., Buscaglia, C. A., Münter, S., Goosmann, C., Frischknecht, F., Brinkmann, V., & Matuschewski, K. (2012). Critical role for heat shock protein 20 (HSP20) in migration of malarial sporozoites. *Journal of Biological Chemistry*. https://doi.org/10.1074/jbc.M111.302109

Moon, R. W., Taylor, C. J., Bex, C., Schepers, R., Goulding, D., Janse, C. J., Waters, A. P., Baker, D. A., & Billker, O. (2009). A Cyclic GMP Signalling Module That Regulates Gliding Motility in a Malaria Parasite. *PLOS Pathogens*, *5*(9), e1000599. https://doi.org/10.1371/journal.ppat.1000599

Morahan, B. J., Wang, L., & Coppel, R. L. (2009). No TRAP, no invasion. In *Trends in Parasitology*. https://doi.org/10.1016/j.pt.2008.11.004

Moreau, C. A., Bhargav, S. P., Kumar, H., Quadt, K. A., Piirainen, H., Strauss, L., Kehrer, J., Streichfuss, M., Spatz, J. P., Wade, R. C., Kursula, I., & Frischknecht, F. (2017). A unique profilin-actin interface is important for malaria parasite motility. *PLoS Pathogens*. https://doi.org/10.1371/journal.ppat.1006412

Moreira, C. K., Templeton, T. J., Lavazec, C., Hayward, R. E., Hobbs, C. V., Kroeze, H., Janse, C. J., Waters, A. P., Sinnis, P., & Coppi, A. (2008). The Plasmodium TRAP/MIC2 family member, TRAP-Like Protein (TLP), is involved in tissue traversal by sporozoites. *Cellular Microbiology*. https://doi.org/10.1111/j.1462-5822.2008.01143.x

Mori, T., Hirai, M., & Mita, T. (2019). See-through observation of malaria parasite behaviors in the mosquito vector. *Scientific Reports*, *9*(1). https://doi.org/10.1038/s41598-019-38529-3

Mota, M. M., Pradel, G., Vanderberg, J. P., Hafalla, J. C. R., Frevert, U., Nussenzweig, R. S., Nussenzweig, V., & Rodriguez, A. (2001). Migration of Plasmodium sporozoites through cells before infection. *Science*. https://doi.org/10.1126/science.291.5501.141

Müller, H. M., Reckmann, I., Hollingdale, M. R., Bujard, H., Robson, K. J., & Crisanti, A. (1993). Thrombospondin related anonymous protein (TRAP) of Plasmodium falciparum binds specifically to sulfated glycoconjugates and to HepG2 hepatoma cells suggesting a role for this molecule in sporozoite invasion of hepatocytes. *The EMBO Journal*. https://doi.org/10.1002/j.1460-2075.1993.tb05950.x

Münter, S., Sabass, B., Selhuber-Unkel, C., Kudryashev, M., Hegge, S., Engel, U., Spatz, J. P., Matuschewski, K., Schwarz, U. S., & Frischknecht, F. (2009). Plasmodium Sporozoite Motility Is Modulated by the Turnover of Discrete Adhesion Sites. *Cell Host and Microbe*. https://doi.org/10.1016/j.chom.2009.11.007

Murakami, T. C., Mano, T., Saikawa, S., Horiguchi, S. A., Shigeta, D., Baba, K., Sekiya, H., Shimizu, Y., Tanaka, K. F., Kiyonari, H., Iino, M., Mochizuki, H., Tainaka, K., & Ueda, H. R. (2018). A three-dimensional single-cell-resolution whole-brain atlas using CUBIC-X expansion microscopy and tissue clearing. *Nature Neuroscience*, *21*(4). https://doi.org/10.1038/s41593-018-0109-1

Muthinja, J. M. (2017). *Dissecting the role of Plasmodium sporozoite curvature in gliding motility*.

Muthinja, M. J., Ripp, J., Hellmann, J. K., Haraszti, T., Dahan, N., Lemgruber, L., Battista, A., Schütz, L., Fackler, O. T., Schwarz, U. S., Spatz, J. P., & Frischknecht, F. (2017). Microstructured Blood Vessel Surrogates Reveal Structural Tropism of Motile Malaria Parasites. *Advanced Healthcare Materials*. https://doi.org/10.1002/adhm.201601178

Nacer, A., Underhill, A., & Hurd, H. (2008). The microneme proteins CTRP and SOAP are not essential for Plasmodium berghei ookinete to oocyst transformation in vitro in a cell free system. *Malaria Journal*. https://doi.org/10.1186/1475-2875-7-82

Oliveira, G. D. A., Lieberman, J., & Barillas-Mury, C. (2012). Epithelial nitration by a peroxidase/NOX5 system mediates mosquito antiplasmodial immunity. *Science*. https://doi.org/10.1126/science.1209678

Otto, T. D., Böhme, U., Jackson, A. P., Hunt, M., Franke-Fayard, B., Hoeijmakers, W. A. M., Religa, A. A., Robertson, L., Sanders, M., Ogun, S. A., Cunningham, D., Erhart, A., Billker, O., Khan, S. M., Stunnenberg, H. G., Langhorne, J., Holder, A. A., Waters, A. P., Newbold, C. I., … Janse, C. J. (2014). A comprehensive evaluation of rodent malaria parasite genomes and gene expression. *BMC Medicine*. https://doi.org/10.1186/s12915-014-0086-0

Pace, T., Grasso, F., Camarda, G., Suarez, C., Blackman, M. J., Ponzi, M., & Olivieri, A. (2019). The Plasmodium berghei serine protease PbSUB1 plays an important role in male gamete egress. *Cellular Microbiology*, *21*(7). https://doi.org/10.1111/cmi.13028

Ponzi, M., Sidén-Kiamos, I., Bertuccini, L., Currà, C., Kroeze, H., Camarda, G., Pace, T., Franke-Fayard, B., Laurentino, E. C., Louis, C., Waters, A. P., Janse, C. J., & Alano, P. (2009). Egress of Plasmodium berghei gametes from their host erythrocyte is mediated by the MDV-1/PEG3 protein. *Cellular Microbiology*. https://doi.org/10.1111/j.1462-5822.2009.01331.x

Pradel, G., Garapaty, S., & Frevert, U. (2002). Proteoglycans mediate malaria sporozoite targeting to the liver. *Molecular Microbiology*, *45*(3). https://doi.org/10.1046/j.1365-2958.2002.03057.x

Prado, M., Eickel, N., De Niz, M., Heitmann, A., Agop-Nersesian, C., Wacker, R., Schmuckli-Maurer, J., Caldelari, R., Janse, C. J., Khan, S. M., May, J., Meyer, C. G., & Heussler, V. T. (2015). Long-term live imaging reveals cytosolic immune responses of host hepatocytes against plasmodium infection and parasite escape mechanisms. *Autophagy*, *11*(9). https://doi.org/10.1080/15548627.2015.1067361

Qian, P., Wang, X., Zhong, C.-Q., Wang, J., Cai, M., Nguitragool, W., Li, J., Cui, H., & Yuan, J. (2022). Inner membrane complex proteomics reveals a palmitoylation cascade regulating intraerythrocytic development of malaria parasite. *BioRxiv*, 2022.01.28.478263. https://doi.org/10.1101/2022.01.28.478263

Quadt, K. A., Streichfuss, M., Moreau, C. A., Spatz, J. P., & Frischknecht, F. (2016). Coupling of Retrograde Flow to Force Production during Malaria Parasite Migration. *ACS Nano*. https://doi.org/10.1021/acsnano.5b06417

Ramakrishnan, C., Dessens, J. T., Armson, R., Pinto, S. B., Talman, A. M., Blagborough, A. M., & Sinden, R. E. (2011). Vital functions of the malarial ookinete protein, CTRP, reside in the A domains. *International Journal for Parasitology*. https://doi.org/10.1016/j.ijpara.2011.05.007

Rédei, G. P. (2008). Major Facilitator Superfamily (MFS). In *Encyclopedia of Genetics, Genomics, Proteomics and Informatics*. https://doi.org/10.1007/978-1-4020-6754-9_9778

Ripp, J., Kehrer, J., Smyrnakou, X., Tisch, N., Tavares, J., Amino, R., Ruiz de Almodovar, C., & Frischknecht, F. (2021). Malaria parasites differentially sense environmental elasticity during transmission. *EMBO Molecular Medicine*, *13*(4). https://doi.org/10.15252/emmm.202113933

Rohrer, J., Schweizer, A., Russell, D., & Kornfeld, S. (1996). The targeting of lamp1 to lysosomes is dependent on the spacing of its cytoplasmic tail tyrosine sorting motif relative to the membrane. *Journal of Cell Biology*, *132*(4). https://doi.org/10.1083/jcb.132.4.565

Rompikuntal, P. K., Foe, I. T., Deng, B., Bogyo, M., & Ward, G. E. (2020). Blocking palmitoylation of Toxoplasma gondii myosin light chain 1 disrupts glideosome composition but has little impact on parasite motility. In *bioRxiv*. https://doi.org/10.1101/2020.08.13.250399

Roux, K. J., Kim, D. I., Raida, M., & Burke, B. (2012). A promiscuous biotin ligase fusion protein identifies proximal and interacting proteins in mammalian cells. *Journal of Cell Biology*. https://doi.org/10.1083/jcb.201112098

RTS, S. C. T. P. (2015). Efficacy and safety of RTS,S/AS01 malaria vaccine with or without a booster dose in infants and children in Africa: Final results of a phase 3, individually randomised, controlled trial. *The Lancet*, *386*(9988). https://doi.org/10.1016/S0140-6736(15)60721-8

Rudzinska, M. A., Trager, W., & Bray, R. S. (1965). Pinocytotic Uptake and the Digestion of Hemoglobin in Malaria Parasites. *The Journal of Protozoology*, *12*(4). https://doi.org/10.1111/j.1550-7408.1965.tb03256.x

Saeed, S., Carter, V., Tremp, A. Z., & Dessens, J. T. (2010). Plasmodium berghei crystalloids contain multiple LCCL proteins. *Molecular and Biochemical Parasitology*. https://doi.org/10.1016/j.molbiopara.2009.11.008

Sala, K. A., Nishiura, H., Upton, L. M., Zakutansky, S. E., Delves, M. J., Iyori, M., Mizutani, M., Sinden, R. E., Yoshida, S., & Blagborough, A. M. (2015). The Plasmodium berghei sexual stage antigen PSOP12 induces anti-malarial transmission blocking immunity both in vivo and in vitro. *Vaccine*, *33*(3). https://doi.org/10.1016/j.vaccine.2014.11.038

Sanchez, T., Welch, D., Nicastro, D., & Dogic, Z. (2011). Cilia-like beating of active microtubule bundles. *Science*. https://doi.org/10.1126/science.1203963

Santos, J. M., Egarter, S., Zuzarte-Luís, V., Kumar, H., Moreau, C. A., Kehrer, J., Pinto, A., da Costa, M., Franke-Fayard, B., Janse, C. J., Frischknecht, F., & Mair, G. R. (2017). Malaria parasite LIMP protein regulates sporozoite gliding motility and infectivity in mosquito and mammalian hosts. *ELife*. https://doi.org/10.7554/eLife.24109

Sassmannshausen, J., Bennink, S., Distler, U., Küchenhoff, J., Minns, A. M., Lindner, S. E., Burda, P. C., Tenzer, S., Gilberger, T. W., & Pradel, G. (2023). Comparative proteomics of vesicles essential for the egress of Plasmodium falciparum gametocytes from red blood cells. *Molecular Microbiology*. https://doi.org/10.1111/mmi.15125

Schloetel, J. G., Heine, J., Cowman, A. F., & Pasternak, M. (2019). Guided STED nanoscopy enables super-resolution imaging of blood stage malaria parasites. *Scientific Reports*, *9*(1). https://doi.org/10.1038/s41598-019-40718-z

Schnider, C. B., Bausch-Fluck, D., Brühlmann, F., Heussler, V. T., & Burda, P.-C. (2018). BioID Reveals Novel Proteins of the Plasmodium Parasitophorous Vacuole Membrane. *MSphere*. https://doi.org/10.1128/msphere.00522-17

Schüler, H., & Matuschewski, K. (2006). Regulation of apicomplexan microfilament dynamics by a minimal set of actin-binding proteins. In *Traffic* (Vol. 7, Issue 11). https://doi.org/10.1111/j.1600-0854.2006.00484.x

Schwach, F., Bushell, E., Gomes, A. R., Anar, B., Girling, G., Herd, C., Rayner, J. C., & Billker, O. (2015). PlasmoGEM, a database supporting a community resource for large-scale experimental genetics in malaria parasites. *Nucleic Acids Research*. https://doi.org/10.1093/nar/gku1143

Sherman, I. W. (1977). Amino acid metabolism and protein synthesis in malarial parasites. In *Bulletin of the World Health Organization* (Vol. 55, Issues 2–3).

Shortt, H., & Garnham, C. (1948). Pre- erythocytic Stage in Mammalian Malaria Parasites. *Nature*, *161(4082)*, 126–126. https://doi.org/10.1038/161126a0

Sinden, R. E., Canning, E. U., & Spain, B. (1976). Gametogenesis and fertilization in Plasmodium yoelii nigeriensis: a transmission electron microscope study. *Proceedings of the Royal Society of London - Biological Sciences*. https://doi.org/10.1098/rspb.1976.0031

Sinden, R. E., & Croll, N. A. (1975). Cytology and kinetics of microgametogenesis and fertilization in Plasmodium yoelii nigeriensis. *Parasitology*. https://doi.org/10.1017/S0031182000048861

Singer, M., & Frischknecht, F. (2023). Still running fast: Plasmodium ookinetes and sporozoites 125 years after their discovery. *Trends in Parasitology*, *39*(12), 991–995.

Sinha, A., Hughes, K. R., Modrzynska, K. K., Otto, T. D., Pfander, C., Dickens, N. J., Religa, A. A., Bushell, E., Graham, A. L., Cameron, R., Kafsack, B. F. C., Williams, A. E., Llinás, M., Berriman, M., Billker, O., & Waters, A. P. (2014). A cascade of DNA-binding proteins for sexual commitment and development in Plasmodium. *Nature*. https://doi.org/10.1038/nature12970

Sinka, M. E., Bangs, M. J., Manguin, S., Rubio-Palis, Y., Chareonviriyaphap, T., Coetzee, M., Mbogo, C. M., Hemingway, J., Patil, A. P., Temperley, W. H., Gething, P. W., Kabaria, C. W., Burkot, T. R., Harbach, R. E.,

& Hay, S. I. (2012). A global map of dominant malaria vectors. *Parasites and Vectors*. https://doi.org/10.1186/1756-3305-5-69

Smith, E. F. (2002). Regulation of flagellar dynein by calcium and a role for an axonemal calmodulin and calmodulin-dependent Kinase. *Molecular Biology of the Cell*. https://doi.org/10.1091/mbc.E02-04-0185

Smith, E. F., & Lefebvre, P. A. (1997). The role of central apparatus components in flagellar motility and microtubule assembly. In *Cell Motility and the Cytoskeleton*. https://doi.org/10.1002/(SICI)1097-0169(1997)38:1<1::AID-CM1>3.0.CO;2-C

Smith, R. C., Vega-Rodríguez, J., & Jacobs-Lorena, M. (2014). The Plasmodium bottleneck: Malaria parasite losses in the mosquito vector. *Memorias Do Instituto Oswaldo Cruz*. https://doi.org/10.1590/0074-0276130597

Soares, A. B., Stäcker, J., Schwald, S., Hoijmakers, W., Metwally, N. G., Schoeler, H., Flemming, S., Höhn, K., Fröhlke, U., Mesén-Ramírez, P., Bergmann, B., Khosh-Naucke, M., Bruchhaus, I., Bártfai, R., & Spielmann, T. (2021). An unusual trafficking domain in MSRP6 defines a complex needed for Maurer's clefts anchoring and maintenance in P. falciparum infected red blood cells. *BioRxiv*, 2021.12.03.471078. https://doi.org/10.1101/2021.12.03.471078

Sologub, L., Kuehn, A., Kern, S., Przyborski, J., Schillig, R., & Pradel, G. (2011). Malaria proteases mediate inside-out egress of gametocytes from red blood cells following parasite transmission to the mosquito. *Cellular Microbiology*. https://doi.org/10.1111/j.1462-5822.2011.01588.x

Spaccapelo, R., Naitza, S., Robson, K. J., & Crisanti, A. (1997). Thrombospondin-related adhesive protein (TRAP) of Plasmodium berghei and parasite motility [1]. *Lancet*. https://doi.org/10.1016/S0140-6736(97)24031-6

Spalteholz, W. (1914). Über das Durchsichtigmachen von menschlichen und tierischen Präparaten und seine theoretischen Bedingungen. In *Leipzig*.

Spreng, B., Fleckenstein, H., Kübler, P., Di Biagio, C., Benz, M., Patra, P., Schwarz, U. S., Cyrklaff, M., & Frischknecht, F. (2019). Microtubule number and length determine cellular shape and function in Plasmodium . *The EMBO Journal*. https://doi.org/10.15252/embj.2018100984

Stanley A. Cohn, & Roy E. Weitzell Jr. (1996). Ecological considerations of Diatom cell motility . I. Characterization of motility and adhesion in four Diatom species. *Journal of Phycology*.

Steinbuechel, M., & Matuschewski, K. (2009). Role for the plasmodium sporozoite-specific transmembrane protein S6 in parasite motility and efficient malaria transmission. *Cellular Microbiology*. https://doi.org/10.1111/j.1462-5822.2008.01252.x

Steward, M. J., & Vanderberg, J. P. (1991). Malaria Sporozoites Release Circumsporozoite Protein from Their Apical End and Translocate It along Their Surface. *The Journal of Protozoology*. https://doi.org/10.1111/j.1550-7408.1991.tb01379.x

Straschil, U., Talman, A. M., Ferguson, D. J. P., Bunting, K. A., Xu, Z., Bailes, E., Sinden, R. E., Holder, A. A., Smith, E. F., Coates, J. C., & Tewari, R. (2010). The armadillo repeat protein PF16 is essential for flagellar structure and function in Plasmodium male gametes. *PLoS ONE*. https://doi.org/10.1371/journal.pone.0012901

Sturm, A., Amino, R., Van De Sand, C., Regen, T., Retzlaff, S., Rennenberg, A., Krueger, A., Pollok, J. M., Menard, R., & Heussler, V. T. (2006). Manipulation of host hepatocytes by the malaria parasite for delivery into liver sinusoids. *Science*. https://doi.org/10.1126/science.1129720

Sultan, A. A., Thathy, V., Frevert, U., Robson, K. J. H., Crisanti, A., Nussenzweig, V., Nussenzweig, R. S., & Ménard, R. (1997). TRAP is necessary for gliding motility and infectivity of Plasmodium sporozoites. *Cell*. https://doi.org/10.1016/S0092-8674(00)80511-5

Tachibana, M., Ishino, T., Takashima, E., Tsuboi, T., & Torii, M. (2018). A male gametocyte osmiophilic body and microgamete surface protein of the rodent malaria parasite Plasmodium yoelii (PyMiGS) plays a critical role in male osmiophilic body formation and exflagellation. *Cellular Microbiology*, *20*(5). https://doi.org/10.1111/cmi.12821

Tainaka, K., Murakami, T. C., Susaki, E. A., Shimizu, C., Saito, R., Takahashi, K., Hayashi-Takagi, A., Sekiya, H., Arima, Y., Nojima, S., Ikemura, M., Ushiku, T., Shimizu, Y., Murakami, M., Tanaka, K. F., Iino, M., Kasai, H., Sasaoka, T., Kobayashi, K., … Ueda, H. R. (2018). Chemical Landscape for Tissue Clearing Based on Hydrophilic Reagents. *Cell Reports*, *24*(8). https://doi.org/10.1016/j.celrep.2018.07.056

Talman, A. M., Lacroix, C., Marques, S. R., Blagborough, A. M., Carzaniga, R., Ménard, R., & Sinden, R. E. (2011). PbGEST mediates malaria transmission to both mosquito and vertebrate host. *Molecular Microbiology*. https://doi.org/10.1111/j.1365-2958.2011.07823.x

Talman, A. M., Prieto, J. H., Marques, S., Ubaida-Mohien, C., Lawniczak, M., Wass, M. N., Xu, T., Frank, R., Ecker, A., Stanway, R. S., Krishna, S., Sternberg, M. J., Christophides, G. K., Graham, D. R., Dinglasan, R. R., Yates, J. R., & Sinden, R. E. (2014). Proteomic analysis of the Plasmodium male gamete reveals the key role for glycolysis in flagellar motility. *Malaria Journal*. https://doi.org/10.1186/1475-2875-13-315

Tanaka, T. Q., Deu, E., Molina-Cruz, A., Ashburne, M. J., Ali, O., Suri, A., Kortagere, S., Bogyo, M., & Williamson, K. C. (2013). Plasmodium dipeptidyl aminopeptidases as malaria transmission-blocking drug targets. *Antimicrobial Agents and Chemotherapy*, *57*(10). https://doi.org/10.1128/AAC.02495-12

Taylor, C. J., McRobert, L., & Baker, D. A. (2008). Disruption of a Plasmodium falciparum cyclic nucleotide phosphodiesterase gene causes aberrant gametogenesis. *Molecular Microbiology*, *69*(1). https://doi.org/10.1111/j.1365-2958.2008.06267.x

Templeton, T. J., & Kaslow, D. C. (1997). Cloning and cross-species comparison of the thrombospondin-related anonymous protein (TRAP) gene from Plasmodium knowlesi, Plasmodium vivax and Plasmodium gallinaceum. *Molecular and Biochemical Parasitology*. https://doi.org/10.1016/S0166-6851(96)02775-2

Templeton, T. J., Kaslow, D. C., & Fidock, D. A. (2000). Developmental arrest of the human malaria parasite Plasmodium falciparum within the mosquito midgut via CTRP gene disruption. *Molecular Microbiology*. https://doi.org/10.1046/j.1365-2958.2000.01821.x

Tian, T., Yang, Z., & Li, X. (2021). Tissue clearing technique: Recent progress and biomedical applications. In *Journal of Anatomy* (Vol. 238, Issue 2). https://doi.org/10.1111/joa.13309

Tomas, A. M., Margos, G., Dimopoulos, G., Van Lin, L. H. M., De Koning-Ward, T. F., Sinha, R., Lupetti, P., Beetsma, A. L., Rodriguez, M. C., Karras, M., Hager, A., Mendoza, J., Butcher, G. A., Kafatos, F., Janse, C. J., Waters, A. P., & Sinden, R. E. (2001). P25 and P28 proteins of the malaria ookinete surface have multiple and partially redundant functions. *EMBO Journal*. https://doi.org/10.1093/emboj/20.15.3975

Torii, M., Nakamura, K.-I.-I., Sieber, K. P., Miller, L. H., & Aikawa, M. (1992). Penetration of the Mosquito (Aedes aegypti) Midgut Wall by the Ookinetes of Plasmodium gallinaceum. *The Journal of Protozoology*. https://doi.org/10.1111/j.1550-7408.1992.tb04830.x

Touray, M. G., Warburg, A., Laughinghouse, A., Krettli, A. U., & Miller, L. H. (1992). Developmentally regulated infectivity of malaria sporozoites for mosquito salivary glands and the vertebrate host. In *Journal of Experimental Medicine*.

Tsai, Y. L., Hayward, R. E., Langer, R. C., Fidock, D. A., & Vinetz, J. M. (2001). Disruption of Plasmodium falciparum chitinase markedly impairs parasite invasion of mosquito midgut. *Infection and Immunity*. https://doi.org/10.1128/IAI.69.6.4048-4054.2001

Tuchin, V. V. (1997). Light scattering study of tissues. *Physics-Uspekhi*, *40*(5). https://doi.org/10.1070/pu1997v040n05abeh000236

Vanderberg, J. P. (1974). Studies on the Motility of Plasmodium Sporozoites. *Journal of Protozoology*, *21*(4), 527–537.

Vega-Rodríguez, J., Ghosh, A. K., Kanzok, S. M., Dinglasan, R. R., Wang, S., Bongio, N. J., Kalume, D. E., Miura, K., Long, C. A., Pandey, A., & Jacobs-Lorena, M. (2014). Multiple pathways for Plasmodium ookinete invasion of the mosquito midgut. *Proceedings of the National Academy of Sciences of the United States of America*, *111*(4). https://doi.org/10.1073/pnas.1315517111

Vincke, I. H., & Lips, M. (1948). Un nouveau plasmodium d'un rongeur sauvage du Congo Plasmodium berghei n. sp. *Annales de La Société Belge de Médecine Tropicale*.

Volz, J. C., Yap, A., Sisquella, X., Thompson, J. K., Lim, N. T. Y., Whitehead, L. W., Chen, L., Lampe, M., Tham, W. H., Wilson, D., Nebl, T., Marapana, D., Triglia, T., Wong, W., Rogers, K. L., & Cowman, A. F. (2016). Essential Role of the PfRh5/PfRipr/CyRPA Complex during Plasmodium falciparum Invasion of Erythrocytes. *Cell Host and Microbe*, *20*(1). https://doi.org/10.1016/j.chom.2016.06.004

Wass, M. N., Stanway, R. S., Blagborough, A. M., Lal, K., Prieto, J. H., Raine, D., Sternberg, M. J., Talman, A. M., Tomley, F. M., Yates, J. R., & Sinden, R. E. (2012). Proteomic analysis of Plasmodium in the mosquito: Progress and pitfalls. *Parasitology*. https://doi.org/10.1017/S0031182012000133

Wengelnik, K., Spaccapelo, R., Naitza, S., Robson, K. J. H., Janse, C. J., Bistoni, F., Waters, A. P., & Crisanti, A. (1999). The A-domain and the thrombospondin-related motif of Plasmodium falciparum TRAP are implicated in the invasion process of mosquito salivary glands. *EMBO Journal*, *18*(19). https://doi.org/10.1093/emboj/18.19.5195

Wichers, J. S., Wunderlich, J., Heincke, D., Pazicky, S., Strauss, J., Schmitt, M., Kimmel, J., Wilcke, L., Scharf, S., von Thien, H., Burda, P. C., Spielmann, T., Löw, C., Filarsky, M., Bachmann, A., & Gilberger, T. W. (2021). Identification of novel inner membrane complex and apical annuli proteins of the malaria parasite Plasmodium falciparum. *Cellular Microbiology*, *23*(9). https://doi.org/10.1111/cmi.13341

Wilson, L. G., Carter, L. M., & Reece, S. E. (2013). High-speed holographic microscopy of malaria parasites reveals ambidextrous flagellar waveforms. *Proceedings of the National Academy of Sciences of the United States of America*. https://doi.org/10.1073/pnas.1309934110

Wirth, C. C., Glushakova, S., Scheuermayer, M., Repnik, U., Garg, S., Schaack, D., Kachman, M. M., Weißbach, T., Zimmerberg, J., Dandekar, T., Griffiths, G., Chitnis, C. E., Singh, S., Fischer, R., & Pradel, G. (2014). Perforin-like protein PPLP2 permeabilizes the red blood cell membrane during egress of Plasmodium falciparum gametocytes. *Cellular Microbiology*. https://doi.org/10.1111/cmi.12288

Wiser, M. F., & Plitt, B. (1987). Plasmodium berghei, P. chabaudi, and P. falciparum: Similarities in phosphoproteins and protein kinase activities and their stage specific expression. *Experimental Parasitology*, *64*(3). https://doi.org/10.1016/0014-4894(87)90043-9

World Health Organization. (2021a). *WHO recommends groundbreaking malaria vaccine for children at risk*.

World Health Organization. (2021b). WHO World malaria report 2021. *WHO World Health Organization*.

Wykes, M. N., & Good, M. F. (2009). What have we learnt from mouse models for the study of malaria? In *European Journal of Immunology*. https://doi.org/10.1002/eji.200939552

Yoeli, M. (1964). Movement of the sporozoites of plasmodium berghei (Vincke et Lips, 1948) [45]. In *Nature*. https://doi.org/10.1038/2011344a0

Yoshida, N., Nussenzweig, R. S., Potocnjak, P., Nussenzweig, V., & Aikawa, M. (1980). Hybridoma produces protective antibodies directed against the sporozoite stage of malaria parasite. *Science*, *207*(4426). https://doi.org/10.1126/science.6985745

Yuda, M., Sakaida, H., & Chinzei, Y. (1999). Targeted disruption of the Plasmodium berghei CTRP gene reveals its essential role in malaria infection of the vector mosquito. *Journal of Experimental Medicine*. https://doi.org/10.1084/jem.190.11.1711

Yuda, M., Yano, K., Tsuboi, T., Torii, M., & Chinzei, Y. (2001). Von Willebrand factor A domain-related protein, a novel microneme protein of the malaria ookinete highly conserved throughout Plasmodium parasites. *Molecular and Biochemical Parasitology*. https://doi.org/10.1016/S0166-6851(01)00304-8

Zieler, H., & Dvorak, J. A. (2000). Invasion in vitro of mosquito midgut cells by the malaria parasite proceeds by a conserved mechanism and results in death of the invaded midgut cells. *Proceedings of the National Academy of Sciences of the United States of America*. https://doi.org/10.1073/pnas.97.21.11516

7 ABBREVIATIONS

°C	degree Celsius
5- FC	5- flourocytosine
A. gambiae	Anopheles gambiae
A. stephensi	Anopheles stephensi
aa	amino acids
BSA	bovine serum albumin
Ca	calcium
CDPK	calcium-dependent protein kinases
CELTOS	cell-traversal protein for ookinetes and sporozoites
cGMP	cyclic guanosine monophosphate
CoA	coenzyme A
CRT	chloroquine resistance transporter
CSP	circumsporozoite protein
CTD	cytoplasmic tail domain
CTRP	circumsporozoite- and TRAP-related protein
d	day
ddH_2O	double-distilled water
DHFR	dihydrofolate reductase
DIC	differential interference contrast
DMSO	dimethylsulfoxid
DNA	desoxyribonucleicsacid
dNTPs	desoxynukleosidtriphosphate
DPAP	dipeptidyl aminopeptidase 2
E. coli	escherichia coli
EDTA	ethylendiamintetraacetat
ef1a	elongation factor 1 alpha
EV	egress vesicles
FACS	fluorescent activated cell sorting
FCS	fetal calf serum
FRAP	fluorescence recovery after photobleaching
FV	food vacuole
g	gram
GAC	glideosome associated connector
GAMA	glycosylphosphatidylinositol-anchored micronemal antigen
GAP	glideosome associated proteins
GAP45	gliding- associated- protein 45

GCα	Guanylyl Cyclase alpha
GEP1	gametogenesis essential protein 1
GEST	gamete egress and sporozoite traversal
GFP	green fluorescent protein
GIMO	gene in marker out
GO	gene ontology
h	hours
HCL	hydrochloricacid
HRP	horseradish peroxidase
HSP20	Heat shock protein 20
i.p.	intra peritoneal
i.v	intra venously
ICM1	Important for Ca2+ mobilization 1
IMC	inner membrane complex
IP3	Inositol-(1,4,5)-trisphosphate
KCL	potassium chloride
kDa	kilo Dalton
KH_2PO_4	potassiumdihydrogenphosphate
KO	knockout
L	liter
MDV/ PEG3	male development-1/ protein of early gametocyte 3
MG	midgut
mg	milligram
MiGS	microgametocyte surface protein
min	minutes
ml	milliliter
mM	millimole
MS	mass- spectrometry
MT	microtubules
MTOC	microtubule organizing center
mTRAP	merozoite TRAP-like protein
NA	numerical aperture
Na_2HPO_4	disodiumhydrogenphosphate
NaCl	sodiumchloride
$NaHCO_3$	sodiumhydrogencarbonate
NaOH	sodiumhydroxide
NH_4CL	ammoniumchloride
nm	nanometer
NS	negative selected
OB	osmiophilic bodies
ORF	open reading frame

PA	pluronic acid
PABA	Para- aminobenzoic acid
PALM	photo-activated localization microscopy
PAT	pantothenic acid transporter
Pb	Plasmodium berghei
PBS	Phosphate buffered saline
PCR	Polymerase chain reaction
Pf	Plasmodium falciparum
PFA	paraformaldehyde
PH	phenylhydrazin
PIP2	phosphatidylinositol (4,5)-bi-phosphate
PKG	protein kinase G
PM	plasma membrane
PPLP2	perforin-like protein 2
PTM	posttranslational modifications
PV	parasitophorous vacuole
PVM	parasitophorous vacuole membrane
Py	Plasmodium yoelii
RBC	red blood cells
RBCM	red blood cell membrane
RPMI	Roswell Park Memorial Institute
RT	Room temperature
s	seconds
s.c.	subcutaneous
SDS	sodium-dodecyl-sulfate
SEM	scanning electron microscopy
SERA5	serine repeat antigen 5
SG	salivary gland
SIAP1	Sporozoite invasion-associated protein 1
SIM	structured illumination microscopy
SOAP	secreted ookinete adhesive protein
SP	signal peptide
SPECT	sporozoite microneme protein essential for cell traversal
SPM	subpellicular microtubules
SS	signal sequence
STED	stochastic emission depletion
STORM	stochastic optical reconstruction microscopy
SUB1	subtilisin-like serine protease 1
SUB2	subtilisin-like serine protease 2
T	temperature
TEM	transmission electron microscopy

TFP1	transporter family protein 1
Tg	Toxoplasma gondii
TLP	TRAP- like protein
TMD	transmembrane domain
TRAP	thrombospondin related anonymous protein
TSR	thrombospondin type-I repeat
UIS2	upregulated in sporozoite 2
vWF	von Willebrand factor
WT	wildtype
XA	xanthurenic acid
yFCU	yeast cytosine deaminase and uridyl phosphoribosyl transferase
µg	microgram

8 LIST OF FIGURES

9 APPENDIX

9.1. The ookinete microneme proteome

Gene ID		TM	SP	pl8 +H2O2	pl8 -H2O2	wt +H2O2	pl8 +H2O2	pl8 -H2O2	wt +H2O2	SUM pl8+	PlasmoGem phenotype	Lal et al.	function
PBANKA_1300700	LCCL domain-containing protein (CCp1)	0	x	**86**	0	0	**49**	0	0	**135**		x	micronemal
PBANKA_1035200	LCCL domain-containing protein (CCp3)	0	x	**71**	0	0	**33**	0	0	**104**		x	micronemal
PBANKA_0204500	LCCL domain-containing protein (CCp5)	0	x	**68**	0	0	**31**	0	0	**99**		x	micronemal
PBANKA_1437300	endoplasmin, putative	0	x	**48**	1	0	**41**	0	0	**89**	L, essential	x	micronemal
PBANKA_1410300	M1-family alanyl aminopeptidase, putative	0	x	**19**	0	10	**54**	0	0	**73**	L, essential	x	micronemal
PBANKA_0702800	protein disulfide isomerase	0	x	**28**	0	0	**28**	0	0	**56**	L, essential	x	micronemal
PBANKA_1318100	aminopeptidase P, putative (APP)	0	x	**6**	0	1	**27**	0	0	**33**	L, essential	x	micronemal
PBANKA_0830200	high molecular weight rhoptry protein 2	0	x	**23**	0	0	**10**	0	0	**33**		x	micronemal
PBANKA_0914300	protein disulfide isomerase related protein, putative	0	x	**19**	0	0	**10**	0	0	**29**		x	micronemal
PBANKA_1319500	LCCL domain-containing protein CCP2 (CCP2)	0	x	**12**	0	0	**16**	0	0	**28**		x	micronemal
PBANKA_1237800	multidrug resistance protein 1, putative	11		**3**	0	1	**20**	0	0	**23**	L, essential	x	micronemal
PBANKA_1214300	enolase, putative	0		**3**	0	0	**19**	0	0	**22**	L, essential	x	micronemal
PBANKA_1102200	merozoite surface protein 8	1	x	**4**	0	5	**18**	0	0	**22**	L, dispensable	x	micronemal
PBANKA_1034400	plasmepsin IV	1		**8**	0	7	**13**	0	0	**21**	Sig slow	x	micronemal
PBANKA_0209200	parasite-infected erythrocyte surface protein	1	x	**14**	0	0	**6**	0	0	**20**	L, dispensable	x	micronemal
PBANKA_1315300	LCCL domain-containing protein Lap5	0	x	**8**	0	0	**7**	0	0	**15**	L, dispensable		micronemal
PBANKA_0932400	berghepain-2	1		**3**	0	0	**11**	0	0	**14**			micronemal
PBANKA_0942500	thioredoxin-like mero protein, putative	0	x	**6**	0	0	**7**	0	0	**13**	L, essential	x	micronemal
PBANKA_1359700	6-cysteine protein p47	2	x	**11**	0	0	**1**	0	0	**12**	L, dispensable	x	micronemal
PBANKA_0931300	dipeptidyl aminopeptidase 1, putative	1	x	**1**	0	0	**11**	0	0	**12**	L, essential	x	micronemal
PBANKA_0826700	parasitophorous vacuolar protein 5	0	x	**3**	0	3	**9**	0	0	**12**		x	micronemal
PBANKA_0416000	high molecular weight rhoptry protein 3, putative	0	x	**6**	0	0	**4**	0	0	**10**	L, essential	x	micronemal
PBANKA_0800500	chitinase	0	x	**0**	0	0	**9**	0	0	**9**	Sig slow	x	micronemal
PBANKA_1137000	bergheilysin	0		**2**	0	0	**6**	0	0	**8**	L, essential	x	micronemal
PBANKA_1113400	secreted ookinete protein	0	x	**7**	0	0	**1**	0	0	**8**		x	micronemal
PBANKA_0304900	serine repeat antigen 3	0		**2**	0	0	**6**	0	0	**8**			micronemal
PBANKA_1321700	berghepain-1	1		**6**	0	0	**1**	0	0	**7**	Sig slow	x	micronemal
PBANKA_0703900	receptor for activated c kinase, putative	0		**2**	0	0	**5**	0	0	**7**		x	micronemal
PBANKA_0207000	calcium-transporting ATPase, putative	8		**6**	0	0	**0**	0	0	**6**	L, essential	x	micronemal
PBANKA_1224500	Dpy-19-like C-mannosyltransferase, putative	11	x	**6**	0	0	**0**	0	0	**6**			micronemal
PBANKA_0514900	ookinete surface protein P28	1	x	**2**	0	0	**3**	0	0	**5**	Sig slow	x	micronemal
PBANKA_1229000	Plasmodium exported protein (PHIST), unknown function	1		**0**	0	0	**5**	0	0	**5**			micronemal
PBANKA_0305000	serine repeat antigen 2	0	x	**1**	0	0	**4**	0	0	**5**	L, dispensable		micronemal
PBANKA_0412900	circumsporozoite- and TRAP-related protein	2	x	**0**	0	0	**4**	0	0	**4**		x	micronemal
PBANKA_0911400	CLPTM1 domain-containing protein, putative	6		**3**	0	0	**1**	0	0	**4**	L, dispensable	x	micronemal
PBANKA_0819000	glideosome-associated protein 50, putative	2	x	**2**	0	0	**2**	0	0	**4**		x	micronemal
PBANKA_1037800	secreted ookinete adhesive protein	0	x	**1**	0	0	**3**	0	0	**4**	L, dispensable	x	micronemal
PBANKA_1228900	von Willebrand factor A domain-related protein	0	x	**0**	0	0	**4**	0	0	**4**		x	micronemal
PBANKA_1338700	plasmepsin V, putative	1	x	**3**	0	0	**1**	0	0	**4**	L, essential		micronemal
PBANKA_1434400	secreted ookinete protein, putative	0	x	**3**	0	0	**1**	0	0	**4**	L, dispensable		micronemal
PBANKA_1101400	rhoptry-associated protein 2/3	0	x	**0**	0	0	**3**	0	0	**3**	Sig slow	x	micronemal
PBANKA_1309900	M17 leucyl aminopeptidase, putative	0		**1**	0	0	**2**	0	0	**3**	Sig slow		micronemal
PBANKA_0919100	parasitophorous vacuolar protein 1	0	x	**0**	0	0	**3**	0	0	**3**	Sig slow		micronemal
PBANKA_0809400	plasma membrane protein 1	2	x	**3**	0	0	**0**	0	0	**3**	L, dispensable		micronemal
PBANKA_0623100	tryptophan-rich protein	1		**0**	0	0	**3**	0	0	**3**			micronemal
PBANKA_1107600	6-cysteine protein	2	x	**0**	0	0	**2**	0	0	**2**	L, dispensable	x	micronemal
PBANKA_0915000	apical membrane antigen 1	1	x	**0**	0	0	**2**	0	0	**2**		x	micronemal
PBANKA_0712200	BEM46-like protein, putative	3	x	**0**	0	0	**2**	0	0	**2**	L, dispensable	x	micronemal
PBANKA_1145800	membrane associated histidine-rich protein 1a	1		**1**	0	2	**1**	0	0	**2**		x	micronemal
PBANKA_0515000	ookinete surface protein P25	2	x	**0**	0	0	**2**	0	0	**2**	L, dispensable	x	micronemal
PBANKA_1008500	translocon component PTEX150	0	x	**0**	0	0	**2**	0	0	**2**	L, essential	x	micronemal
PBANKA_0408500	parasite-infected erythrocyte surface protein PIESP	0	x	**2**	0	0	**0**	0	0	**2**			micronemal
PBANKA_1335800	protein disulfide-isomerase, putative	0	x	**2**	0	0	**0**	0	0	**2**	L, dispensable		micronemal
PBANKA_0619200	secreted ookinete protein, PSOP1	0	x	**0**	0	0	**2**	0	0	**2**	L, dispensable		micronemal
PBANKA_0522500	transmembrane emp24 domain-containing protein, putative	2	x	**2**	0	0	**0**	0	0	**2**			micronemal
PBANKA_1105300	**conserved Plasmodium protein, unknown function**	**4**	**x**	**13**	**0**	**0**	**3**	**0**	**0**	**16**			**unknown**
PBANKA_0407300	conserved Plasmodium protein, unknown function	0	x	**4**	0	0	**2**	0	0	**6**	L, dispensable		unknown
PBANKA_1243600	conserved Plasmodium protein, unknown function	2	x	**1**	0	0	**4**	0	0	**5**	L, essential		unknown
PBANKA_0620700	conserved Plasmodium protein, unknown function	0	x	**4**	0	0	**1**	0	0	**5**			unknown
PBANKA_0403800	conserved Plasmodium membrane protein, unknown function	12		**0**	0	0	**3**	0	0	**3**			unknown
PBANKA_0806400	conserved protein, unknown function	2	x	**3**	0	0	**0**	0	0	**3**	L, dispensable		unknown
PBANKA_1454200	conserved Plasmodium protein, unknown function	0		**2**	0	0	**0**	0	0	**2**	L, essential		unknown
PBANKA_0818900	endoplasmic reticulum chaperone BiP, putative	0	x	**46**	1	2	**40**	0	1	**86**			Chaperone
PBANKA_1357200	heat shock protein 110, putative	0	x	**21**	0	0	**24**	0	0	**45**	L, essential	x	Chaperone
PBANKA_0711900	heat shock protein 70	0		**13**	0	4	**26**	1	1	**39**	L, essential	x	Chaperone
PBANKA_0805700	heat shock protein 90, putative	0		**4**	1	1	**20**	0	0	**24**	Sig slow	x	Chaperone
PBANKA_1127800	DnaJ protein, putative	0	x	**9**	0	0	**1**	0	0	**10**	Sig slow	x	Chaperone
PBANKA_0938300	heat shock protein J2, putative	1	x	**9**	0	0	**1**	0	0	**10**	L, essential	x	Chaperone
PBANKA_0706800	DnaJ protein, putative	3		**7**	0	0	**1**	0	0	**8**	Sig slow	x	Chaperone
PBANKA_1219300	heat shock protein 110, putative	0		**0**	0	0	**7**	0	0	**7**			Chaperone
PBANKA_0310900	T-complex protein 1 subunit theta, putative	0		**0**	0	0	**4**	0	0	**4**			Chaperone

PBANKA_0820000	DnaJ protein, putative	6		**3**	0	0	**0**	0	0	**3**	L, essential	x	Chaperone
PBANKA_0916200	T-complex protein 1 subunit alpha, putative	0		**0**	0	0	**3**	0	0	**3**		x	Chaperone
PBANKA_0405200	T-complex protein 1 subunit beta, putative	0		**0**	0	0	**3**	0	0	**3**	L, essential	x	Chaperone
PBANKA_0406500	T-complex protein 1 subunit eta, putative	0		**0**	0	0	**3**	0	0	**3**	L, essential	x	Chaperone
PBANKA_0929900	heat shock protein 90, putative	0		**1**	0	0	**2**	0	0	**3**			Chaperone
PBANKA_1463900	HSP20-like chaperone, putative	0	x	**2**	0	0	**1**	0	0	**3**			Chaperone
PBANKA_1444100	T-complex protein 1 subunit gamma, putative	0		**0**	0	0	**3**	0	0	**3**	L, essential		Chaperone
PBANKA_1224200	DnaJ protein, putative	0		**0**	0	0	**2**	0	0	**2**			Chaperone
PBANKA_1134100	T-complex protein 1 subunit delta, putative	0		**0**	0	0	**2**	0	0	**2**	L, essential		Chaperone
PBANKA_1218200	T-complex protein 1 subunit epsilon, putative	0		**0**	0	0	**2**	0	0	**2**	L, essential		Chaperone
PBANKA_0522700	alpha tubulin 2	0		**9**	0	0	**12**	0	0	**21**			contaminant
PBANKA_1206900	tubulin beta chain, putative	0		**3**	0	1	**14**	0	0	**17**	L, essential	x	contaminant
PBANKA_0938400	endoplasmic reticulum-resident calcium binding protein	0	x	**9**	0	0	**7**	0	0	**16**		x	contaminant
PBANKA_1030600	p1/s1 nuclease, putative	0	x	**3**	0	3	**13**	0	0	**16**		x	contaminant
PBANKA_1459300	actin I	0		**3**	0	1	**12**	0	0	**15**	L, essential	x	contaminant
PBANKA_1326400	glyceraldehyde-3-phosphate dehydrogenase	0		**2**	0	1	**12**	0	0	**14**	L, essential	x	contaminant
PBANKA_1337400	nucleoside-diphosphatase, putative	1	x	**9**	0	0	**4**	0	0	**13**	L, essential	x	contaminant
PBANKA_1125600	pyruvate kinase, putative	0		**3**	0	0	**10**	0	0	**13**	L, essential	x	contaminant
PBANKA_1133300	elongation factor 1-alpha	0		**4**	0	0	**9**	0	0	**13**			contaminant
PBANKA_1315500	sortilin, putative	2	x	**9**	0	0	**3**	0	0	**12**		x	contaminant
PBANKA_1314800	elongation factor 2, putative	0		**0**	0	0	**12**	0	0	**12**	L, essential	x	contaminant
PBANKA_1365500	exported protein IBIS1	1		**1**	0	1	**9**	0	0	**10**		x	contaminant
PBANKA_1429300	integral membrane protein GPR180, putative	8	x	**8**	0	0	**2**	0	0	**10**	L, dispensable		contaminant
PBANKA_1217700	ATP-dependent RNA helicase DDX6	0		**0**	0	0	**9**	0	0	**9**	L, dispensable	x	contaminant
PBANKA_1329300	40S ribosomal protein S3, putative	0		**3**	0	0	**5**	0	0	**8**		x	contaminant
PBANKA_1308600	fructose-bisphosphate aldolase 2	0		**0**	0	0	**8**	0	0	**8**	L, essential	x	contaminant
PBANKA_1365200	thioredoxin-related protein, putative	1	x	**5**	0	0	**3**	0	0	**8**		x	contaminant
PBANKA_0924300	endoplasmic reticulum oxidoreductin, putative	2	x	**7**	0	0	**1**	0	0	**8**			contaminant
PBANKA_1426300	ER membrane protein complex subunit 1, putative	3	x	**7**	0	0	**0**	0	0	**7**	L, essential	x	contaminant
PBANKA_1122900	hexokinase, putative	0		**1**	0	0	**6**	0	0	**7**	L, essential		contaminant
PBANKA_1302800	thioredoxin peroxidase 1	0		**2**	0	0	**4**	0	0	**6**	L, dispensable	x	contaminant
PBANKA_0712600	14-3-3 protein	0		**1**	0	0	**4**	1	0	**5**	L, essential	x	contaminant
PBANKA_1450300	ATP synthase subunit beta, mitochondrial	0		**1**	0	0	**4**	0	0	**5**	Sig slow	x	contaminant
PBANKA_1118600	cell division cycle protein 48 homologue, putative	0		**0**	0	0	**5**	0	0	**5**	L, essential	x	contaminant
PBANKA_1331900	eukaryotic initiation factor 4a, putative	0		**2**	0	1	**3**	0	0	**5**		x	contaminant
PBANKA_0930300	GTP-binding nuclear protein RAN/TC4, putative	0		**0**	0	0	**5**	0	0	**5**	L, essential	x	contaminant
PBANKA_1231800	60S ribosomal protein L12, putative	0		**2**	0	1	**3**	0	0	**5**	L, essential		contaminant
PBANKA_0520200	ADP/ATP transporter on adenylate translocase, putative	3		**3**	0	1	**2**	0	0	**5**	Sig slow		contaminant
PBANKA_1418300	golgi protein 1, putative	0	x	**5**	0	0	**0**	0	0	**5**			contaminant
PBANKA_1032700	CUGBP Elav-like family member 2, putative	0		**0**	0	0	**4**	0	0	**4**	L, dispensable	x	contaminant
PBANKA_1238800	karyopherin beta, putative	0		**0**	0	0	**4**	0	0	**4**	L, dispensable	x	contaminant
PBANKA_1141700	ubiquitin-60S ribosomal protein L40, putative	0		**2**	0	1	**2**	0	0	**4**		x	contaminant
PBANKA_0619100	40S ribosomal protein S5, putative	0		**1**	0	0	**3**	0	0	**4**			contaminant
PBANKA_1317500	glucose-6-phosphate dehydrogenase-6-phosphogluconolactonase	0		**0**	0	0	**4**	0	0	**4**	Sig slow		contaminant
PBANKA_0104700	long chain polyunsaturated fatty acid elongation enzyme	7		**2**	0	0	**2**	0	0	**4**	L, dispensable		contaminant
PBANKA_1326000	GTP-binding protein, putative	3	x	**3**	0	0	**0**	0	0	**3**		x	contaminant
PBANKA_1301300	trailer hitch homolog CITH	0		**0**	0	0	**3**	0	0	**3**		x	contaminant
PBANKA_1201900	40S ribosomal protein S20e, putative	0		**0**	0	0	**3**	0	0	**3**			contaminant
PBANKA_0505100	ADP-ribosylation factor, putative	0		**1**	0	0	**2**	0	0	**3**			contaminant
PBANKA_1426900	ATP-dependent RNA helicase DBP1, putative	0		**0**	0	0	**3**	0	0	**3**	Sig slow		contaminant
PBANKA_1003800	V-type proton ATPase subunit B, putative	0		**0**	0	0	**3**	0	0	**3**			contaminant
PBANKA_0924800	golgi protein 2	1	x	**2**	0	0	**0**	0	0	**2**		x	contaminant
PBANKA_0522800	40S ribosomal protein S19, putative	0		**0**	0	0	**2**	0	0	**2**		x	contaminant
PBANKA_1364200	60S ribosomal protein L17, putative	0		**0**	0	0	**2**	0	0	**2**		x	contaminant
PBANKA_0417700	alpha tubulin 1	0		**0**	0	0	**2**	0	0	**2**	L, dispensable	x	contaminant
PBANKA_0306800	ATP-dependent RNA helicase UAP56, putative	0		**0**	0	0	**2**	0	0	**2**	L, essential	x	contaminant
PBANKA_1406700	carbamoyl phosphate synthetase, putative	0		**0**	0	0	**2**	0	0	**2**	L, essential	x	contaminant
PBANKA_1423300	DNA/RNA-binding protein Alba 1, putative	0		**0**	0	0	**2**	0	0	**2**		x	contaminant
PBANKA_0941800	histone H2B, putative	0		**0**	0	0	**2**	0	0	**2**	L, essential	x	contaminant
PBANKA_1135000	YOP1-like protein, putative	3	x	**0**	0	0	**2**	0	0	**2**		x	contaminant
PBANKA_0510900	40S ribosomal protein S2, putative	0		**0**	0	0	**2**	0	0	**2**	L, essential		contaminant
PBANKA_1202400	60S ribosomal protein L13, putative	0		**0**	0	0	**2**	0	0	**2**	L, essential		contaminant
PBANKA_0407600	asparagine synthetase [glutamine-hydrolyzing]	0		**0**	0	0	**2**	0	0	**2**	Sig slow		contaminant
PBANKA_0919900	ATP-dependent 6-phosphofructokinase, putative	0		**0**	0	0	**2**	0	0	**2**	L, dispensable		contaminant
PBANKA_0816400	ATP-dependent 6-phosphofructokinase, putative	0		**0**	0	0	**2**	0	0	**2**			contaminant
PBANKA_0819100	cytochrome b5, putative	1	x	**0**	0	0	**2**	0	0	**2**	Sig slow		contaminant
PBANKA_0505800	deoxyribose-phosphate aldolase, putative	0		**0**	0	0	**2**	0	0	**2**			contaminant
PBANKA_1364300	glycerol kinase, putative	0		**0**	0	0	**2**	0	0	**2**			contaminant
PBANKA_1220200	lysophospholipase, putative	0		**0**	0	0	**2**	0	0	**2**			contaminant
PBANKA_1210900	phosphoglucomutase, putative	0		**0**	0	0	**2**	0	0	**2**	L, dispensable		contaminant
PBANKA_1223300	ras-related protein Rab-18, putative	0		**0**	0	0	**2**	0	0	**2**			contaminant
PBANKA_0611600	ribonucleoside-diphosphate reductase large subunit, putative	0		**0**	0	0	**2**	0	0	**2**	L, essential		contaminant

9.2. The sporozoite secretome

Gene ID	Gene ID PY		TM	SP	ExpI	ExpII	ExpIII	SUM	PlasmoGem phenotype	Lindner et al 2013 MCP WCL	Lindner et al 2013 MCP surface	FPKM PY Spz
PBANKA_1450300	PY17X_1452800	ATP synthase subunit beta, mitochondrial	0		11	9	10	30	Sig slow	x	x	6,33
PBANKA_1006200	PY17X_1007600	**sporozoite invasion-associated protein 1**	**0**	**x**	**15**	**3**	**8**	**26**	**L. dispensable**	x		3331,83
PBANKA_1459300	PY17X_1461900	actin I	0		8	8	8	24	L. essential	x		495,91
PBANKA_0818900	PY17X_0822200	endoplasmic reticulum chaperone BiP, putative	0	x	14	3	6	23		x		1,12
PBANKA_1133300	PY17X_1134800	elongation factor 1-alpha	0		8	4	10	22		x		18,68
PBANKA_1349800	PY17X_1354800	**thrombospondin-related anonymous protein**	**1**	**x**	**10**	**3**	**4**	**17**	**L. dispensable**	x		30290,12
PBANKA_1141700	PY17X_1143100	ubiquitin-60S ribosomal protein L40, putative	0		5	4	6	15		x		4225,36
PBANKA_1206900	PY17X_1210100	tubulin beta chain, putative	0		5	3	5	13	L. essential	x		**8,82**
PBANKA_0417700	PY17X_0420500	alpha tubulin 1	0		4	3	4	11	L. dispensable	x		14,84
PBANKA_040320	PY17X_0405400	**circumsporozoite (CS) protein**	**1**	**x**	**4**	**4**	**3**	**11**		x	**x**	**43073,31**
PBANKA_0701900	PY17X_0702200	**GPI-anchored micronemal antigen, putative**	**1**	**x**	**4**	**1**	**6**	**11**		x		1882,67
PBANKA_071190	PY17X_0712100	heat shock protein 70	0		5	2	3	10	L. essential	x		8345,83
PBANKA_1217600	PY17X_1220800	histone H2A.Z, putative	0		3	4	3	10	L. essential	x		251,85
PBANKA_0712600	PY17X_0712800	14-3-3 protein	0		2	3	4	9	L. essential	x		246,06
PBANKA_0520200	PY17X_0521300	ADP/ATP transporter on adenylate translocase, putative	3		3	3	3	9	Sig slow	x		2,25
PBANKA_0805700	PY17X_0808800	heat shock protein 90, putative	0		3	2	4	9	Sig slow	x		1221,36
PBANKA_0941900	PY17X_0944400	histone H4, putative	0		4	2	3	9	L. essential	x	x	667,47
PBANKA_0702800	PY17X_0703100	protein disulfide isomerase	0	x	5	1	2	8	L. essential	x		26,65
PBANKA_1305100	PY17X_1308900	60S ribosomal protein L1, putative	0		1	2	4	7	L. essential	x		6,31
PBANKA_1312700	PY17X_1316500	**gamete egress and sporozoite traversal protein**	**0**	**x**	**3**	**1**	**3**	**7**	**L. dispensable**	x	**x**	13095,08
PBANKA_1326400	PY17X_1330200	glyceraldehyde-3-phosphate dehydrogenase	0		3	1	3	7	L. essential	x	x	3,44
PBANKA_1028300	PY17X_1030700	serine/threonine protein phosphatase PP1	0		2	1	2	5		x		19,99
PBANKA_1410400	PY17X_1412200	V-type proton ATPase catalytic subunit A, putative	0		1	2	2	5	L. essential	x		1,86
PBANKA_1231000	PY17X_1234400	40S ribosomal protein S11, putative	0		2	1	1	4	L. essential	x		422,82
PBANKA_0710100	PY17X_0710300	2-oxoglutarate dehydrogenase E1 component, putative	0		1	1	1	3	L. dispensable	x		239,03
PBANKA_0922100	PY17X_0924100	40S ribosomal protein S18, putative	0		1	1	1	3		x		47,82
PBANKA_1231800	PY17X_1235200	60S ribosomal protein L12, putative	0		1	1	1	3	L. essential			77,54
PBANKA_1319400	PY17X_1323200	conserved Plasmodium protein, unknown function	0		1	1	1	3	L. dispensable			5,17
PBANKA_1411500	PY17X_1413300	conserved Plasmodium protein, unknown function	0		1	1	1	3		x		12,12
PBANKA_1351600	PY17X_1356800	conserved Plasmodium protein, unknown function	0		1	1	1	3				0,13
PBANKA_1231900	PY17X_1235300	conserved protein, unknown function	0		1	1	1	3	L. essential			0,38
PBANKA_1208600	PY17X_1211800	DNA2/NAM7 helicase, putative	0		1	1	1	3		x		7,18
PBANKA_1346500	PY17X_1351400	protein tyrosine phosphatase-like protein	6	x	1	1	1	3	L. dispensable			76,74
PBANKA_1354100	PY17X_1359500	ras-related protein Rab-11B, putative	0		1	1	1	3	L. essential	x		32,16
PBANKA_1112300	PY17X_1113400	ras-related protein Rab-1B, putative	0		1	1	1	3		x		2,85
PBANKA_1212700	PY17X_1215900	SPRY domain-containing protein, putative	2		1	1	1	3				153,87
PBANKA_1422900	PY17X_1424900	conserved protein, unknown function	0		1	0	6	7		x		2374,56
PBANKA_143730	PY17X_1439800	endoplasmin, putative	0	x	1	0	6	7	L. essential	x	x	1,68
PBANKA_1107600	PY17X_1108700	6-cysteine protein	2	x	5	0	1	6	L. dispensable	x		483,87
PBANKA_1340100	PY17X_1344800	L-lactate dehydrogenase	1	x	0	1	3	4	L. essential	x		507,55
PBANKA_0505100	PY17X_0506200	ADP-ribosylation factor, putative	0		2	0	1	3		x		5,8
PBANKA_0915000	PY17X_0916500	**apical membrane antigen 1**	1	x	2	0	1	3		x		351,36
PBANKA_1019800	PY17X_1021700	calcium-dependent protein kinase, putative	0		0	1	2	3	L. dispensable	x	x	**18**
PBANKA_1432300	PY17X_1434600	**cell traversal protein for ookinetes and sporozoites**	**1**	**x**	**2**	**0**	**1**	**3**		x		27165,99
PBANKA_1214300	PY17X_1217500	enolase, putative	0		1	0	2	3	L. essential	x		374,3
PBANKA_1125600	PY17X_1127000	pyruvate kinase, putative	0		1	0	2	3	L. essential	x		1264,56
PBANKA_0301000	PY17X_0301500	**repetitive organellar protein, putative**	0		1	0	2	3	L. dispensable	x		5,07
PBANKA_0510900	PY17X_0512000	40S ribosomal protein S2, putative	0		1	0	1	2	L. essential	x		206,83
PBANKA_0619100	PY17X_0621800	40S ribosomal protein S5, putative	0		1	1	0	2				187,02
PBANKA_1230600	PY17X_1234000	conserved oligomeric Golgi complex subunit 4, putative	0		1	0	1	2	Insufficient data			0,22
PBANKA_0106300	PY17X_0107800	conserved Plasmodium protein, unknown function	0		1	1	0	2	Sig slow			0,37
PBANKA_0915300	PY17X_0916800	conserved Plasmodium protein, unknown function	0		0	1	1	2	L. essential			116,13
PBANKA_0804700	PY17X_0807800	conserved Plasmodium protein, unknown function	0		0	1	1	2				1,16
PBANKA_0940400	PY17X_0942900	conserved Plasmodium protein, unknown function	0	x	1	0	1	2				0,41
PBANKA_1229900	PY17X_1233400	conserved protein, unknown function	0		1	1	0	2	L. dispensable			32,72
PBANKA_0606700	PY17X_0609200	**cysteine repeat modular protein 3**	10	x	0	1	1	2				18,54
PBANKA_0811900	PY17X_0815200	cytosolic Fe-S cluster assembly factor NBP35, putative	1		0	1	1	2	L. essential	x		2,59
PBANKA_1223500	PY17X_1226700	DNA helicase PSH3, putative	0		0	1	1	2	L. essential			114,12
PBANKA_0613200	PY17X_0615900	DNA polymerase alpha catalytic subunit A, putative	0		1	1	0	2		x		36,21
PBANKA_1314800	PY17X_1318600	elongation factor 2, putative	0		1	0	1	2	L. essential	x		13,09
PBANKA_1306100	PY17X_1309900	GTP-binding protein, putative	0		1	1	0	2	L. essential	x		0,08
PBANKA_0413800	PY17X_0416600	**microneme associated antigen (MA), putative**	**0**		**1**	**0**	**1**	**2**	**L. dispensable**			6,78
PBANKA_0929600	PY17X_0931600	nucleolar protein 56, putative	0		1	1	0	2	L. essential	x		67,7
PBANKA_1432400	PY17X_1434700	**perforin-like protein 2**	0		1	1	0	2				47,06
PBANKA_1039800	PY17X_1042300	pseudouridine synthase, putative	0		1	0	1	2	L. dispensable	x		2,52
PBANKA_1445800	PY17X_1448300	ras-related protein Rab-2, putative	0		1	0	1	2	L. essential	x		**1,34**
PBANKA_0820800	PY17X_0824100	regulator of chromosome condensation-PP1-interacting prot	0		1	1	0	2				2,55
PBANKA_0936500	PY17X_0938500	replication factor C subunit 5, putative	0		0	1	1	2	L. essential	x		16,09
PBANKA_0310800	PY17X_0311300	RTR1 domain-containing protein, putative	0		1	0	1	2				57,63
PBANKA_1444900	PY17X_1447400	vacuolar transporter chaperone, putative	3		1	0	1	2	L. dispensable	x		0,06

PBANKA_1355700	PY17X_1361400	myosin A	**0**		**4**	**0**	**0**	**4**	L. essential	x	x	1433,62
PBANKA_1328000	PY17X_1332700	**serine/threonine protein phosphatase UIS2**	0	x	4	0	0	4	L. essential	x		1146,16
PBANKA_0313800	PY17X_0314300	ATP synthase subunit alpha, mitochondrial, putative	0		0	0	2	2	Sig slow	x		52,3
PBANKA_0701200	PY17X_0701500	conserved Plasmodium protein, unknown function	0		0	2	0	2	L. essential			3,01
PBANKA_090240	PY17X_0942100	conserved Plasmodium protein, unknown function	0		0	0	2	2	L. dispensable			130,08
PBANKA_0214000	PY17X_0215400	dynein heavy chain, putative	0		0	0	2	2		x		0,34
PBANKA_1308600	PY17X_1312400	fructose-bisphosphate aldolase 2	0		0	0	2	2	L. essential	x	x	**1272,89**
PBANKA_1108100	PY17X_1109200	guanidine nucleotide exchange factor, putative	0		0	0	2	2	L. essential			**16,67**
PBANKA_0304700	PY17X_0305300	**serine repeat antigen 5**	**0**	**x**	**2**	**0**	**0**	**2**	**L. dispensable**	x		1776,2
PBANKA_0912300	PY17X_0913800	tudor staphylococcal nuclease, putative	0		0	0	2	2	L. dispensable	x		1,45
PBANKA_0918000	PY17X_0919700	60S acidic ribosomal protein P0, putative	0		0	0	1	1		x		150,26
PBANKA_1353300	PY17X_1358700	ABC transporter B family member 5, putative	5		1	0	0	1	Sig slow	x		61,01
PBANKA_1103100	PY17X_1104200	actin-depolymerizing factor 1	0		0	0	1	1	L. essential	x		521,78
PBANKA_1125900	PY17X_1127400	ankyrin-repeat protein, putative	0		0	0	1	1		x		217,55
PBANKA_0214300	PY17X_0215700	AP-4 complex subunit beta, putative	0		0	1	0	1		x		1,8
PBANKA_0112100	PY17X_0113700	AP2 domain transcription factor, putative	0		0	0	1	1	L. essential			1,13
PBANKA_0617900	PY17X_0620600	apoptosis-inducing factor, putative	1		0	0	1	1		x		1,8
PBANKA_1448200	PY17X_1450700	asparagine/aspartate rich protein, putative	0		1	0	0	1	Sig slow	x		17,52
PBANKA_0816400	PY17X_0819700	ATP-dependent 6-phosphofructokinase, putative	0		0	0	1	1		x		81,18
PBANKA_1439100	PY17X_1441600	BRO1 domain-containing protein, putative	0		0	1	0	1	L. dispensable	x		**190,72**
PBANKA_0517500	PY17X_0518600	bromodomain protein 1, putative	0		1	0	0	1	L. essential	x		35,83
PBANKA_0938600	PY17X_0941100	casein kinase 2, alpha subunit	0		0	1	0	1	L. essential	x		0,69
PBANKA_1434700	PY17X_1437100	clathrin heavy chain, putative	0		1	0	0	1	L. essential	x		**0,5**
PBANKA_1349600	PY17X_1354600	conserved oligomeric Golgi complex subunit 3, putative	1		0	1	0	1				1,98
PBANKA_1316300	PY17X_1320100	conserved Plasmodium protein, unknown function	2		1	0	0	1	Sig slow			7,46
PBANKA_0403600	PY17X_0405800	conserved Plasmodium protein, unknown function	4		0	0	1	1	L. essential			54,93
PBANKA_1362300	PY17X_1368000	conserved Plasmodium protein, unknown function	0		1	0	0	1	L. essential			40,03
PBANKA_1451800	PY17X_1454300	conserved Plasmodium protein, unknown function	1		1	0	0	1	L. essential			26,83
PBANKA_0309400	PY17X_0309900	conserved Plasmodium protein, unknown function	0		0	0	1	1	L. essential			8,2
PBANKA_0809600	PY17X_0812900	conserved Plasmodium protein, unknown function	0		1	0	0	1	L. essential			5,27
PBANKA_0402900	PY17X_0405100	conserved Plasmodium protein, unknown function	0		0	0	1	1	L. essential			4,72
PBANKA_0206800	PY17X_0208200	conserved Plasmodium protein, unknown function	2		1	0	0	1	L. essential			3,5
PBANKA_0800700	PY17X_0803400	conserved Plasmodium protein, unknown function	1		0	1	0	1	L. essential			1,52
PBANKA_1322000	PY17X_1325800	conserved Plasmodium protein, unknown function	5		0	1	0	1	L. dispensable			31,25
PBANKA_0105300	PY17X_0106800	conserved Plasmodium protein, unknown function	0		0	0	1	1	L. dispensable	x		9,69
PBANKA_0703500	PY17X_0703800	conserved Plasmodium protein, unknown function	0		0	1	0	1	L. dispensable			7,75
PBANKA_0603000	PY17X_0605500	conserved Plasmodium protein, unknown function	0		0	1	0	1	L. dispensable			1,93
PBANKA_1341000	PY17X_1345700	conserved Plasmodium protein, unknown function	0		1	0	0	1	L. dispensable			0,44
PBANKA_0621600	PY17X_0624300	conserved Plasmodium protein, unknown function	0		0	1	0	1		x		104,62
PBANKA_0605600	PY17X_0608100	conserved Plasmodium protein, unknown function	0		1	0	0	1				98,36
PBANKA_1106100	PY17X_1107200	conserved Plasmodium protein, unknown function	0		1	0	0	1				88,03
PBANKA_0620900	PY17X_0623600	conserved Plasmodium protein, unknown function	0		0	1	0	1		x		60,73
PBANKA_1452100	PY17X_1454600	conserved Plasmodium protein, unknown function	0		0	1	0	1				**52,49**
PBANKA_0617400	PY17X_0620100	conserved Plasmodium protein, unknown function	0		0	0	1	1				31,58
PBANKA_1120600	PY17X_1122000	conserved Plasmodium protein, unknown function	0		0	0	1	1				27,37
PBANKA_1220600	PY17X_1223800	conserved Plasmodium protein, unknown function	0		1	0	0	1				13,92
PBANKA_0925800	PY17X_0927800	conserved Plasmodium protein, unknown function	0		0	1	0	1				11,34
PBANKA_1145100	PY17X_1146400	conserved Plasmodium protein, unknown function	0		0	0	1	1				4,27
PBANKA_0942600	PY17X_0945100	conserved Plasmodium protein, unknown function	0		0	1	0	1				3,2
PBANKA_1134500	PY17X_1136000	conserved Plasmodium protein, unknown function	0		0	0	1	1				2,52
PBANKA_1402300	PY17X_1403900	conserved Plasmodium protein, unknown function	0		0	0	1	1				2,19
PBANKA_0802000	PY17X_0804700	conserved Plasmodium protein, unknown function	4		1	0	0	1				0,38
PBANKA_1403800	PY17X_1405500	conserved Plasmodium protein, unknown function	0		1	0	0	1		x		0,21
PBANKA_0801500	PY17X_0804200	conserved Plasmodium protein, unknown function	0		0	0	1	1				0,13
PBANKA_1025100		conserved Plasmodium protein, unknown function	1		0	0	1	1				
PBANKA_0812200	PY17X_0815500	conserved protein, unknown function	0		0	1	0	1	L. essential			24,16
PBANKA_0822200	PY17X_0825500	conserved protein, unknown function	0		0	1	0	1				57,35
PBANKA_0907700	PY17X_0909100	conserved protein, unknown function	0		0	0	1	1				0,55
PBANKA_0805200	PY17X_0808300	cytoskeleton associated protein, putative	0		0	1	0	1	L. essential	x		1,61
PBANKA_1360300	PY17X_1366000	DNA/RNA-binding protein Alba 4, putative	0		1	0	0	1	Sig slow	x		0,29
PBANKA_1426300	PY17X_1428400	ER membrane protein complex subunit 1, putative	3	x	1	0	0	1	L. essential	x		35,61
PBANKA_1126900	PY17X_1128400	eukaryotic translation initiation factor 2-alpha kinase	1		0	0	1	1	Sig slow			5,39
PBANKA_0834300	PY17X_0837700	gamma-tubulin complex component, putative	0		1	0	0	1				8,4
PBANKA_1428500	PY17X_1430600	glycerol-3-phosphate 1-O-acyltransferase, putative	3	x	0	1	0	1		x		**8,2**
PBANKA_1126800	PY17X_1128300	HECT-domain (ubiquitin-transferase), putative	0		0	1	0	1	L. essential	x		24,45
PBANKA_1364400	PY17X_1370200	inner membrane complex protein 1f, putative	0		1	0	0	1	Sig slow	x		**24,02**
PBANKA_0202700	PY17X_0204100	kinesin-8, putative	0		0	1	0	1	L. dispensable			199,36
PBANKA_1302300	PY17X_1306100	metacaspase-2, putative	0		0	0	1	1	L. dispensable			0,57
PBANKA_1354200	PY17X_1359600	mitochondrial pyruvate carrier protein 1, putative	1		1	0	0	1				1,01
PBANKA_1013300	PY17X_1014800	mitogen-activated protein kinase 1	0		0	1	0	1	L. dispensable	x		39,86
PBANKA_0401600	PY17X_0403800	N-ethylmaleimide-sensitive fusion protein, putative	0		0	1	0	1	L. essential	x		55,08
PBANKA_1025500	PY17X_1027900	NOT family protein, putative	0		1	0	0	1	L. essential	x		38,2
PBANKA_0315300	PY17X_0315800	patatin-like phospholipase, putative	2		1	0	0	1				3,4
PBANKA_1006300	PY17X_0827500	**perforin-like protein 1**	0	x	0	0	1	1		x		3,17
PBANKA_1229000	PY17X_1232500	Plasmodium exported protein (PHIST), unknown function	1		0	0	1	1				0
PBANKA_1445500	PY17X_1448000	pre-mRNA-splicing regulator, putative	0		0	1	0	1		x		5,6
PBANKA_0620600	PY17X_0623300	protein CPH1, putative	1		0	0	1	1				12,29
PBANKA_082690	PY17X_0830200	protein kinase, putative	0		0	0	1	1	Sig slow			24,75

PBANKA_1103200	PY17X_1104300	protein kinase, putative	0		0	1	0	1	L. dispensable			4,54
PBANKA_1409100	PY17X_1410900	ras-related protein Rab-5B, putative	0		0	1	0	1	L. essential			26,45
PBANKA_0811600	PY17X_0814900	selenide water dikinase, putative	0		0	1	0	1		x		0,48
PBANKA_0615400	PY17X_0618100	serine--tRNA ligase, putative	0		0	0	1	1	L. dispensable	x		16,27
PBANKA_0802200	PY17X_0804900	serine/threonine protein kinase, putative	0		0	0	1	1	Sig slow			0,07
PBANKA_0718800	PY17X_0718900	small GTP-binding protein sar1, putative	0		1	0	0	1		x		87,71
PBANKA_1355600	PY17X_1361300	**sporozoite protein essential for cell traversal**			**1**	**0**	**0**	**1**		x		4060,9
PBANKA_0917500	PY17X_0919100	structural maintenance of chromosomes protein 1, putative	0		0	1	0	1		x		34,49
PBANKA_0314900	PY17X_0315400	SUZ domain-containing protein, putative	0		1	0	0	1	L. dispensable			17,21
PBANKA_0927800	PY17X_0929800	tRNA nucleotidyltransferase, putative	0	x	0	1	0	1	L. essential	x		21,46
PBANKA_1036100	PY17X_1038500	tubby domain-containing protein, putative	0		0	0	1	1				1,84
PBANKA_1134000	PY17X_1135500	U3 small nucleolar RNA-associated protein 21, putative	0		1	0	0	1	L. essential	x		7,08
PBANKA_1011500	PY17X_1013000	zinc finger protein, putative	6		0	1	0	1	L. essential			21,36

9.3. Multiple sequence alignment of PbANKA_1105300

```
PbANKA_1105300      1 ------------------------------------------------------------------------------------
P.yoelii_110640     1 ------------------------------------------------------------------------------------
Pf3D7_0505700       1 MRLNTICFFLLLIYVINCFSSQFVKNKDFKNGEVNVSGDVDNNGKANKPGEVNKMGQVNKPDQVNKNEKGNTLDKSDKKR
P.vivax_1028300     1 ------------------------------------------------------------------------------------

PbANKA_1105300      1 ------------------------------------------------------------------------------------
P.yoelii_110640     1 ------------------------------------------------------------------------------------
Pf3D7_0505700      81 ESKYASTVEQVNKKEGENKLDEVGISEKAKNPNQVGKKGEVKVVKVVKEVKEAKEAKEAKEVKEAKEAKEAKEVKEAKEV
P.vivax_1028300     1 ----------------------------------------MKLCRAVFFLLAACALHLVACRSGGDEGVAVGAV---

PbANKA_1105300      1 ------------------------------------------------MKLGKVWIFIALVYVVTSLKCENV-----NNKK
P.yoelii_110640     1 ------------------------------------------------MKLGKVWLFIGFAYVATTLKCENG-----VSTK
Pf3D7_0505700     161 KEAKEAKEEKEMKEAKGAKGAKEANTSDQDRNNGGAKKENRSDHNDKKDEAKNASSSGQVSNDRGINKPNQ-----VGKK
P.vivax_1028300    35 --GKAAGKGRGVPTAGKTANGKTAN--GKTTNVGGVASQAPTKKMHRVISEEEGVQEGPNVEASEGDTPNGDAPEELKKV

PbANKA_1105300     29 NGNNVERNSEIDNMNRE-QILENNINEAHRKIKECENQKNELAIQIKNVQNSLYKYTENNKNELNLCISQMSKTENLFKK
P.yoelii_110640    29 DGND-----EINNMSRE-QILENNINEAQRKIKECENQKNELAIKIKNVQNSLHEYIENNKNELNLCVSQMNETKNLFKN
Pf3D7_0505700     236 GEERKTGSPDQVNNNGE-TNKHGAVKTTSDETKECQAEKNAILQEIKGVQKSLQECTKSSSRDLNKCMTKINESQTQLNT
P.vivax_1028300   111 RAELKTAKEELKTAKKEAKQLEEDLQKAKDRALKCEKQKRETLQAAQTAQKNLKECTESGALNLTQCKAQLGDREKHLDV

PbANKA_1105300    108 CKEKELKHSEEIKNITNEYKENLNKKENEKKNFEDKISNLEIKIANAEYKLNNCNKKYENYYYNN-GY---------ENAE
P.yoelii_110640   103 CKEKELKNSEEIKNIRNEYNENLNKKENENKNLESKINKLEIKIANTEYKLNDCSKKYEKYYYNNNGY---------ENGE
Pf3D7_0505700     315 CKENEYKCNGKVKDISSKCSESLNKKEKEAVELKVKISNLENKIVYVQSKLNSCTKNSKSSYRNR-----------DNKE
P.vivax_1028300   191 CRENEDKCYAKMKDLGKQHEERVSRKEDEAAQLREKVLRLERALEDMELKLNAHSQSKPPSTLNENSSAGGGGRHGEGED

PbANKA_1105300    179 -NYLISYDMIKGYFYKIYKIYKTIYIIIIENTYLFEIFNKIYIIYYNLIKYAKMYGTLAISRIYEFYEFILNNNITNIII
P.yoelii_110640   175 -NYLISYNMIKIYFHKIYKIYKTIYIIIIENTYLFEILNRIYIIYYNLIKYTKMYGTLTISKIYEFYEFINNNKINIII
Pf3D7_0505700     384 SNYLISYEIIKNYFLKIFKIYKTFFIIIDEKTFFSELFRKICYLKDMFIKYGKIYSILIITKVYIYFKVIVNSNIVKSSM
P.vivax_1028300   271 SDYLISFPMVRSYFVKVLKIYKTFYIIAFEQTNLAGLLSQVALHKDALVTHLKLYGRLTMERLHDYESFIRESDWVTRLM

PbANKA_1105300    258 NIYNNYISKYYHLFLKNKVNNSILSPSYDLILKH-----IKNIIPILLTLKDGYFKYVE--YFVQKLNINAENLVNKINT
P.yoelii_110640   254 NIYNDYIYKYYHLFLKNKIN-TILSHSYDLILKH-----VKNVIPILLSLKDGYFKYVE--HFVQKLNINAENFVNKINT
Pf3D7_0505700     464 NYYESCFLYQYVTSIKDKII------YVSLIVKVYFMDIINSIIPKFLTLKESLKQNLE--IFVQKLSINSQVLVNKINT
P.vivax_1028300   351 SLYESSPLSQYAQMMKRKAA-SFVSTVRRLLLQKVVHPVSRELYPQMIQSMRNKYMSIEWDLFLQKLHNNSEVLVVKLNS

PbANKA_1105300    331 INPELKGIIPTNLLDQIIFLLFFTIVNFIHIYILFYIIYISFKYSIKTITCLLGNIWFFISSIFQLIIFILTLPIRFFIP
P.yoelii_110640   326 INPELKGIIPTNLLDQILFLLFFTIVNFIHIYILFYIIYISFKYSIKIIIWLLRWICFFISSIFQLIIFILTLPIRFFIS
Pf3D7_0505700     536 INPELNGIIPASLLDQIILLIFFTIVNVIHLYILFYVLFVLYKFFKKITIFTFTWTYFLTTRTYKYIFFFVTLPMRFCMP
P.vivax_1028300   430 INPELQGVISPRLEDQLILLIFFTAVNIIHLYLLFYLLFLLVKLFKRVSICLFVWGFFFVSVAYRCTVFVLTLPIRFCLR

PbANKA_1105300    411 KKNHKNRKIYRRHDDN-AYDNSERLSYQQHEYKKLYKSQNAYQRKF
P.yoelii_110640   406 KKNRKNRKTYRRHDDNNAYDNSERISYQQQEYKKLYKSQNAYQRKF
Pf3D7_0505700     616 KRNSKSRKVYKRHDEQ-VYSNPERTSYQQQEFKKMYKNQSIHQRKF
P.vivax_1028300   510 KRGNRSRKAYRRHEER-TCANPERVSYQQQEIKKMHRGHSVHQRRG
```

ClustalW alignment. Highlighted in black are the bases conserved in all 4 species

9.4. Multiple sequence alignment of PbANKA_1422900

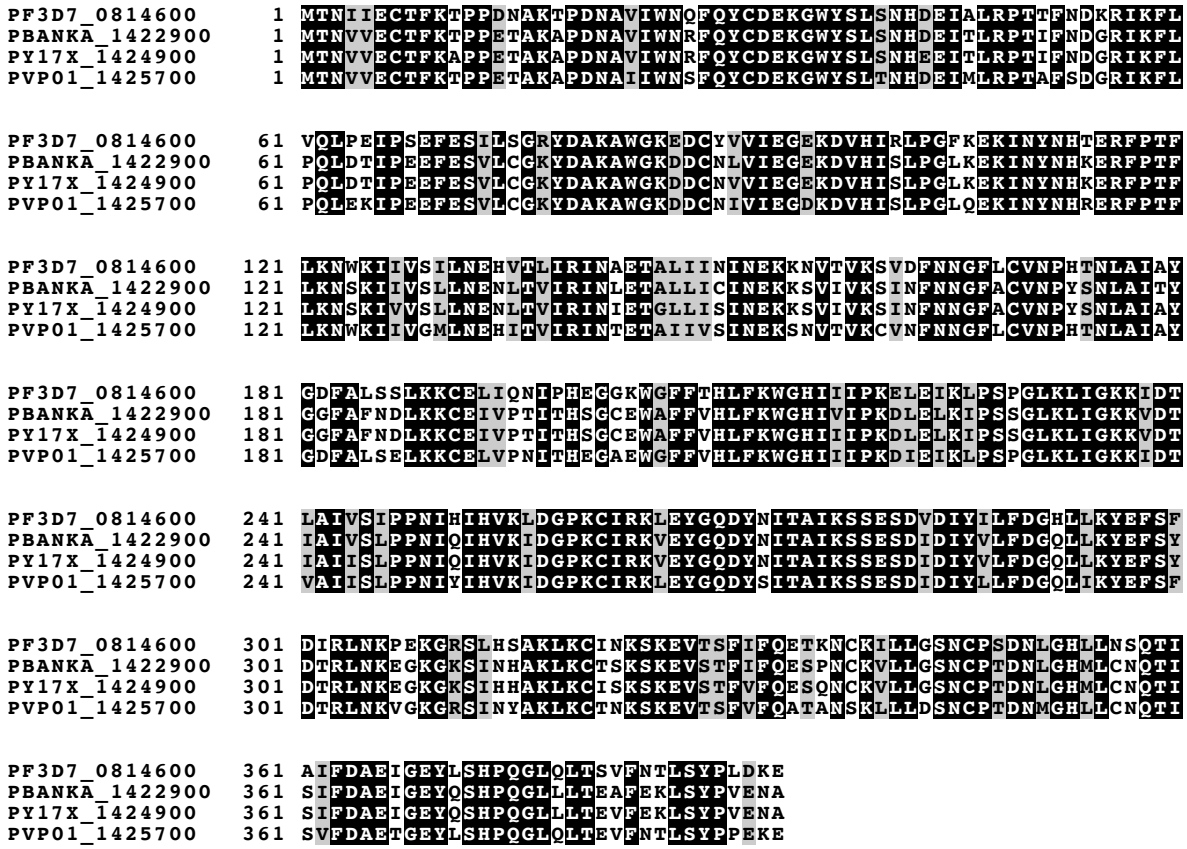

ClustalW alignment. Highlighted in black are the bases conserved in all 4 species